A

Stability and Mechanistic Study

of

Pendant Arm Ligand Complexes

A thesis submitted for the degree of Doctor of Philosophy

at the University of Adelaide (Faculty of Science)

by

Sonya L. Whitbread

B. Sc. (Honours) (Adelaide)

Department of Chemistry
June 1999

TABLE OF CONTENTS

ERRATUM

1. (page 4 Figure 1.2)

   The correct structures for BHE-C21 and BME-C21 are as shown below:

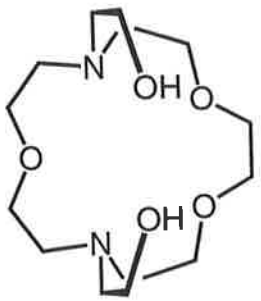

BHE-C21

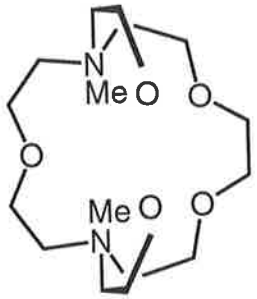

BME-C21

2. (pages 8-14, 29, 32-34, 49, 61-63, 66, 84, 99, 116, 119, 135, 143, and 146)

   The word "conformation" should be replaced by "configuration" in these instances, as interconversion between the C12 or C9 isomeric forms involves bond cleavage.

ACKNOWLEDGMENTS

I would like to thank Professor Stephen F. Lincoln for supervising my postgraduate studies and for the knowledge he has shared. Thank you to the NMR Officer, Phil Clements, for giving me so much time on the CXP-300 and for helping with difficulties. Thank you also to the Lincoln group colleagues, especially Ramesh Dhillon, Ashley Stephens and Phil Clarke, for their helpful advice and instruction, and to the General staff in the Chemistry Department (particularly Rob Morris, Graham Bull, Peter Apoefis, Tony Snigg and Gavin Duthie) for their assistance and expert knowledge of their field.

I would like to thank Kevin Wainwright and Peter Valente for their assistance and guidance with synthetic work and for providing various ligands, and John Sheldon for supporting my tutoring ambitions and for his insight and benevolence.

To Brothers Rob (Morris), Graham (Bull) and Peter (Roberts) I extend my sincerest gratitude for not only allowing me to work for them, but also for their friendship and conviction. To my dearest friends Reina, Ramesh, Sara, Khiet and Mrs D; thank you for all the support, encouragement, food and understanding – which I could not have done without. I would like to acknowledge Gary for his friendship, tutoring partnership and teaching me the value of persistence with work, and Frank for his friendship and thoughtfulness.

Last, but certainly not least, I would like to thank my Mum, Reina, Freya and Greg for being such a supportive family who have always stood by me throughout my studies, and to my beautiful nephew Aiden, for his inspiration and joy of life.

STATEMENT

To the best of my knowledge and belief, this thesis contains no material which has been submitted for any other degree or diploma in any University, nor any material previously published or written by another author except where due reference is made in the text.

I consent to making this thesis available for copying or loan.

Signed

Sonya Whitbread
June 1999

ABSTRACT

This study investigates alkali and alkaline earth metal complexes of pendant arm ligands. The alkali metal ions are of particular interest because complexes involving less labile metal ions have been extensively studied, but those of alkali metal ions need to be explored further. A study of the chiral ligand (*R*)-THPEC12 (1,4,7,10-tetrakis((*R*)-2-hydroxy-2-phenylethyl)-1,4,7,10-tetraazacyclododecane) will provide further insight into the effects of chiral pendant arms on the overall chirality of macrocyclic ligands and their metal complexes.

Stability constants of alkali metal and Ag^+ ion complexes of (*R*)-THPEC12, THEC12 (1,4,7,10-tetrakis(2-hydroxyethyl)-1,4,7,10-tetraazacyclododecane), CYCLEN (1,4,7,10-tetraazacyclododecane) and THEC9 (1,4,7-tris(2-hydroxyethyl)-1,4,7-triazacyclononane) were determined by potentiometric titration. To explore the kinetic origin of macrocyclic ligand selectivity for metal ions, Li^+ and Na^+ exchange on (*R*)-THPEC12, THEC12 and CYCLEN were studied by variable temperature ^7Li and ^{23}Na NMR spectroscopy, respectively. The rate constants and kinetic parameters for this exchange were determined and are discussed in relation to the nature and solvation energy of the metal ion, flexibility and topology of the ligand, nature of pendant arms, and solvent.

The protonation constants of THEC12 and THEC9 and the stability constants of their alkaline earth metal complexes were determined in aqueous solution by pH-metric titration. Stabilities of $[ML]^{2+}$ and $[ML]^+$ were compared, and it is apparent that the same factors influence equilibrium processes for $[ML]^{n+}$ in aqueous and non-aqueous solution, but protonation of nitrogen atoms in the ligand are important in aqueous solution.

Variable temperature ^{13}C NMR spectroscopy, invaluable for elucidating coordination geometries of metal complexes in solution, was used to study intramolecular exchange processes in $[M((R)\text{-THPEC12})]^+$, $[M(THEC12)]^{n+}$, $[M(THEC9)]^{n+}$, and $[Zn(THEC12)]^{2+}$. Intramolecular exchange in $[M(THEC12)]^{n+}$ and $[M(THEC9)]^+$ results in the interconversion of two enantiomers. In (*R*)-THPEC12 and $[M((R)\text{-THPEC12})]^+$, diastereomerisation of single diastereomers occurs through double nitrogen inversion. In the $[M(THEC9)]^{2+}$ system, exchange between $[M(THEC9)]^{2+}$ and $[M(THEC9)(methanol)_n]^{2+}$ may be significant at low temperature. In $[Zn(THEC12)]^{2+}$, the enantiomerisation process involves transannular oscillation of 6-coordinate Zn^{2+}.

Intermolecular ligand exchange on alkaline earth metal complexes of THEC12, TMEC12 (1,4,7,10-tetrakis(2-methoxyethyl)-1,4,7,10-tetraazacyclododecane) and (*S*)-THPC12 (1,4,7,10-tetrakis((*S*)-2-hydroxypropyl)-1,4,7,10-tetraazacyclododecane) was shown to be in very slow exchange on the NMR timescale, excepting $[Mg(TMEC12)]^{2+}$ as a result of steric strain. Similar rate parameters for M^+ and (*R*)-THPEC12 or THEC12 exchange on $[ML]^+$ confirm both processes occur through the same monomolecular mechanism. In contrast, the different activation parameters for intramolecular and ligand exchange on $[M((R)\text{-THPEC12})]^+$ and $[M(THEC12)]^+$, for $M^+ = Li^+$ and Na^+, confirm these two processes follow different reaction pathways overall.

ABBREVIATIONS

The following abbreviations have been used in this study:

Å	angström (10^{-10} m)
$[Ag^+]$	silver ion concentration (mol dm^{-3})
[12]aneN_3	1,5,9-triazacyclododecane
[9]aneN_2S	1-thia-4,7-diaazacyclononane
[9]aneS_3	1,4,7-trithiacyclononane
υ	absorption mode lineshape
BHE-C21	1,7-bis(2-hydroxyethyl)-4,10,13-trioxa-1,7-diaza-cyclopentadecane
BME-C21	1,7-bis(2-methoxyethyl)-4,10,13-trioxa-1,7-diaza-cyclopentadecane
$CHCl_3$	chloroform
$CDCl_3$	deuterated chloroform
C_2H_4O	ethylene oxide
CH_3CH_2OH	ethanol
$ClCH_2CH_2Cl$	dichloroethane
$ClCH_2CH_2OCH_3$	chloroethylmethyl ether
CYCLAM	1,4,8,11-tetraazacyclotetradecane
CYCLEN	1,4,7,10-tetraazacyclododecane
18C6	1,4,7,10,13,16-hexaoxacyclooctadecane
DB-18C6	2,3,11,12-dibenzo-1,4,7,10,13,16-hexaoxacyclo-octadecane
C221	4,7,13,16,21-pentaoxa-1,10-diazabicyclo[8.8.5]-tricosane
C222	4,7,13,16,21,24-hexaoxa-1,10-diazabicyclo[8.8.8]-hexacosane
DB-C222	5,6,14,15-dibenzo-4,7,13,16,21,24-hexaoxa-1,10-diazabicyclo[8.8.8]hexacosane
C22C2	4,7,13,16-tetraoxa-1,10-diazabicyclo[8.8.2]eicosane
δ	chemical shift (ppm)
χ	mole fraction
DNMR	dynamic nuclear magnetic resonance (spectroscopy)

D_N	Gutmann donor number
DMF	*N,N*-dimethylformamide
d_n	*n*-deuterated
d_7-DMF	deuterated dimethylformamide
DIEN	1,4,7-triazaheptane
DOTMA	1,4,7,10-tetrakis((*R*)-methylacetato)-1,4,7,10-tetra-azacyclododecane
DOTA	1,4,7,10-tetraazacyclododecane-*N,N',N'',N'''*-tetra-acetic acid
E	observed potential (volts)
E_0	standard electrode potential (volts)
EMF	electromotive force (volts)
exp	experimental
FID	free induction decay
F	Faraday's constant (9.6487×10^4 C mol^{-1})
$\Delta G^{\ddagger}$	free energy of activation (kJ mol^{-1})
γ	gyromagnetic ratio
$\Delta H^{\ddagger}$	enthalpy of activation (kJ mol^{-1})
H_2O	water
H_2SO_4	sulphuric acid
$HClO_4$	perchloric acid
Hz	hertz (s^{-1})
h	Planck's constant (6.6262×10^{-34} J s)
ISE	ion selective electrode
I	ionic strength
intra	intramolecular (exchange)
inter	intermolecular (exchange)
K_e	equilibrium constant
K_s	stability constant
K_{th}	thermodynamic stability constant

k	rate constant (s^{-1})
k_B	Boltzmann's constant (1.3806×10^{-23} J K^{-1})
K_a	acid dissociation constant
pK_a	$-\log_{10}[K_a]$
L	unspecified ligand
log	logarithm (base 10)
ln	logarithm (base e)
mm Hg	1 mm Hg = 101325 kg m^{-1} s^{-2}
ms	milliseconds (10^{-3} s)
mV	millivolts (10^{-3} volts)
MHz	megahertz (10^6 s^{-1})
MeCN	acetonitrile
MeOH	methanol
$MgSO_4$	magnesium sulphate
NMR	nuclear magnetic resonance (spectroscopy)
NaOH	sodium hydroxide
NEt_4ClO_4	tetraethylammonium perchlorate
NEt_4OH	tetraethylammonium hydroxide
NOTA	1,4,7-triazacyclononane-*N,N',N''*-triacetic acid
P_2O_5	phosphorous pentoxide
PC	propylene carbonate (1,2-propanediol cyclic carbonate)
pH	$-\log_{10}[H^+]$
pOH	$-\log_{10}[OH^-]$
ppm	parts per million
pm	picometer (10^{-12} m)
pK_w	$-\log_{10}[K_w]$
ω	resonant frequency (rad s^{-1})
R	gas constant (8.3143 J K^{-1} mol^{-1})
r	radius (Å)
$\Delta S^{\ddagger}$	entropy of activation (J mol^{-1} K^{-1})

TACN	1,4,7-triazacyclononane
TACN-TM	1,4,7-tris(2-mercaptoethyl)-1,4,7-triazacyclononane
THEC9	1,4,7-tris(2-hydroxyethyl)-1,4,7-triazacyclononane
TRIEN	3,6-diaza-1,8-diaminooctane
(*R*/*S*)-THPC9	1,4,7-tris((*R*/*S*)-2-hydroxypropyl)-1,4,7-triazacyclononane
(*R*/*S*)-THPEC9	1,4,7-tris((*R*/*S*)-2-hydroxy-2-phenylethyl)-1,4,7-triazacyclononane
THEC12	1,4,7,10-tetrakis(2-hydroxyethyl)-1,4,7,10-tetraazacyclododecane
TMEC12	1,4,7,10-tetrakis(2-methoxyethyl)-1,4,7,10-tetraazacyclododecane
(*R*)-THPEC12	1,4,7,10-tetrakis((*R*)-2-hydroxy-2-phenylethyl)-1,4,7,10-tetraazacyclododecane
(*S*)-THPC12	1,4,7,10-tetrakis((*S*)-2-hydroxypropyl)-1,4,7,10-tetraazacyclododecane
THEC14	1,4,8,11-tetrakis(2-hydroxyethyl)-1,4,8,11-tetraazacyclotetradecane
TMC	1,4,8,11-tetramethyl-1,4,8,11-tetraazacyclotetradecane
TCMC	1,4,8,11-tetrakis(carbamoylmethyl)-1,4,7,10-tetraazacyclododecane
Ts	tosyl (*p*-toluene sulphonyl)
tosylate	*p*-toluene sulphonate
triflic acid	trifluoromethane sulphonic acid
triflate	trifluoromethane sulphonate
theor	theoretical
τ	mean lifetime (s)
T	temperature (K)
T_1	longitudinal relaxation time (s)
T_2	transverse relaxation time (s)
[X]	concentration of species X (mol dm^{-3})
$W_{1/2}$	full width at half maximum amplitude

CHAPTER 1

INTRODUCTION

1.1 GENERAL INTRODUCTION

Pendant arm polyaza macrocyclic ligands are cyclic polyamines in which substituents, which often contain donor atoms, are attached to the cyclic backbone of their parent polyaza macrocycles.[1-5] They are defined as containing at least three donor atoms with a minimum of nine atoms in the polyaza ring.[6,7] The pendant arm macrocyclic ligands which are the subject of this study are the *N*-functionalised macrocycles 1,4,7,10-tetrakis((*R*)-2-hydroxy-2-phenylethyl)-1,4,7,10-tetraazacyclododecane, 1,4,7,10-tetrakis(2-hydroxyethyl)-1,4,7,10-tetraazacyclododecane and 1,4,7-tris(2-hydroxyethyl)-1,4,7-triazacyclononane, conveniently abbreviated to (*R*)-THPEC12, THEC12 and THEC9, respectively (Figure 1.1). The trivial nomenclature is based on the shorthand names for the ring and pendant arms. For tetraaza ligands derived from CYCLEN, the systematic name 1,4,7,10-tetrakis((*R*)-2-hydroxy-2-phenylethyl)-1,4,7,10-tetraazacyclododecane is abbreviated to (*R*)-THPEC12; **t**etrakis((***R***)-2-**h**ydroxy-2-**p**heny**l**ethyl)**C**YCLEN, where the (*R*) indicates the configuration of the four chiral carbons of the pendant arms (Figure 1.1), and the systematic name 1,4,7,10-tetrakis(2-hydroxyethyl)-1,4,7,10-tetraazacyclododecane is abbreviated to THEC12; **t**etrakis(2-**h**ydroxy**e**thyl)**C**YCLEN. The number 12 indicates that these pendant arm ligands are derived from the 12-membered parent macrocycle CYCLEN (1,4,7,10-tetraazacyclododecane). Similarly, the systematic name of the triaza ligand 1,4,7-tris(2-hydroxyethyl)-1,4,7-triazacyclononane is abbreviated to THEC9; **t**ris(2-**h**ydroxy**e**thyl)-TA**C**N, where this pendant arm ligand is derived from the 9-membered parent macrocycle TACN (1,4,7-**tri**a**z**a**cyclo**n**onane).

Initial interest in polyaza macrocycles was stimulated by the unusual properties exhibited by their metal complexes, which are not observed for their non-cyclic analogues. These properties include their high degree of thermodynamic and kinetic stability, a degree of metal ion selectivity, interesting spectral and magnetic properties, novel coordination geometries and their ability to stabilise uncommon oxidation states.[6-11] (The high stability of these complexes, compared with their linear chain analogues, is known as the macrocyclic effect).[12] In addition, many naturally occurring polyaza macrocyclic ligands have important biological functions, so considerable research has been directed towards the design of macrocyclic coordination

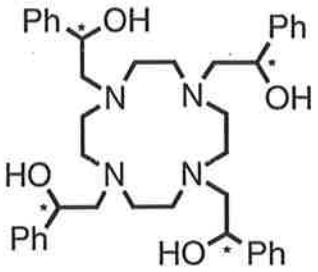

(*R*)-THPEC12

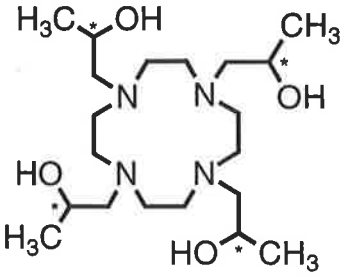

(*S*)-THPC12

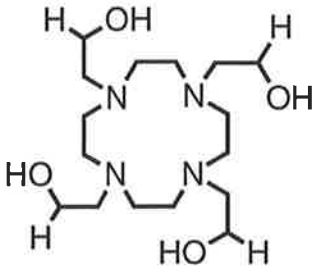

THEC12

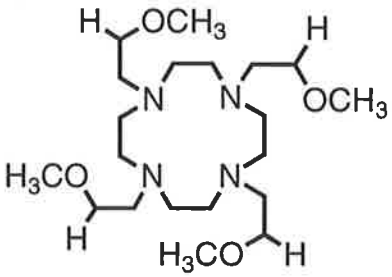

TMEC12

CYCLEN

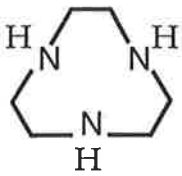

TACN

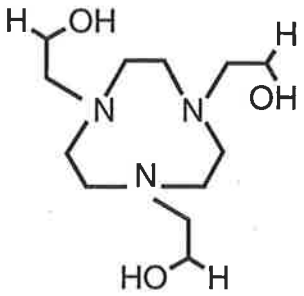

THEC9

Figure 1.1: Structures and trivial nomenclature of the tetraaza and triaza macrocycles discussed in this study.

compounds to model those in biological systems. This aspect is discussed in more detail in Section 1.4.

Metal complexes of the rigid cryptands (shown in Figure 1.2) have received a great deal of attention since their initial synthesis by J.-M. Lehn in 1968.[13] These ligands were largely designed to complex alkali metal ions within a rigid three-dimensional cavity, and many cryptands have subsequently been synthesised.[13] Cryptands form highly stable and selective complexes, or cryptates, with numerous metal ions, and the stability of their metal ion complexes strongly depends on the match between the size of the metal ion and the intramolecular cavity of the cryptand ("size-match" selectivity).[14,15]

These studies prompted further investigation into the effects of ligand flexibility on complex stability and metal ion selectivity, and so lariat ethers (Figure 1.2) were synthesised. These ligands were designed to mimic naturally occurring compounds, specifically the antibiotics monactin, nonactin and valinomycin, by combining the flexibility of crown ethers with the three-dimensional binding characteristics of the more rigid cryptands.[16] There are two types of lariat ethers, the *N*-pivot and *C*-pivot, in which pendant arms are attached to a nitrogen or carbon atom in the azacrown or polyether ring, respectively. Since nitrogens are able to invert easily, the *N*-pivot lariat ethers are more flexible and dynamic than the *C*-pivot analogues.[17] This factor, together with the relative ease of alkylation of amines, has led to *N*-pivot lariat ethers and polyaza macrocycles being more extensively studied, in which a wide range of pendant arms carrying additional potential donors have been incorporated into the ligand. Extensive solution and solid state studies of the complexation of alkali metal ions by lariat ethers have shown that the pendant arms play a significant role in the binding of a metal ion.[18,19] Thermodynamic and kinetic studies have revealed that although lariat ethers show similar complexation properties to those of cryptands, they tend to form cavities around the metal ion during the complexation process, and because of their greater flexibility are less selective and their complexes are more labile.

To extend this understanding, pendant arm macrocycles were designed. It was intended that these ligands should combine the properties of the relatively rigid and kinetically stable macrocyclic structural element with those of the more flexible and kinetically labile open chain ligands.[2c,6]

The selective complexation of divalent and trivalent transition and main group metal ions by tetraaza macrocyclic ligands and their pendant arm derivatives is well established, as is the complexation of divalent and trivalent

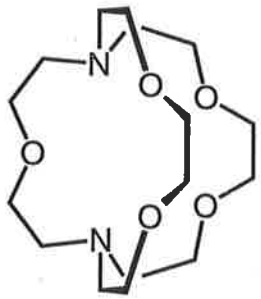

C221

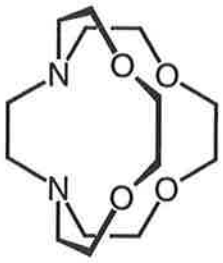

$C22C_2$

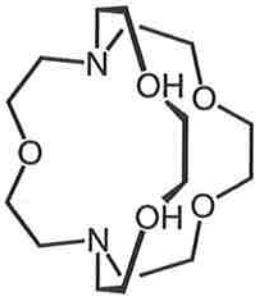

BHE-C21

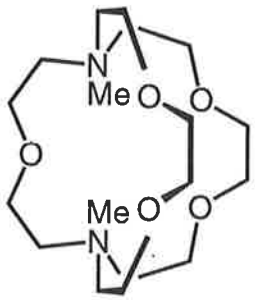

BME-C21

Figure 1.2: Structures of the cryptands C221 and $C22C_2$, and the *N*-pivot lariat ethers BHE-C21 and BME-C21 based on the diaza crown ether C21.

transition metal ions by cyclononane derived ligands, because of their propensity for octahedral coordination.[1c,2a,6,20] However, although the ability of the former type of ligand to complex alkali metal ions has been studied in the solid state, there appear to be fewer quantitative studies of such complexation in solution.[20c,21-23] In addition, the majority of alkali metal ion complexes studied have involved ligands containing predominantly oxygen donor atoms, such as cryptands, crown ethers and lariat ethers,[14a,15a,24-29] because unsubstituted polyaza macrocycles strongly complex transition and heavy metal ions, but only weakly complex alkali metal ions in aqueous solution.[2c,10a,30,31] To enhance their affinity for alkali metal ions, oxygen donor groups can added to these ligands, either by incorporation into the macrocyclic ring or more readily, by attaching pendant arms containing oxygen donor groups to the macrocyclic ring, thus creating pendant arm macrocyclic ligands.

One of the earliest investigations of alkali metal complexation by a pendant arm macrocyclic ligand concerned the macrocyclic ligand THEC12.[1a,32] The solid state structures of $[M(THEC12)]^+$, for $M^+ = Li^+$, Na^+ and K^+, are illustrated in Figure 1.3. In these structures, the metal ion is coordinated by all four ring nitrogens and sits slightly above their common plane. The metal ions Li^+, Na^+ and K^+ in $[M(THEC12)]^+$ are coordinated within the three-dimensional cavity formed by these four ring nitrogens and one, three and four hydroxyethyl pendant arms, respectively, with the pendant arms all coordinated on the same side of the ring. These results demonstrate that the mode of complexation of THEC12 in the solid state is dependent on the size of the metal ion, with an increase in coordination number as the ionic radius of the metal ion increases. Thus, it is anticipated that pendant arm macrocyclic ligands will be effective complexing agents for alkali metal ions, since they are closely related to lariat ethers, and will exhibit some of the complexation characteristics possessed by cryptands, particularly the ability of cryptands to form selective and highly stable complexes with alkali and alkaline earth metal ions as a consequence of their three-dimensional cavity. However, pendant arm macrocyclic ligands are generally more flexible than cryptands, and generally do not have a rigid, preformed cavity or exist as a single preferred conformer, but adopt an encapsulating conformation around the metal ion. Therefore, pendant arm macrocycles can more readily adapt to the size of a metal ion without enhancing the inherent conformational strain associated with binding an ill-fitting metal ion, and the metal ion is often coordinated out of the plane of the nitrogen donor atoms.

The coordination chemistry of pendant arm macrocyclic ligands has attracted keen interest in recent years.[1c,2c,3b,4,14a,24-26,33-36] (It is surprising that, although numerous studies have been devoted to the application of tetraaza macrocyclic compounds in inorganic chemistry, until 1978 only a limited number of triaza macrocycles was known and their coordination chemistry has received comparatively little attention). The addition of substituents at the nitrogen atom of a macrocyclic ring generally incurs a loss of ring flexibility and modified chemical behaviour to that of the unsubstituted parent macrocycle. In particular, metal complexes involving unsubstituted tetraaza macrocyclic ligands are often kinetically inert, but attachment of donor groups onto pendant arms of the macrocyclic ligand substantially increases metal incorporation rates.[6] This has been demonstrated for a vast array of macrocycles including the attachment of acetate arms to porphyrins,[37a] divalent and trivalent metal ion complexes of tetraaza macrocycles,[3a,20a,30a,36b,37b-37d] and is clearly evident for pendant arm derivatives of CYCLAM. Several hours are required for metal complexation to reach equilibrium for ligands based on

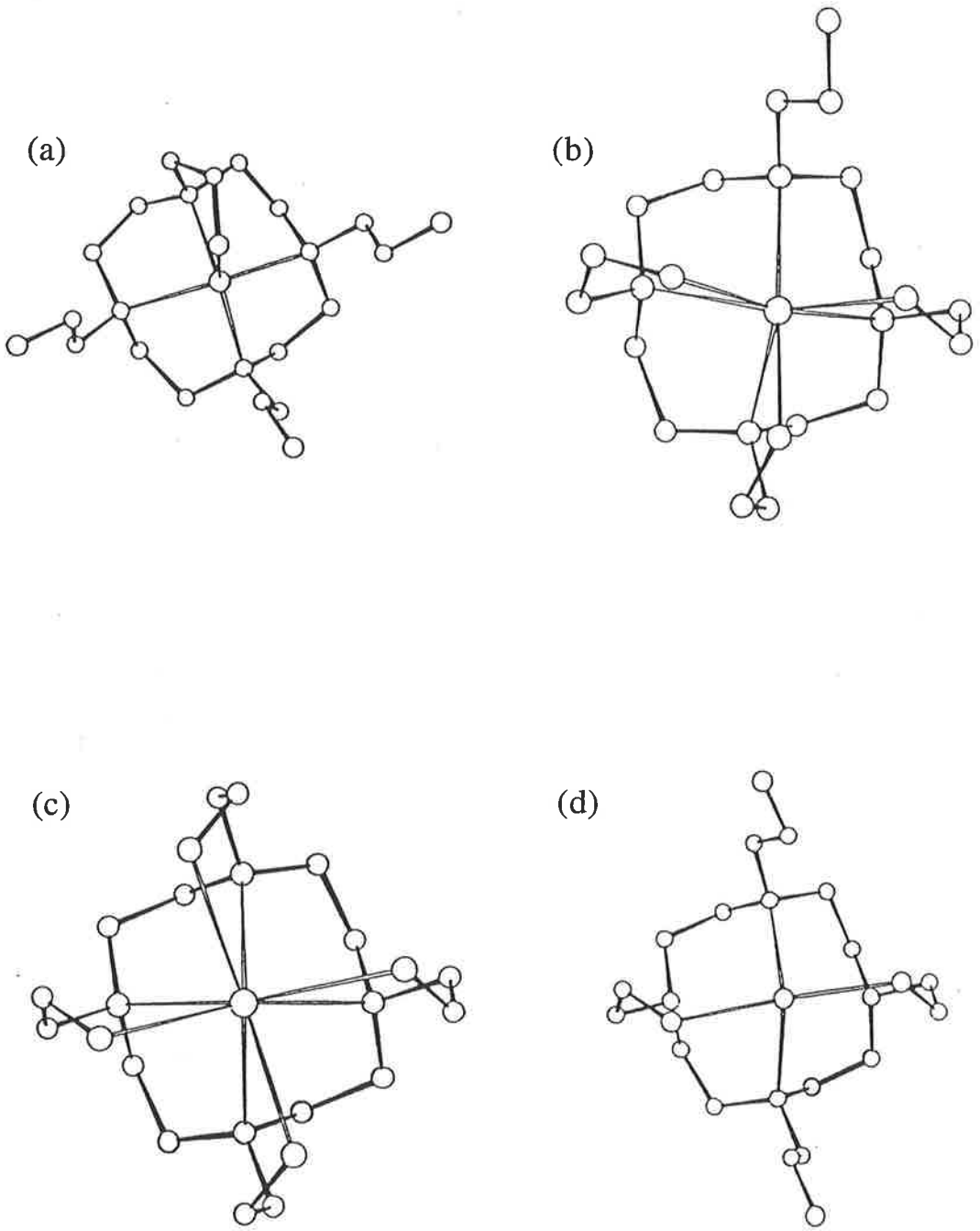

Figure 1.3: Solid state structures of the alkali metal complexes of THEC12. (Reproduced from References 1a and 32).
(a) $[Li(THEC12)]^+$ (b) $[Na(THEC12)]^+$
(c) $[K(THEC12)]^+$ (d) $THEC12.H_2O$

CYCLAM which lack donor groups in the pendant arms, but only seconds are necessary for incorporation of metal ions by pendant hydroxy-, acetato- or amino- arm derivatives of CYCLAM.[1c,2a,3a,3c,37e] This observed increase in the rate of complexation may be attributed to a fast initial coordination of the metal ion by the flexible pendant arms of the ligand, followed by coordination of the tetraaza ring. (The attachment of weak donor pendant arms, such as 2-cyanoethyl, or non-bonding pendant arms, such as methyl, to 14-membered macrocyclic ligands do not cause the significantly increased metal complexation rates observed for other pendant arm derivatives.[1c,3a] However, if the coordinating ability of the pendant arms is increased over that of 2-cyano-ethyl, as for pendant arms containing 2-aminoethyl, 3-aminopropyl, or 2-pyridylmethyl groups, the metal ion may be coordinated by two pendant arms and only two or three tetraaza ring nitrogens.[3b,4,38a] In this circumstance, the metal ion remains outside the macrocyclic ring and the potential discrimination of the metal ion by the ring size of the ligand is lost. Therefore, pendant arms incorporating hydroxyethyl groups may be optimal types of donor pendant arms, with the potential to accelerate metal ion complexation and retain the metal ion selectivity of the macrocyclic ligand).

The nature of the pendant arm is often influential in determining both the structure and lability of metal complexes involving pendant arm polyaza macrocyclic ligands.[1c-3a,3c-5,33a] That is, the attachment of potentially coordinating groups to the periphery of the macrocycle increases the ligating ability of the macrocycle, and can allow the ligand to fulfil the coordination number requirements of the metal ion by complete encapsulation on complexation. Moreover, the increased denticity of a pendant arm macrocyclic ligand over the parent macrocyclic ligand affords its metal complexes stereochemistries and intramolecular processes which are not available to complexes of the parent macrocyclic ligand. Such phenomena have been observed in the intramolecular exchange processes of several metal complexes of TMEC12,[21c] (*S*)-THPC12,[23c] TMEC14 and (*S*)-THPC14,[38b,38c] heavy metal complexes of THEC12,[38d] and THEC14.[20a,20b] However, much less is known about the effects of *N*-substitution of triaza macrocycles on metal ion selectivity and intramolecular exchange processes.[39]

In this study, much of the ensuing discussion on the chemical behaviour of the macrocyclic ligands (*R*)-THPEC12, THEC12, CYCLEN and THEC9 involves comparisons of the structural features of these ligands. Therefore, it is pertinent to include a discussion here of the structural features of macrocyclic ligands, such as complex configuration, hole size and flexibility, which influence the thermodynamic and kinetic properties of the metal complexes of (*R*)-THPEC12, THEC12, CYCLEN and THEC9.

1.2 CONFIGURATIONS OF MACROCYCLIC LIGANDS

The configuration of the ligand strongly influences its thermodynamic and kinetic behaviour. There are two general coordination modes for metal complexes of tetraaza macrocyclic ligands. These are planar coordination (square planar or *trans*-octahedral arrangements) and folded coordination (trigonal bipyramidal or *cis*-octahedral arrangements). Bosnich *et al* developed the terminology of TRANS I - V for planar coordination and CIS II and CIS V for the folded coordination.[40] These configurations are illustrated in Figure 1.4. The relative energy of a particular configuration in a planar or folded coordination is largely determined by the possible conformations of the individual chelate rings comprising the macrocyclic complex.[7] It is important to note that the flexibility of lariat ethers and pendant arm macrocycles does not preclude the formation of dominant free ligand conformations in solution, as observed from studies of (*S*)-THPC12.[23c]

For open-chain ligands, it is mainly the size of the chelate ring rather than the macrocyclic ring in the pendant arm macrocycle which determines the stability of the metal ion complex, except for very small macrocyclic rings, or where the ring is structurally reinforced and thus fairly rigid.[1c,2b,2b,41-43] (The term "chelate", from the Greek word *chele*, meaning crab's claw, was introduced in 1920 to describe those complexes in which the ligand bonds through at least two donor groups such that a ring system is formed. Ligands which have the potential to form such rings are called chelating agents).[44] Minimum strain in the 5-membered (1,2-diaminoethane) chelate ring occurs with M-N bond lengths of 2.5 Å and N-M-N bond angles of 69°, which corresponds to the stabilisation of metal ions with an ionic radius of ~ 1.0 Å. For the 6-membered (1,3-diaminopropane) chelate ring, minimum strain is achieved for M-N bond lengths of 1.6 Å and N-M-N bond angles of 109.5°, corresponding to the stabilisation of smaller metal ions.[2b,41,42] A comparison of CYCLEN and its 14-membered analogue CYCLAM by these theoretical calculations suggests that the 6-membered chelate rings of the 1,3-diaminopropane type present in CYCLAM have an optimal arrangement of the hydrogen atoms with respect to torsional effects. That is, for very small metal ions, the 6-membered chelate ring has all its hydrogen atoms in the more favoured staggered position. However, as the size of the metal ion increases, the hydrogens are increasingly forced into the less favoured eclipsed position, resulting in an increase in strain energy and a decrease in complex stability. For the 5-membered chelate rings of the 1,2-diaminoethane type present in CYCLEN, the hydrogens cannot achieve such a staggered arrangement, and the effect of increasing metal ion size is much less marked.[41a] The cumulative

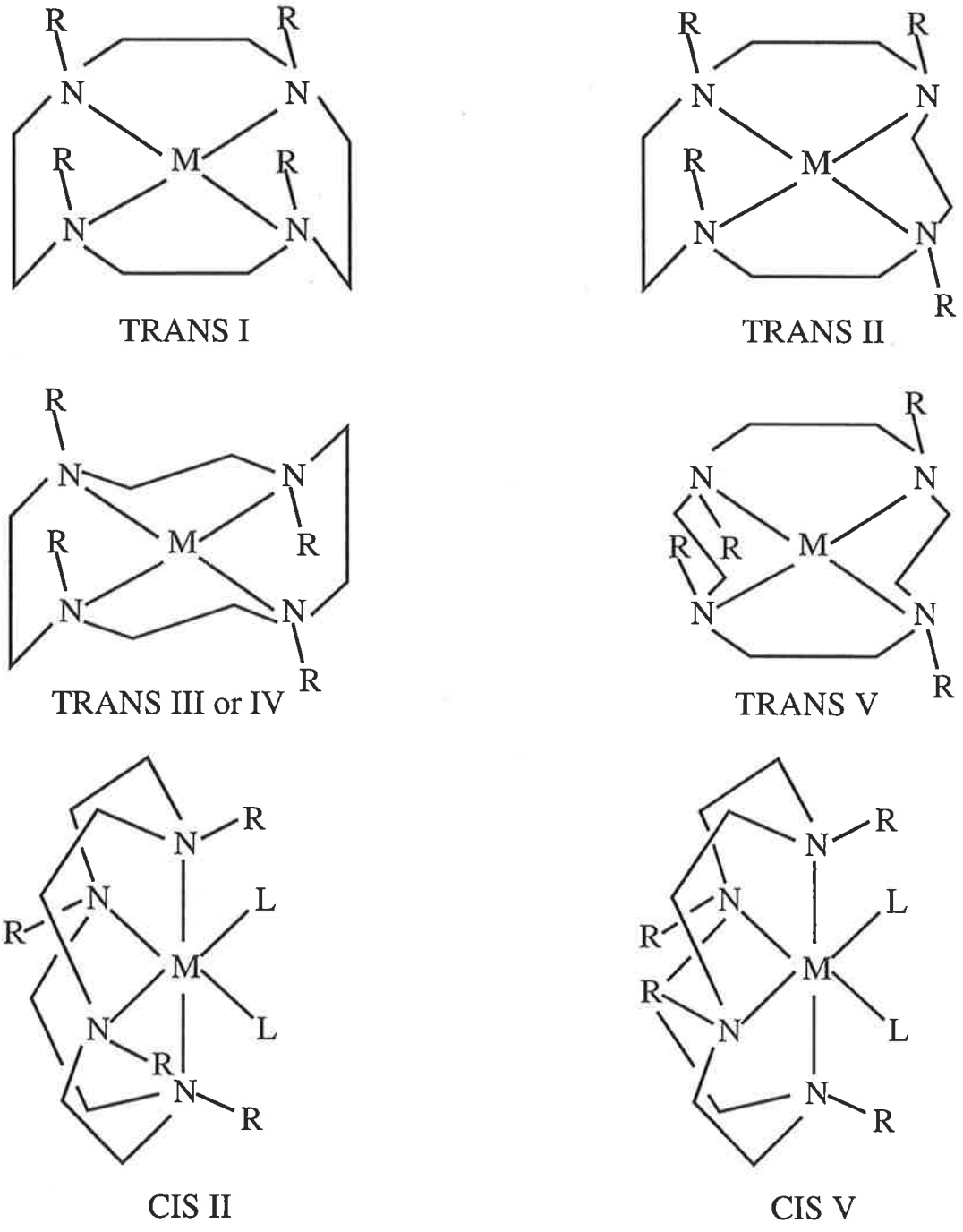

Figure 1.4: Possible configurational isomers of CYCLEN based tetraaza macrocyclic ligands, where the pendant arms, denoted R, are shown uncoordinated. The TRANS III and TRANS IV conformations are equivalent in the completely symmetrical THEC12 and (*R*)-THPEC12 systems.

strain of chelate rings in a macrocyclic ligand complex may be relieved by the complex distorting to a tetrahedral arrangement, which relieves the coplanarity requirement of the M-donor set.[7] Furthermore, chelate angle constraints are less for the macrocycle adopting a folded configuration, which may account for the observation of 12- and 13-membered tetraaza macrocycles often adopting a folded configuration in their metal complexes.[7,30b,44a]

The attachment of substituents to amine donor groups of the macrocyclic ring severely limits the flexibility of the coordinated ligand.[7] Consequently, the macrocyclic ligand is expected to adopt a configuration with the least strain energy to minimise the additional factor of steric repulsion between the pendant arms.[7] Molecular mechanics calculations indicate that the TRANS I configuration (Figure 1.4) is the lowest energy configuration and has the ability to accommodate a range of metal ion sizes, provided the metal ion does not require octahedral coordination.[42a,42b] This conformer allows square planar, square pyramidal, heptacoordination and square antiprismatic geometries. In the TRANS I configuration, the metal ion is coordinated by the four coplanar nitrogens and is often coordinated by up to 0.5 Å above the plane of the macrocycle.[30c,44b] This is most noticeable for the alkali and alkaline earth metal ions, which are generally too large to be coordinated within the macrocyclic ring plane without inducing considerable strain in the complex.[42a] (The degree of extrusion from this plane decreases for smaller metal ions preferring planar coordination).[44a,45a] These theoretical calculations are supported by the recent solution studies of several metal complexes of TMEC12, (*S*)-THPC12 and THEC12,[21b,21c,22,23c,38d] and the adoption of 5,7 and 8-coordinate geometries for various metal complexes of CYCLEN and THEC12 in the solid state, in which the ligand adopts the TRANS I configuration.[1a,30c,32]

The TRANS I configuration is usually not observed for metal ions which have a strong preference for remaining octahedral. This is because in the TRANS I configuration, the alkyl bridges linking the nitrogens together all lie on one side of the macrocycle, effectively below the plane of the four nitrogens, and block off coordination on that side. If the metal ion is too large, the most likely result will be a folded complex, by adoption of a folded TRANS V configuration (Figure 1.4).[45b,45c] The adoption of the TRANS V configuration by a ligand requires coordination of the metal ion by pendant arms above and below the plane of the ring, so that the metal ion is coordinated within the tetraaza ring plane. The torsional strain exhibited by such a conformation, most clearly apparent for alkali and alkaline earth metal ions, makes this coordination geometry thermodynamically unfavourable, particularly for an 8-coordinate complex. (Molecular mechanics calculations have shown, however, that it is possible for a small metal ion to adopt an in-

plane coordination geometry with a macrocyclic ligand. For example, for THEC12, the optimum strain free internuclear distance between the metal ion and a ring nitrogen is 1.82 Å which, in principle, corresponds to a metal ion of radius ~ 0.6 Å).[41a]

No particular macrocyclic constraints are present for folded conformations, and the M-N bond lengths are similar to those observed for analogous non-cyclic ligands.[7] Octahedral geometry can occur for the tetraaza ring folding about a diagonal axis delineated by two nitrogens, so that these two nitrogen donor atoms occupy *trans* coordination sites of an octahedral metal ion and the other two nitrogen donor atoms occupy *cis* coordination sites. Other donor groups occupy the remaining two coordination sites. The CIS II and CIS V configurations (Figure 1.4) describe such conformations. For the CIS V configuration, there is considerable steric crowding between the substituents bonded to the nitrogen donor atoms located in the *cis* sites of an octahedral complex,[43b] which becomes more evident with bulkier pendant arms. This steric interaction can be reduced by a shift from octahedral to trigonal bipyramidal geometry or by adoption of the CIS II configuration. In this configuration, the substituents bonded to the nitrogen donor atoms located in the *cis* sites of an octahedral complex are on opposite sides of the molecular plane.[43b,45b-45d] The CIS II conformation has been observed in several solid state transition metal complexes of CYCLEN,[30b,30c,31a,31c,43b,45a,46,47a] whereas related macrocycles have been shown to complex transition metal ions in the CIS V conformation.[47b]

The TRANS III configuration is a conformation that has also been adopted by macrocyclic ligands. For instance, the TRANS III conformation has been observed in the solid state for complexes between Zn^{2+} and 1,4,8,11-tetraaza-cyclotetradecane, 1,4,8,12-tetraazacyclopentane and related ligands,[31b,45c,47a] in which the metal ion is coordinated above the tetraaza ring plane. In addition, the least strain energy structure for metal complexes of CYCLAM and its pendant arm derivatives, such as THEC14, with alternating 5- and 6-membered chelate rings is one that adopts the TRANS III configuration. Therefore, this configuration has been adopted in heavy metal complexes of CYCLAM, and pendant arm derivatives, as well as complexes of 15-membered macrocyclic ligands.[1c,2a,15a,20a,20b,21a,48c]

It is noteworthy that the TRANS III/IV configuration is not often observed with 12-membered tetraaza macrocyclic ligands in 8-coordinate metal complexes because, as for adoption of a TRANS V configuration, it places the metal ion in the plane of the ring thus generating steric strain in the complex. In addition, the observed variable temperature spectra of metal complexes of 12-

membered macrocyclic ligands are often inconsistent with the adoption of the TRANS III/IV configuration by an 8-coordinate complex. It has been proposed from molecular mechanics calculations that the ideal M-N bond length for adoption of the TRANS III configuration by CYCLEN based macrocyclic ligands is 1.81 Å, and that octahedral geometry is allowed, provided that the metal ion is not too large for the macrocyclic cavity by more than 0.05 Å.[42b] The TRANS III configuration displays a lesser tolerance of variation in metal ion size than the TRANS I form.[42b] With increasing metal ion size, the nitrogens in the TRANS I configuration simply rotate so that the metal ion is raised further and further above the plane of the donor atoms. This is not possible for the TRANS III configuration, where two nitrogens are oriented above the plane of the macrocycle and two are oriented below the plane. Therefore, the TRANS III configuration cannot produce the concerted movement available to the TRANS I configuration, with all lone pairs oriented on the same side of the macrocycle.

In contrast to the number of configurations available to tetraaza macrocyclic ligands, there are only two general configurations with coplanar nitrogens coordinating a metal ion available to 9-membered macrocyclic ligands. These are the + + + and + − + configurations (Figure 1.5). Molecular mechanics calculations have shown that the + + +, or [333], configuration is the most energetically favourable configuration for planar coordination of metal ions, and is thus expected to be the most commonly adopted conformation of 9-membered macrocyclic ligands in their metal complexes.[41b,49] In this configuration, the metal ion is coordinated above the triaza ring to the three coplanar nitrogens, with the coordinated pendant arms on the same side of the ring. For a 6-coordinate complex, the + − + configuration is thermodynamically unfavourable because it places the metal ion in the plane of the triaza nitrogens, a geometry which, depending on the size of the metal ion, generates considerable steric strain in the complex. These proposals are supported by the computed structures of $[M(THEC9)]^+$ in this study, and the solid state structures of related metal complexes.[23a,36c] It has been postulated that metal complexes of THEC9, and related macrocyclic ligands, should experience considerable trigonal distortion because the hydroxyethyl arms are too short to permit regular octahedral coordination.[36c,50]

The only other conformer that has been observed is the [234] conformer (Figure 1.6), found in $[Cu([9]aneN_2S)Br_2]$, where $[9]aneN_2S$ is 1-thia-4,7-diazacyclononane.[49a] For the [333] and [234] conformers, the numbers in the square brackets indicate the lengths of the sides which are present in the macrocycle. That is, the [333] conformer is considered to be a triangle with

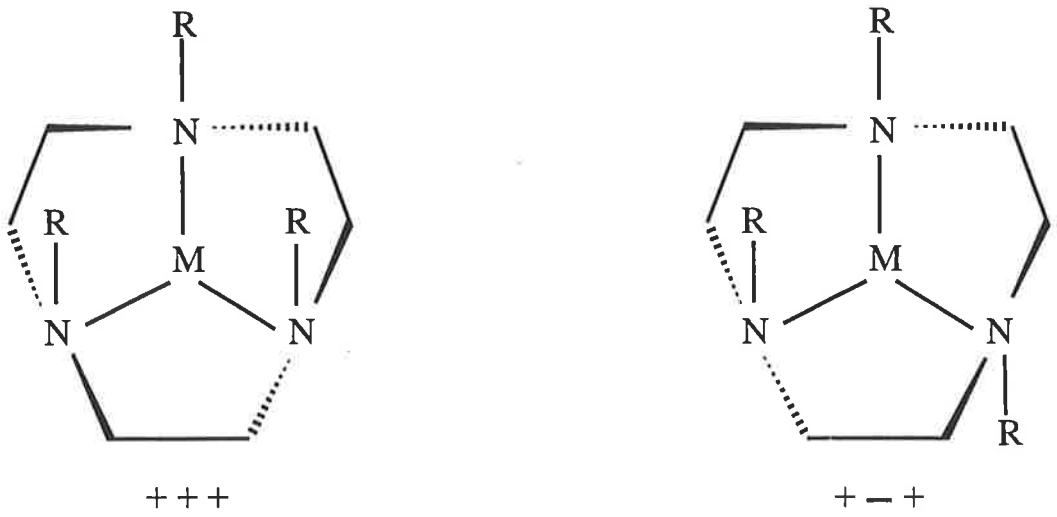

Figure 1.5: Possible configurational isomers of $[M(THEC9)]^{+}$, where the hydroxyethyl pendant arms, denoted R, are shown uncoordinated. The R groups oriented above the nitrogen plane are indicated with a +, while those below the plane are indicated with a –.

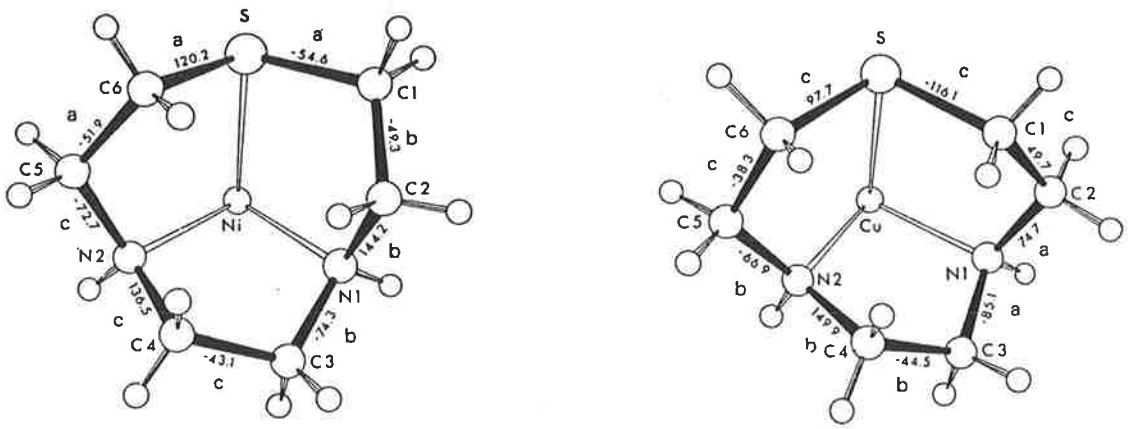

Figure 1.6: The macrocycle [9]aneN_2S shown bound to Ni^{2+} and Cu^{2+} to illustrate the difference between the [333] and [234] conformers. (Reproduced from Reference 49a).

three sides each comprised of three bonds, indicated as *a*, *b* and *c* in Figure 1.6. For the [234] conformer, the macrocycle is considered to have three sides of unequal length, comprising a short side consisting of two bonds (denoted *a* in Figure 1.6), a longer side consisting of three bonds (denoted *b*), and the longest side consisting of four bonds (denoted *c*). The steric difference between these two conformers is that the ring atom C_1 lies more or less flat at a corner position in the [333] conformer, but is twisted up out of the plane in the [234] conformer, so that the corner for the [234] conformer occurs at ring atom C_2.[49a] The adoption of this unusual conformation may be due to the mismatch in bond length between the Cu-N and Cu-S bonds, which is unusually large because the sulphur donor occupies the axial site on the tetragonally distorted Cu^{2+} ion. For cyclononane derived macrocycles, molecular mechanics calculations indicate that the [333] conformer is always a lower energy configuration than the [234] conformer, in agreement with the rarity of the [234] conformer. However, the difference in strain energy between these two conformers is small for complexes of [9]aneN_2S compared to that for TACN and [9]aneS_3 (1,4,7-trithiacyclononane), allowing adoption of such a conformation.

1.3 LIGAND HOLE SIZE AND FLEXIBILITY

Two fundamental factors influencing the complexation properties of metal complexes of macrocyclic ligands are the macrocyclic hole size and flexibility of the ligand.[6,7] The hole size of a macrocyclic ligand is determined by many structural factors such as the number of atoms in the macrocyclic ring, the flexibility of the ligand to expand or contract to accommodate ideal M-donor atom bond lengths, and the nature of the donor atoms.[6,7] The flexibility of a macrocyclic ligand is determined by the size of the macrocyclic ring, and the degree of substitution on the donor atoms or cyclic backbone.[6,7]

Macrocyclic hole sizes have been determined by molecular mechanics calculations, on the basis that hole size is the M-N bond length that produces minimum strain in the complex. That is, the best-fit hole size refers to the situation where the metal ion is constrained to lie in the plane of the polyaza ring, so that a metal ion having this ideal M-N distance chelates with minimum strain of the macrocyclic ligand. Molecular mechanics calculations have established M-N distances for the least strained conformation with approximately coplanar nitrogen atoms for tetraaza and triaza macrocycles. For the commonly adopted TRANS I configuration by tetraaza macrocyclic ligands based on CYCLEN, the ideal M-N bond length is 2.11 Å, and for the adoption of the + + + configuration by triaza macrocyclic ligands based on TACN the

ideal M-N bond length is 1.40 Å.[6,7,42b,51] There is an ideal ring size for any metal ion having a given M-donor atom distance. A ring size slightly smaller (0.1–0.2 Å in terms of M-N distance) than the best-fit ring shows abnormally strong M-donor bonds, whereas an oversized ring shows substantially decreased M-donor interactions.[52] It must be noted, however, that for conformations such as the TRANS I configuration, where the metal ion lies above the macrocyclic ring plane, cavity size plays only a minor part in determining stability patterns, and chelate ring size effects are stability determining.

The cyclic structure of a macrocycle confers additional stereochemical constraints on the ligand which depend on the size of the macrocyclic ring, and the number and nature of chelate rings formed on coordination.[6,7] These factors influence the positions of the donor atoms with respect to each other and to the coordinated metal ion, and these constraints may limit configurations and coordination modes of the ligand in the metal complex. Depending on the rigidity of the macrocyclic ring and degree of substitution on the donor atoms or cyclic backbone, ligand folding can increase the steric strain in a metal complex, so much so that it can be more energetically favourable for the metal ion to be coordinated above the macrocyclic ring plane.[30c] Therefore, the ring strain of a macrocyclic complex may account for the adoption of less commonly observed coordination geometries for particular metal ions, M-donor atom bond lengths and angles which differ from the ideal, and the unusual spectrochemical and electrochemical behaviour associated with these complexes.[6,7] The effect of macrocyclic ring size of a pendant arm macrocyclic ligand on its complexation characteristics with metal ions is investigated in this study by comparison of the 12-membered macrocyclic ligands (*R*)-THPEC12 and THEC12 with the 9-membered ligand THEC9.

1.4 APPLICATIONS

Systematic variation of the pendant arms, and thus modification to the properties of the parent macrocycle, has led to the synthesis of ligands with interesting and useful applications. Certainly, the ability to predict the metal ion selectivity of a macrocyclic ligand is of great interest in many fields. For instance, synthetic polyaza macrocycles have been designed and developed as potential iron sequestering reagents for the treatment of acute iron poisoning and aluminium intoxication,[53,54a] and as selective metal extractants in hydrometallurgy.[54b] Synthetic pendant arm macrocyclic ligands have been used as biofunctional chelating agents, which attach metal ions to proteins, because of the ability of these reagents to incorporate a strong metal chelating

group and a chemically reactive group. Substantial progress has been made in the application of such reagents to areas such as cancer therapy and diagnosis, clinical immunoassays, and DNA footprinting.[3c,43a,55] The treatment of heavy metal intoxication, in the cases of metal poisoning and contamination by radioactive metals, is of great concern in analytical and environmental chemistry and complexotherapy. Therefore, one of the major areas of current interest is in the design of macrocyclic ligands which selectively complex toxic heavy metals (Cd^{2+}, Hg^{2+} and Pb^{2+}) over biologically important ones (Cu^{2+}, Zn^{2+}, Ca^{2+} and Mg^{2+}),[36a,47a,56a] where studies have shown that the attachment of pendant arms containing oxygen donor groups alters the metal ion selectivity of such ligands.[2b,36a,41] Preliminary results of studies on test animals have shown that (*S*)-THPC12 is able to remove Cd^{2+} from aged deposits in rats, is non-toxic and non-carcinogenic, and does not appear to remove any other metal ions.[36a] Synthetic macrocycles have also found uses in metal ion promoted reactions, such as ester, amide and nitrile hydrolysis, where a weakly binding or even non-coordinating organic group is covalently coupled to a macrocycle which binds a metal ion, so that the properties and reactivity of the organic group might be changed.[3a,56b,56c] Other applications of synthetic macrocycles include the design of complexing agents for use in detergents,[56d] the potential for attachment to other substituents via their appended functional groups to produce, for example, immobilised systems for metal ion scavenging,[57] and the ability of macrocyclic ligands containing chiral centres to separate racemic mixtures into their enantiomers, yielding a number of important applications such as the resolution of amino acids.[58,59a] Several divalent and trivalent metal complexes of the macrocyclic polyamines CYCLEN and CYCLAM, and their pendant arm derivatives, have a degree of effectiveness against human immunodeficiency virus type 1 (HIV-1).[59b] It is hoped, in the near future, that research into various structural modifications to macrocyclic polyamine compounds and drug combinations will lead to the development of more selective and potent anti-HIV agents.

Synthetic polyaza macrocycles may be a helpful tool in understanding metal complexes of naturally occurring macrocycles and the mechanisms occurring in biological systems. For example, synthetic 16-membered porphyrins and their Fe^{2+} complexes have been examined to elucidate the factors governing the reversible uptake of iron by haemoglobin. Fundamental kinetic and thermodynamic data have also been obtained on synthetic vitamin B_{12} model compounds, where modified Schiff-base ligands imitate the natural 15-membered corrin system, to further the understanding of the factors affecting the stability of the Co-C bond in vitamin B_{12}.[2c,6,60,61] These are only two examples of the extensive studies carried out on synthetic polyaza macrocycles to explore the possibility of their use as models for biological

systems.[7,62,63] Studies of this kind are associated with the development of the scientific field of biomimetic chemistry ("biomimetics").

In addition, knowledge of the principles of selectivity are invaluable in developing the understanding of metal ion selectivity displayed by biological systems and how metal ions are distributed in the environment. For instance, in recent years macrocyclic complexes of trivalent lanthanides have received considerable attention because they are inert to metal ion dissociation, a prerequisite for many medicinal applications of metal complexes in blood serum and *in vivo*, they are active in catalysing ribonucleic acid cleavage or cleavage of phosphate esters or phosphoric anhydrides,[64] and they have been tested as potential lanthanide ion selective reagents.[64e,65] A variety of molecules based on the iron-transport ligand enterobactin have been synthesised in an effort to mimic the ability of enterobactin to treat iron-overload diseases such as Cooley's anemia.[66] These synthetic macrocyclic ligands are geometrically capable of encapsulating the ferric ion in an octahedral cavity analogous to that of enterobactin, and since the usefulness of enterobactin is limited by its rapid hydrolysis in the human body, the synthetic molecules do not contain the ester group that subject enterobactin to hydrolysis. The biological significance of pyrazole- and imidazole-functionalised macrocycles is also of current interest, where these macrocycles model the donor properties of histidine residues in the binding sites of metalloproteins,[46] and the analogy between haem-containing proteins such as catalases and peroxidases and tetraaza macrocyclic transition metal complexes suggested that the latter may exhibit catalase or peroxidase activity. This has since been established.[46] It has been recently reported that the achiral macrocycle TMEC12 produces chiral complexes, and chiral (*S*)-THPC12 produces homochiral metal complexes.[21c,23b,23c] The existence of chiral metal complexes of synthetic macrocycles, apart from the intrinsic interest, also has biological implications because many naturally occurring molecules are chiral, but for reasons which remain unclear, exist in only one of the two possible enantiomers or diastereomers. Many drug molecules are also chiral, but their enantiomers often have very different, and sometimes devastating, effects. Chiral metal complexes of macrocyclic ligands, such as the Co^{2+} complexes of chiral macrocycles containing the CYCLEN skeleton, have been examined in a number of studies, which include the selective hydrolysis of specific *N*-terminal groups of peptides and the conversion of L-alanine.[46c]

Since the recent discovery of the usefulness of the triazacyclononane ring, for both its synthetic versatility and its selectivity for binding Mg^{2+} over Ca^{2+}, a series of 1,4,7-triazacyclononane based ligands have been studied for their use in determining free Mg^{2+} levels in plasma or for monitoring changes in the

levels of free Mg^{2+} in perfusates during ^{31}P NMR studies of perfused organs.[67] These findings are particularly important because most interest has focused on Ca^{2+}, largely because of its well established role as an intracellular messenger,[68a] whereas there has been mounting evidence in recent years that Mg^{2+} may play a pivotal role in regulations of a much wider variety of intracellular events.[68b] The selectivity of certain 9-membered ligands for Mg^{2+} over Ca^{2+} is especially useful in the development of Mg^{2+}-specific membrane electrode systems, where current technology requires a substantial correction for both pH and the ubiquitous Ca^{2+}.[69a] Changes to the ligating group attached to the triazacyclononane ring allow fine-tuning of complex stability and metal ion selectivity, and 1,4,7-triazacyclononane derivatives containing a combination of acetate and ethylphosphinate side chains have shown great promise for *in vivo* applications.[67c,67d] The ligand TACN-TM (1,4,7-tris(2-mercaptoethyl)-1,4,7-triazacyclononane), with mercapto donor groups, is of interest in studying enzyme models which have protein-bound non-haem iron.[69b] The high stability of TACN-TM with Ga^{3+} allows this complex to maintain its integrity *in vivo*, preventing hydrolysis or competition with natural carriers of trivalent metal ions, such as the blood protein transferrin.[69c] In addition, this high stability constant, together with the lipophilic nature of the complex, makes TACN-TM an attractive candidate for functionalisation in the labelling of antibodies and other proteins.[70] The formation of stable complexes between lanthanides and TACN-TM, as well as for related triaza ligands, may be useful in radiopharmacology for imaging purposes and as biofunctional chelating agents.[69b,70]

1.5 OBJECTIVES OF THIS STUDY

This study addresses the equilibrium, thermodynamic, kinetic and mechanistic aspects of metal complexation by macrocyclic ligands through an examination of the stability and lability of alkali and alkaline earth metal complexes of the tetraaza macrocycles (*R*)-THPEC12, THEC12 and CYCLEN, and the triaza macrocycle THEC9. The addition of oxygen containing pendant arms, such as hydroxyethyl, to a polyaza macrocycle increases the denticity of the ligand, but also increases steric crowding in the metal complex. This has the effect of increasing the selectivity of the ligand for larger rather than smaller metal ions, because a larger metal ion (with an ionic radius ~ 1.0 Å) can more readily adopt a higher coordination number without steric strain. In addition, the oxygen donor atoms of the pendant arms form part of a 5-membered chelate ring in the metal complex. Therefore, this study explores the effect of the attachment of $-CH_2CH_2R-$ (where R is a donor group)

type of pendant arms to tetraaza and triaza macrocyclic ligands in enhancing the selectivity of the ligand for particular alkali and alkaline earth metal ions.

It is intended that the results from these studies will complement and extend the current understanding of metal complexes of macrocyclic ligands. It is important to note that the metal complexation characteristics of pendant arm macrocyclic ligands depend on the nature and solvation energy of the complexing metal ion, the nature of the solvent, and the topology and steric constraints of the ligand.[1c,3-5,33,34c,36b] It is known that even minor variations in the structure of the macrocycle may lead to considerable differences in the behaviour of the metal complex that cannot be anticipated. Therefore, an indication of these effects on complex stability and lability is sought through a comparison with analogous metal complexes of the related macrocyclic ligands TMEC12 and (*S*)-THPC12. In this respect, the stability and lability of metal complexes of the parent macrocyclic ligand CYCLEN can be compared with those of pendant arm ligands with varying degrees of potential steric hindrance in the pendant arms. Thus, stability and lability data of the less sterically hindered macrocycle THEC12 is compared with that of (*R*)-THPEC12, which contains bulkier phenyl substituents at the αcarbon (αC). These results are then compared and contrasted with those for ligands containing methyl substituents at the αC of the ligand ((*S*)-THPC12), and relatively bulky methyl groups at the coordinating oxygen of the pendant arms (TMEC12). Studies of related macrocyclic ligands and lariat ethers support the supposition that placement of methyl groups on the ethylene bridges of a macrocyclic ring or at the αC of a pendant arm causes less steric hindrance than placement on the coordinating oxygen or nitrogen donor atoms of the ligand.[71]

Included in this discussion is the kinetic study of $[Zn(THEC12)]^{2+}$. The Zn^{2+} ion is of interest because it is a trace element of biological importance. That is, it is involved in inhibitory control as well as catalysis,[72a] and increasing numbers of hydrolytic enzymes, such as carboxypeptidases and carbonic anhydrase, are found to contain Zn^{2+} in their active sites.[72b] Apart from its biological importance, Zn^{2+} also has some special chemical features. These include its ready formation of low coordination number complexes, and its ability to change coordination number to adapt to the geometry of the ligand. In addition, its metal complexes generally undergo rapid intramolecular and intermolecular exchange. Various metal complexes have been designed to account for or mimic the functions displayed by Zn^{2+}. The majority of these complexes, however, have employed Co^{3+} or Cu^{2+} ions, which are not common in metalloenzymes, whereas fewer models with Zn^{2+} complexes have been reported. The Zn^{2+} complexes of TMC and [12]aneN_3, discussed below, are two complexes which show promise for mimicking naturally occurring sites.

The Zn^{2+} complex of TMC (1,4,8,11-tetramethyl-1,4,8,11-tetraazacyclotetradecane) behaves as a reversible CO_2 acceptor in alcoholic solution,[63b,73] in which Zn^{2+}, coordinated by three nitrogens, is in the active site, and is very efficient at fixing CO_2 and converting it to carbonic acid *in vivo*.[72a,74] More recently, it has been proposed that from the macrocyclic triamines and tetraamines tested, the 12-membered triamine [12]aneN_3 (1,5,9-triazacyclododecane) is the most appropriate ligand to mimic the ligand field surrounding Zn^{2+} in carbonic anhydrase where, like the Zn^{2+}-enzymes, the $[Zn[12]aneN_3(OH)]^+$ species catalyses metal acetate hydrolysis and acetaldehyde hydration.[73c] The use of the analogy between the active centres of metalloenzymes and a metal ion with its immediate environment in a macrocyclic complex provides further insight into this type of metal ion environment, which is of considerable importance in living systems. Therefore, an investigation of $[Zn(THEC12)]^{2+}$ will extend the existing understanding of zinc complexes of related macrocyclic ligands, and may provide a basis for a better knowledge of the metal environment in some metalloenzymes and metalloproteins.

BIBLIOGRAPHY

1. (a) S. Buøen, J. Dale, P. Groth, J. Krane, *J. Chem. Soc., Chem. Commun.* **1982**, 1172-1174.
   (b) R.W. Hay, D.M.S. Clark, *Inorg. Chim. Acta.* **1984**, 83, L23.
   (c) C.M. Madeyski, J.P. Michael, R.D. Hancock, *Inorg. Chem.* **1984**, 23, 1487-1489.
2. (a) R.W. Hay, M.P. Pujari, W.T. Moodie, S. Craig, D.T. Richens, A. Perotti, L. Ungaretti, *J. Chem. Soc., Dalton Trans.* **1987**, 2605-2613.
   (b) R.D. Hancock, R. Bhavan, P.W. Wade, J.C.A. Boeyens, S.M. Dobson, *Inorg. Chem.* **1989**, 28, 187-194.
   (c) T.A. Kaden, *Topp. Curr. Chem.* **1984**, 121, 157-179.
3. (a) K.P. Wainwright, *J. Chem. Soc., Dalton Trans.* **1980**, 2117-2120.
   (b) I. Murase, M. Mikuriya, H. Sonoda, Y. Fikuda, S. Kida, *J. Chem. Soc., Dalton Trans.* **1986**, 953-959.
   (c) M.K. Moi, Y. Yanuck, S.V. Deshpande, H. Hope, S.J. DeNardo, C.F. Meares, *Inorg. Chem.* **1987**, 26, 3458-3463.
4. N.W. Alcock, K.P. Balakrishnan, P. Moore, *J. Chem. Soc., Dalton Trans.* **1986**, 1743-1745.
5. A. Reisen, M. Zehnder, T.A. Kaden, *Acta. Crystallogr., Sect. C: Cryst. Struct. Commun.* **1988**, C44, 1740-1742.
6. L.F. Lindoy, *"The Chemistry of Macrocyclic Ligand Complexes"*, Cambridge University Press, Cambridge, **1990**.
7. *"Coordination Chemistry of Macrocyclic Compounds"*, G.A. Melson (Editor), Plenum Press, New York, **1979**.
8. (a) D.K. Cabbiness, D.W. Margerum, *J. Am. Chem. Soc.* **1970**, 92, 2151.
   (b) S.C. Jackels, K. Farmery, E.K. Barefield, N.J. Rose, D.H. Busch, *Inorg. Chem.* **1972**, 11, 2893-2901.
   (c) D.C. Olsen, J. Vasilevskis, *Inorg. Chem.* **1969**, 8, 1611.
9. (a) F.V. Lovecchio, E.S. Gore, D.H. Busch, *J. Am. Chem. Soc.* **1974**, 96, 3109.
   (b) F.P. Hinz, D.W. Margerum, *Inorg. Chem.* **1974**, 13, 2941-2949.
   (c) M. Kodama, E. Kimura, *J. Chem. Soc., Dalton Trans.* **1976**, 116-120.
10. (a) M. Kodama, E. Kimura, *J. Chem. Soc., Dalton Trans.* **1976**, 1720-1724.
    (b) M. Kodama, E. Kimura, *J. Chem. Soc., Dalton Trans.* **1976**, 2341-2345.
    (c) A. Anichini, L. Fabbrizzi, P. Paoletti, R.M. Clay, *J. Chem. Soc., Dalton Trans.* **1978**, 577-583.
11. (a) R.M. Clay, H. McCormac, M. Micheloni, P. Paoletti, *Inorg. Chem.* **1982**, 21, 2494-2496.

(b) L. Fabbrizzi, *Comments Inorg. Chem.* **1985**, 4, 33.
(c) E.K. Barefield, G.M. Freeman, D.G. Van Derveer, *Inorg. Chem.* **1986**, 25, 552-558.

12. (a) D.H. Busch, K. Farmery, V. Goedken, V. Katovic, A.C. Melnyk, C.R. Sperati, N. Tokel, *Adv. Chem. Ser.* **1971**, 100, 44.
(b) D.K. Cabbiness, D.W. Margerum, *J. Am. Chem. Soc.* **1969**, 91, 6540-6541.
(c) J.J. Christensen, D.J. Eatough, R.M. Izatt, *Chem. Rev.* **1974**, 74, 351.
13. (a) B. Dietrich, J.-P. Sauvage, *Tetrahedron Lett.* **1969**, 2885.
(b) B. Dietrich, J.-P. Sauvage, *New J. Chem.* **1988**, 12, 725-728.
(c) J.-M. Lehn, *Angew. Chem. Ed. Engl.* **1972**, 11, 16-25.
14. (a) J.-M. Lehn, *Struct. Bond. (Berlin)* **1973**, 16, 1-69.
(b) B. Dietrich, J.-M. Lehn, J.-P. Sauvage, J.B. Lanzat, *Tetrahedron* **1973**, 29, 1629-1658.
(c) B. Dietrich, J.-M. Lehn, J.-P. Sauvage, J.B. Lanzat, *Tetrahedron* **1973**, 29, 1647-168.
15. (a) J.-M. Lehn, J.-P. Sauvage, *J. Am. Chem. Soc.* **1975**, 97, 6700-6707.
(b) C.J. Pederson, *J. Am. Chem. Soc.* **1967**, 89, 2459.
16. (a) G.W. Gokel, *"Crown Ethers and Cryptands"*, The Royal Society of Chemistry, Cambridge, **1991**.
(b) G.W. Gokel, *Chem. Soc. Rev.* **1992**, 39-47.
17. (a) D.M. Dishong, C.J. Diamond, M.I. Cinoman, G.W. Gokel, *J. Am. Chem. Soc.* **1983**, 105, 586-593.
(b) R.A. Schultz, B.D. White, D.M. Dishong, K.A. Arnold, G.W. Gokel, *J. Am. Chem. Soc.* **1985**, 107, 6659.
18. (a) R.D. Gandour, F.R. Fronczek, V.J. Gatto, C. Minganti, R.A. Schultz, B.D. White, K.A. Arnold, D. Mazzocchi, S.R. Miller, G.W. Gokel, *J. Am. Chem. Soc.* **1986**, 108, 4078.
(b) K.A. Arnold, L. Echegoyen, F.R. Fronczek, R.D. Gandour, V.J. Gatto, B.D. White, G.W. Gokel, *J. Am. Chem. Soc.* **1987**, 109, 3716.
(c) L. Echegoyen, A. Kaifer, H. Durst, R.A. Schultz, D.M. Dishong, D.M. Goli, G.W. Gokel, *J. Am. Chem. Soc.* **1984**, 106, 5100-5103.
19. (a) T. Rodopoulos, P.-A. Pittet, S.F. Lincoln, *J. Chem. Soc., Dalton Trans.* **1993**, 1055-1060.
(b) J. Lucas, S.F. Lincoln, *J. Chem. Soc., Dalton Trans.* **1994**, 423-427.
(c) J. Lucas, S.F. Lincoln, *Inorg. Chim. Acta.* **1994**, 219, 217-220.
20. (a) P. Clarke, A.M. Hounslow, R.A. Keough, S.F. Lincoln, K.P. Wainwright, *Inorg. Chem.* **1990**, 29, 1793-1797.
(b) P. Clarke, S.F. Lincoln, K.P. Wainwright, *Inorg. Chem.* **1990**, 30, 134-139.
(c) P.-A. Pittet, G.S. Laurence, S.F. Lincoln, M.L. Turonek, K.P. Wainwright, *J. Chem. Soc., Chem. Commun.* **1991**, 1205-1206.

21. (a) M.L. Turonek, P. Clarke, G.S. Laurence, S.F. Lincoln, P.-A. Pittet, S. Politis, K.P. Wainwright, *Inorg. Chem.* **1993**, 32, 2195-2198.
(b) S.L. Whitbread, S. Politis, A.K.W. Stephens, J. Lucas, R.S. Dhillon, S.F. Lincoln, K.P. Wainwright, *J. Chem. Soc., Dalton Trans.* **1996**, 1379-1384.
(c) A.K.W. Stephens, R.S. Dhillon, S.E. Madback, S.L. Whitbread, S.F. Lincoln, *Inorg. Chem.* **1996**, 35, 2019-2024.
22. R.S. Dhillon, A.K.W. Stephens, S.L. Whitbread, S.F. Lincoln, K.P. Wainwright, *J. Chem. Soc., Chem. Commun.* **1995**, 1, 97-98.
23. (a) S.L. Whitbread, J.M. Weeks, P. Valente, M.A. Buntine, S.F. Lincoln, K.P. Wainwright, *Aust. J. Chem.* **1997**, 50, 853-856.
(b) A.K.W. Stephens, S.F. Lincoln, *J. Chem. Soc., Dalton Trans.* **1993**, 2123-2126.
(c) R.S. Dhillon, S.E. Madback, F.G. Ciccone, M.A. Buntine, S.F. Lincoln, K.P. Wainwright, *J. Am. Chem. Soc.* **1997**, 119, 6126-6134.
24. (a) M. Shamsipur, A.I. Popov, *J. Phys. Chem.* **1986**, 90, 5997-5999.
(b) R.M. Izatt, K. Pawlak, J.S. Bradshaw, R.L. Bruening, *Chem. Rev.* **1991**, 91, 1721-2085.
25. (a) B.G. Cox, J. Garcia-Rosas, H. Schneider, *J. Am. Chem. Soc.* **1981**, 103, 1054-1059.
(b) S.F. Lincoln, A.K.W. Stephens, *Inorg. Chem.* **1991**, 30, 3529-3534.
(c) J.M. Ceraso, J.L. Dye, *J. Am. Chem. Soc.* **1973**, 95, 4432-4434.
26. (a) R. Gresser, D.W. Boyd, A.M. Albrecht-Gary, J.P. Schwing, *J. Am. Chem. Soc.* **1980**, 102, 651-653.
(b) B.G. Cox, D. Knop, H. Schneider, *J. Am. Chem. Soc.* **1978**, 100, 6002-6007.
(c) J.M. Ceraso, P.B. Smith, J.S. Landers, J.L. Dye, *J. Phys. Chem.* **1977**, 81, 760-766.
(d) E. Schchori, J. Jagur-Grodzinski, Z. Luz, H. Shporer, *J. Am. Chem. Soc.* **1971**, 93, 7133-7138.
27. (a) J.-M. Lehn, *Pure. Appl. Chem.* **1979**, 51, 979-997.
(b) B.G. Cox, H. Schneider, J.J. Stroka, *J. Am. Chem. Soc.* **1978**, 100, 4746-4749.
(c) B.G. Cox, J. Garcia-Rosas, H. Schneider, *J. Am. Chem. Soc.* **1981**, 103, 1384-1389.
28. (a) A. Abou-Hamdan, S.F. Lincoln, *Inorg. Chem.* **1991**, 30, 462-466.
(b) S.F. Lincoln, I.M. Brereton, T.M. Spotswood, *J. Am. Chem. Soc.* **1986**, 108, 8134-8138.
(c) Y.M. Cahen, J.L. Dye, A.I. Popov, *J. Phys. Chem.* **1975**, 79, 1292-1295.
29. B.G. Cox, N.V. Truong, H. Schneider, *J. Am. Chem. Soc.* **1984**, 106, 1273.

30. (a) S.P. Kapsprzyk, R.G. Wilkins, *Inorg. Chem.* **1982**, 21, 3349-3352.
(b) B. Scott, K.J. Brewer, L.O. Spreer, C.A. Craig, J.W. Otves, M. Calvin, S. Taylor, *J. Coord. Chem.* **1990**, 21, 307-313.
(c) R. Clay, P. Murray-Rust, J. Murray-Rust, *J. Acta. Cryst.* **1979**, B35, 1894-1895.
31. (a) Y. Iitaka, M. Shima, E. Kimura, *Inorg. Chem.* **1974**, 13, 2886-2891.
(b) N. Matsumoto, A. Hirano, T. Hara, A. Ohyoshi, *J. Chem. Soc., Dalton Trans.* **1983**, 2405.
(c) M. Kojima, K. Nakabayashi, S. Ohba, S. Okumoto, Y. Saito, J. Fujita, *Bull. Chem. Soc. Jpn.* **1986**, 59, 277-283.
32. (a) P. Groth, *Acta. Chem. Scand.* **1983**, A37, 71-77.
(b) P. Groth, *Acta. Chem. Scand.* **1983**, A37, 283-291.
33. (a) I. Murase, M. Mikuriya, H. Sonoda, S. Kida, *J. Chem. Soc., Chem. Commun.* **1984**, 692-694.
(b) I. Murase, I. Ueda, N. Marbuayashi, S. Kida, N. Matsumoto, M. Kudo, M. Toyohara, K. Hiate, M. Mikuriya, *J. Chem. Soc., Dalton Trans.* **1990**, 2763-2769.
(c) E. Asato, H. Tofthund, S. Kida, M. Mikuriya, K.S. Murray, *Inorg. Chim. Acta.* **1989**, 165, 207-214.
34. (a) G. Vuckovic, E. Asato, N. Matsumoto, S. Kida, *Inorg. Chim. Acta.* **1990**, 171, 45-52.
(b) M. Takahashi, S. Takamoto, *Bull. Chem. Soc. Jpn.* **1977**, 50, 3413-3414.
(c) H. Häfliger, T.A. Kaden, *Helv. Chim. Acta.* **1979**, 62, 683-688.
35. (a) N.W. Alcock, K.P. Balakrishnan, A. Berry, P. Moore, C.J. Reader, *J. Chem. Soc., Dalton Trans.* **1989**, 1089-1093.
(b) B.A. Sayer, J.P. Michael, R.D. Hancock, *Inorg. Chim. Acta.* **1983**, 77, 63-64.
(c) P. Clarke, A.M. Hounslow, R.A. Keough, S.F. Lincoln, K.P. Wainwright, *Inorg. Chem.* **1990**, 29, 1793-1797.
36. (a) R.D. Hancock, *J. Coord. Chem.* **1993**, 129-151.
(b) H. Stetter, W. Frank, *Angew. Chem. Ed. Engl.* **1976**, 15, 686.
(c) M.J. Van der Merwe, J.C.A. Boeyens, R.D. Hancock, *Inorg. Chem.* **1985**, 24, 1208-1213.
(d) A. Evers, R.D. Hancock, I. Murase, *Inorg. Chem.* **1986**, 25, 2160-2163.
37. (a) D.A. Buckingham, C.R. Clarke, W.S. Webley, *J. Chem. Soc., Chem. Commun.* **1981**, 192-194.
(b) J.R. Morrow, S. Amin, C.H. Lake, M.R. Churchill, *Inorg. Chem.* **1993**, 32, 4566-4572.
(c) J.F. Desreux, *Inorg. Chem.* **1980**, 19, 1319-1324.

(d) J.F. Desreux, E. Merciny, M.F. Loncin, *Inorg. Chem.* **1981**, 20, 987-991.
(e) E.K. Barefield, F. Wagner, *Inorg. Chem.* **1973**, 12, 2435-2439.
38. (a) K.P. Wainwright, Flinders University of South Australia. Unpublished material.
(b) A.K.W. Stephens, PhD Thesis, University of Adelaide, **1994**.
(c) J.B. Lucas, PhD Thesis, University of Adelaide, **1994**.
(d) S.F. Lincoln, G.S. Laurence, P.-A. Pittet, M.L. Turonek, K.P. Wainwright, *J. Chem. Soc., Chem. Commun.* **1991**, 1205.
39. (a) P. Chaudhuri, K. Weighardt, *Prog. Inorg. Chem.* **1987**, 35, 329-436.
(b) R. Luckay, R.D. Hancock, J. Cukrowski, J.H. Reibenspies, *Inorg. Chim. Acta.* **1996**, 246, 159-169.
40. B. Bosnich, C.K. Poon, M.L. Tobe, *Inorg. Chem.* **1965**, 4, 1102-1108.
41. (a) R.D. Hancock, *Pure. Appl. Chem.* **1986**, 58, 1445-1452.
(b) R.D. Hancock, A.E. Martell, *Chem. Rev.* **1989**, 89, 1875-1914.
(c) R.D. Hancock, *Perspect. Coord. Chem.* **1993**, 65, 941-946.
(d) L. Carlton, R.D. Hancock, H. Maumela, K.P. Wainwright, *J. Chem. Soc., Chem. Commun.* **1994**, 1007-1008.
42. (a) V.J. Thöm, G.D. Hosken, R.D. Hancock, *Inorg. Chem.* **1985**, 24, 2378-3381.
(b) V.J. Thöm, C.C. Fox, J.C.A. Boeyens, R.D. Hancock, *J. Am. Chem. Soc.* **1984**, 106, 5947-5955.
(c) R.D. Hancock, *Prog. Inorg. Chem.* **1989**, 37, 187-291.
(d) R.D. Hancock, M.P. Ngwenya, A.S. deSousa, K.V. Damu, *Inorg. Chem.* **1990**, 29, 1968-1974.
43. (a) *"The Present Status of Chelating Agents in Medicine"*, P.M. May, R.A. Bulman in *Prog. Medicinal Chem.* **1983**, 20, 225-317.
(b) C.M. Sarther, E.L. Blinn, *Inorg. Chem.* **1976**, 15, 3083-3087.
44. (a) J.H. Coates, D.M.M.A. Hadi, T.W. Hambley, S.F. Lincoln, J.R. Rodgers, *Cryst. Struct. Commun.* **1982**, 11, 815-821.
(b) R.L. Webb, M.L. Mino, E.L. Blinn, A.A. Pinkerton, *Inorg. Chem.* **1993**, 32, 1396-1402.
45. (a) T. Ito, M. Kato, H. Ito, *Bull. Chem. Soc. Jpn.* **1984**, 57, 2634-2640.
(b) E.K. Barefield, A. Bianchi, E.J. Billo, P.J. Connolly, P. Paoletti, J.S. Summers, D.G. Van Derveer, *Inorg. Chem.* **1986**, 25, 4197-4202.
(c) J.H. Lochlin, E.B. Fleischer, *J. Acta. Cryst.* **1976**, B32, 3063-3066.
(d) R. Smierciak, J. Passariello, E.L. Blinn, *Inorg. Chem.* **1977**, 16, 2646-2648.
46. (a) M. Di Vaira, F. Mani, P. Stoppioni, *J. Chem. Soc., Dalton Trans.* **1992**, 1127-1130.
(b) G. de Martino Norante, M. Di Vaira, F. Mani, S. Mazzi, P. Stoppioni, *Inorg. Chem.* **1990**, 29, 2822-2829.

(c) K.B. Yatsimirskii, *Russian Chem. Rev.* **1990**, 59, 1150-1156.

47. (a) K.R. Adam, B.J. McCool, A.J. Leong, L.F. Lindoy, C.W.G. Ansell, P.J.Baillie, K.P. Dancey, L.A. Drummond, K. Henrick, M. McPartlin, D.K. Uppal, P.A. Tasker, *J. Chem. Soc., Dalton Trans.* **1990**, 3435-3444.
(b) J. Guisti, S. Chimichi, M. Ciampolini, *Inorg. Chim. Acta.* **1984**, 88, 51-54.
48. (a) C.W.G. Ansell, K.P. Dancey, M. McPartlin, P.A. Tasker, L.F. Lindoy, *J. Chem. Soc., Dalton Trans.* **1983**, 1789-1791.
(b) M. Kato, T. Ito, *Inorg. Chem.* **1985**, 24, 509-514.
(c) N.W. Alcock, N. Herron, P. Moore, *J. Chem. Soc., Dalton Trans.* **1978**, 1282-1288.
49. (a) R.D. Hancock, S.M. Dobson, J.C.A. Boeyens, *Inorg. Chim. Acta.* **1987**, 133, 221-231.
(b) *"Stereochemical and Stereophysical Behaviour of Macrocycles"*, Volume 2, Ivan Bernal (Editor), **1987**.
50. (a) R.S. Glass, G.S. Wilson, W.N. Setzer, *J. Am. Chem. Soc.* **1980**, 102, 5068-5069.
(b) B.A. Sayer, J.P. Michael, R.D. Hancock, *Inorg. Chim. Acta.* **1983**, 77, L63-L64.
(c) K. Weighardt, U. Bossek, P. Chaudhuri, W. Hermann, B.C. Menke, J. Weiss, *Inorg. Chem.* **1982**, 21, 4308-4314.
51. V.J. Thöm, J.C.A. Boeyens, G.J. McDougall, R.D. Hancock, *J. Am. Chem. Soc.* **1984**, 106, 3198-3207.
52. L.Y. Martin, L.J. DeHayes, L.J. Zompa, D.H. Busch, *J. Am. Chem. Soc.* **1974**, 96, 4046-4048.
53. F.L. Weitl, K.N. Raymond, *J. Am. Chem. Soc.* **1979**, 101, 2728-2731.
54. (a) A.E. Martell, R.J. Motekaitis in *"The Environmental Chemistry and Toxicology of Aluminium"*, T.E. Lewis (Editor), Lewis Publishers, Chelsea, MI, **1989**.
(b) B.R. Green, R.D. Hancock, *J. S. Afr. Inst. Min. Metall.* **1982**, 82, 303.
55. (a) M. Studer, T.A. Kaden, H.R. Mäcke, *Helv. Chim. Acta.* **1990**, 73, 149-153.
(b) D. Parker, J.R. Morphy, K. Jankowski, J. Cox, *Pure. Appl. Chem.* **1989**, 61, 1637-1641.
56. (a) H. Adams, N.A. Bailley, D.E. Fenton, I.G. Ford, S.J. Kitchen, M.G. Williams, P.A. Tasker, A.J. Leong, L.F. Lindoy, *J. Chem. Soc., Dalton Trans.* **1991**, 1665-1674.
(b) D. Tschudin, T.A. Kaden, *Pure. Appl. Chem.* **1988**, 60, 489-493.
(c) T.A. Kaden, *Pure. Appl. Chem.* **1988**, 60, 1117-1122.
(d) M.M. Crutchfield, *J. Am. Oil. Chem. Assoc.* **1978**, 55, 58.

57. (a) V. Dudler, L.F. Lindoy, D. Sallin, C.W. Schlaepfer, *Aust. J. Chem.* **1987**, 40, 1557.
(b) J.S. Bradshaw, R.M. Izatt, J.J. Christensen, K.E. Krakowiak, B.J. Tarbet, R.L. Breuning, *J. Inclusion Phenom.* **1989**, 7, 127.
58. D.J. Cram, *J. Inclusion Phenom.* **1988**, 6, 397.
59. (a) J.-P. Joly, B. Gross, *Tetrahedron Lett.* **1989**, 30, 4231.
(b) Y. Inouye, T. Kanamori, T. Yoshida, X. Bu, M. Shinoya, T. Koike, E. E. Kimura, *Biol. Pharm. Bull.* **1994**, 17, 243-350.
60. R.M. Izatt, J.J. Christensen *"The Design of Selective Complexing Agents"* in *"Synthesis of Macrocycles"*, Wiley, New York, **1987**.
61. A.I. Popov, J.-M. Lehn in *"Coordination Chemistry of Macrocyclic Compounds"*, G.A. Melson (Editor), Plenum Press, New York, **1979**.
62. (a) K. Kodama, E. Kimura, *J. Chem. Soc., Dalton Trans.* **1980**, 327-333.
(b) M. Kato, T. Ito, *Inorg. Chem.* **1985**, 24, 504-508 and 509-514.
63. (a) E. Fujita, D.J. Szalda, C. Creutz, N. Sutin, *J. Am. Chem. Soc.* **1988**, 110, 4870-4871.
(b) D.J. Szalda, E. Fujita, T. Koike, M. Shiro, M. Kodama, *J. Am. Chem. Soc.* **1990**, 112, 5805-5811.
64. (a) M. Komiyama, K. Matsumura, Y. Matsumoto, *J. Chem. Soc., Chem. Commun.* **1992**, 640-641.
(b) R. Breslow, D.L. Huang, *Proc. Natl. Acad. Sci. USA* **1991**, 88, 4080-4083.
(c) K.O.A. Chin, J.R. Morrow, C.H. Lake, M.R. Churchill, *Inorg. Chem.* **1994**, 33, 656-664.
(d) J.R. Morrow, L.A. Buttrey, K.A. Berbeck, *Inorg. Chem.* **1992**, 31, 16-20.
(e) L.L. Chappell, D.A. Vaas Jr., W. DeW. Horrocks Jr., J.R. Morrow, *Inorg. Chem.* **1998**, 37, 3989-3998.
65. (a) C.A. Chang, V.O. Ochaya, *Inorg. Chem.* **1986**, 25, 355.
(b) C.A. Chang, PH.-L. Chang, V.K. Manchanda, S.P. Kasprzyk, *Inorg. Chem.* **1988**, 27, 3786-3789.
66. (a) K.N. Raymond, G. Mueller, B.F. Matzanke, *Topp. Curr. Chem.* **1984**, 123, 49.
(b) A.E. Martell, R.J. Motekaitis, E.T. Clarke, Y. Sun, *Drugs Today* **1992**, 28, 11.
67. (a) R. Ramasamay, I. Lazar, E. Brucher, A.D. Sherry, C.R. Malley, *FEBS Lett.* **1991**, 280, 121-124.
(b) I. Lazar, R. Ramasamay, E. Brucher, C.F.G.C. Geraldes, A.D. Sherry, *Inorg. Chim. Acta.* **1992**, 195, 89-93.
(c) J. Van Haveren, L. De Leon, R. Ramasamay, J. Van Westrenen, A.D. Sherry, *NMR Biomed.* **1995**, 8, 197-205.
(d) J. Huskens, A.D. Sherry, *J. Am. Chem. Soc.* **1996**, 118, 4396-4404.

68. (a) H. Rasmussen, P.Q. Barrett, *Physiol. Rev.* **1984**, 64, 938-984.
(b) R. Grubbs, M.E. Maguire, *Magnesium* **1987**, 6, 113-127.
69. (a) J. Huskens, A.D. Sherry, *J. Chem. Soc., Chem. Commun.* **1997**, 845-984.
(b) R. Ma, M.J. Welch, J. Reibenspies, A.E. Martell, *Inorg. Chim. Acta.* **1995**, 236, 75-82.
(c) D.A. Moore, P.E. Fanwick, M.J. Welch, *Inorg. Chim. Acta.* **1990**, 19, 672.
70. (a) J.R. Morphy, D. Parker, R. Alexander, A. Bains, A.F. Carne, M.A.W. Eaton, A. Harrison, A. Millican, A. Phipps, S.K.Rhind, R. Titmans, D. Weatherby, *J. Chem. Soc., Chem. Commun.* **1988**, 156.
(b) A.S. Craig, I.M. Helps, K.J. Jankowski, D. Parker, N.R.A. Beeley, B.A. Boyce, M.A.W. Eaton, A.T. Millican, K. Millar, A. Phipps, S.K. Rhind, A. Harrison, C. Walker, *J. Chem. Soc., Chem. Commun.* **1989**, 794.
71. R.D. Hancock, B.S. Nakani, F. Marsicano, *Inorg. Chem.* **1983**, 22, 2531.
72. (a) R.J.P. Williams, *Endeavour, New Series* **1984**, 8, 65-70.
(b) I. Bertini, C. Luchinat, W. Maret, M. Zeppezauer, *"Zinc Enzymes"*, Birkhäuser, Boston MA, **1986**.
73. (a) J. Szalda, E. Fujita, C. Creutz, *Inorg. Chem.* **1989**, 28, 1446-1450.
(b) E. Fujita, D.J. Szalda, C. Creutz, N. Sutin, *J. Am. Chem. Soc.* **1988**, 110, 4870-4871.
(c) E. Kimura, T. Shiota, T. Koike, M. Shiro, M. Kodama, *J. Am. Chem. Soc.* **1990**, 112, 5805-5811.
74. R. Montgomery, R.L. Dryer, T.W. Conway, A.A. Spector, *"Biochemistry"*, **1977**, Second Edition, The CV Mosby Company.

CHAPTER 2

EQUILIBRIUM STUDIES OF MONOVALENT METAL ION COMPLEXES WITH (*R*)-THPEC12

2.1 INTRODUCTION

In non-aqueous solution, an equilibrium exists between the solvated monovalent metal ion, M^+, the macrocyclic ligand, L, and the alkali metal ion complex, $[ML]^+$. This is described by Equation 2.1:

$$M^+ + L \underset{}{\overset{K_S}{\rightleftharpoons}} [ML]^+ \qquad 2.1$$

where the stability constant, K_S, is defined by:

$$K_s = \frac{[ML^+]}{[M^+][L]} \qquad 2.2$$

In general, K_S is only an average stability constant for the system at thermodynamic equilibrium with respect to conformation and complexation, because the solvated ligand may not necessarily have the same conformation as the complexed ligand. For example, ^{13}C NMR solution studies indicate that free (*R*)-THPEC12 and $[Na((R)\text{-THPEC12})]^+$ adopt the Δ diastereomer, whereas $\Lambda[M((R)\text{-THPEC12})]^+$ dominates for $M^+ = K^+$, Rb^+ and Cs^+.[1] Similarly, calculated structures, modelled using the *ab initio* molecular orbital program Gaussian 94, indicate that although (*S*)-THPEC12 exists as the Λ diastereomer when uncomplexed, it adopts the Δ form in several of its alkali metal complexes.[1,2] In addition, the X-ray crystal structures for several of the divalent transition metal ion complexes of CYCLEN show that complexed and uncomplexed CYCLEN adopt different conformations.[3-8] On the other hand, although THEC12 and THEC9 may adopt several conformations, the X-ray crystal structures[9,10] of $[M(THEC12)]^+$ and the calculated structures[11] of $[M(THEC9)]^+$ indicate that THEC12 and THEC9 adopt the TRANS I and + + + conformation, respectively, when both complexed and uncomplexed.

Until recently, much of the focus on macrocyclic ligand complexes with alkali metal ions has been either for cryptand and coronand ligands in solution or pendant arm macrocyclic ligands in the solid state.[12,13] Since rigid cryptands form metal complexes, or cryptates, which have higher stabilities and

selectivities than their linear chain analogues (reflected by the macrobicyclic and cryptate effects), [14,15] studies have been extended to include the more flexible tetraaza macrocyclic ligands, such as THEC12, to examine their complex stabilities and selectivities. The metal ion complexation characteristics and selectivity patterns[12,16] exhibited by THEC12 has prompted investigation of the related ligands TMEC12, (*S*)-THPC12, and now (*R*)-THPEC12.

While the alkali metal cryptate stabilities are primarily governed by the "size-match" compatibility of the metal ion size to the predetermined size of the ligand cavity,[17,18] studies of pendant arm macrocyclic ligands have shown that this is not necessarily the dominating factor for complexes of these more flexible ligands.[19-22] In general, pendant arm macrocyclic ligands do not have as rigid or preformed a cavity as those of cryptands or exist as a single preferred conformer, but adopt an encapsulating conformation around the metal ion. These ligands have the ability to form a cavity of appropriate size when complexing a metal ion, with the metal ion often coordinated out of the plane of the nitrogen donor atoms. As for the open-chain ligands, it is mainly the size of the chelate ring, not the macrocyclic ring, which determines their complex stability with metal ions of different sizes.[23-30] A 5-membered chelate ring gives minimum strain energy and increased stability for coordination of larger metal ions, which can adopt high coordination numbers, relative to the stabilisation of smaller metal ions by a 6-membered chelate ring.[19,22,25-30] Hence, the attachment of $-CH_2CH_2O-$ type of pendant arms to a tetraaza macrocycle generally enhances the selectivity of the ligand for a larger metal ion (with an ionic radius of ~ 1.0 Å) because of their ability to form 5-membered chelate rings in the complex. Pendant arm macrocyclic ligands generally retain the metal ion selectivity of their parent macrocycles, and the attachment of pendant arms increases both the denticity of the ligand and often the extent of steric crowding in the complex, which is particularly evident for bulky substituents on the pendant arms. Nonetheless, many of the factors determining the stability of alkali metal cryptates also apply to tetraaza macrocyclic complexes.[31-39] These include the ionic radius of the metal ion, the solvation energy of the metal ion and possibly of the ligand, the nature of the solvent, and the topology and steric constraints of the ligand.

The summation of all these effects are examined in this study of the complexation of 1,4,7,10-tetrakis((*R*)-2-hydroxy-2-phenylethyl)-1,4,7,10-tetra-azacyclododecane, abbreviated as (*R*)-THPEC12 (Figure 2.1), with alkali, Ag^+, alkaline earth and Zn^{2+} ions in a range of solvents. The alkali metal ions are of particular interest because while the existence of enantiomeric complexes involving less labile metal ions is well established,[40] both their identification and kinetic characterisation with alkali metal ions needs to be explored further.

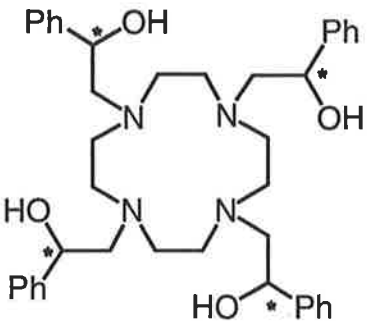

(*R*)-THPEC12

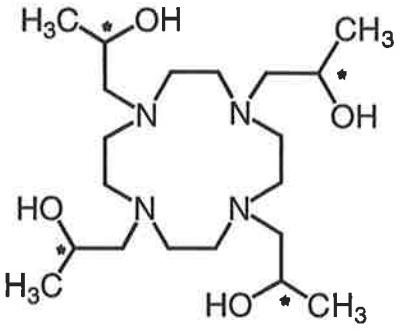

(*S*)-THPC12

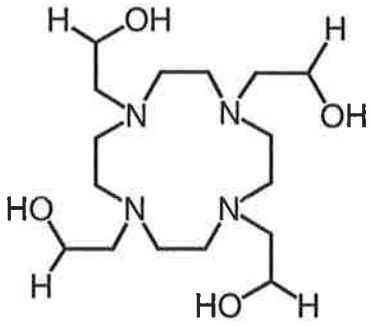

THEC12

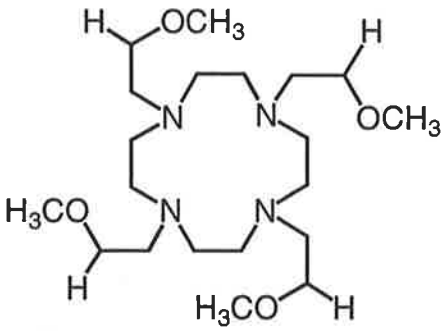

TMEC12

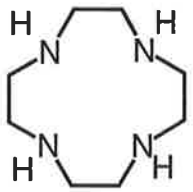

CYCLEN

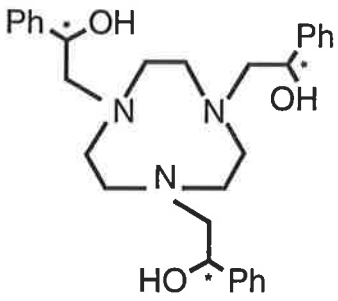

(*R*)-THPEC9

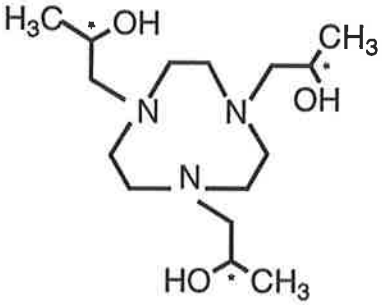

(*S*)-THPC9

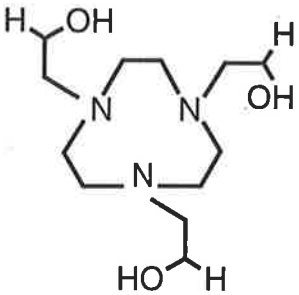

THEC9

Figure 2.1: The tetraaza and triaza macrocyclic ligands examined in this study.

The unexpected homochirality exhibited by (*S*)-THPC12 and its alkali metal complexes[41-44] has led to the study of (*R*)-THPEC12 to examine more fully the effect of chiral pendant arms on the overall chirality of this macrocyclic ligand and its metal ion complexes. The selectivity patterns for (*R*)-THPEC12 are compared with those for the related ligands (*S*)-THPC12, THEC12, TMEC12, the smaller THEC9 and the parent macrocycle CYCLEN (Figure 2.1). The factors determining the stabilities and selectivities of the alkaline earth metal ion complexes (Chapter 3) are then collated and contrasted with these results.

2.2 STABILITY OF $[M((R)\text{-THPEC12})]^+$

The stability constants for the alkali metal ion complexes of (*R*)-THPEC12, denoted $[M((R)\text{-THPEC12})]^+$, have been determined in DMF (*N,N*-dimethyl-formamide) and are shown in Table 2.1. (*R*)-THPEC12 is Na^+ selective, and the order of stability for $[M((R)\text{-THPEC12})]^+$ is $Li^+ < Na^+ > K^+ > Rb^+ > Cs^+$. This occurrence is discussed below.

No crystals suitable for solid state structure determination by X-ray diffraction of $[M((R)\text{-THPEC12})]^+$ have yet been obtained. The macrocyclic hole radius in (*R*)-THPEC12 is estimated as ~ 1.27 Å from literature data,[45] which should be sufficient to bind Li^+, Na^+, and possibly K^+ with some strain (with 8-coordinate radii of 0.92 Å, 1.18 Å and 1.51 Å, respectively).[46] The solid state structures of $[M(THEC12)]^+$, for $M^+ = Li^+$, Na^+ and K^+, have, however, been determined.[9,10] In these structures, the metal ion is coordinated by all four ring nitrogens and sits slightly above their common plane, with THEC12 in a TRANS I conformation (Figure 2.2). The metal ions Li^+, Na^+ and K^+ are coordinated within the cavity formed by these four ring nitrogens and one, three, and four hydroxy groups, respectively, of the pendant arms. If a similar situation prevailed for $[M((R)\text{-THPEC12})]^+$, then the different coordination number of the metal ion in the complex may account for the observed trend in stability constants. However, ^{13}C NMR studies (Chapter 5) demonstrate that the metal ion in $[M(THEC12)]^+$ and $[M((R)\text{-THPEC12})]^+$ is 8-coordinate in solution. These results are further corroborated by the approximately cubic global energy minimised Λ(*S*)-THPEC12 and alkali metal ion complex structures[1] calculated using Gaussian 94.[2] Therefore, the different coordination geometry of the metal ion is not a factor that can explain the metal ion selectivity of (*R*)-THPEC12.

Chiral (*R*)-THPEC12, in principle, can form Δ or Λ diastereomers in the free ligand form or in its metal ion complexes. The convention used in this study assigns the phenyl groups (of the (*R*)-2-hydroxy-2-phenylethyl pendant

Figure 2.2: The TRANS I conformer of the 1,4,7,10-tetraazacyclododecane ring. The pendant arms, denoted R, are shown uncoordinated.

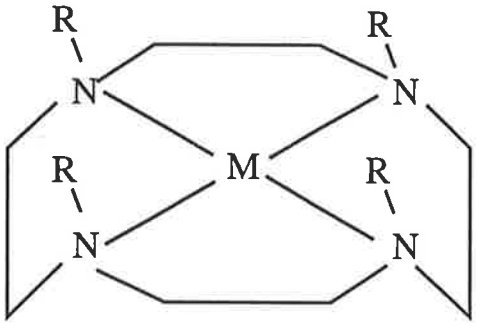

TRANS I

Table 2.1: Stability constants for the complexation of monovalent metal ions by (*R*)-THPEC12 and other ligands in DMF, at 298.2 K and I = 0.05 mol dm^{-3} NEt_4ClO_4 supporting electrolyte.

	log (K_s/dm^3 mol^{-1})					
Ligand	Li^+	Na^+	K^+	Rb^+	Cs^+	Ag^+
(*R*)-THPEC12[a]	3.13	4.25	4.10	3.57	3.47	8.14
(*S*)-THPC12[b]	3.24	3.76	3.63	3.56	3.41	11.3
THEC12[c]	2.99	3.37	1.59	1.39	1.23	11.16
TMEC12[d]	3.61	5.68	3.62	2.73	2.28	13.73
CYCLEN[b]	2.10	< 2	< 2	< 2	< 2	9.10

[a]This work. Errors of ± 0.05 and ± 0.03 apply to the alkali metal and Ag^+ complex ions, respectively, and represent 1 standard deviation. [b]Reference 42. [c]Reference 16. [d]Reference 53.

arms) in respective equatorial or axial positions (Figure 5.7) and the pendant arms in a clockwise or anticlockwise orientation, respectively, when viewed down the C_4 axis from the plane of the four oxygens, so that the phenyl groups point outwards from the coordinated structure. The square plane delineated by the four oxygens of (*R*)-THPEC12 above M^+, and parallel to the square plane delineated by the four nitrogens below M^+, is rotated about the C_4 axis of the complex to give a distorted square antiprismatic first coordination sphere. As shown in Table 2.2 and Figures 2.3 and 2.4, the hydroxy protons point towards the adjacent hydroxy oxygens at distances where weak hydrogen bonding can occur.[47] In NMR solution studies (Chapter 5), only the sterically less crowded Δ(*R*)-THPEC12 diastereomer is present in detectable concentrations in solution in the Na^+ complex, but Λ[M((*R*)-THPEC12)]$^+$ predominates for $M^+ = K^+$, Rb^+ and Cs^+. Conversely, the molecular orbital calculations refer to Δ[M((*S*)-THPEC12)]$^+$, for $M^+ = K^+$, Rb^+ and Cs^+, Λ[Na((*S*)-THPEC12)]$^+$ and Λ(*S*)-THPEC12.[1]

Molecular orbital calculations demonstrate that when (*S*)-THPEC12 assumes a TRANS I conformation, it is able to form a three-dimensional cavity around the metal ion on complexation. The cavity is defined by the four nitrogens of the macrocyclic ring and the four oxygens of the (*S*)-2-hydroxy-2-phenylethyl pendant arms. Apart from Li^+, the alkali metal ions are positioned in the centre of this ligand cavity. On complexation, the metal ion is coordinated to both the nitrogen and oxygen donor atoms. Due to the hard acid nature of the alkali metal ions, they have a higher affinity for the oxygen donor atoms than for the nitrogen donor atoms.[48-51]

The computed structures of Λ[Na((*S*)-THPEC12)]$^+$ and Λ(*S*)-THPEC12 show that they have similar dimensions (Table 2.2, and Figures 2.3 and 2.4), in which Λ[Na((*S*)-THPEC12)]$^+$ retains the C_4 symmetry and chiral characteristics of Λ(*S*)-THPEC12. This suggests that Na^+ is probably of optimum size for the Λ(*S*)-THPEC12 cavity or more appropriately, establishes optimum bonding distances and induces minimum steric strain in Λ[Na((*S*)-THPEC12)]$^+$ compared with the other alkali metal ion complexes of (*S*)-THPEC12 in DMF.

From Na^+ to Cs^+, charge density systematically decreases and metal ion size increases. Therefore, along this progression, the metal ions form weaker interactions with the hard base oxygen donor atoms of the pendant arms, and significant conformational strain may be induced in their complexes with (*S*)-THPEC12. Molecular orbital calculations show that as the alkali metal ion size increases from Na^+ to Cs^+, the O-O, N-N and O-N distances all increase, the M-O plane distances decrease, and the M-N plane distances increase

Table 2.2: Parameters derived from molecular orbital calculations[1] for L = (*S*)-THPEC12 and $[ML]^+$ = alkali metal ion complexes of (*S*)-THPEC12 using the Gaussian 94 LanL2DZ basis set.[a]

Distance (pm)	L	$[ML]^+$				
		$M^+ = Li^+$	Na^+	K^+	Rb^+	Cs^+
O-O distance	272	O1-O2 = 267 O2-O3 = 262 O3-O4 = 268 O4-O1 = 269	276	370	408	446
N-N distance	317	N1-N2 = 301 N2-N3 = 302 N3-N4 = 302 N4-N1 = 304	311	321	325	328
O-N distance	292	O1-N1 = 296 O2-N2 = 281 O3-N3 = 296 O4-N4 = 290	292	302	306	310
M-O distance	-	Li-O1 = 288 Li-O2 = 239 Li-O3 = 292 Li-O4 = 277	254	282	299	318
M-N distance	-	Li-N1 = 232 Li-N2 = 227 Li-N3 = 232 Li-N4 = 236	254	294	314	338
M-O plane distance	-	-[b]	163	106	79	48
M-N plane distance	-	-[c]	128	188	215	245
H-O distance[d]	97	97	96	95	95	95
H-O distance[e]	176	H1-O4 = 176 H2-O1 = 172 H3-O2 = 178 H4-O3 = 179	193[f]	395[f]	439[f]	483[f]
Twist angle ϕ (°)[g]	-2.5	-[h]	-2.5	14.5	13.5	12.0
Angle between phenyl and O planes (°)[i]	36.1	-[j]	33.9	23.4	18.6	13.5

[a]Reference 2. The globalised minimum energies for (*S*)-THPEC12 and its Li^+, Na^+, K^+, Rb^+ and Cs^+ complex ions are –2061.6107, -2069.0531, -2061.7770, -2089.4281, and -2081.1503 H, respectively, where 1 H = 2617.13 kJ mol^{-1}. [b]The oxygen atoms have no common plane. [c]The nitrogen atoms have no common plane. [d]Distance between H and O in hydroxy groups. [e]Distance between the H and O of adjacent hydroxy groups. [f]No hydrogen bonding. [g]Twist angle ϕ = 0° for a cubic structure. [h]No meaningful ϕ as C_4 symmetry is absent. [i]An angle of 0° exists when the phenyl and the oxygen planes are parallel. [j]No meaningful angle as C_4 symmetry is absent.

Figure 2.3: View approximately down the C_4 axes of the global energy minimised structures[1] of Λ(*S*)-THPEC12 (A), Λ[Na((*S*)-THPEC12)]$^+$ (B), Δ[K((*S*)-THPEC12)]$^+$ (C), and Δ[Cs((*S*)-THPEC12)]$^+$ (D) determined through Gaussian 94 using the LanL2DZ basis set.[2] In A and B, the oxygens mask the nitrogens. Hydrogen bonds are shown as broken lines in A, but these bonds are not shown in B, C or D.

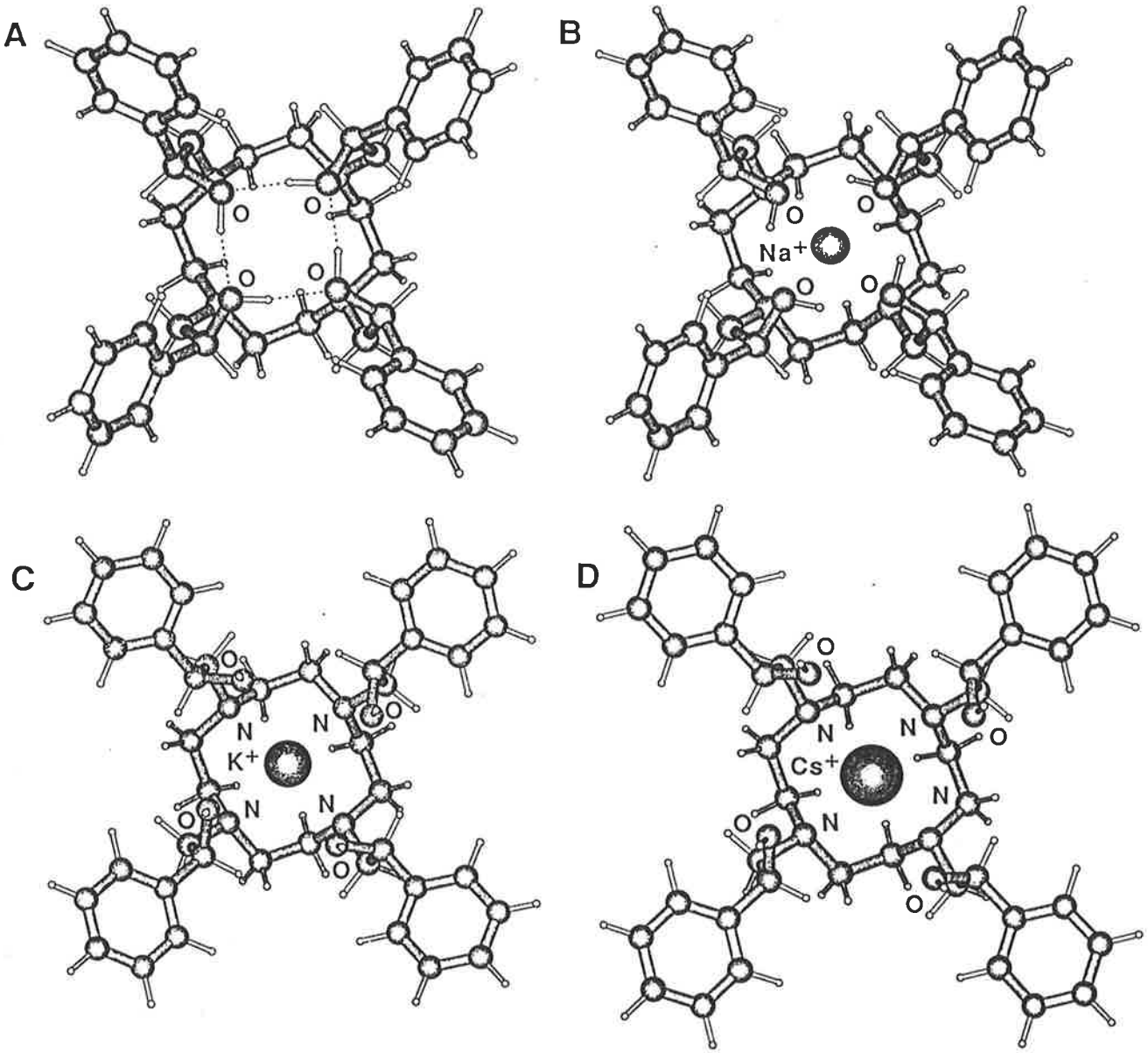

Figure 2.4: Side views of the global energy minimised structures[1] of Λ(*S*)-THPEC12 (A), Λ[Na((*S*)-THPEC12)]$^+$ (B), Δ[K((*S*)-THPEC12)]$^+$ (C), and Δ[Cs((*S*)-THPEC12)]$^+$ (D) determined through Gaussian 94 using the LanL2DZ basis set.[2] In all four structures, other atoms mask either the nitrogens or oxygens or both. Hydrogen bonds are shown as broken lines in A, but these bonds are not shown in B, C or D.

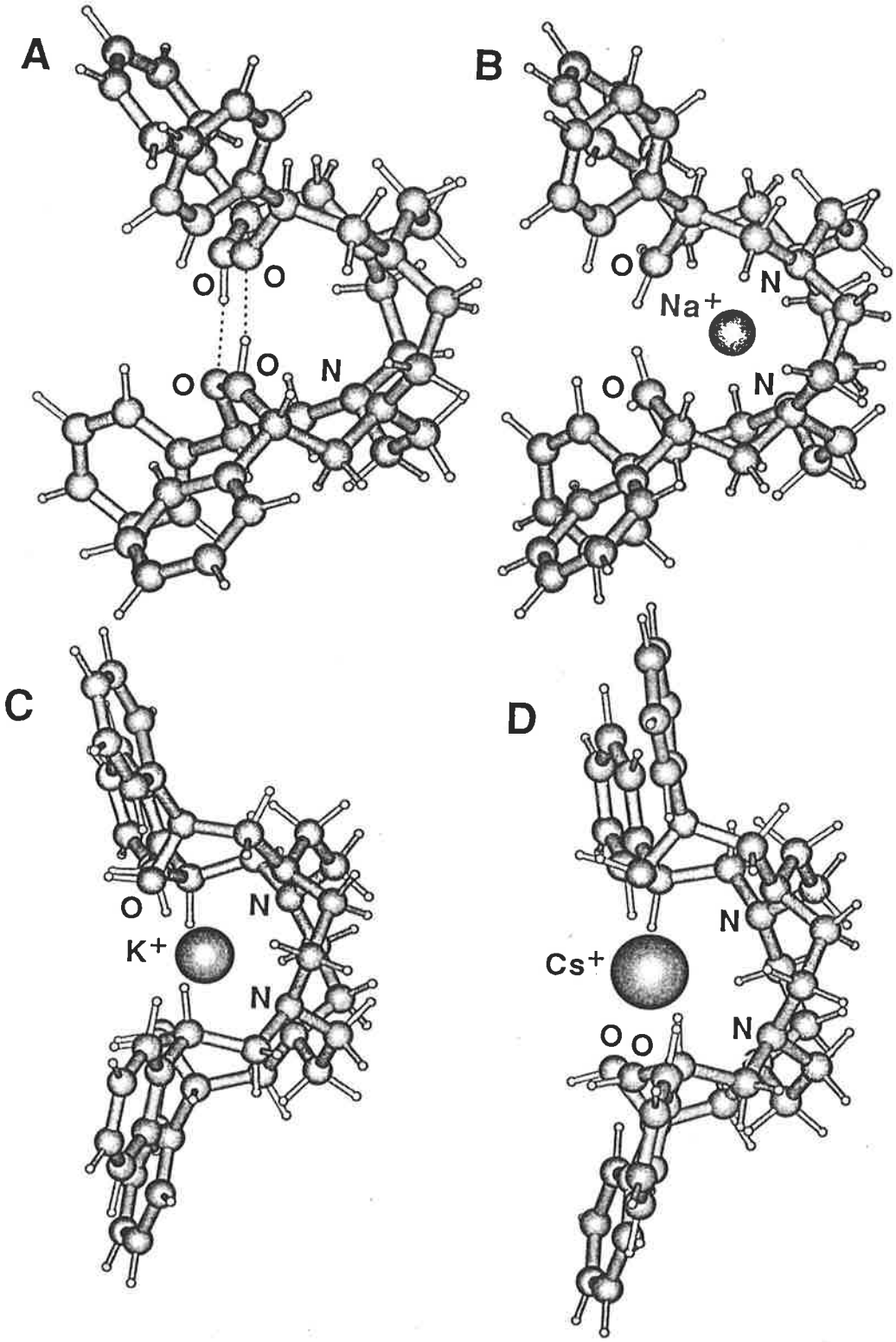

(Table 2.2, and Figures 2.3 and 2.4). That is, the "basket-like" structure of (*S*)-THPEC12, defined by its four phenyl groups, opens out and becomes more shallow, and the four oxygens move further apart, indicating that the larger metal ions are less well accommodated by the (*S*)-THPEC12 cavity. This is evident by the decreasing angle between the plane of the phenyl rings and the oxygen plane as the metal ion size increases. As a consequence, the computed structures of Δ[M((*S*)-THPEC12)]$^+$, for $M^+ = K^+$, Rb^+ and Cs^+, show no hydrogen bonding between adjacent hydroxy groups. These computed structure variations coincide with a decrease in the stability of [M((*R*)-THPEC12)]$^+$ as M^+ changes from Na^+ to Cs^+.

The Li^+ ion is the hardest of the alkali metal ions, and should have the strongest electrostatic interactions with the hard base oxygen atoms of (*S*)-THPEC12, but it is also the most highly solvated alkali metal ion. Molecular orbital calculations show that all the [M((*S*)-THPEC12)]$^+$ complexes have a C_4 symmetry, except for $M^+ = Li^+$ (Table 2.2). Although Li^+ is 8-coordinate in the calculated structure of [Li((*S*)-THPEC12)]$^+$, the variation in the computed Li–O and Li–N distances is consistent with Li^+ being too small to give an optimum fit into the (*S*)-THPEC12 cavity and inducing steric hindrance between the coordinating pendant arms in their effort to form Li–O bonds. So, Li^+ may not bond as effectively as the larger alkali metal ions with the donor atoms of the ligand, resulting in [Li((*R*)-THPEC12)]$^+$ being less stable than [Na((*R*)-THPEC12)]$^+$. The significantly different Li–O distances in [Li((*S*)-THPEC12)]$^+$, with one small distance and three larger ones, indicates the complex approaches a 5-coordinate structure similar to that found for the X-ray crystal structure of [Li(THEC12)]$^+$.[9b] In the X-ray crystal structure of [Li(THEC12)]$^+$, the three uncoordinated hydroxy groups form intermolecular hydrogen bonds, whereas in the calculated structure of [Li((*S*)-THPEC12)]$^+$ intramolecular hydrogen bonding occurs.

2.3 EFFECT OF PENDANT ARMS

2.3.1 COMPARISON OF (*R*)-THPEC12 WITH (*S*)-THPC12 AND THEC12

The alkali metal complexes of (*R*)-THPEC12, (*S*)-THPC12 and THEC12 in DMF show similar stability patterns, and are all Na^+ selective (as shown in Table 2.1). The selectivity of these three ligands for Na^+ over Li^+ in DMF may be due to their ability to give optimum bonding to Na^+ over Li^+, as supported by the molecular orbital studies for [M((*S*)-THPEC12)]$^+$ (Section 2.2) and [M((*S*)-THPC12)]$^+$.[42] These three ligands are all derived from the same parent

macrocycle, CYCLEN, and differ only by the substituent on the hydroxy pendant arms (Figure 2.1), with a $-CH_2CH_2OH$ moiety for THEC12, a $-CH_2CH(CH_3)OH$ moiety for (*S*)-THPC12, and a $-CH_2CH$(phenyl)OH moiety for (*R*)-THPEC12. It is likely that their similar stability patterns in DMF are due to the similar size and arrangement of donor atoms in these three ligands.

The ^{13}C NMR spectroscopic studies indicate that M^+ is 8-coordinate in $[M(THEC12)]^+$ (Chapter 5), $[M((S)\text{-}THPC12)]^+$,[41-44] and $[M((R)\text{-}THPEC12)]^+$ (Chapter 5), with the ligand in the TRANS I conformation. The stabilities of $[M(THEC12)]^+$, for $M^+ = K^+$, Rb^+ and Cs^+, were not sufficiently high enough to ensure that the concentrations of M^+, THEC12 and $[M(THEC12)]^+$ in the solutions used in the NMR studies were those arising from the stoichiometric complexation of M^+ by THEC12. However, it is likely that K^+, Rb^+ and Cs^+ are also 8-coordinate in their complexes with THEC12. Hence, the metal complex stabilities cannot be explained in terms of the different coordination geometry of the metal ion.

The alkali metal complex stabilities in DMF decrease in the order $[M((R)\text{-}THPEC12)]^+ > [M((S)\text{-}THPC12)]^+ > [M(THEC12)]^+$ (Table 2.1). As these ligands only differ by the substituent on the pendant arm, the ligand binding energy may be divided into the three following areas: (i) intramolecular and intermolecular hydrogen bonding ability of the ligand; (ii) steric hindrance between the coordinating pendant arms on complexation; and (iii) effect of the substituent groups in enhancing or hindering complexation.

The ligands (*R*)-THPEC12, (*S*)-THPC12, and THEC12 are all capable of forming both intramolecular and intermolecular hydrogen bonds.[1,42,52] Intramolecular hydrogen bonding takes place between the hydroxy groups on the pendant arms of the ligand, and intermolecular hydrogen bonding occurs between the hydroxy groups and the solvent, DMF. Intramolecular hydrogen bonding favours a tighter structure, and suppresses segmental motions in the pendant arms. Intermolecular hydrogen bonding, as well as decreasing the intramolecular component, has the effect of decreasing the availability of the ligand for metal-ligand coordination. This results in lower metal complex stabilities, as these interactions must be disrupted for complexation to occur.

On progression from hydroxyethyl to (*S*)-2-hydroxypropyl to (*R*)-2-hydroxy-2-phenylethyl pendant arms, the substituent size on the –CH(R)OH centre increases significantly, from R = –H to $-CH_3$ to a –phenyl group. This may result in considerable steric hindrance between these groups on complexation. Consequently, as the substituent size increases, the metal ion may be coordinated further out of the plane of the tetraaza ring and closer to

the coordinating oxygens. The steric hindrance effect lowers the overall stabilities on progression from THEC12 through to (*R*)-THPEC12. In addition, the increasing size of the substituent gives the ligand less stereochemical flexibility, which may result in its greater selectivity for metal ions. However, from Table 2.1 it is evident that the selectivity of (*R*)-THPEC12 and (*S*)-THPC12 for Na^+ over the larger metal ions K^+, Rb^+ and Cs^+ is not that substantial. Hence, the effect of substituent size on ligand flexibility may not be a dominating factor of metal complex stability.

The third factor that may account for the different stabilities of the three ligands is the electron donating ability of the pendant arms on the ligand. On progression from THEC12 to (*S*)-THPC12 to (*R*)-THPEC12, the electron donating ability of the substituent increases dramatically, where hydrogen has no such ability and methyl is weak by comparison with phenyl. This electron pair donating ability (or Lewis basicity) has the effect of helping to stabilise the complex, and enhancing complex stability.

Since the stability order is $[M((R)\text{-THPEC12})]^+ > [M((S)\text{-THPC12})]^+ > [M(THEC12)]^+$ as M^+ changes from Na^+ to Cs^+ in DMF, the effects of the substituent in stabilising the complex and inferring less stereochemical flexibility to the ligand outweigh the steric effect of the increasing substituent size on the pendant arm. The hydrogen bonding ability is probably a less dominant factor in determining the stability patterns for these ligands because all three ligands are capable of forming both intramolecular and intermolecular hydrogen bonds.

Since Li^+ is the smallest alkali metal ion, steric hindrance in the ligand is expected to play a larger role for complexes of this metal ion. This results in $[Li((R)\text{-THPEC12})]^+$ being marginally less stable than $[Li((S)\text{-THPC12})]^+$ but more stable than $[Li(THEC12)]^+$.

2.3.2 COMPARISON OF (*R*)-THPEC12 WITH TMEC12

The $[M(TMEC12)]^+$ complexes in DMF show the same stability sequence $Li^+ < Na^+ > K^+ > Rb^+ > Cs^+$ (Table 2.1) as $[M((R)\text{-THPEC12})]^+$, and $[Na(TMEC12)]^+$ is the most stable complex of those discussed here. The ^{13}C NMR spectroscopic studies have shown that in $[M(TMEC12)]^+$, for $M^+ = Li^+$, Na^+ and K^+, the ligand adopts the TRANS I conformation and the metal ion is 8-coordinate.[53] (It is likely that Rb^+ and Cs^+ are also 8-coordinate in their complexes with TMEC12, although their low stabilities precluded NMR

studies). Hence, coordination changes are unlikely to contribute to the variations in stability.

The relative stabilities of the TMEC12 complexes result from the balance between the following effects: (i) steric effect of the methyl group on the pendant arms of TMEC12; (ii) inductive effect of the methyl group; (iii) hydrogen bonding capacity of the ligand; and (iv) nature and solvation energy of the metal ion in the complex. By comparison with (*R*)-THPEC12, TMEC12 (Figure 2.1) has a bulky methyl group on the coordinating oxygen of the pendant arm. This methyl group may cause steric crowding in the $[M(TMEC12)]^+$ complexes, thus lowering the coordinating ability of TMEC12 and the complex stability by comparison with $[M((R)\text{-}THPEC12)]^+$, particularly because of the presence of these groups on the four pendant arms of a relatively small 12-membered ring. On the other hand, the presence of this methyl group makes the methoxy moiety a stronger electron pair donor (or Lewis base) than the hydroxy group,[29] which should help stabilise $[M(TMEC12)]^+$. TMEC12 cannot take part in either intramolecular or intermolecular hydrogen bonding, making it more available than (*R*)-THPEC12 for complexation.

Since the Li^+ and Na^+ complexes of TMEC12 are more stable than those of THEC12, (*S*)-THPC12, or (*R*)-THPEC12, it is likely that the steric crowding effect in TMEC12 is counterbalanced by both the better electron pair donating ability of the methoxy group compared with the hydroxy group, and the lack of hydrogen bonding available to TMEC12. As for the complexes discussed in Section 2.3.1, it is likely that $[Li(TMEC12)]^+$ is less stable than $[Na(TMEC12)]^+$ because the smaller Li^+ ion induces more steric strain in the coordinating pendant arms of TMEC12 and has the highest solvation energy of the alkali metal ions.

The stabilities of $[M(TMEC12)]^+$ follow the same sequence of $K^+ > Rb^+ > Cs^+$ as for the other ligands discussed here, because of the systematic decreasing charge density of the metal ion and increasing induced strain in the complex. $[M(TMEC12)]^+$ complexes are more stable than $[M(THEC12)]^+$, as expected because of the methyl inductive effect, but are less stable than those of (*S*)-THPC12 and (*R*)-THPEC12. This may be because TMEC12 has less stereochemical flexibility and is therefore more selective than the latter two ligands, as reflected by TMEC12 having the highest Na^+ selectivity in DMF. In addition, steric hindrance between coordinating pendant arms is probably greater in $[M(TMEC12)]^+$ than in $[M((S)\text{-}THPC12)]^+$ or $[M((R)\text{-}THPEC12)]^+$ as a result of the bulky methyl group on the coordinating oxygen of the pendant arms of TMEC12.

2.3.3 COMPARISON OF (*R*)-THPEC12 WITH CYCLEN

The K_S values for $[M(CYCLEN)]^+$ in DMF are shown in Table 2.1. CYCLEN (Figure 2.1) is a 12-membered macrocycle with only ring nitrogen donor atoms, and no pendant arms. Therefore, it has only four donor atoms to stabilise the metal complex, and can only form a two-dimensional cavity via these nitrogens to bind the metal ion. The lowest strain energy form for the $[M(CYCLEN)]^+$ complexes is the TRANS I isomer.[23] (*R*)-THPEC12 is able to form a three-dimensional cavity around the metal ion by binding the metal ion to the ring nitrogens and oxygen donor atoms of the pendant arms. In addition, alkali metal ions have a stronger affinity for the hard base oxygen donor atoms than for softer nitrogen donor atoms, and the tertiary amine (*R*)-THPEC12 is a stronger donor than the secondary amine CYCLEN.[19,29] These factors all account for the much lower stabilities of $[M(CYCLEN)]^+$ by comparison with $[M((R)\text{-THEPC12})]^+$ in DMF. A similar trend holds for $[M(THEC12)]^+$, $[M((S)\text{-THPC12})]^+$, and $[M(TMEC12)]^+$, as shown in Table 2.1.

In DMF, CYCLEN is Li^+ selective, whereas (*R*)-THPEC12 and the other pendant arm macrocyclic ligands listed in Table 2.1 are Na^+ selective. This may be attributed to the ability of the coordinating pendant arms of (*R*)-THPEC12 (and the other pendant arm macrocyclic ligands listed in Table 2.1) to enhance stability as well as Na^+ selectivity. It is important to note, however, that the choice of solvent is also a crucial factor in determining whether a ligand is Li^+ or Na^+ selective, and this aspect is discussed below.

2.4 EFFECT OF SOLVENT

Another factor influencing the formation and stability of metal ion macrocyclic complexes, apart from those mentioned in the previous sections, is the effect of solvent. The properties of the solvent, such as dipole moment, donor ability and potential hydrogen bonding capacity, affect each $[ML]^+$ complexation differently. These effects for a range of pendant arm macrocyclic ligand complexes are examined below.

Due to the highly insoluble nature of (*R*)-THPEC12 and its complex ions in most common solvents, the stability constants of $[M((R)\text{-THPEC12})]^+$ were only determined in DMF. However, alkali metal ion complexes of THEC12, (*S*)-THPC12, TMEC12 and CYCLEN were soluble in a range of solvents, and their stabilities are shown in Table 2.3. For L = THEC12, (*S*)-THPC12 and TMEC12, $[LiL]^+$ is more stable than $[NaL]^+$ in MeCN (acetonitrile), whereas in both MeOH (methanol) and DMF there is a shift in selectivity from Li^+ to

Na^+. In PC (1,2-propanediol cyclic carbonate), only TMEC12 is Na^+ selective. This shows that the complex stabilities and selectivities cannot be rationalised by the preference of a ligand for a metal ion of particular size alone.

As the solvent changes from MeCN to MeOH, DMF and H_2O, the shift in selectivity from Li^+ to Na^+ is due to the balance between the following factors: (i) electron donating ability of the solvent (and solvation energy of the metal ion); (ii) coordinating power of the ligand donor groups; and (iii) ability of the ligand to assume a conformation which optimises bonding with the metal ion.

Complexation involves the substitution of several solvent molecules from the inner coordination sphere of the metal ion. Thus, in solution, complexation of a metal ion by a macrocyclic ligand involves competition between the ligand and the solvent for coordination of the metal ion. The Gutmann donor number, D_N,[54,55] is proportional to the electron donating strength of a solvent, and is used as a measure of the cation solvation energy. The D_N's for the solvents studied here are shown in Table 2.3. The nitrogen donor solvent MeCN has a relatively low D_N of 14.1 by comparison with those of the other solvents studied, and so competes less with the ligand for metal ion coordination. PC is an intermediate oxygen donor solvent with a D_N of 15.1, and the hard base oxygen donor solvents MeOH, DMF, and H_2O compete more effectively for the metal ion, as reflected by their larger D_N's of 23.5, 26.6, and 33.0, respectively. As the D_N of the solvent increases, consistent with increasingly strong metal ion solvation, complex stability generally decreases.

The solvation energy of the alkali metal ions increase as their size decreases, so that Li^+ has the highest solvation energy. In addition, since the alkali metal ions have a hard acid nature they have a preference for hard base oxygen donor atoms in the ligand and solvent than for the softer base nitrogen donor atoms.[48] Therefore, they have higher solvation energies in MeOH, DMF and H_2O than in MeCN, and, in general, the stability of $[ML]^+$ follows the sequence H_2O << DMF < MeOH < PC < MeCN, for L = THEC12, (*S*)-THPC12 and TMEC12.

In solution, the number of pendant arms coordinated to the metal ion may vary depending on the solvent. The ^{13}C NMR spectra of $[M((R)\text{-THPEC12})]^+$ in DMF (Chapter 5), $[M(THEC12)]^+$ in MeOH (Chapter 5), and $[M((S)\text{-THPC12})]^+$ in MeOH[42] are consistent with M^+ being 8-coordinate in the complex. Since the hard base oxygen donor solvents MeOH and DMF do not alter the 8-coordinate nature of the metal ion in the complex, it is unlikely that PC and MeCN, which compete less effectively with the pendant arms of the ligand for coordination of the metal ion, will do so either.

Table 2.3: Stability constants for $[ML]^+$ complexes in a range of solvents at 298.2 K and $I = 0.05$ mol dm^{-3} NEt_4ClO_4 supporting electrolyte.

		log (K_s /dm^3 mol^{-1})					
Ligand	D_N	Li^+	Na^+	K^+	Rb^+	Cs^+	Ag^+
	14.1[h]			MeCN			
(*S*)-THPC12[a]		7.65	5.98	3.20	3.16	3.10	8.51
THEC12[b]		8.07	6.66	3.40	3.00	2.90	9.35
TMEC12[c]		9.34	9.13	6.07	4.85	3.55	12.30
CYCLEN[d]		6.90	3.60	2.90	2.82	2.78	9.43
	15.1[h]			PC			
(*S*)-THPC12[a]		6.7	5.3	5.3	4.8	4.1	15.3
THEC12[b]		8.90	7.49	5.91	4.23	4.04	14.00
TMEC12[d]		8.02	8.15	6.65	6.12	-	15.30
CYCLEN[d]		5.60	5.45	4.78	4.10	-	11.25
	23.5[i]			MeOH			
(*S*)-THPC12[a]		4.0	4.8	3.5	3.4	3.2	12.8
THEC12[e]		3.09	4.53	2.43	2.20	1.90	12.57
TMEC12[c]		4.10	6.20	3.90	3.00	2.50	14.20
THEC9[d]		3.13	3.52	3.23	2.78	2.47	7.65
(*S*)-THPC9[f]		3.47	3.77	3.01	-	-	7.18
	26.6[h]			DMF			
(*R*)-THPEC12[d]		3.13	4.25	4.10	3.57	3.47	8.14
(*S*)-THPC12[a]		3.24	3.76	3.63	3.56	3.41	11.30
THEC12[e]		2.99	3.37	1.59	1.39	1.23	11.16
TMEC12[c]		3.61	5.68	3.62	2.73	2.28	13.73
CYCLEN[b]		2.10	< 2	< 2	< 2	< 2	9.10
	33.0[i]			H_2O[j]			
(*S*)-THPC12[a]		< 2	< 2	< 2	< 2	< 2	11.86
THEC12[d]		< 2	< 2	< 2	< 2	< 2	12.16
TMEC12[g]		< 2	2.20	< 2	< 2	< 2	12.62

[a]Reference 42. [b]Reference 16. [c]Reference 53. [d]This work. Errors of ± 0.05 and ± 0.1 apply to $[M(CYCLEN)]^+$ in MeCN and PC, respectively. Errors of ± 0.05 and ± 0.03 apply to $[M((R)\text{-THPEC12})]^+$ and $[Ag((R)\text{-THPEC12})]^+$, respectively, in DMF. Errors of ± 0.1 apply to $[M(TMEC12)]^+$ in PC. Errors of ± 0.09, ± 0.05, ± 0.1, ± 0.08, and ± 0.07 apply to $[M(THEC9)]^+$, with $M^+ = Li^+$, Na^+ and K^+, Rb^+, Cs^+, and Ag^+, respectively. [e]Reference 12. [f]Reference 57. [g]Reference 13. [h]D_N's from Reference 54. [i]D_N's from Reference 55. [j]Determined by pH titration in 0.1 mol dm^{-3} NEt_4ClO_4 supporting electrolyte.

In the absence of solvent, the Li^+ ion has the strongest interactions of the alkali metal ions with the macrocyclic ligands THEC12, (*S*)-THPC12, and TMEC12 because of its greater charge density. However, Li^+ is the most strongly solvated alkali metal ion in solution. This is clearly evident by the lower stability of $[LiL]^+$ compared with $[NaL]^+$, for L = THEC12, (*S*)-THPC12, and TMEC12, in the hard base oxygen donor solvents H_2O, DMF and MeOH. As the D_N of the solvent progressively decreases from DMF to MeCN, the solvation energy of the alkali metal ions decrease, such that in a poorer solvating medium complexation of Li^+ is favoured relative to that of Na^+, compared with complexation in the hard base oxygen donor solvents. This results in a shift in selectivity from Na^+ to Li^+ along the solvent progression DMF to MeCN.

This marked selectivity shift is less apparent for the K^+, Rb^+ and Cs^+ complexes. These larger metal ions have lower solvation energies than either Li^+ or Na^+, and there is a much smaller difference in the solvation energy between K^+, Rb^+ and Cs^+ than between Li^+ and Na^+. Therefore, the K^+, Rb^+ and Cs^+ complexes show a smaller variation in stability with changing solvent.

2.5 EFFECT OF RING SIZE

Molecular mechanics calculations have shown that for larger macrocyclic ligands, such as pendant arm macrocyclic ligands based on the 12-membered macrocycle CYCLEN, the small effect of the macrocyclic ring on complex stability is due to the flexibility of these ligands.[22] That is, for these 12-membered macrocyclic ligands, the size of the macrocyclic ring is less important than that of the chelate ring because the ligand is able to change its conformation depending on the size of the metal ion. For smaller 9-membered ring ligands, the macrocyclic ring may be rigid enough to compete with the chelate ring as a factor governing selectivity.[30] Many triazamacrocycles coordinate main group metal ions strongly,[56] and the stabilities of these complexes exceed those of their open-chain analogues, thus exhibiting the expected macrocyclic effect. These aspects are now discussed with respect to the alkali metal ion complexes of the 9-membered ligand THEC9 (Figure 2.1).

The stabilities of $[M((R)\text{-THPEC9})]^+$ have not yet been determined (where (*R*)-THPEC9 has identical pendant arms to (*R*)-THPEC12 but only a 9-membered triaza ring). However, stability constants have been obtained for $[M(THEC9)]^+$ and $[M((S)\text{-THPC9})]^+$,[57] as shown in Table 2.3. These results show that, as for the 12-membered ring systems discussed in the previous sections, $[NaL]^+$ is more stable than $[LiL]^+$ in MeOH. For the 9-membered ring

systems, this selectivity appears only marginal. In addition, these complexes are generally less stable than their tetraaza ligand analogues in MeOH. This may be attributed to the fewer donor atoms in these smaller ligands, where they have a smaller cavity defined by only three triaza ring nitrogens and three oxygen donor atoms in the hydroxy arms to coordinate the metal and stabilise the complex. In keeping with the larger pendant arm macrocyclic ligands, as the degree of stereochemical flexibility decreases from THEC9 to (*S*)-THPC9, the complex stabilities in MeOH generally increase (Table 2.3).

Molecular orbital studies of THEC9 and $[M(THEC9)]^+$, for $M^+ = Li^+$, Na^+, K^+, Rb^+ and Cs^+, (Figure 2.5) predict M^+ to be 6-coordinate and the Λ and Δ enantiomers to have distorted trigonal prismatic structures (Figure 2.6).[11] These computed structures are consistent with the commonly adopted + + + configuration (Figure 2.7) of a cyclononane derived ligand in its metal complexes, where the metal ion is coordinated above the triaza ring to the three coplanar nitrogens.[26] The hydroxy protons point away from adjacent hydroxy oxygens so that no intramolecular hydrogen bonding occurs. This is consistent with the smaller ring in THEC9 making intramolecular hydrogen bonding between the pendant arms less favoured. The convention used in this study refers to the pendant arms exhibiting a clockwise or anticlockwise rotation, designated by Δ or Λ, respectively, (Figure 2.6) when viewed down the C_3 axis from the plane of the three oxygens, so that the methylene groups point outwards. The M-O and M-N bond distances (Table 2.4) show that the metal ion is coordinated in the centre of the cavity. The similarity between the free ligand and Na^+ complex dimensions that was found for the 12-membered systems is not present for THEC9. Therefore, the optimum bonding between Na^+, with a 6-coordinate radius of 1.02 Å,[46] and the donor atoms of THEC12 (and the other related 12-membered ligands) is not as apparent for the smaller THEC9.

The computed structure of $[Li(THEC9)]^+$ does not show the variation in Li–O and Li–N bond distances that was found for the 12-membered systems. Hence, Li^+, with a 6-coordinate radius of 0.76 Å,[46] may be better accommodated by the smaller cavity of THEC9 than that of the 12-membered macrocyclic ligands, resulting in the higher stability of $[Li(THEC9)]^+$ compared with $[Li(THEC12)]^+$. Since Li^+ is the smallest, hardest alkali metal ion and therefore the most solvated ion, it is the most affected by solvent. This results in $[Li(THEC9)]^+$ being less stable than $[Na(THEC9)]^+$.

The 6-coordinate geometry of M^+ in $[Li(THEC9)]^+$ and $[Na(THEC9)]^+$ predicted by molecular orbital calculations is in accord with the interpretation of the ^{13}C NMR solution spectra (Chapter 5). It is apparent from ^{13}C NMR

Figure 2.5: The global energy minimised structures[11] of $[Li(THEC9)]^+$ (A), $[K(THEC9)]^+$ (B) and $[Cs(THEC9)]^+$ (C) determined through Gaussian 94 using the LanL2DZ basis set.[2]

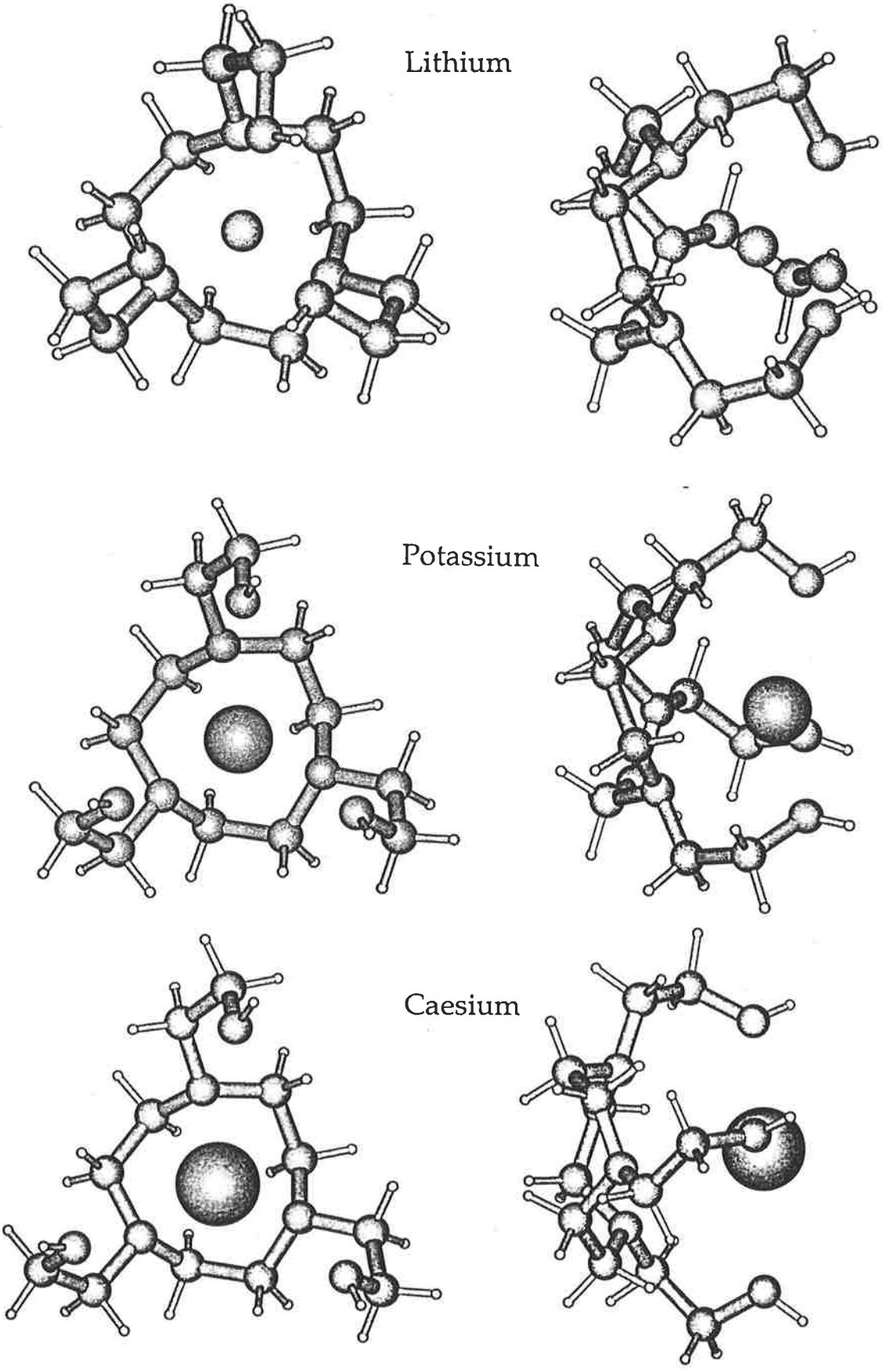

Figure 2.6: The computed structures[11] of Δ and Λ[Na(THEC9)]$^+$ determined through Gaussian 94 using the LanL2DZ basis set.[2]

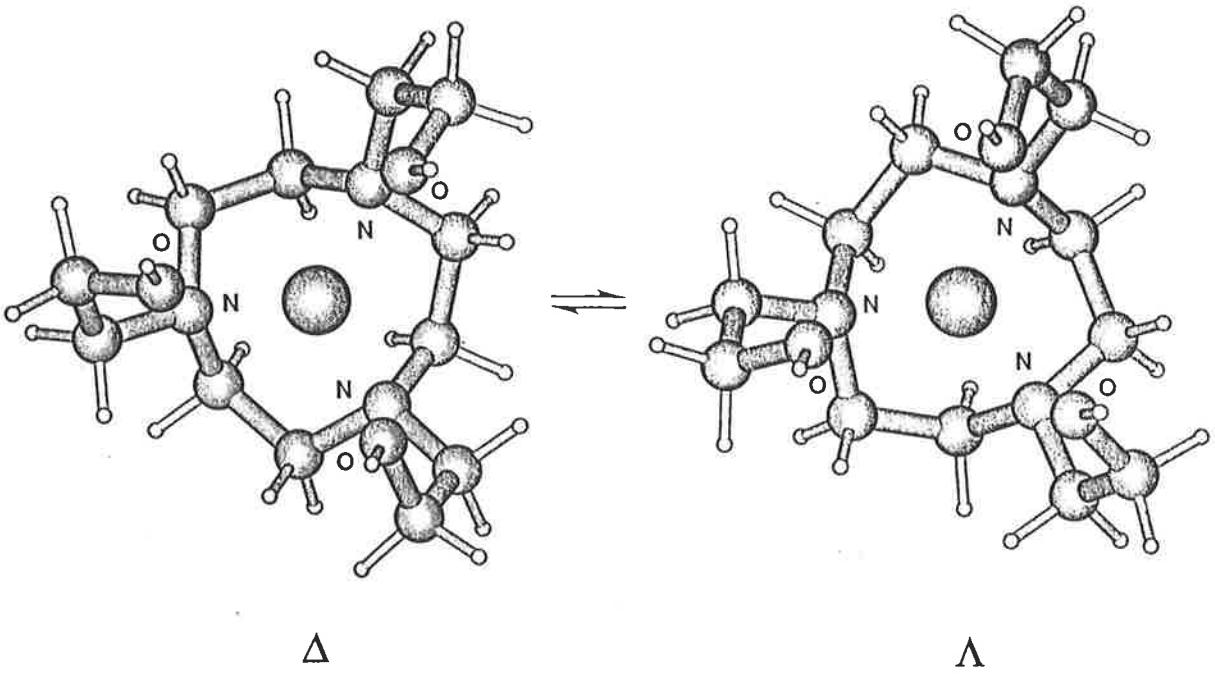

Δ Λ

studies, however, that K^+ in $[K(THEC9)]^+$ is not 6-coordinate, but that it increases its coordination number by coordinating THEC9 and the solvent, MeOH. Although the $[Rb(THEC9)]^+$ and $[Cs(THEC9)]^+$ complexes were insufficiently soluble at the high concentrations needed for NMR solution studies, they were sufficiently soluble for their stability constants to be determined. It is likely that, as with K^+ (with a 6-coordinate radius of 1.38 Å),[46] these metal ions (with 6-coordinate radii of 1.52 Å and 1.67 Å, respectively)[46] also increase their coordination number by coordinating MeOH in addition to THEC9. Therefore, it is not possible to compare their stability values with those of the 8-coordinate metal ions in $[ML]^+$, where L = THEC12, (*S*)-THPC12, TMEC12 and (*R*)-THPEC12. The ^{13}C NMR spectra[57] of $[K((S)\text{-THPC9})]^+$ indicates that K^+ in this complex may also increase its coordination number, by coordinating(*S*)-THPC9 and MeOH. It is likely that a similar situation exists for the Rb^+ and Cs^+ analogues, which precludes a more detailed comparison.

Figure 2.7: The + + + conformer of the 1,4,7-triazacyclononane ring. The pendant arms, denoted R, are shown uncoordinated.

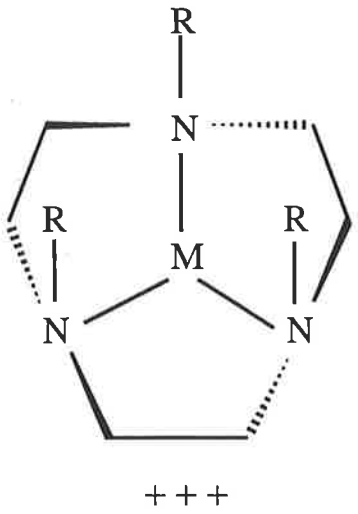

Table 2.4: Parameters derived from molecular orbital calculations[11] for THEC9 and $[M(THEC9)]^+$ using the Gaussian 94 LanL2DZ basis set.[2]

Distance (pm)	THEC9	$[M(THEC9)]^+$	
		$M^+ = Li^+$	Na^+
O - O distance	470	294	348
N - N distance	311	294	304
O - N distance	265	273	285.7
M - O distance	-	208	235
M - N distance	-	230	258
M - O plane distance	-	117	96.7
M - N plane distance	-	156	189
Twist angle ϕ (°)[a]	32.75	9.3	10.0

[a]Twist angle $\phi = 0°$ for trigonal prismatic stereochemistry.

2.6 STABILITY OF Ag^+ COMPLEXES

In DMF, $[Ag((R)\text{-THPEC12})]^+$ is more stable than the corresponding alkali metal complexes (as shown in Table 2.1). This may be rationalised by the different interactions that Ag^+ and the alkali metal ions have with the macrocyclic ligand. The alkali metal ions are hard acids whereas Ag^+ is a soft acid,[47-51] so that Ag^+ has a much higher affinity for the four nitrogen donor atoms of (*R*)-THEPC12 than the alkali metal ions do. This is substantiated by the bond energy of a Ag-N bond (23 kJ mol^{-1}) being significantly higher than that of a Ag-O bond (6 kJ mol^{-1}).[51] In addition, the alkali metal ions have non-directional metal-ligand bonding, whereas Ag^+ has directional bonding and tends to form two strong coaxial bonds.[30] The 8-coordinate radius of Ag^+ (1.28 Å) is very similar to that of Na^+ (1.18 Å),[46] and since it has been shown that Na^+ has optimum bonding with the donor atoms of (*R*)-THPEC12, Ag^+ may show a similar trend.

For L = THEC12, (*S*)-THPC12 and TMEC12, $[AgL]^+$ is more stable than the corresponding alkali metal complexes in DMF (Table 2.1). The stability of these Ag^+ complexes, like those of the alkali metal ions, are solvent dependant (Table 2.3), but $[AgL]^+$ is always more stable than $[ML]^+$, where M^+ = alkali metal ion. As the D_N of the solvent increases from PC to MeOH to DMF, the $[AgL]^+$ stability decreases, consistent with the increasing degree of competition by the solvent for the Ag^+ ion. In MeCN, however, there is a marked decrease in the $[AgL]^+$ stability. This is because MeCN is a nitrogen donor solvent and can compete more effectively for Ag^+ than the hard base oxygen donor solvents do, so that Ag^+ has a much higher solvation energy in MeCN than in the other solvents studied, and hence its complexes are of lower stability.

It could be surmised that the stability of $[Ag((R)\text{-THPEC12})]^+$ should be higher than that of $[Ag(CYCLEN)]^+$ in DMF because the extra donor atoms in (*R*)-THPEC12 help to stabilise the Ag^+ complex. In addition, the donor strength of a tertiary amine is greater than that of a secondary amine,[19,29] so that $[Ag((R)\text{-THPEC12})]^+$ should be more stable. However, this is not observed. This may indicate that the large phenyl substituent on the chiral pendant arms of (*R*)-THPEC12 may hinder the proximity of the metal ion to the donor atoms of the ligand on coordination. For the alkali metal ions, which bind both the nitrogen and oxygen donor atoms, this may not be such a significant factor, as discussed in Section 2.3.1. The Ag^+ ion, however, has a preference for nitrogen over oxygen. Therefore, from THEC12 to (*R*)-THPEC12, the increasing size of the substituent on the pendant arms may cause progressively greater steric hindrance between the coordinating pendant arms, so that Ag^+ is coordinated further out of the plane of the tetraaza ring and

the Ag-N interactions are reduced. This results in $[Ag((R)\text{-THPEC12})]^+$ being less stable than those of the other pendant arm macrocyclic ligand complexes listed in Table 2.3 and $[Ag(CYCLEN)]^+$.

In MeOH, the observation that $[Ag(THEC9)]^+$ is less stable than $[AgL]^+$, where L = THEC12, (*S*)-THPC12 and TMEC12, is consistent with the fewer nitrogen donor atoms in the ring (and one less pendant arm) in THEC9 to stabilise the complex. In addition, the 6-coordinate radius of Ag^+ (1.15 Å) is larger than that of Li^+ (0.76 Å) or Na^+ (1.02 Å).[46] So, Ag^+ has a poorer fit in the cavity of THEC9 and induces more strain in the complex than the smaller Li^+ or Na^+, by comparison with the similar 8-coordinate radii of Ag^+ and Na^+ in the 12-membered ring macrocyclic complexes.

BIBLIOGRAPHY

1. S.L. Whitbread, P. Valente, M.A. Buntine, P. Clements, S.F. Lincoln, K.P. Wainwright, *J. Am. Chem. Soc.* **1998**, 120, 2862-2869.
2. Guassian 94, Revision C.3: M.J. Frisch, G.W. Trucks, H.B. Schegel, P.M.W. Gill, B.G. Johnson, M.A. Robb, J.R. Cheeseman, T. Keith, G.A. Petersson, J.A. Montgomery, K. Raghavachari, M.A. Al-Laham, V.G. Zakrzewski, J.V. Ortiz, J.B. Foresman, J. Cioslowski, B.B. Stefanov, A. Nanayakkara, M. Challacombe, C.Y. Peng, P.Y. Ayala, W. Chen, M.W. Wong, J.L. Andres, E.S. Replogle, R. Gomperts, R.L. Martin, D.J. Fox, J.S. Binkley, D.J. Defrees, J. Baker, J.P. Stewart, M. Head-Gordon, C. Gonzalez, J.A. Pople, *Gaussian Inc.*, Pittsburgh, Pennsylvania, **1995**.
3. B. Scott, K.J. Brewer, L.O. Spreer, C.A. Craig, J.W. Otves, M. Calvin, S. Taylor, *J. Coord. Chem.* **1990**, 21, 307-313.
4. R. Clay, P. Murray-Rust, J. Murray-Rust, *J. Acta. Cryst.* **1979**, B35, 1894-1895.
5. Y. Iitaka, M. Shima, E. Kimura, *Inorg. Chem.* **1974**, 13, 2886-2891.
6. J.H. Loehlin, E.B. Fleischer, *Acta. Crystallogr. Sect. B* **1976**, 32, 3063-3066.
7. N. Matsumoto, A. Hirano, T. Hara, A. Ohyoshi, *J. Chem. Soc., Dalton Trans.* **1983**, 2405.
8. M. Kojima, K. Nakabayashi, S. Ohba, S. Okumoto, Y. Saito, J. Fujita, *Bull. Chem. Soc. Jpn.* **1986**, 59, 277-283.
9. (a) S. Buøen, J. Dale, P. Groth, J. Krane, *J. Chem. Soc., Chem. Commun.* **1982**, 1172-1174.
   (b) P. Groth, *Acta. Chem. Scand.* **1983**, A37, 71-77.
10. P. Groth, *Acta. Chem. Scand.* **1983**, A37, 283-291.
11. S.L. Whitbread, J.M. Weeks, P. Valente, M.A. Buntine, S.F. Lincoln, K.P. Wainwright, *Aust. J. Chem.* **1997**, 50, 853-856.
12. M.L. Turonek, P. Clarke, G.S. Laurence, S.F. Lincoln, P.-A. Pittet, S. Politis, K.P. Wainwright, *Inorg. Chem.* **1993**, 32, 2195-2198.
13. A.K.W. Stephens, S.F. Lincoln, *J. Chem. Soc., Dalton Trans.* **1993**, 2123-2126.
14. J.-M. Lehn, *Struct. Bond. (Berlin)* **1973**, 16, 1-69.
15. J.-M. Lehn, J.-P. Sauvage, *J. Am. Chem. Soc.* **1975**, 97, 6700-6707.
16. S.L. Whitbread, S. Politis, A.K.W. Stephens, J. Lucas, R.S. Dhillon, S.F. Lincoln, K.P. Wainwright, *J. Chem. Soc., Dalton Trans.* **1996**, 7, 1379-1384.
17. (a) B.G. Cox, J. Garcia-Rosas, H. Schneider, *J. Am. Chem. Soc.* **1981**, 103, 1384-1389.
    (b) J.-M. Lehn, *Acc. Chem. Res.* **1978**, 11, 49-57.
18. J.-M. Lehn, *J. Inclusion Phenom.* **1988**, 6, 351-396.

19. R.D. Hancock, *Pure. Appl. Chem.* **1986**, 58, 1445-1452.
20. C.M. Madeyski, J.P. Michael, R.D. Hancock, *Inorg. Chem.* **1984**, 23, 1487-1489.
21. J.R. Morrow, K.O.A. Chin, *Inorg. Chem.* **1993**, 32, 3357-3361.
22. V.J. Thöm, C.C. Fox, J.C.A. Boeyens, R.D. Hancock, *J. Am. Chem. Soc.* **1984**, 106, 5947-5955.
23. R.D. Hancock, *Pure. Appl. Chem.* **1993**, 65, 941-946.
24. R.D. Hancock, *Acc. Chem. Res.* **1990**, 65, 253-257.
25. R.D. Hancock, R. Bhavan, P.W. Wade, J.C.A. Boeyens, S.M. Dobson, *Inorg. Chem.* **1989**, 28, 187-194.
26. R.D. Hancock, A.E. Martell, *Chem. Rev.* **1989**, 89, 1875-1914.
27. V.J. Thöm, G.D. Hosken, R.D. Hancock, *Inorg. Chem.* **1985**, 24, 3378-3381.
28. R.D. Hancock, *Prog. Inorg. Chem.* **1989**, 37, 187-291.
29. R.D. Hancock, *Perspect. Coord. Chem.* **1993**, 65, 941-946.
30. R.D. Hancock, P.W. Wade, M.P. Ngwenya, A.S. de Sousa, K.V. Damu, *Inorg. Chem.* **1990**, 29, 1968-1974.
31. H.J. Buschmann, *Inorg. Chim. Acta.* **1986**, 125, 31-35.
32. S.F. Lincoln, A.K.W. Stephens, *Inorg. Chem.* **1992**, 31, 5067.
33. B.G. Cox, H. Schneider, J.J. Stroka, *J. Am. Chem. Soc.* **1978**, 100, 4746-4749.
34. Y.M. Cahen, J.L. Dye, A.I. Popov, *J. Phys. Chem.* **1975**, 79, 1292-1295.
35. T.A. Kaden, *Topp. Curr. Chem.* **1984**, 121, 157-179.
36. D.J. Cram, *Angew. Chem. Ed. Engl.* **1986**, 25, 1039-1057.
37. D.J. Cram, *J. Inclusion Phenom.* **1988**, 6, 397-413.
38. L.F. Lindoy, *"The Chemistry of Macrocyclic Ligand Complexes"*, Cambridge University Press, Cambridge, U.K., **1989**.
39. G.W. Gokel, *Chem. Soc. Rev.* **1992**, 39-47.
40. D.F. Shriver, P.W. Atkins, C.H. Langford, *"Inorganic Chemistry"*, Chapter 6, Oxford University Press:Oxford, **1994**.
41. R.S. Dhillon, A.K.W. Stephens, S.L. Whitbread, S.F. Lincoln, K.P. Wainwright, *J. Chem. Soc., Chem. Commun.* **1995**, 1, 97-98.
42. R.S. Dhillon, S.E. Madback, F.G. Ciccone, M.A. Buntine, S.F. Lincoln, K.P. Wainwright, *J. Am. Chem. Soc.* **1997**, 119, 6126-6134.
43. R.D. Hancock, M.S. Shaikjee, S.M. Dobson, J.C.A. Boeyens, *Inorg. Chim. Acta.* **1988**, 154, 229-238.
44. R. Luckay, J.H. Reibenspies, R.D. Hancock, *J. Chem. Soc., Chem. Commun.* **1995**, 2365-2366.
45. K. Henrick, P. Tasker, L.F. Lindoy, *Prog. Inorg. Chem.* **1985**, 33, 1-58.
46. R.D. Shannon, *Acta. Crystallogr. Sect. A: Cryst. Phys. Diffr. Theor. Gen. Crystallogr.* **1976**, 32, 751-767.
47. J. Emsley, *Chem. Soc. Rev.* **1980**, 9, 91-124.

48. R.G. Pearson, *J. Am. Chem. Soc.* **1963**, 85, 3533-3539.
49. R.G. Pearson, *Coord. Chem. Rev.* **1990**, 100, 403-425.
50. F.A. Cotton, G. Wilkinson, *"Advanced Inorganic Chemistry"*, 5th Edition, Inter-Science, New York, **1988**.
51. H.J. Buschmann, *Inorg. Chim. Acta.* **1985**, 102, 95-98.
52. D.S.B. Grace, J. Krane, *J. Chem. Research(S)* **1983**, 162-163.
53. A.K.W. Stephens, R.S. Dhillon, S.E. Madback, S.L. Whitbread, S.F. Lincoln, *Inorg. Chem.* **1996**, 35, 2019-2024.
54. V. Gutmann, *"Coordination Chemistry in Non-Aqueous Solvents"*, Springer-Verlag:Wien, **1968**.
55. (a) W.J. Dewitte, A.I. Popov, *J. Solution Chem.* **1976**, 5, 231-240.
(b) R.H. Erlich, E. Roach, A.I. Popov, *J. Am. Chem. Soc.* **1970**, 92, 4989-4990.
56. P. Chaudhuri, K. Weighardt, *Prog. Inorg. Chem.* **1987**, 35, 329-436.
57. F.G. Ciccone, Honours Thesis, University of Adelaide, **1996**.

CHAPTER 3

EQUILIBRIUM STUDIES OF DIVALENT METAL ION COMPLEXES WITH THEC12

3.1 PROTONATION CONSTANTS OF THEC12

The factors influencing the equilibrium processes for the complexation of metal ions by macrocyclic ligands in non-aqueous solvents (Chapter 2) are also applicable to metal ion complexation processes in aqueous solution. However, in aqueous solution the ability of the nitrogen atoms in the macrocyclic ligand to be protonated is a factor that must also be considered. Thus, in aqueous solution at 298.2 K and I = 0.1 mol dm^{-3} NEt_4ClO_4, the pendant arm tetraaza macrocycle THEC12 (1,4,7,10-tetrakis(2-hydroxyethyl)-1,4,7,10-tetraaza-cyclododecane) denoted L, acts as a tetrabasic species due to its four tertiary amine nitrogen atoms. The four protonations of THEC12 are described by Equations 3.1 – 3.4, with the four successive protonation constants K_1, K_2, K_3 and K_4 defined by Equations 3.5 – 3.8:

$$H^+ + L \overset{K_1}{\rightleftharpoons} HL^+ \qquad 3.1$$

$$H^+ + HL^+ \overset{K_2}{\rightleftharpoons} H_2L^{2+} \qquad 3.2$$

$$H^+ + H_2L^{2+} \overset{K_3}{\rightleftharpoons} H_3L^{3+} \qquad 3.3$$

$$H^+ + H_3L^{3+} \overset{K_4}{\rightleftharpoons} H_4L^{4+} \qquad 3.4$$

$$K_1 = \frac{[HL^+]}{[H^+][L]} \qquad 3.5$$

$$K_2 = \frac{[H_2L^{2+}]}{[H^+][HL^+]} \qquad 3.6$$

$$K_3 = \frac{[H_3L^{3+}]}{[H^+][H_2L^{2+}]} \qquad 3.7$$

$$K_4 = \frac{[H_4L^{4+}]}{[H^+][H_3L^{3+}]} \qquad 3.8$$

The protonation constants of THEC12 are shown in Table 3.1, together with those of related macrocyclic ligands. The non-bonded electron pairs of the amine nitrogens are probably initially directed towards the centre of the tetraaza ring to minimise repulsion and maximise interactions between the nitrogen lone pairs and protons. Therefore, the first protonation is facilitated by an increase in the electron density in the macrocyclic ring. The second protonation of THEC12 occurs at an amine group in the tetraaza ring diagonally opposite the protonated amine in $HTHEC12^+$, thus minimising electrostatic repulsions between the incoming proton and the one already bound. The much lower value of K_3 is due to the third protonation occurring at an amine group adjacent to those already protonated, so that the electrostatic repulsions are much larger than for the first two protonation steps, and this results in $K_3 << K_2 < K_1$. Electrostatic repulsions are increased even further still when the fourth protonation occurs, culminating in K_4 for THEC12 being too low to be determined.

The macrocycles THEC12, (*S*)-THPC12, and TMEC12 (Figure 2.1) all have similar protonation constants (Table 3.1),[1,2] consistent with the different donor groups on the pendant arms having little influence on the protonation of these ligands. A similar comparison with the alkaline earth metal complexes of (*R*)-THPEC12 (Figure 2.1) in aqueous solution cannot be made because (*R*)-THPEC12 and its metal complexes were insoluble in most common solvents.

These pendant arm tetraaza macrocycles exhibit a lower basicity than their parent macrocyclic ligand CYCLEN (Table 3.1 and Figure 2.1).[3-5] This is consistent with tertiary amine nitrogens having a lower basicity than their secondary amine analogues,[6,7] which can be rationalised by the balance

Table 3.1: Protonation constants[a] for THEC12 and related ligands at 298.2 K.

Ligand	log K_1 K_1 /dm^3 mol^{-1}	log K_2 K_2 /dm^3 mol^{-1}	log K_3 K_3 /dm^3 mol^{-1}	log K_4 K_4 /dm^3 mol^{-1}
TACN[b]	10.42	6.82	-	
THEC9[c]	11.12	3.41	-	
CYCLEN[d]	11.32	9.72	< 2.30	< 2.30
THEC12[c]	10.74	8.16	1.94	-
(*S*)-THPC12[e]	10.75	8.32	2.36	-
TMEC12[f]	10.92	8.04	2.17	-

[a]In 0.1 mol dm^{-3} NEt_4ClO_4 supporting electrolyte unless stated otherwise. [b] Reference 15. In 0.1 mol dm^{-3} KNO_3. [c]This work. Errors of ± 0.05 apply to the log K values. [d]Reference 3. In 0.1 mol dm^{-3} $NaNO_3$. [e]Reference 2. [f]Reference 1.

Table 3.2: Stability constants[a] for the complexation of divalent metal ions by THEC12 and other ligands at 298.2 K.

	log (K_S /dm^3 mol^{-1})			
Ligand	Mg^{2+}	Ca^{2+}	Sr^{2+}	Ba^{2+}
THEC9[b]	< 2	< 2	< 2	< 2
CYCLEN	2.25[c]	3.12[d]	-	-
THEC12[b]	2.86	7.41	6.47	4.84
(*S*)-THPC12[e]	3.26	7.17	6.75	5.42
TMEC12[f]	2.47	5.47	5.00	4.72

[a]In 0.1 mol dm^{-3} NEt_4ClO_4 supporting electrolyte unless stated otherwise. [b]This work. Errors of ± 0.05 apply to the $[M(THEC12)]^{2+}$ complexes. [c]Reference 4. In 0.1 mol dm^{-3} KNO_3. [d]Reference 5. In 0.1 mol dm^{-3} $NaNO_3$. [e]Reference 2. [f]Reference 1.

between steric and inductive effects. That is, the conversion of secondary amine nitrogens to tertiary amines confers a greater basicity on the tertiary amine nitrogen because of the inductive effect of the pendant arm. However, this is outweighed by the greater steric hindrance around a tertiary amine nitrogen, limiting the hydrogen bonding ability of the tertiary amine.[6] Therefore, these pendant arm macrocycles have lower first and second protonation constants by comparison with CYCLEN. Their differences, however, are less significant for subsequent protonations because of increased electrostatic repulsions within the ligand.

A similar situation occurs for related macrocycles with larger rings[3,8,9] and it has been established that the addition of hydroxyethyl groups to amines usually decreases their protonation constants relative to the unsubstituted analogues.[10-13] This is probably due to the combination of induced steric strain and electron withdrawing ability of the hydroxyethyl group. This does not seem to be the case for the smaller macrocycle THEC9 (Figure 2.1), as discussed below.

The first protonation constant (Table 3.1) of THEC9 is higher than that of its parent macrocyclic ligand TACN (1,4,7-triazazcyclononane),[14] (Figure 2.1) which may be due to intramolecular hydrogen bonding involving the hydroxyethyl arms. The low second protonation constant suggests that this hydrogen bonding type of structure breaks down and the normal electron withdrawing properties of the hydroxyethyl group become apparent.[15] Another possibility put forward by other workers to explain this phenomenon is the "cage effect" of THEC9.[12] The first proton may be considered to be bonded to the three oxygen and three nitrogen donor atoms of THEC9, so that they form a cage surrounding the proton and thus hold it very strongly. This "cage" type structure is shown in Figure 3.1. The proton may not be bound to any specific donor atom but shared by all six donor atoms of THEC9. This proposal may explain the significantly higher value of K_1 for not only THEC9 compared with TACN, but also for other related triaza pendant arm macrocycles.[12]

The second protonation constant for THEC9 is significantly lower than that for the tetraaza macrocycle THEC12 and its related analogues. This is because as the degree of protonation increases, the smaller triaza ligand experiences stronger electrostatic repulsions between the positive charges that accumulate in the ring due to the closer proximity of the protonated amines. These increased electrostatic repulsion effects are the reason why the third protonation constant for THEC9 is too low to be determined.

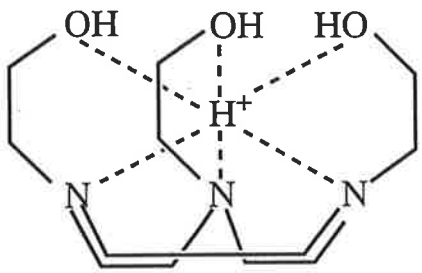

Figure 3.1: Possible structure for the monoprotonated form of THEC9, showing the proposed "cage effect" of THEC9.

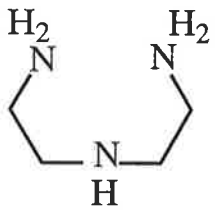

DIEN

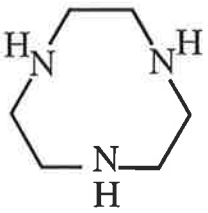

TACN

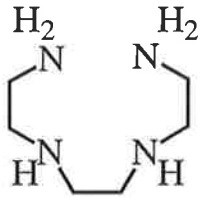

TRIEN

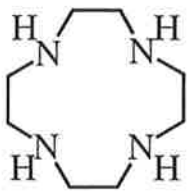

CYCLEN

Figure 3.2: Structures of DIEN and TRIEN, with their respective cyclised analogues TACN and CYCLEN.

The 9-membered macrocyclic ligands have higher nitrogen basicity for the first proton, and lower nitrogen basicities for subsequent protonation, relative to their linear counterparts. For instance, when the linear triamine DIEN (1,4,7-triazaheptane) (Figure 3.2) is cyclised to TACN, the basicity of the first amine increases (log K_1 = 9.70 *vs* 10.42), but the basicities of the second and third amines decrease (log K_2 = 8.98 *vs* 6.82 and log K_3 = 4.25 *vs* < 1).[11,15-17] This is rationalised by the increased electron density in the macrocyclic cavity facilitating the first proton uptake, resulting in the higher K_1 value. Subsequent protonations, however, induce electrostatic repulsions from protons already coordinated, and thus a lowering of the protonation constants. A similar situation holds for tetraaza macrocycles. For example, when TRIEN (3,6-diaza-1,8-diaminooctane) (Figure 3.2) is cyclised to CYCLEN, the basicities of CYCLEN for the first and second protons are higher (log K_1 = 11.32 *vs* 10.09 and log K_2 = 9.72 *vs* 9.31) and subsequent basicities for the third and fourth protons are much lower (log K_3 < 2.30 *vs* 6.75 and log K_4 < 2.30 *vs* 3.39) than the corresponding basicities for TRIEN.[3,18,19]

It must be noted that the protonation constants determined for complexes between alkali metal ions and pendant arm macrocyclic ligands using alkali metal salts as the supporting electrolyte are considerably lower than for those with an inert electrolyte.[20] This is due to the ability of pendant arm tetraaza macrocyclic ligands to complex alkali metal ions strongly. However, since the stabilities of alkali metal ion complexes with CYCLEN and TACN in aqueous solution are probably very low, it is likely their effect on the protonation constants of CYCLEN and TACN is negligible.

3.2 STABILITY OF $[M(THEC12)]^{2+}$

The complexation of an alkaline earth metal ion, denoted M^{2+}, by a pendant arm macrocyclic ligand, denoted L, is described by:

$$M^{2+} + L \underset{}{\overset{K_S}{\rightleftharpoons}} [ML]^{2+} \qquad 3.9$$

where the stability constant, K_S, is defined by:

$$K_S = \frac{[ML^{2+}]}{[M^{2+}][L]} \qquad 3.10$$

The stability constants for $[M(THEC12)]^{2+}$ have been determined in aqueous solution and, as shown in Table 3.2, follow the sequence of $Mg^{2+} < Ca^{2+} > Sr^{2+} > Ba^{2+}$. The factors responsible for variations in K_S with the nature of M^{2+} are: (i) size of the metal ion;[21] (ii) solvation energy of the metal ion;[22] and (iii) hard or soft nature of the metal ion and its consequent variation in affinity for oxygen or nitrogen donor atoms.[23,24] The alkaline earth metal ions are hard acids, and have a preference for hard oxygen donor atoms rather than softer nitrogen donor atoms.[23,24] Therefore, like the alkali metal ions, they bind more strongly to the oxygen donor atoms in the hydroxyethyl pendant arms of THEC12 than to the tetraaza ring nitrogens.

The ^{13}C NMR solution studies (Chapter 5) have shown that M^{2+} in $[M(THEC12)]^{2+}$, for $M^{2+} = Mg^{2+}$, Ca^{2+} and Ba^{2+}, is 8-coordinate, with the M^{2+} ion coordinated to the four nitrogen donor atoms and the four oxygen donor atoms of THEC12. As for the $[M(THEC12)]^{+}$ complexes, $[M(THEC12)]^{2+}$ has a square antiprismatic coordination geometry, THEC12 adopts the TRANS I conformation (Figure 2.2), and the M^{2+} ion sits above the plane of the ring nitrogens. Although $[Sr(THEC12)]^{2+}$ has not been the subject of NMR solution studies, it is likely Sr^{2+} is also 8-coordinate in the complex. Hence, as for $[M(THEC12)]^{+}$, the different coordination geometry of M^{2+} in $[M(THEC12)]^{2+}$ is not a factor determining the variation of stability observed in Table 3.2.

The variation of K_S in the sequence $Mg^{2+} < Ca^{2+} > Sr^{2+} > Ba^{2+}$ for $[M(THEC12)]^{2+}$ is similar to the sequence $Li^{+} < Na^{+} > K^{+} > Rb^{+} > Cs^{+}$ observed in Chapter 2 for $[M(THEC12)]^{+}$ in most solvents studied. The selectivity of THEC12 for Ca^{2+} may be due to Ca^{2+}, with an 8-coordinate radius of 1.12 Å,[21] being able to establish optimum bonding distances and inducing minimum strain in $[Ca(THEC12)]^{2+}$ compared with the other $[M(THEC12)]^{2+}$ complexes. This seems feasible since Ca^{2+} and Na^{+} have very similar 8-coordinate radii (1.12 Å and 1.18 Å, respectively)[21] and, as shown in Chapter 2, the high stability of $[Na(THEC12)]^{+}$ is consistent with the strain energy in THEC12 being minimised with Na^{+}. These results suggest that for THEC12 adopting the TRANS I conformation in $[M(THEC12)]^{n+}$ (where n = 1 or 2) optimum bonding and least induced strain results with a metal ion of radius between 1.12 – 1.18 Å. This would also explain the much lower stability of $[Mg(THEC12)]^{2+}$ compared with the other $[M(THEC12)]^{2+}$ complexes. The Mg^{2+} ion is the smallest, hardest alkaline earth metal ion and is therefore the most strongly solvated ion. Although NMR studies have shown that Mg^{2+} in $[Mg(THEC12)]^{2+}$ is 8-coordinate, the higher solvation energy of Mg^{2+} and its smaller size is consistent with Mg^{2+} being too small to give optimum bonding with THEC12 and inducing steric strain between the coordinating pendant arms of THEC12 as they form Mg–O bonds. This is analogous to the situation

described for $[Li(THEC12)]^+$ where Li^+, with an 8-coordinate radius of 0.92 Å,[21] induces considerable steric strain in the complex because of its small size.

As the charge density systematically decreases with increasing metal ion size from Ca^{2+} to Ba^{2+}, there is a concomitant decrease in the electrostatic attraction between M^{2+} and THEC12, and the larger M^{2+} ions induce more conformational strain in $[M(THEC12)]^{2+}$. Therefore, the stability of $[M(THEC12)]^{2+}$ decreases in the order $Ca^{2+} > Sr^{2+} > Ba^{2+}$. The decrease in stability along this progression is not as significant as for $[M(THEC12)]^+$ where K^+, Rb^+ and Cs^+ have larger 8-coordinate radii (1.38 Å, 1.52 Å and 1.67 Å, respectively) than Sr^{2+} or Ba^{2+} (1.26 Å and 1.42 Å, respectively).[21] However, as for $[M(THEC12)]^+$, the observed complexing ability of THEC12 with M^{2+} ions of significantly different size is consistent with the flexibility of THEC12, allowing it to adapt to variations in the size of the metal ion.

3.3 EFFECT OF PENDANT ARMS

3.3.1 COMPARISON OF THEC12 WITH (S)-THPC12 AND TMEC12

The stabilities of $[M((S)\text{-}THPC12)]^{2+}$ and $[M(TMEC12)]^{2+}$ follow the same sequence $Mg^{2+} < Ca^{2+} > Sr^{2+} > Ba^{2+}$ observed for $[M(THEC12)]^{2+}$ (Table 3.2).[1,2] In addition, these three ligands show a similar trend for the alkaline earth metal ions as for the alkali metal ions, with stabilities in the order $Li^+ < Na^+ > K^+ > Rb^+ > Cs^+$ (Chapter 2). Therefore, as for $[NaL]^+$, where L = THEC12, (*S*)-THPC12 and TMEC12, Ca^{2+} probably establishes optimum bonding and minimum induced strain in $[CaL]^{2+}$. As for $[M(THEC12)]^{2+}$, the ^{13}C NMR solution studies show that the M^{2+} ion in $[M((S)\text{-}THPC12)]^{2+}$, for $M^{2+} = Mg^{2+}$, Ca^{2+} and Ba^{2+},[25] and $[M(TMEC12)]^{2+}$, for $M^{2+} = Ca^{2+}$ and Ba^{2+},[25] is 8-coordinate, and the ligand adopts the TRANS I conformation. NMR solution[26] and X-ray diffraction[25] studies, however, show that although TMEC12 adopts the TRANS I conformation, Mg^{2+} in $[Mg(TMEC12)]^{2+}$ is 7-coordinate. Furthermore, the complexes generally follow the stability sequence $[M((S)\text{-}THPC12)]^{2+} > [M(THEC12)]^{2+} > [M(TMEC12)]^{2+}$, in contrast to the trend observed in Chapter 2 for the corresponding alkali metal complexes. These phenomena are discussed below.

The $[M(TMEC12)]^+$ complexes are more stable than $[M(THEC12)]^+$, with the factors responsible for this phenomenon outlined in Chapter 2, but the reverse is true for $[ML]^{2+}$. Therefore, either additional factors may be important for $[ML]^{2+}$ or the balance between the factors discussed in Chapter 2 changes. Since M^{2+} in $[ML]^{2+}$ is 8-coordinate, for $M^{2+} = Ca^{2+}$, Sr^{2+} and Ba^{2+},

differences in coordination number or geometry is not a factor determining the stability of $[ML]^{2+}$. The effect of solvation, however, may be important for the alkaline earth metal ions. On complexation, the ligand donor atoms replace the first solvation shell of the hydrated metal ion. However, the second solvation shell still has ion-dipole interactions with the metal ion. With an increasing lipophilic moiety of the ligand, the second solvation shell is pushed further away from the metal ion and the complex stability decreases. That is, the ligand forms a lipophilic layer separating the complexed M^{2+} ion from the solvent, and the thickness of this layer will influence the stability of the complex.[27] Molecular models show that for TMEC12 in the TRANS I conformation, the methyl groups on its pendant arms point outwards in the $[ML]^{2+}$ complexes. The larger methyl moiety on the pendant arm of TMEC12 may shield the complexed M^{2+} ion more from the solvent than the hydroxyethyl arms of THEC12 can, which may destabilise $[M(TMEC12)]^{2+}$ relative to $[M(THEC12)]^{2+}$.

The following two examples, for complexes involving the K^+ and Ba^{2+} ions with their similar 8-coordinate radii of 1.51 Å and 1.42 Å, respectively,[21] lend support to the solvation effect being more important for $[ML]^{2+}$ than $[ML]^+$. Firstly, complexes of K^+ and Ba^{2+} with 18C6 (1,4,7,10,13,16-hexaoxacyclooctadecane) and DB-18C6 (2,3,11,12-dibenzo-1,4,7,10,13,16-hexaoxacyclooctadecane) (Figure 3.3) in H_2O show that $[K(DB\text{-}18C6)]^+$ is only 2.3 times less stable than $[K(18C6)]^+$ whereas $[Ba(DB\text{-}18C6)]^{2+}$ is 83.2 times less stable than $[Ba(18C6)]^{2+}$.[28] An even more pronounced effect is evident for the K^+ and Ba^{2+} complexes of C222 (4,7,13,16,21,24-hexaoxa-1,10-diaza-bicyclo-[8.8.8]hexacosane) and DB-C222 (5,6,14,15-dibenzo-4,7,13,16,21,24-hexaoxa-1,10-diazabicyclo[8.8.8]hexacosane) (Figure 3.3). $[K(DB\text{-}C222)]^+$ is only 7.1 times less stable than $[K(C222)]^+$ but $[Ba(DB\text{-}C222)]^{2+}$ is 1000 times less stable than $[Ba(C222)]^{2+}$.[29,30] These results are consistent with the presence of the two benzene groups in DB-18C6 and DB-C222 hindering the approach of solvent to the complexed metal ion, and this destabilising effect is more pronounced for divalent Ba^{2+} than monovalent K^+.

The increased steric hindrance in TMEC12 caused by the bulky methyl group on the coordinating oxygen of its pendant arms may account for the observations that Mg^{2+} in $[Mg(TMEC12)]^{2+}$ is 7-coordinate (while Mg^{2+} in $[Mg(THEC12)]^{2+}$ and $[Mg((S)\text{-}THPC12)]^{2+}$ is 8-coordinate) and the stability order is $[Mg(TMEC12)]^{2+} < [Mg(THEC12)]^{2+} < [Mg((S)\text{-}THPC12)]^{2+}$ (Table 3.2). The increased steric hindrance and lack of flexibility of TMEC12 compared with THEC12 and (*S*)-THPC12 is more evident for the smaller Mg^{2+} ion than for the other alkaline earth metal ions. In addition, the pendant arms of

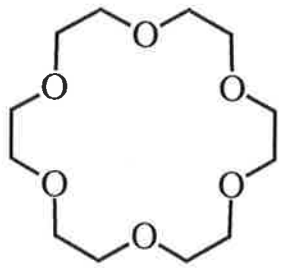

18C6

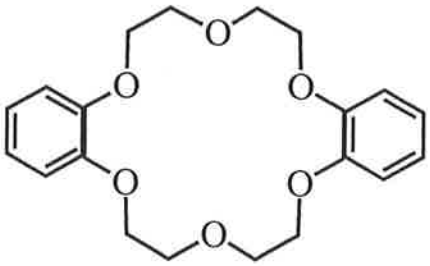

DB-18C6

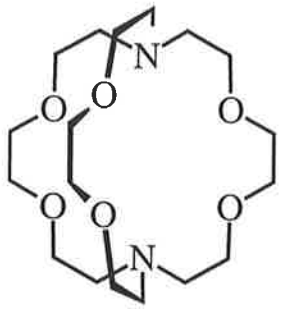

C222

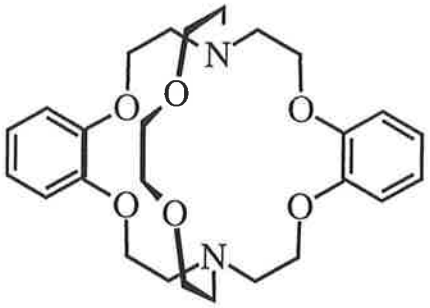

DB-C222

Figure 3.3: The crown ethers 18C6 and DB-18C6, and the cryptands C222 and DB-C222.

TMEC12 and THEC12 contribute to 5-membered chelate rings when coordinated to M^{2+}, and as discussed in Chapter 2, 5-membered chelate rings enhance the selectivity of a ligand for larger metal ions (with an ionic radius of ~ 1.0 Å).[7,31] The combination of these two factors may result in the decreased selectivity of TMEC12 for Mg^{2+}.

As for the alkali metal ion complexes (in Chapter 2), generally the stabilities of $[M((S)\text{-THPC12})]^{2+} > [M(THEC12)]^{2+}$. This may be attributed to the factors discussed in Chapter 2. That is, the effects of both the substituent on the pendant arm of (*S*)-THPC12 enhancing selectivity and the lesser

stereochemical flexibility of (*S*)-THPC12 compared with THEC12 outweigh the steric effect of the increasing substituent size in the pendant arms. Although the lipophilic layer causes significant destabilisation of $[M(TMEC12)]^{2+}$, this effect may be less significant for (*S*)-THPC12, where the methyl group is not attached to the coordinating oxygen of the pendant arms directly involved in bonding.

3.3.2 COMPARISON OF THEC12 WITH CYCLEN

The $[M(THEC12)]^{2+}$ complexes are more stable than $[M(CYCLEN)]^{2+}$ (Table 3.2).[3-5] This is consistent with CYCLEN having fewer donor atoms, and thus only a two-dimensional cavity, to coordinate M^{2+} and stabilise the complex. Attachment of pendant arms onto CYCLEN increases the rigidity of the tetraaza ring and the extent of steric crowding when M^{2+} is coordinated. However, the pendant arm macrocycles are able to more fully encapsulate M^{2+} in a three-dimensional cavity by use of their pendant arms. In addition, the oxygen donor atoms in the pendant arms further enhance stability of the complex because the hard M^{2+} ions have a stronger affinity for oxygen donor atoms than for nitrogen donor atoms. Hence, for L = THEC12, (*S*)-THPC12 and TMEC12, the stabilities of $[ML]^{2+} > [M(CYCLEN)]^{2+}$ and these pendant arm macrocyclic ligands have a much higher selectivity for Ca^{2+} over Mg^{2+} than CYCLEN. A similar relationship was shown for the $[ML]^{+}$ complexes (Chapter 2).

3.4 EFFECT OF RING SIZE

The stabilities for $[M(THEC9)]^{2+}$ determined by potentiometric titration techniques are very low, with values of log $K_S < 2$ quoted in Table 3.2. Other workers have found a selectivity, K_{Sel} (= K_{MgL}/K_{CaL}), of only 0.18 by ^{13}C NMR solution studies in MeCN.[32] (Their work confirms the poor discrimination of THEC9 for Mg^{2+} or Ca^{2+} ions in aqueous solution). In addition, ^{13}C NMR solution studies (Chapter 5) have shown that M^{2+} in $[M(THEC9)]^{2+}$, for M^{2+} = Mg^{2+}, Ca^{2+} and Ba^{2+}, may not necessarily adopt a dominant 6-coordinate structure.

The much lower stabilities of $[M(THEC9)]^{2+}$ by comparison with $[ML]^{2+}$, where L = THEC12, (*S*)-THPC12 and TMEC12, are due to the smaller ring size, the fewer donor atoms to stabilise the complex, and the increased rigidity of THEC9. THEC9 has fewer donor atoms, with only three triaza ring nitrogens and three oxygen donor atoms in the hydroxyethyl arms to coordinate

M^{2+} and stabilise the complex. Furthermore, molecular mechanics calculations have shown that for triaza macrocyclic ligands, the macrocyclic ring may be rigid enough to compete with the chelate ring as a factor governing stability.[31,33] Previous studies have shown that 9-membered macrocyclic ligands tend to show a size selectivity.[17,34-38] This is not the "size–match" selectivity of the metal ion to the preformed cavity size observed by cryptands, but, rather triaza macrocyclic ligands are less flexible than their 12-membered analogues and are not able to accommodate an ill–fitting metal ion as readily as the 12-membered macrocyclic ligands can.[39,40]

Molecular orbital calculations[41] for THEC9 and $[M(THEC9)]^+$ (Figures 2.5 and 2.6) and X-ray diffraction studies[40,42-44] show that the triaza ring of 9-membered ligands is too small to coordinate the metal ion completely within the triaza ring. Therefore, THEC9 adopts a + + + conformation (Figure 2.7) and the metal ion sits above the plane of the three ring nitrogens. A similar situation is envisaged to hold for $[M(THEC9)]^{2+}$, for $M^{2+} = Mg^{2+}$, Ca^{2+}, Sr^{2+} and Ba^{2+}, where the 6-coordinate radii of these alkaline earth metal ions are 0.72 Å, 1.00 Å and 1.35 Å, respectively.[21] This is supported by molecular mechanics calculations where three possible structures denoted AAA, BBB and CCC (Figure 3.4), are available for $[M(THEC9)]^{2+}$, with $M^{2+} = Mg^{2+}$ and Ca^{2+}.[32] Since the carbon atoms of the macrocyclic ring are alternatively above and below the plane of the ring nitrogens, there is an inherent twist of the plane of side-chain carbon atoms directly connected to the ring nitrogens. The twist angle, α, is thus defined by the rotation of the oxygen plane relative to that of the ring nitrogens. The AAA structure is only favoured for $[MgL]^{2+}$ when substituents on the pendant arms of the ligand, denoted R and R' in Figure 3.4, are large enough for there to be a driving force on the side-chains to orientate these groups away from the centre, with no steric hindrance between the side-chains.

For $[M(THEC9)]^{2+}$ there is no such driving force, as the hydroxyethyl pendant arms are not particularly bulky, and so the BBB structure is favoured. In addition, the large twist angle for the AAA structure makes the cavity for the M^{2+} ion quite small, with a more evident effect on the larger Ca^{2+} ion. Thus, $[CaL]^{2+}$ complexes usually adopt the BBB structure.

For L = (*R/S*)-THPC9 and (*R/S*)-THPEC9 (Figure 2.1), with the bulkier (*R/S*)-2-hydroxypropyl and (*R/S*)-2-hydroxy-2-phenyethyl pendant arms respectively, the $[MgL]^{2+}$ complexes adopt the AAA structure.[32] The $[CaL]^{2+}$ complexes adopt the BBB structure seen for $[Ca(THEC9)]^{2+}$ rather than the AAA structure because of the larger size of Ca^{2+} compared with Mg^{2+} and the

Table 3.3: Selectivities, K_{Sel} (= K_{MgL}/K_{CaL}),[a] for L = THEC9 and related macrocycles from ^{13}C NMR competition studies.

		Mode		Twist Angle, α[b]	
Ligand	K_{Sel}	$[MgL]^{2+}$	$[CaL]^{2+}$	$[MgL]^{2+}$	$[CaL]^{2+}$
THEC9	0.18	BBB	BBB	10	5
(*R/S*)-THPC9	590	AAA	BBB	40	5
(*R/S*)-THPEC9	16	AAA		40	

[a] ± 5%. Reproduced from Reference 32. [b] Twist angle refers to the rotation of the oxygen plane relative to that of the ring nitrogens.

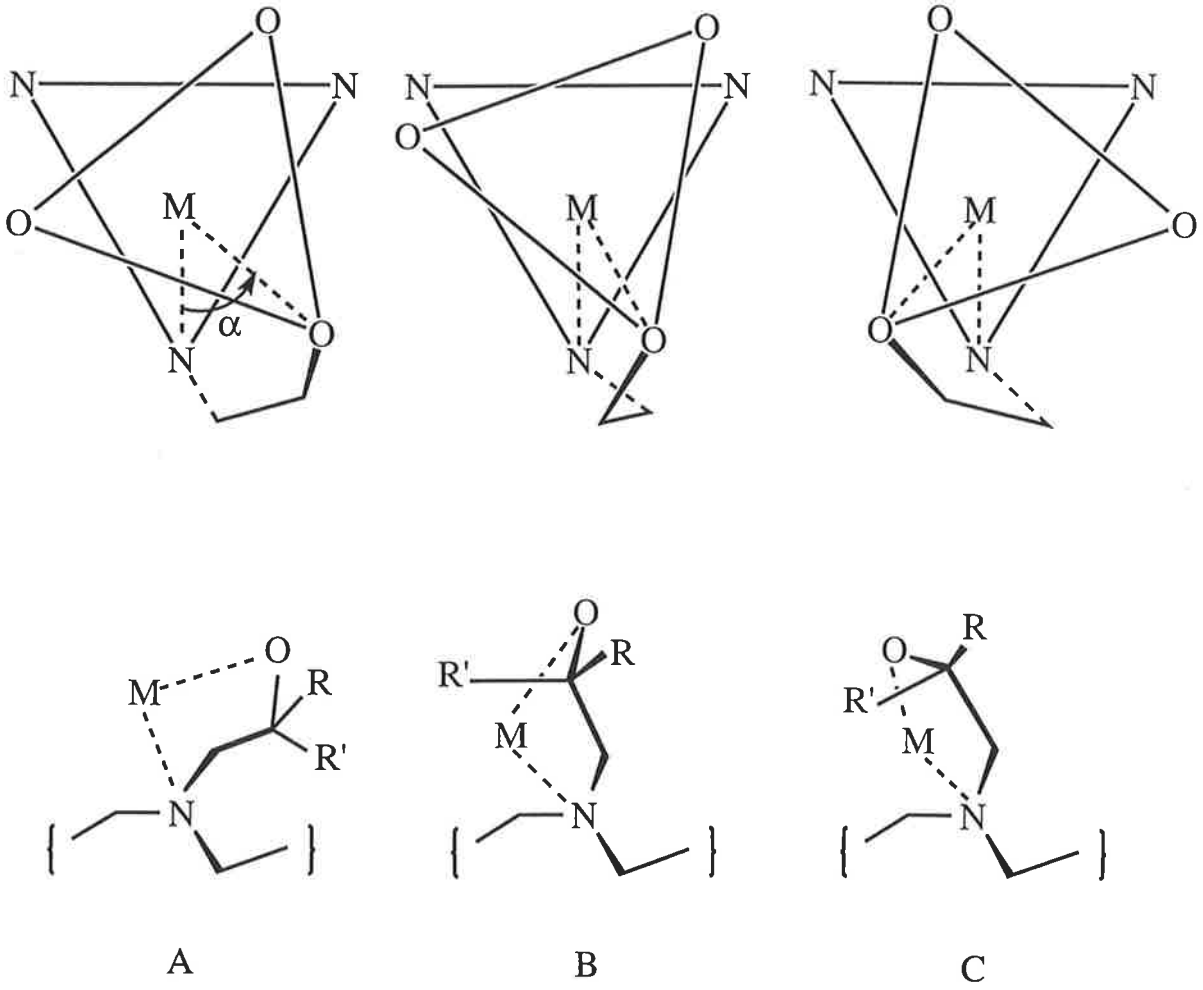

Figure 3.4: Schematic front and top views of the possible coordination modes of the $[M(THEC9)]^{2+}$ complexes for which energy minima were observed by molecular mechanics calculations. (Reproduced from Reference 32).

smaller cavity defined by the AAA structure. It may be postulated that the adoption of these different structures may account for the larger selectivity seen in Table 3.3 of (*R/S*)-THPC9 and (*R/S*)-THPEC9 over THEC9 for Mg^{2+}, but more studies are needed to extend the existing information.

The triaza ligand NOTA (1,4,7-triazacyclononane-*N,N',N''*-triacetic acid), based on the same parent ligand TACN as THEC9, but with carboxylate pendant arms (Figure 3.5), has been shown to be marginally selective for Mg^{2+} over Ca^{2+} (where log K_S = 9.69 and 8.92, respectively).[45] In contrast, DOTA (1,4,7,10-tetraazacyclododecane-*N,N',N'',N'''*-tetraacetic acid), the 12-membered analogue of NOTA (Figure 3.5), shows a marked selectivity for Ca^{2+} (log K_S = 17.23) over Mg^{2+} (log K_S = 11.92).[46] These results lend support to the above discussion for THEC9 and THEC12, where the triaza ligand has a smaller ring size and fewer donor atoms to stabilise the complex, resulting in much lower stabilities for the 9-membered macrocyclic ligands compared with their 12-membered analogues, and a change in selectivity from the larger Ca^{2+} ion to the smaller Mg^{2+} ion as the ring size decreases. Therefore, it is envisaged that since the stabilities of $[M(THEC12)]^{2+}$ << $[M(DOTA)]^{2+}$, the stabilities of $[M(THEC9)]^{2+}$ << $[M(NOTA)]^{2+}$, and this is in accord with the very low stabilities of $[M(THEC9)]^{2+}$ in Table 3.2.

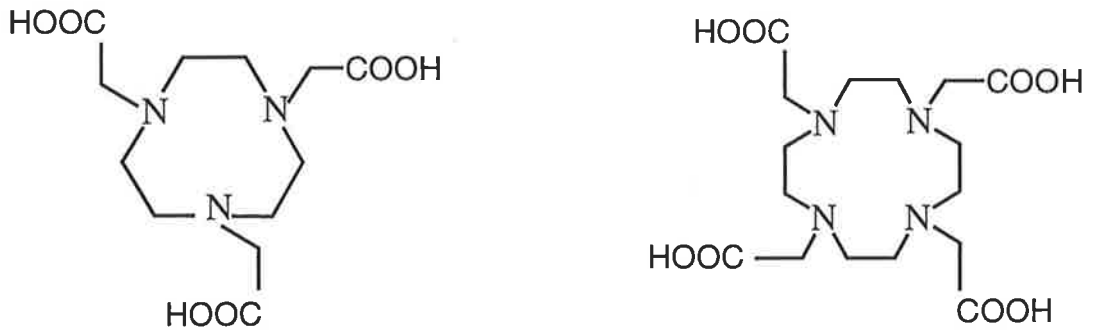

Figure 3.5: The triaza macrocyclic ligand NOTA and its tetraaza macrocyclic analogue DOTA.

BIBLIOGRAPHY

1. A.K.W. Stephens, S.F. Lincoln, *J. Chem. Soc., Dalton Trans.* **1993**, 2123-2126.
2. R.S. Dhillon, S.F. Lincoln. Unpublished material.
3. M.L. Turonek, PhD Thesis, University of Adelaide, **1993**.
4. V.W. Ruangpornvisuti, M.M. Probst, B.M. Rode, *Inorg. Chim. Acta.* **1988**, 144, 21-23.
5. M. Kojima, K. Nakabayaski, S. Ohba, S. Okumoto, J. Fujita, *Bull. Chem. Soc. Jpn.* **1986**, 59, 277-283.
6. R.W. Hay, M.P. Pujari, W.T. Moodie, S. Craig, D.T. Richens, A. Perotti, L. Ungaretti, *J. Chem. Soc., Dalton Trans.* **1987**, 2605-2613.
7. (a) R.D. Hancock, *Prog. Inorg. Chem.* **1989**, 37, 187-291.
   (b) M. Ciampolini, M. Micheloni, N. Nardi, P. Paoletti, P. Dapporto, F. Zanobini, *J. Chem. Soc., Dalton Trans.* **1984**, 1357-1362.
8. D. Bosnich, C.K. Poon, M.L. Tobe, *Inorg. Chem.* **1965**, 4, 1102-1108.
9. D.K. Cabbiness, D.W. Margerum, *J. Am. Chem. Soc.* **1970**, 92, 2151-2153.
10. R.D. Hancock, *Inorg. Chim. Acta.* **1981**, 49, 145-148.
11. R.M. Smith, A.E. Martell, *"Critical Stability Constants Volume 2: Amines"*, Plenum Press, New York, **1975**.
12. M.J. Welch, J. Reibenspies, A.E. Martell, *Inorg. Chim. Acta.* **1995**, 236, 75-82.
13. (a) A.P. Leugger, L. Hertli, T.A. Kaden, *Helv. Chim. Acta.* **1978**, 61, 2296-2306.
    (b) K. Kumar, T. Jin, X. Wang, J.F. Desreux, M.F. Tweedle, *Inorg. Chem.* **1994**, 33, 3823-3929.
    (c) K. Kumar, C.A. Chang, L.C. Francesconi, D. Dischino, M.F. Malley, J.Z. Gougoutas, M.F. Tweedle, *Inorg. Chem.* **1994**, 33, 3567-3575.
14. R. Yang, L.J. Zompa, *Inorg. Chem.* **1976**, 15, 1499-1502.
15. F. Cabral, J. Costa, R. Delgado, J.J.R.F. DaSilva, M.F. Vilhena, *Polyhedron* **1990**, 9, 2847-2857.
16. M. Kodama, E. Kimura, *J. Chem. Soc., Dalton Trans.* **1977**, 1473-1478.
17. S.M. Hart, J.C.A. Boeyens, J.P. Michael, R.D. Hancock, *J. Chem. Soc., Dalton Trans.* **1983**, 1601-1603.
18. M. Kodama, E. Kimura, *J. Chem. Soc., Dalton Trans.* **1976**, 116-120.
19. (a) M. Kodama, E. Kimura, *J. Chem. Soc., Chem. Commun.* **1975**, 326-327.
    (b) R.M. Clay, H. McCormac, M. Micheloni, P. Paoletti, *Inorg. Chem.* **1982**, 21, 2494-2496.
20. (a) R. Delgado, L.C. Siegried, T.A. Kaden, *Helv. Chim. Acta.* **1990**, 73, 140-148.

(b) R. Delgado, J.J.R.F. DaSilva, *Talanta.* **1982**, 29, 815.
21. R.D. Shannon, *Acta. Crystallogr. Sect. A: Cryst. Phys. Diffr. Theor. Gen. Crystallogr.* **1976**, 32, 751-767.
22. J. Burgess, *"Metal Ions in Solution"*, Ellis Horwood, Chichester, **1978**.
23. R.G. Pearson, *J. Am. Chem. Soc.* **1963**, 85, 3533-3539.
24. R.G. Pearson, *Coord. Chem. Rev.* **1990**, 100, 403-425.
25. S. Madback, Honours Thesis, University of Adelaide, **1994**.
26. A.K.W. Stephens, S.F. Lincoln. Unpublished material.
27. J.-M. Lehn, *Struct. Bond. (Berlin)* **1973**, 16, 1-69.
28. G.A. Melson, *"Coordination Chemistry of Macrocyclic Compounds"*, Plenum Press, New York, **1979**.
29. B. Dietrich, *J. Chem. Educ.* **1985**, 62, 954-964.
30. B. Dietrich, J.-M. Lehn, J.-P. Sauvage, *J. Chem. Soc., Chem. Commun.* **1973**, 15-16.
31. R.D. Hancock, P.W. Wade, M.P. Ngwenya, A.S. de Sousa, K.V. Damu, *Inorg. Chem.* **1990**, 29, 1968-1974.
32. J. Huskens, A.D. Sherry, *J. Chem. Soc., Chem. Commun.* **1997**, 845-846.
33. V.J. Thöm, C.C. Fox, J.C.A. Boeyens, R.D. Hancock, *J. Am. Chem. Soc.* **1984**, 106, 5947-5955.
34. W.N. Setzer, C.A. Ogle, G.S. Wilson, R.S. Glass, *Inorg. Chem.* **1983**, 22, 266-271.
35. K. Weighardt, K. Pohl, I. Jibril, G. Huttner, *Angew. Chem. Ed. Engl.* **1984**, 23, 77-78.
36. H.J. Kuppers, A. Neves. C. Pomp, D. Ventur, K. Weighardt, B. Nuber, J. Weiss, *Inorg. Chem.* **1986**, 25, 2400-2408.
37. R.D. Hancock, V.J. Thöm, *J. Am. Chem. Soc.* **1982**, 104, 291-292.
38. R.D. Hancock, S.M. Dobson, J.C.A. Boeyens, *Inorg. Chim. Acta.* **1987**, 221-231.
39. V.J. Thöm, J.C.A. Boeyens, G.J. McDougall, R.D. Hancock, *J. Am. Chem. Soc.* **1984**, 106, 3198-3207.
40. M.J. Van der Merwe, J.C.A. Boeyens, R.D. Hancock, *Inorg. Chem.* **1985**, 24, 1208-1213.
41. S.L. Whitbread, J.M. Weeks, P. Valente, M.A. Buntine, S.F. Lincoln, K.P. Wainwright, *Aust. J. Chem.* **1997**, 50, 853-856.
42. L.J. Zompa, T.N. Margulis, *Inorg. Chim. Acta.* **1978**, 28, L157-L159.
43. J.C.A. Boeyens, A. Forbes, R.D. Hancock, K. Weighardt, *Inorg. Chem.* **1985**, 24, 2926-2931.
44. D.L. Roger, C.A. Swift, L. Lebioda, *Inorg. Chem.* **1984**, 23, 349-354.
45. A. Bevilacqua, R.I. Gelb, W.R. Hebard, L.J. Zompa, *Inorg. Chem.* **1987**, 26, 2699-2706.
46. H. Stetter, W. Frank, *Angew. Chem. Ed. Engl.* **1976**, 15, 686.

CHAPTER 4

COMPLEXATION DYNAMICS OF [M((*R*)-THPEC12)]$^{+}$

4.1 INTRODUCTION

Metal complexes involving unsubstituted tetraaza macrocyclic ligands are often kinetically inert.[1] Attachment of donor groups onto pendant arms of the macrocyclic ligand substantially increases metal incorporation rates. This has been shown for a vast array of macrocycles including the attachment of acetate pendant arms to porphyrins,[2] attachment of pendant arms to CYCLAM,[3-5] and for divalent and trivalent metal ion complexes.[6-12] The selectivities and labilities observed by alkali metal ion complexes of cryptands, crown ethers and related ligands have been widely researched.[13-23] However, there are fewer kinetic studies characterising alkali metal complexes of unsubstituted tetraaza macrocyclic ligands and their pendant arm derivatives.[24-30] Exploration into the kinetic origin of the selectivity of pendant arm macrocycles for particular metal ions will give a more complete understanding of the complexes and of the mechanisms describing the complexation and decomplexation processes. Subsequently, the behaviour of these synthetic ionophores can be compared with that of naturally occurring antibiotics and other carrier molecules (which regulate the transport of alkali metal ions across membranes in biological systems) and to naturally occurring metal-macrocycle centres found in proteins.

Complexation between an alkali metal ion, denoted M^{+}, and the pendant arm macrocycle (*R*)-THPEC12 (1,4,7,10-tetrakis((*R*)-2-hydroxy-2-phenyl-ethyl)-1,4,7,10-tetraazacyclododecane) denoted L, is illustrated by Equation 4.1. This equation demonstrates the interrelation between the kinetic and thermodynamic aspects of complexation since the stability constant, K_S, may be expressed in terms of the complexation rate constant, k_c, and the decomplexation rate constant, k_d:

$$M^{+} + L \underset{k_d}{\overset{k_c}{\rightleftharpoons}} [ML]^{+} \qquad 4.1$$

where

$$K_S = \frac{k_c}{k_d} \qquad 4.2$$

Complexation in solution involves a combination of conformational and solvational changes in the ligand and metal ion, where each step contributes to the overall rate. This may be described by a simplified reaction scheme, called the Eigen–Winkler mechanism:[31-34]

Scheme 4.1

$$M^+ + L \underset{k_{-1}}{\overset{k_1}{\rightleftharpoons}} M^+ \cdots L$$

$$M^+ \cdots L \underset{k_{-2}}{\overset{k_2}{\rightleftharpoons}} ML^+$$

$$ML^+ \underset{k_{-3}}{\overset{k_3}{\rightleftharpoons}} [ML]^+$$

This is a simplified mechanism because desolvation of the metal ion is thought to be a concerted process, where solvent molecules coordinated to the metal ion are replaced by ligand donor atoms in a stepwise manner. Thus, overall complexation probably involves several steps.[35-38] Nonetheless, the steps for complexation may be combined into three main sequences. The first sequence, characterised by the rate constant k_1, involves formation of an outer sphere encounter complex ($M^+ \cdots L$) between the fully solvated metal ion and solvated ligand occurring at a diffusion controlled rate. The second sequence, characterised by the rate constant k_2, involves formation of the first metal ion-ligand bonds, partial desolvation of the metal ion, and partial conformational rearrangements of the ligand. The third sequence, characterised by k_3, involves formation of the remaining metal ion-ligand bonds and progressive desolvation of the metal ion.

The rate constants k_c and k_d determined in this study correspond to the rate-determining steps for complexation and decomplexation, respectively, but cannot be assigned to any individual step in the overall process shown in Scheme 4.1.

Three possible mechanisms may operate to describe the exchange of an alkali metal ion, M^+, between the solvated and complexed environments with (*R*)-THPEC12, denoted L:[13,23,39,40]

(i) Mechanism I: The dissociative (unimolecular) mechanism, described by Equation 4.3. This is a first order process and the rate-determining step is the decomplexation of M^+:

$$M^+ + L \underset{k_d}{\overset{k_c}{\rightleftharpoons}} [ML]^+ \qquad 4.3$$

where k_c is the complexation rate constant
k_d is the decomplexation rate constant
$K_S = \frac{k_c}{k_d}$ is the stability constant.

The second order complexation rate constant, k_c, is the product of the stability constant for the encounter complex and the rate constant for the slowest unimolecular complexation step.

For this process, the rate of exchange is independent of the concentration of solvated M^+ and is expressed as:

$$\text{rate} = k_d [ML^+] \qquad 4.4$$

$$\text{with} \quad \tau_c = \frac{1}{k_d} = \frac{\tau_S \chi_C}{\chi_S} \qquad 4.5$$

where τ_c and τ_s are the mean lifetimes of $[ML]^+$ and solvated M^+, respectively, and χ_c and χ_s are the corresponding mole fractions.

(ii) Mechanism II: The associative (bimolecular) mechanism, described by Equation 4.6. This is a second order process and the rate-determining step involves displacement of complexed M^+ by a second M^+ ion, denoted $^*M^+$:

$$^*M^+ + [ML]^+ \underset{k_b}{\overset{k_b}{\rightleftharpoons}} [^*ML]^+ + M^+ \qquad 4.6$$

where k_b is the bimolecular exchange rate constant.

In contrast to the unimolecular mechanism, the rate of exchange for this process is dependent on the concentration of solvated M^+ and is expressed as:

$$\text{rate} = k_b\,[ML^+][M^+] \qquad 4.7$$

$$\text{with} \quad \tau_c = \frac{1}{k_b[M^+]} = \frac{\chi_s}{\tau_s \chi_c} \qquad 4.8$$

where τ_c and τ_s are the mean lifetimes of $[ML]^+$ and solvated M^+, respectively, and χ_c and χ_s are the corresponding mole fractions.

In the bimolecular mechanism, the ligand should have a conformation such that the simultaneous arrival of a free M^+ ion and departure of the complexed M^+ ion can easily occur.

(iii) Mechanism III: The interchange mechanism, which involves a concerted exchange of solvent and ligand between the inner and outer coordination spheres of M^+. That is, the ligand and solvent in the first and second coordination spheres, respectively, interchange synchronously through an encounter complex. Operation of either of the two subclasses of interchange mechanism, associative (I_a) or dissociative (I_d), depend on the relative importance of bond formation and bond breakage, respectively.

A number of factors, other than the geometrical structure of the complex, determine which mechanism is observed. These factors include temperature, concentration, and nature of the solvent and anion.[23,39,41-46] Although decomplexation of alkali metal ion macrocyclic complexes operate predominantly through the unimolecular exchange mechanism,[13,22,24,26,29,30] the bimolecular mechanism has been found to dominate in solvents with high dielectric constants.[39]

For the unimolecular mechanism, the standard state activation parameters characterising the exchange process may be derived from the temperature dependence of τ_c according to Equations 4.9 and 4.10:[47,48]

$$k_d = \frac{1}{\tau_c} = \frac{k_B T}{h} \exp\left(\frac{-\Delta G_d^{\ddagger}}{RT}\right) \qquad 4.9$$

$$= \frac{k_B T}{h} \exp\left(\frac{-\Delta H_d^{\ddagger}}{RT} + \frac{\Delta S_d^{\ddagger}}{R}\right) \qquad 4.10$$

where τ_c is the mean lifetime of $[ML]^+$
k_B is Boltzmann's constant
h is Planck's constant
R is the gas constant
T is temperature
$\Delta G_d^{\ddagger}$, $\Delta H_d^{\ddagger}$, and $\Delta S_d^{\ddagger}$ are the free energy, enthalpy and entropy of activation, respectively, for the decomplexation process.

A similar equation may be derived for a bimolecular mechanism from the temperature variation of k_b.

For decomplexation to occur, substantial ligand rearrangement is often required with the concomitant sequential resolvation of the metal ion and the ligand. Therefore, complex lability depends on a number of factors: (i) nature and solvation energy of M^+; (ii) flexibility and topology of the pendant arm macrocycle; (iii) number and type of ligand donor atoms; and (iv) solvent. These factors were discussed in Chapters 2 and 3 with respect to variations in the thermodynamic stabilities of alkali and alkaline earth metal ion complexes with (*R*)-THPEC12 and related macrocycles. In this chapter, the influence of these factors on complex lability will be investigated. Thus, exchange of M^+ on $[M((R)\text{-THPEC12})]^+$, where $M^+ = Li^+$ and Na^+, has been studied in DMF (*N,N*-dimethylformamide) by ^{7}Li and ^{23}Na NMR spectroscopy, and their kinetic data are compared with those for complexes of related ligands based on the 12-membered macrocycle CYCLEN.

4.2 EXCHANGE KINETICS OF M^+ ON $[M((R)\text{-THPEC12})]^+$

4.2.1 EXCHANGE OF Na^+ ON $\Delta[Na((R)\text{-THPEC12})]^+$

The temperature dependent coalescence of the ^{23}Na resonances arising from solvated Na^+ and $\Delta[Na((R)\text{-THPEC12})]^+$ as Na^+ exchanges between these environments in DMF (Figure 4.1) yielded the kinetic parameters for the decomplexation of $\Delta[Na((R)\text{-THPEC12})]^+$ (Equation 4.11) shown in Table 4.1:

$$Na^+ + \Delta(R)\text{-THPEC12} \underset{k_d}{\overset{k_c}{\rightleftharpoons}} \Delta[Na((R)\text{-THPEC12})]^+ \qquad 4.11$$

These parameters were derived from the temperature dependence of τ_c, the mean lifetime of Δ[Na((*R*)-THPEC12)]$^+$, through Equation 4.10. The τ_c values were obtained from complete lineshape analysis[49] of the coalescing ^{23}Na resonances observed for the three solutions whose compositions are given in Table 4.1. From Table 4.1 and Figure 4.2, it is apparent that the magnitudes and temperature variations of τ_c for each of the solutions in DMF are indistinguishable. This indicates that τ_c is independent of the concentration of solvated Na^+, so that solvated Na^+ is not involved in the rate-determining step of the dominant pathway for Na^+ exchange on Δ[Na((*R*)-THPEC12)]$^+$. This is consistent with the unimolecular mechanism (Equation 4.3) describing the decomplexation of Na^+ from Δ[Na((*R*)-THPEC12)]$^+$.

The decomplexation rate constant, k_d, is given in Table 4.1 at two different temperatures: (i) at the coalescence temperature, where the most reliable values for k_d are obtained because the exchange induced modification of the spectra is at a maximum; and (ii) at 298.2 K, to allow comparisons of kinetic data between different systems.

4.2.2 EXCHANGE OF Li^+ ON [Li((*R*)-THPEC12)]$^+$

The temperature dependent coalescence of the ^{7}Li resonances arising from solvated Li^+ and [Li((*R*)-THPEC12)]$^+$ in DMF (Figure 4.3) yielded the kinetic parameters for the decomplexation of [Li((*R*)-THPEC12)]$^+$ (Equation 4.12) shown in Table 4.2:

$$Li^+ + (R)\text{-THPEC12} \underset{k_d}{\overset{k_c}{\rightleftharpoons}} [Li((R)\text{-THPEC12})]^+ \qquad 4.12$$

(where it is important to note that neither the Δ or Λ chirality can be assigned to [Li((*R*)-THPEC12)]$^+$ as the calculated structure, discussed in Chapter 2, shows significant distortion).

The kinetic parameters were obtained through the temperature dependence of τ_c, the mean lifetime of [Li((*R*)-THPEC12)]$^+$, through Equation 4.10. The τ_c values were obtained from complete lineshape analysis[49] of the coalescing ^{7}Li resonances observed for three solutions of different concentrations, as shown in Table 4.2. It is apparent from Table 4.2 and Figure 4.2 that the magnitudes and temperature variations of τ_c for each of these solutions in DMF are indistinguishable. This is consistent with τ_c being independent of the

Table 4.1: Solution composition and kinetic parameters[a] for Na^+ exchange on $\Delta[(NaL)]^+$, where L = (R)-THPEC12, in DMF.

Soln.	$[Na^+_{solvated}]$ mol dm^{-3}	$[\Delta(NaL)^+]$ mol dm^{-3}	k_d(329.6 K) s^{-1}	k_d(298.2 K) s^{-1}	$\Delta H_d^{\ddagger}$ kJ mol^{-1}	$\Delta S_d^{\ddagger}$ J K^{-1} mol^{-1}
i	0.0835	0.0495	934 ± 13	70.5 ± 1.6	64.6 ± 0.4	7.1 ± 1.4
ii	0.0512	0.0498	1015 ± 18	73.0 ± 1.9	65.9 ± 0.5	11.8 ± 1.8
iii	0.0360	0.0670	997 ± 16	76.8 ± 1.6	64.1 ± 0.5	6.2 ± 1.7
(i – iii)[b]	–	–	982 ± 16	73.4 ± 1.7	64.9 ± 0.5	8.4 ± 1.6

[a]Errors represent 1 standard deviation from the least squares fit of the experimental τ_c data to Equation 4.10.
[b]Simultaneous fit of all data.

Table 4.2: Solution composition and kinetic parameters[a] for Li^+ exchange on $[(LiL)]^+$, where L = (R)-THPEC12, in DMF.

Soln.	$[Li^+_{solvated}]$ mol dm^{-3}	$[(LiL)^+]$ mol dm^{-3}	k_d(260.1 K) s^{-1}	k_d(298.2 K) s^{-1}	$\Delta H_d^{\ddagger}$ kJ mol^{-1}	$\Delta S_d^{\ddagger}$ J K^{-1} mol^{-1}
i	0.0132	0.0069	27.5 ± 0.6	400 ± 14	43.0 ± 0.6	-50.9 ± 2.5
ii	0.0125	0.0119	27.3 ± 0.4	392 ± 9	42.8 ± 0.4	-51.7 ± 1.7
iii	0.0071	0.0130	27.7 ± 0.4	382 ± 12	42.1 ± 0.5	-54.3 ± 2.1
(i – iii)[b]	–	–	27.5 ± 0.5	391 ± 12	42.6 ± 0.5	-52.3 ± 2.1

[a]Errors represent 1 standard deviation from the least squares fit of the experimental τ_c data to Equation 4.10.
[b]Simultaneous fit of all data.

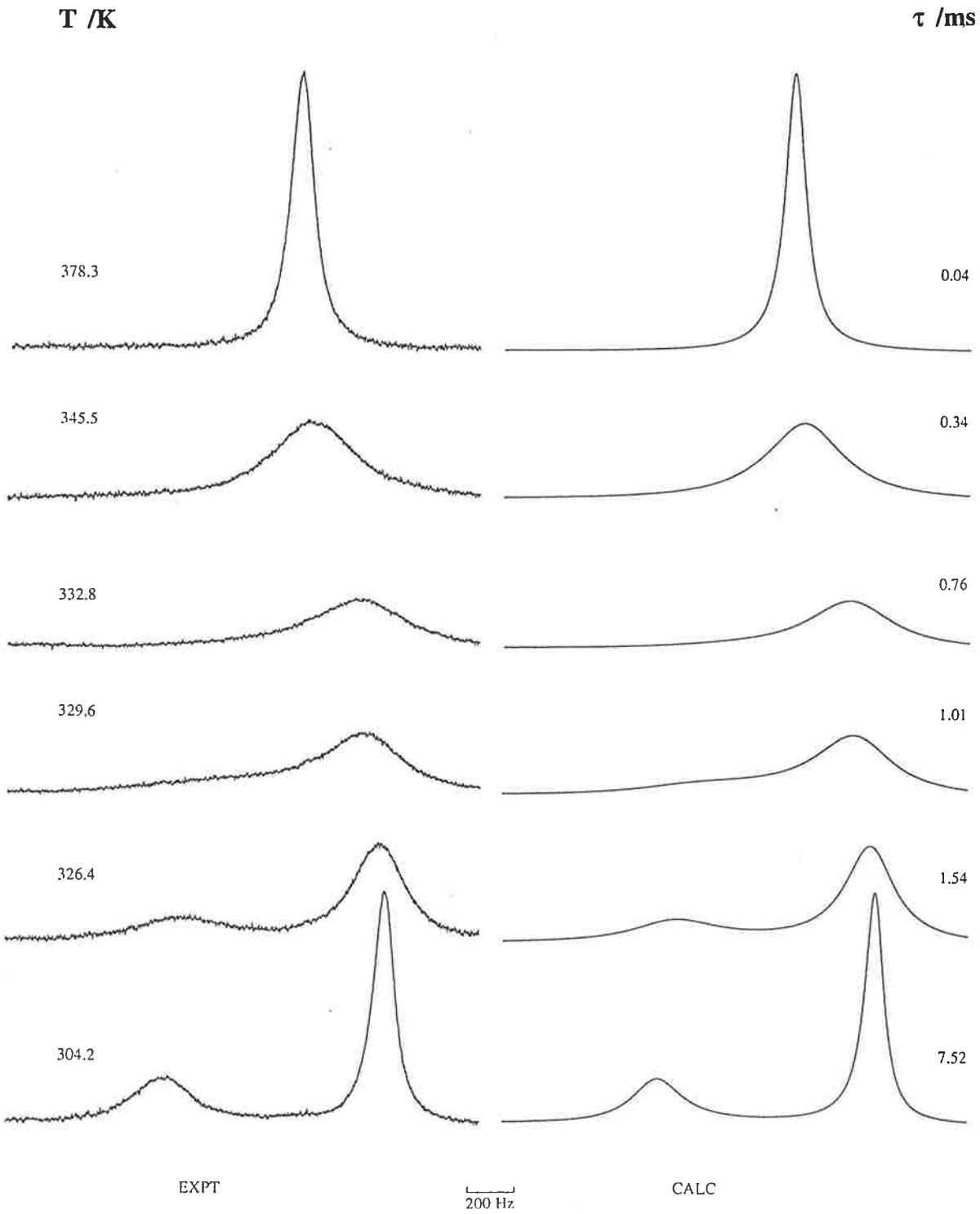

Figure 4.1: Typical exchange-modified 79.39 MHz NMR spectra of a DMF solution of $NaClO_4$ (0.0835 mol dm^{-3}) and Δ[Na((*R*)-THPEC12)]$^+$ (0.0495 mol dm^{-3}). Experimental temperatures and spectra appear to the left of the figure and the best-fit calculated lineshapes and corresponding τ_c values appear to the right. The resonance of solvated Na^+ appears downfield from that of Δ[Na((*R*)-THPEC12)]$^+$.

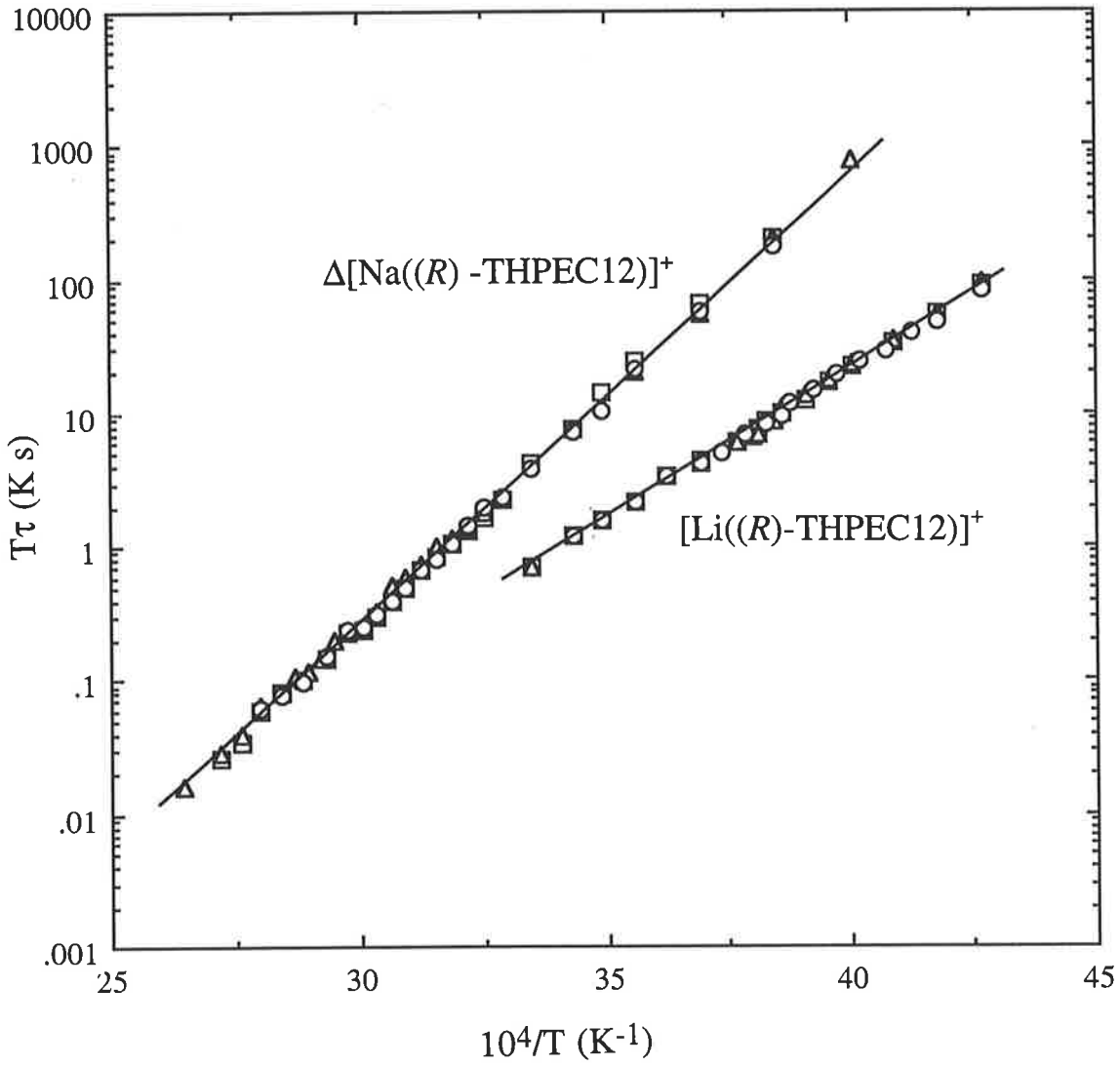

Figure 4.2: Temperature variations of τ_c for $[M((R)\text{-THPEC12})]^+$, where $M^+ = Li^+$ and Na^+, in DMF. Data points for the $\Delta[Na((R)\text{-THPEC12})]^+$ solutions i – iii in Table 4.1 are represented by triangles, squares and circles, respectively. Data points for the $[Li((R)\text{-THPEC12})]^+$ solutions i – iii in Table 4.2 are represented by triangles, squares and circles, respectively. The solid lines represent the simultaneous best-fit of the data derived from each set of three solutions to Equation 4.10.

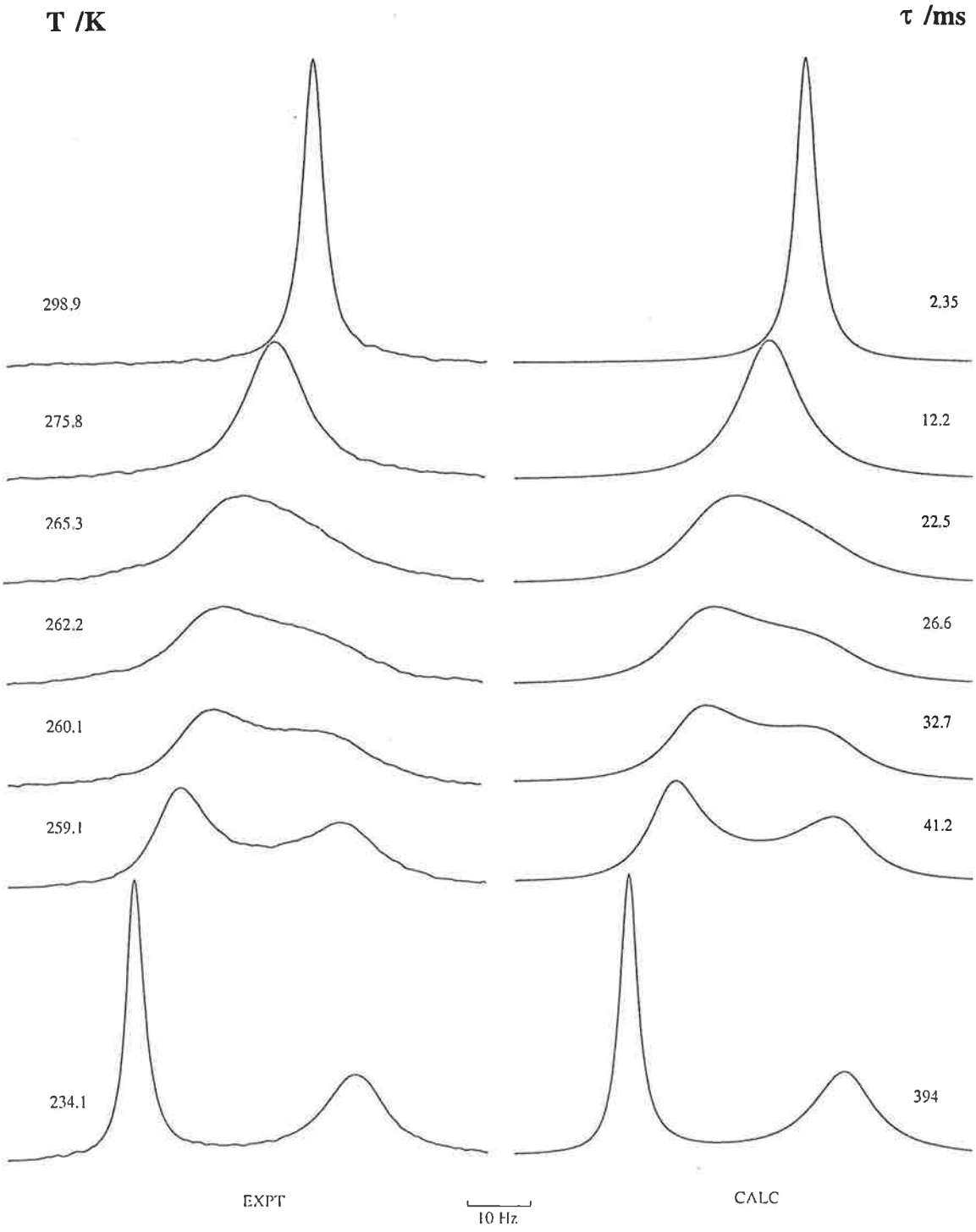

Figure 4.3: Typical exchange-modified 116.64 MHz NMR spectra of a DMF solution of $LiClO_4$ (0.0132 mol dm^{-3}) and $[Li((R)\text{-THPEC12})]^+$ (0.0069 mol dm^{-3}). Experimental temperatures and spectra appear to the left of the figure and the best-fit calculated lineshapes and corresponding τ_c values appear to the right. The resonance of solvated Li^+ appears downfield from that of $[Li((R)\text{-THPEC12})]^+$.

Table 4.3: Kinetic and equilibrium parameters[a] for M^+ exchange on $[ML]^+$, where L = (*R*)-THPEC12, and other complexes in DMF at 298.2 K.

Complex	10^{-5} k_c [b] $dm^3mol^{-1}s^{-1}$	k_d s^{-1}	$\Delta H_d^{\ddagger}$ $kJmol^{-1}$	$\Delta S_d^{\ddagger}$ $JK^{-1}mol^{-1}$	log K_S (K_S/dm^3mol^{-1})
$[LiL]^+$	5.27	391	42.6	-52.3	3.13
$\Delta[NaL]^+$	13.1	73.4	64.9	8.4	4.25
[c]$[Li(THEC12)]^+$	5.74	587	41.8	-51.9	2.99
[c]$[Na(THEC12)]^+$	7.00	299	56.4	-8.4	3.37
[d]$[Li(TMEC12)]^+$	1.3	31.4	54.3	-34.3	3.61
[d]$[Na(TMEC12)]^+$	36.4	7.6	76.2	27.7	5.68

[a]This work unless stated otherwise. [b]$k_c = k_dK_S$. [c]Reference 24. [d]Reference 26.

concentration of solvated Li^+ and the operation of a unimolecular mechanism (Mechanism I) for the decomplexation of Li^+ from $[Li((R)\text{-THPEC12})]^+$.

In DMF, the 13 fold greater stability of $\Delta[Na((R)\text{-THPEC12})]^+$ compared with $[Li((R)\text{-THPEC12})]^+$ (Table 4.3) results from the 5.3 times smaller decomplexation rate constant, k_d(298.2 K), and the 2.5 times larger complexation rate constant, k_c(298.2 K), of $\Delta[Na((R)\text{-THPEC12})]^+$ over $[Li((R)\text{-THPEC12})]^+$. The ^{13}C NMR solution studies in DMF (Chapter 5) show that both Li^+ and Na^+ are 8-coordinate in $[M((R)\text{-THPEC12})]^+$, so that the different $\Delta H_d^{\ddagger}$ and $\Delta S_d^{\ddagger}$ values (Table 4.3) for $[Li((R)\text{-THPEC12})]^+$ and $\Delta[Na((R)\text{-THPEC12})]^+$ are not due to a different number of pendant arms coordinating the metal ions.

Contributions from $\Delta H_d^{\ddagger}$ to the activation energy of decomplexation correspond to the resolvation of M^+, opening of the complex and M^+-ligand bond breakage.[19] Thus the smaller k_d(298.2 K) and larger $\Delta H_d^{\ddagger}$ for $\Delta[Na((R)\text{-THPEC12})]^+$ compared with $[Li((R)\text{-THPEC12})]^+$ are consistent with the more optimum bonding of Na^+ over Li^+ by (*R*)-THPEC12, and less induced

strain in Δ[Na((*R*)-THPEC12)]$^+$. That is, the greater electrostatic interaction between Na^+ and (*R*)-THPEC12 results in an increase in the activation enthalpy required to dissociate Na^+ from (*R*)-THPEC12 in the decomplexation process. In addition, since Li^+ is smaller than Na^+, Li^+ probably induces steric hindrance between the coordinated pendant arms of (*R*)-THPEC12 (as discussed in Chapter 2), resulting in a higher lability of [Li((*R*)-THPEC12)]$^+$ towards decomplexation.

The smaller k_c(298.2 K) characterising [Li((*R*)-THPEC12)]$^+$ compared with Δ[Na((*R*)-THPEC12)]$^+$ may be attributed to the larger solvation energy, or stronger solvent-metal ion interactions, of Li^+ compared with Na^+ giving a larger contribution from desolvation of the metal ion to the activation energy for complexation. This solvation effect is also reflected in the contribution from $\Delta S_d^{\ddagger}$ to the activation energy of decomplexation. That is, the significantly more negative $\Delta S_d^{\ddagger}$ characterising [Li((*R*)-THPEC12)]$^+$ compared with that of Δ[Na((*R*)-THPEC12)]$^+$ is consistent with the greater coordination of solvent molecules by Li^+ in the transition state while still bound to (*R*)-THPEC12.

4.2.3 PATHWAYS FOR M^+ EXCHANGE ON [M((*R*)-THPEC12)]$^+$

Two possible pathways for the exchange of M^+ on [M((*R*)-THPEC12)]$^+$ are illustrated by the reaction scheme in Figure 4.4. This is a simplified scheme because it shows neither the solvational changes in M^+ nor the conformational and coordination changes in (*R*)-THPEC12 required for complexation and decomplexation. The final state [M((*R*)-THPEC12)]$^+$ species is based on the structures proposed by the ^{13}C NMR solution studies in DMF (Chapter 5), where both Li^+ and Na^+ are 8-coordinate, with a square antiprismatic geometry.

Pathway A involves initial coordination of M^+ to the four ring nitrogens of (*R*)-THPEC12, where M^+ sits above the plane of the tetraaza ring. The four (*R*)-2-hydroxy-2-phenylethyl pendant arms are then sequentially coordinated. Pathway B involves initial coordination of M^+ to two ring nitrogens and two (*R*)-2-hydroxy-2-phenylethyl pendant arms of (*R*)-THPEC12 so that M^+ is bound perpendicularly to the plane of the tetraaza ring. This is followed by coordination of the remaining two ring nitrogens and the other two (*R*)-2-hydroxy-2-phenylethyl pendant arms. Decomplexation is the reverse of either Pathway A or B.

Pathway A is plausible because stable [M(CYCLEN)]$^+$ complexes have been observed, where CYCLEN has no pendant arms to coordinate M^+. On the

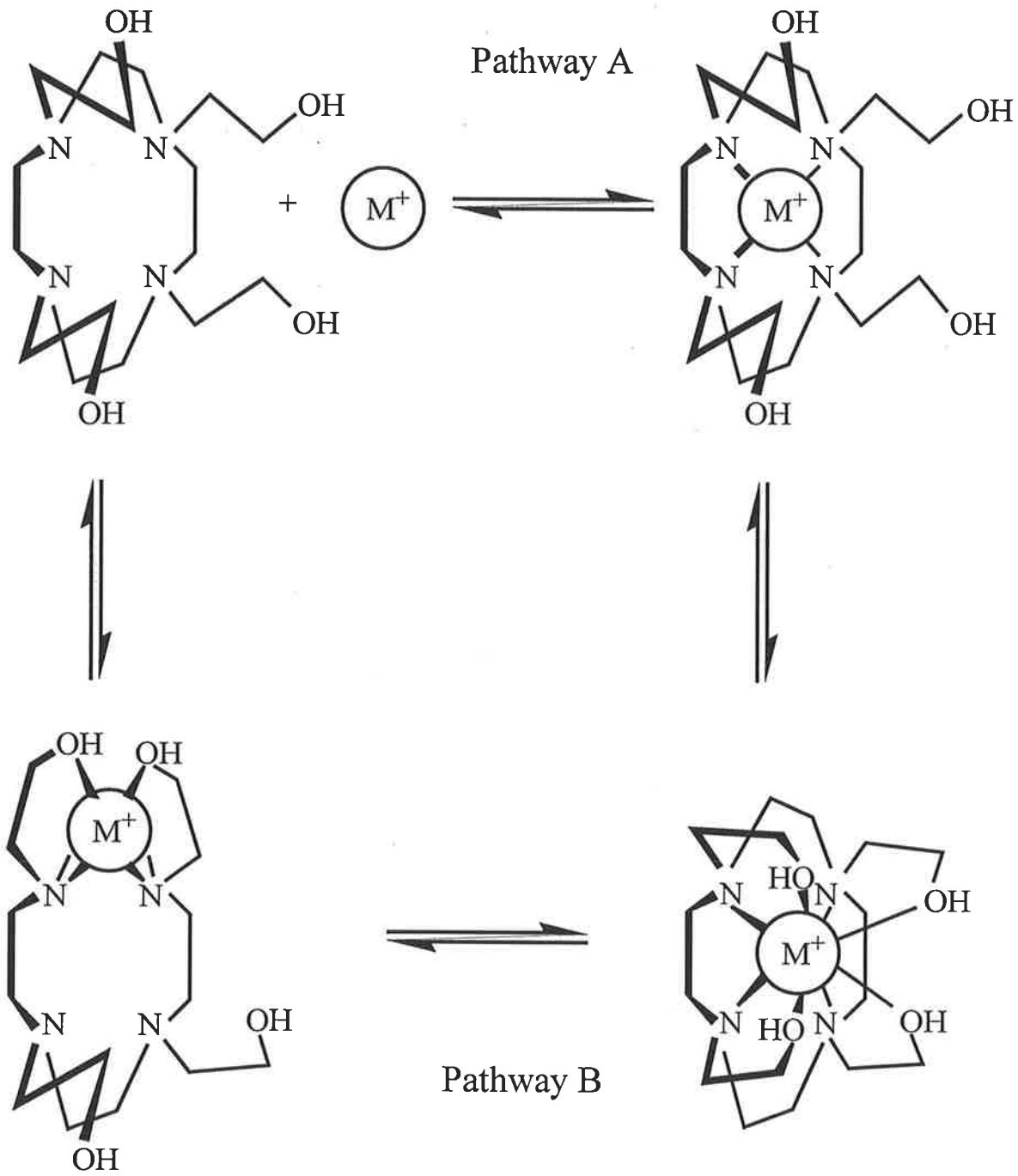

Figure 4.4: Simplified proposed pathways for the exchange of M^+ on $[M((R)\text{-THPEC12})]^+$. For simplicity, the phenyl substituents on the pendant arms of (*R*)-THPEC12 have been omitted from the diagram. Pathway A involves initial coordination of M^+ by the four tetraaza nitrogens of (*R*)-THPEC12, followed by coordination of the four (*R*)-2-hydroxy-2-phenyl-ethyl pendant arms. Pathway B involves initial coordination of M^+ by two nitrogens and two pendant arms, followed by subsequent coordination to the remaining two nitrogens and pendant arms of (*R*)-THPEC12.

other hand, the pendant arms of macrocyclic ligands may enhance complexation by providing initial points of attachment outside the macrocyclic ring for the incoming metal ion, as proposed by Pathway B. However, it is not possible to distinguish between the two complexation pathways from the available NMR data and, although the k_d(298.2 K) values in this study represent the slowest step for the sequential decomplexation of $[M((R)\text{-THPEC12})]^+$, it is not clear which step they can be assigned to. It is possible that a double inversion at each nitrogen of (*R*)-THPEC12 may characterise k_d, as proposed for metal complexes of related pendant arm macrocycles and by similar rate-limiting conformational changes associated with complexes involving crown ethers. [29,30,42-45,50-55]

4.3 EFFECT OF PENDANT ARMS ON LABILITY

A greater insight into the kinetic characteristics of $[M((R)\text{-THPEC12})]^+$, for $M^+ = Li^+$ and Na^+, may be gained by comparison with systems for which k_d(298.2 K) characterises the unimolecular decomplexation process. As for $[M((R)\text{-THPEC12})]^+$ in Section 4.2, it has been shown that the decomplexation of M^+ from $[M(THEC12)]^+$ and $[M(TMEC12)]^+$ in DMF operates by the unimolecular mechanism.[21,22] As discussed in Chapter 2, M^+ in each of these complexes is 8-coordinate and $[ML]^+$ adopts the TRANS I conformer. Therefore, the ability of these ligands to bind M^+ without significant structural changes to the TRANS I conformer decreases the activation energy contribution from stereochemical changes in the ligand associated with the decomplexation mechanism. The stabilities, K_S, decrease in the sequence $[M(TMEC12)]^+ > [M((R)\text{-THPEC12})]^+ > [M(THEC12)]^+$, which is mainly due to k_d(298.2 K) increasing (and $\Delta H_d^{\ddagger}$ decreasing) along this progression (Table 4.3). These trends are discussed in more detail below.

The factors influencing the labilities of these complexes are the same as those affecting their stabilities. These factors include: (i) effect of substituent groups on the pendant arms to enhance or hinder complexation; (ii) steric hindrance between the pendant arms in the complex; and (iii) hydrogen bonding ability of the ligand. It was apparent in Chapter 2 that the alkali metal complexes of (*R*)-THPEC12 are more stable than $[M(THEC12)]^+$. The smaller k_d(298.2 K) and larger $\Delta H_d^{\ddagger}$ characterising $[M((R)\text{-THPEC12})]^+$ compared with $[M(THEC12)]^+$ indicate that, as for the trends in K_S, addition of a phenyl substituent at the αcarbon (αC) of the pendant arms of THEC12 culminates in stabilisation of the complex and less stereochemical flexibility of the ligand. Although k_c(298.2 K) is larger for $\Delta[Na((R)\text{-THPEC12})]^+$ than for $[Na(THEC12)]^+$, the reverse is true for the analogous Li^+ complexes. This is

probably because the effect of steric hindrance is more pronounced for Li^+, due to both the smaller size of Li^+ compared with Na^+ and the steric effect of the substituent on the pendant arms of the ligand being more significant for $[Li((R)\text{-THPEC12})]^+$ than for $[Li(THEC12)]^+$. That is, as the substituent size at the αC of the ligand increases from a hydrogen (in THEC12) to a phenyl group (in (*R*)-THPEC12), the steric strain in the Li^+ complexes imposed by the smaller size of Li^+ compared with Na^+ may be increased further still by steric crowding in the pendant arms. This is corroborated by the computed structure of $[Li((S)\text{-THPEC12})]^+$ (Chapter 2), which exhibits significant distortion from the C_4 symmetry observed for the other alkali metal ion complexes of (*S*)-THPEC12.[56] The smaller k_c characterising $[LiL]^+$ compared with $[NaL]^+$, for L = (*R*)-THPEC12 and THEC12, (Table 4.3) is consistent with the greater solvation energy of Li^+ compared with Na^+, which also gives a substantially more negative contribution from $\Delta S_d^{\ddagger}$ to the activation energy of decomplexation.

The same factors discussed above are applicable for the $[M(TMEC12)]^+$ complexes. For TMEC12, the bulkier methyl group on the coordinating oxygen may cause steric hindrance in the complex. Conversely, the methoxy group may enhance complex stability by the inductive effect of the methyl group. In Chapter 2 it was apparent that the $[M(TMEC12)]^+$ complexes are more stable than $[M((R)\text{-THPEC12})]^+$, and that TMEC12 shows the highest selectivity for Na^+ of all the pendant arm macrocycles studied in that chapter. Thus, the smaller k_d(298.2 K) and larger $\Delta H_d^{\ddagger}$ (Table 4.3) for $[M(TMEC12)]^+$ compared with $[M((R)\text{-THPEC12})]^+$ are consistent with the methoxy donor group of TMEC12 being a stronger electron pair donor than the hydroxy group of (*R*)-THPEC12. This results in greater electrostatic attraction between M^+ and TMEC12, thus slowing the rate of release of M^+ from $[M(TMEC12)]^+$ and increasing the activation energy required for decomplexation.

As for $[Li((R)\text{-THPEC12})]^+$ and $[Li(THEC12)]^+$, k_c is smaller for $[Li(TMEC12)]^+$ than for $[Na(TMEC12)]^+$, which is probably due to the smaller Li^+ being more affected than Na^+ by steric hindrance in TMEC12. Indeed, the steric hindrance for Li^+ and the inductive effect of the methyl group of TMEC12 is reflected in the 28 times larger k_c (and 4.1 times smaller k_d) of $[Na(TMEC12)]^+$ compared with $[Li(TMEC12)]^+$ in DMF. By comparison, k_c for $[Na(THEC12)]^+$ is only 1.2 times higher (and k_d is 2.0 times lower) than that of $[Li(THEC12)]^+$, and k_c for $\Delta[Na((R)\text{-THPEC12})]^+$ is only 2.5 times higher (and k_d is 5.3 times lower) than that of $[Li((R)\text{-THPEC12})]^+$. This demonstrates the substantially higher selectivity of TMEC12 for Na^+ over Li^+ compared with THEC12 and (*R*)-THPEC12, and the importance of bond breaking in the decomplexation process.

4.4 EFFECT OF SOLVENT ON LABILITY

The highly insoluble nature of (*R*)-THPEC12 and its metal complexes in most common solvents prevents a further study into the effects of solvent on lability for this ligand. However, such studies for the related ligands THEC12 and TMEC12 are possible in a range of solvents, and the results in MeCN (acetonitrile) and PC (1,2-propanediol cyclic carbonate) appear with those in DMF in Table 4.5.

The exchange of Na^+ on $[Na(THEC12)]^+$ falls within the NMR timescale in MeCN, however due to boiling point limitations of the solvent, kinetic data could only be obtained up to 350.1 K. The temperature dependent coalescence of the ^{23}Na resonances characterising this exchange appears in Figure 4.5. The kinetic parameters shown in Tables 4.4 and 4.5 were obtained from the temperature dependence of τ_c, the mean lifetime of $[Na(THEC12)]^+$, through Equation 4.10. The τ_c values were determined by complete lineshape analysis[49] of the coalescing ^{23}Na resonances observed for each of the three solutions in Table 4.4 of different Na^+ to $[Na(THEC12)]^+$ ratios and constant total Na^+ concentration. It is apparent from Table 4.4 that τ_c is concentration independent over the concentration range for this system. Thus, the decomplexation of Na^+ from $[Na(THEC12)]^+$ in MeCN proceeds by a unimolecular mechanism.

Table 4.4: Solution composition and kinetic parameters[a] for Na^+ exchange on $[(NaL)]^+$, where L = THEC12, in MeCN.

Soln.	$[Na^+_{solvated}]$ mol dm^{-3}	$[(NaL)^+]$ mol dm^{-3}	k_d(350.1 K) s^{-1}	k_d(298.2 K) s^{-1}	$\Delta H_d^{\ddagger}$ kJ mol^{-1}	$\Delta S_d^{\ddagger}$ J K^{-1} mol^{-1}
i	0.0615	0.0398	1841 ± 12	74.6 ± 1.3	51.0 ± 0.4	-38.2 ± 1.2
ii	0.0452	0.0561	1751 ± 24	78.0 ± 2.8	49.4 ± 0.8	-43.1 ± 2.4
iii	0.0266	0.0747	1738 ± 11	78.8 ± 1.3	49.1 ± 0.3	-44.1 ± 1.1
(i – iii)[b]	–	–	1742 ± 9	78.5 ± 1.0	49.2 ± 0.3	-43.7 ± 0.9

[a]Errors represent 1 standard deviation from the least squares fit of the experimental τ_c data to Equation 4.10.
[b]Simultaneous fit of all data.

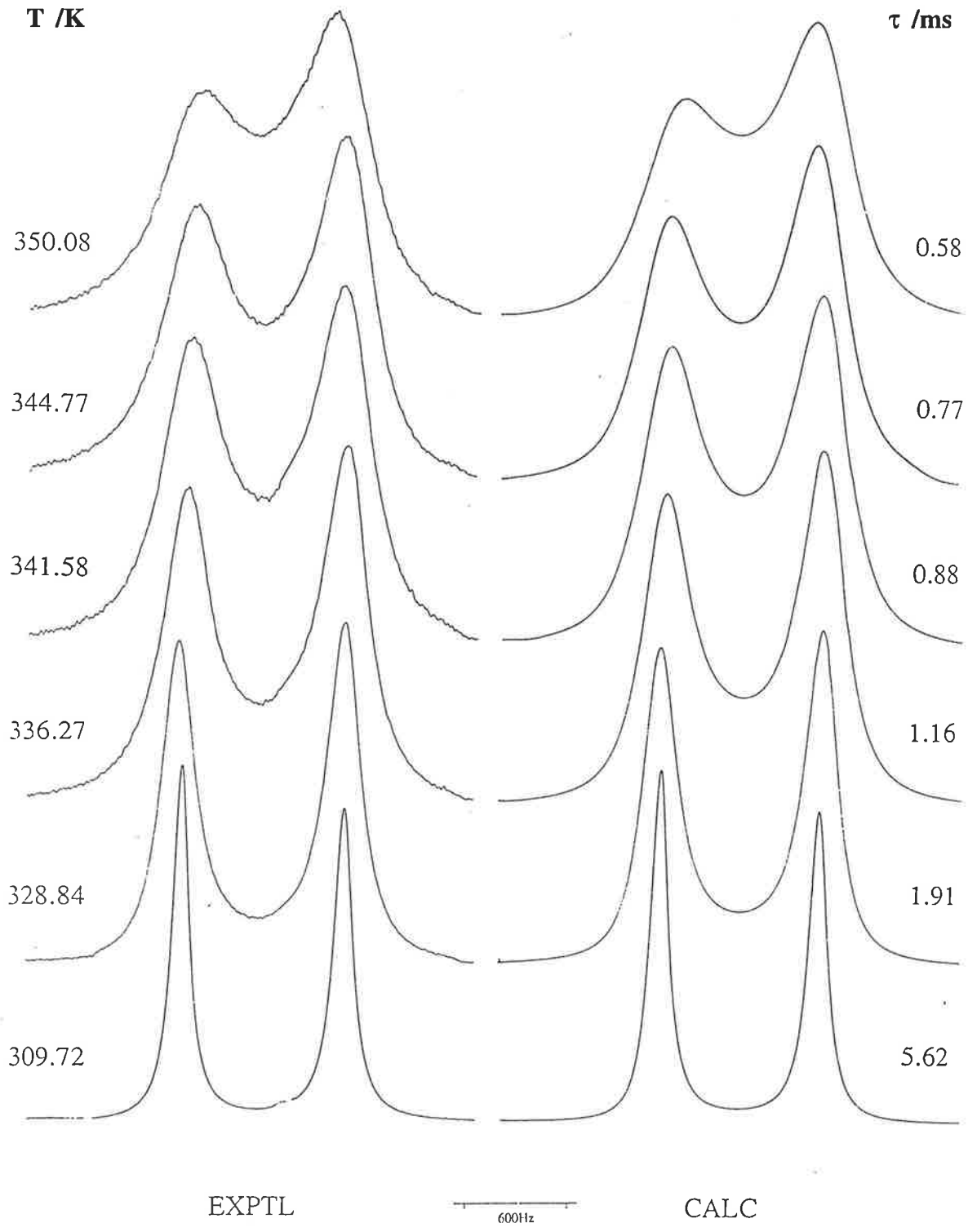

Figure 4.5: Exchange-modified 79.39 MHz NMR spectra of a MeCN solution of $NaClO_4$ (0.0452 mol dm^{-3}) and $[Na(THEC12)]^+$ (0.0561 mol dm^{-3}). Experimental temperatures and spectra appear to the left of the figure and the best-fit calculated lineshapes and corresponding τ_c values appear to the right. The resonance of solvated Na^+ is downfield from that of $[Na(THEC12)]^+$.

Table 4.5: Kinetic and equilibrium parameters for M^+ exchange on [M((*R*)-THPEC12)]$^+$ and other complexes in a range of solvents at 298.2 K.

Complex	Solvent	D_N [a]	$10^{-5}\ k_c$ [b] $dm^3\ mol^{-1}\ s^{-1}$	k_d s^{-1}	$\Delta H_d^{\ddagger}$ $kJ\ mol^{-1}$	$\Delta S_d^{\ddagger}$ $J\ K^{-1}\ mol^{-1}$	$\log K_s$ (K_s/$dm^3\ mol^{-1}$)
[c][Na(CYCLEN)]$^+$	MeCN	14.1	–	> 705	–	–	3.60
[c][Na(CYCLEN)]$^+$	PC	15.1	–	> 2440	–	–	5.45
[c][Na(THEC12)]$^+$	MeCN	14.1	3588	78.5	49.2	-43.7	6.66 [d]
[d][Na(THEC12)]$^+$	PC	15.1	8066	26.1	57.7	-24.0	7.49
[e][Na(THEC12)]$^+$	DMF	26.6	7.00	299	56.4	-8.4	3.37
[f][Na(TMEC12)]$^+$	MeCN	14.1	–	< 41	–	–	9.13
[f][Na(TMEC12)]$^+$	PC	15.1	–	< 87	–	–	8.2 [c]
[f][Na(TMEC12)]$^+$	DMF	26.6	36.4	7.6	76.2	27.7	5.68
[c]Δ[Na((*R*)-THPEC12)]$^+$	DMF	26.6	13.1	73.4	64.9	8.4	4.25
[c][Li(CYCLEN)]$^+$	PC	15.1	–	fast [g]	–	–	5.60

Table 4.5 continued.

[c][Li(THEC12)]$^+$	MeCN	14.1	–	fast [g]	–	–	8.07 [d]
[c][Li(THEC12)]$^+$	PC	15.1	–	fast [g]	–	–	8.90 [d]
[e][Li(THEC12)]$^+$	DMF	26.6	5.74	587	41.8	-51.9	2.99
[f][Li(TMEC12)]$^+$	MeCN	14.1	–	< 8.5	–	–	9.34
[f][Li(TMEC12)]$^+$	PC	15.1	–	< 11.9	–	–	8.0 [c]
[f][Li(TMEC12)]$^+$	DMF	26.6	1.3	31.4	54.3	-34.3	3.61
[c][Li((*R*)-THPEC12)]$^+$	DMF	26.6	5.27	391	42.6	-52.3	3.13

[a]D_N's from Reference 64. [b]$k_c = k_d K_S$. [c]This work. [d]Reference 25. [e]Reference 24. [f]Reference 26. [g]In the fast exchange limit on the NMR timescale.

In MeCN and PC, a single narrow ^{7}Li resonance is observed for a solution containing $[Li(THEC12)]^+$ and solvated Li^+ over the solvent liquid temperature range. Thus, Li^+ exchange on $[Li(THEC12)]^+$ in these solvents is in the very fast exchange limit of the ^{7}Li NMR timescale, where no kinetic data could be derived.

From Table 4.5 it is evident that there is a substantial variation in k_c and k_d with the nature of the solvent for $[Na(THEC12)]^+$, where the magnitude of k_d(298.2 K) for $[Na(THEC12)]^+$ varies with the nature of the solvent in the sequence DMF > PC < MeCN. For the range of solvents for which quantitative data for $[Na(THEC12)]^+$ is available, there is a more significant change in k_c than k_d with the nature of the solvent. That is, k_c characterising $[Na(THEC12)]^+$ in PC is 1152 times larger (while k_d is only 11.4 times smaller) than that in DMF, and k_c characterising $[Na(THEC12)]^+$ in MeCN is 2.25 times smaller (while k_d is 3.01 times larger) than that in PC. Thus, variations in k_c mainly dominate variations in the stability of $[Na(THEC12)]^+$, where variations in k_c for $[Na(THEC12)]^+$ follow the sequence DMF << PC > MeCN. The dramatic increase in k_c as the electron donating ability, D_N, of the solvent decreases from DMF to PC is consistent with the rate-determining step for complexation involving considerable desolvation of Na^+. The less marked effect on k_d(298.2 K) for $[Na(THEC12)]^+$ with changing solvent reflects the lesser involvement of solvent in the rate-determining step for decomplexation. Therefore, the transition state for decomplexation probably more closely resembles the equilibrium solution structure of $[Na(THEC12)]^+$ than that of solvated Na^+ and free THEC12. Similar variations in k_c and k_d with the nature of the solvent are observed for $[Na(TMEC12)]^+$.[26]

The lower k_c (and higher k_d) for $[Na(THEC12)]^+$ in MeCN compared with those in PC is in accord with the stability trend of $[Na(THEC12)]^+$ in these solvents (Chapter 2). In addition, in the oxygen donor solvents $[Na(THEC12)]^+$ is more stable than $[Li(THEC12)]^+$ but in MeCN this order is reversed. Unfortunately, since no quantitative kinetic data characterising $[Li(THEC12)]^+$ in MeCN or PC could be obtained, it is not possible to ascertain to what extent changes in k_c and k_d effect this selectivity shift. Although there is only minimal kinetic data available for $[LiL]^+$, where L = (*R*)-THPEC12, THEC12, and TMEC12, in all cases $[LiL]^+$ is characterised by a smaller k_c than for $[NaL]^+$ in DMF. This is probably due to the combination of increased steric strain induced in the metal complex by the smaller Li^+ ion compared with Na^+ (Section 4.3), greater steric hindrance between coordinating pendant arms in $[LiL]^+$ by comparison with $[NaL]^+$, and the effect of solvation. That is, the small size of Li^+ and the degree of bulkiness of the pendant arms on the ligand may prevent Li^+ from bonding with the oxygen donor atoms of the pendant

arms as effectively as Na^+. In addition, the rate-determining step for formation of $[ML]^+$ is likely to involve considerable desolvation of M^+, so that the greater solvation energy of Li^+ compared with Na^+ results in an increase in the activation enthalpy required to sequentially desolvate Li^+ in the complexation process.

The observation that variations in k_c dominate variations in K_S for many complexes involving pendant arm macrocyclic ligands contrasts with the behaviour exhibited by cryptands. That is, for alkali metal cryptates, variations in K_S with the nature of the solvent are principally a consequence of larger variations in k_d(298.2 K) rather than k_c(298.2 K).[13,21,33,57-59] This may be a reflection of the greater rigidity of the cryptands compared with the more flexible pendant arm macrocycles. Kinetic studies of copper complexes with TACN and its pendant arm derivatives have shown that they have similar dissociation rates but significantly different stabilities.[60-62] This indicates that, as for the tetraaza macrocyclic ligands in this study, variations in k_c and not k_d for triaza analogues account for the observed trend in their stability constants.

The ^{7}Li spectra of a solution containing $[Li(CYCLEN)]^+$ and solvated Li^+ in both MeCN and PC show only a single narrow resonance at temperatures approaching the solvent freezing points (232 K and 218 K, respectively). Therefore, Li^+ exchange on $[Li(CYCLEN)]^+$ in MeCN and PC is in the very fast exchange limit of the ^{7}Li NMR timescale, and no kinetic data could be obtained.

Although the exchange of Na^+ on $[Na(CYCLEN)]^+$ falls within the NMR timescale in MeCN and PC, the substantial baseline curvature of these spectra prevented the quantitative derivation of exchange rate constants for these systems. Thus, an estimate of τ_c was derived from the square-top approximation method[63] (Chapter 7), giving a lower limit for k_d characterising $[Na(CYCLEN)]^+$ in MeCN and PC as shown in Table 4.5. In MeCN and PC, the lower stability of $[Na(CYCLEN)]^+$ compared with $[Na(THEC12)]^+$ (Table 4.5) is a result of the much larger k_d characterising $[Na(CYCLEN)]^+$. This is consistent with the fewer donor atoms in CYCLEN to stabilise the complex and the ability of the pendant arms in THEC12 to participate in the formation of a three-dimensional cavity, which can more fully encapsulate Na^+ than the two-dimensional cavity available to CYCLEN. Thus, the greater electrostatic attraction between Na^+ and THEC12 compared with CYCLEN results in $[Na(THEC12)]^+$ being less labile than $[Na(CYCLEN)]^+$.

BIBLIOGRAPHY

1. L.F. Lindoy, *"The Chemistry of Macrocyclic Ligand Complexes"*, Cambridge University Press, Cambridge, U.K., **1989**.
2. D.A. Buckingham, C.R. Clark, W.S. Webley, *J. Chem. Soc., Chem. Commun.* **1981**, 192-194.
3. C.M. Madeyski, J.P. Michael, R.D. Hancock , *Inorg. Chem.* **1984**, 23, 1487-1489.
4. R.W. Hay, M.P. Pujari, W.T. Moodie, S. Craig, D.T. Richens, A. Perotti, L. Ungaretti, *J. Chem. Soc., Dalton Trans.* **1987**, 2605-2613.
5. E.K. Barefield, F. Wagner, *Inorg. Chem.* **1973**, 12, 2435-2439.
6. K.P. Wainwright, *J. Chem. Soc., Dalton Trans.* **1980**, 2117-2120.
7. S.P. Kasprzyk, G.R. Wilkins, *Inorg. Chem.* **1982**, 21, 3349-3352.
8. P. Clarke, A.M. Hounslow, R.A. Keough, S.F. Lincoln, K.P. Wainwright, *Inorg. Chem.* **1990**, 1793-1797.
9. J.R. Morrow, S. Amin, C.H. Lake, M.R. Churchill, *Inorg. Chem.* **1993**, 32, 4566-4572.
10. H.S. Stetter, W. Frank, *Angew. Chem. Ed. Engl.* **1976**, 15, 686.
11. J.F. Desreux, *Inorg. Chem.* **1980**, 19, 1319-1324.
12. J.F. Desreux, E. Merciny, M.F. Loncin, *Inorg. Chem.* **1981**, 20, 987-991.
13. M. Shamsipur, A.I. Popov, *J. Phys. Chem.* **1986**, 90, 5997-5999.
14. J.-M. Lehn, *Struct. Bond. (Berlin)* **1973**, 16, 1-69.
15. R.M. Izatt, K. Pawlak, J.S. Bradshaw, R.L. Bruening, *Chem. Rev.* **1991**, 91, 1721-2085.
16. B.G. Cox, J. Garcia-Rosas, H. Schneider, *J. Am. Chem. Soc.* **1981**, 103, 1054-1059.
17. S.F. Lincoln, A.K.W. Stephens, *Inorg. Chem.* **1991**, 30, 3529-3534.
18. J.M. Ceraso, J.L. Dye, *J. Am. Chem. Soc.* **1973**, 95, 4432-4434.
19. (a) A. Abou-Hamdan, S.F. Lincoln, *Inorg. Chem.* **1991**, 30, 462-466. (b) A. Anichini, L. Fabbrizzi, P. Paoletti, R.M. Clay, *J. Chem. Soc., Dalton Trans.* **1986**, 577-583.
20. R. Gresser, D.W. Boyd, A.M. Albrecht-Gary, J.P. Schwing, *J. Am. Chem. Soc.* **1980**, 102, 651-653.
21. B.G. Cox, D. Knop, H. Schneider, *J. Am. Chem. Soc.* **1978**, 100, 6002-6007.
22. J.M. Ceraso, P.B. Smith, J.S. Landers, J.L. Dye, *J. Phys. Chem.* **1977**, 81, 760-766.
23. E. Schchori, J. Jagur-Gordzinski, Z. Luz, H. Shporer, *J. Am. Chem. Soc.* **1971**, 93, 7133-7138.
24. M.L. Turonek, P. Clarke, G.S. Laurence, S.F. Lincoln, P.-A. Pittet, S. Politis, K.P. Wainwright, *Inorg. Chem.* **1993**, 32, 2195-2198.

25. S.L. Whitbread, S. Politis, A.K.W. Stephens, J. Lucas, R.S. Dhillon, S.F. Lincoln, K.P. Wainwright, *J. Chem. Soc., Dalton Trans.* **1996**, 1379-1384.
26. A.K.W. Stephens, R.S. Dhillon, S.E. Madback, S.L. Whitbread, S.F. Lincoln, *Inorg. Chem.* **1996**, 35, 2019-2024.
27. R.S. Dhillon, A.K.W. Stephens, S.L. Whitbread, S.F. Lincoln, K.P. Wainwright, *J. Chem. Soc., Chem. Commun.* **1995**, 1, 97-98.
28. S.L. Whitbread, J.M. Weeks, P. Valente, M.A. Buntine, S.F. Lincoln, K.P. Wainwright, *Aust. J. Chem.* **1997**, 50, 853-856.
29. A.K.W. Stephens, S.F. Lincoln, *J. Chem. Soc., Dalton Trans.* **1993**, 2123-2126.
30. R.S. Dhillon, S.E. Madback, F.G. Ciccone, M.A. Buntine, S.F. Lincoln, K.P. Wainwright, *J. Am. Chem. Soc.* **1997**, 119, 6126-6134.
31. W. Burgenmeister, R. Winkler-Oswatitsch, *Topp. Curr. Chem.* **1977**, 69, 91-196.
32. M. Eigen, R. Winkler, *"The Neurosciences, Second Study Program"*, Rockefeller University Press, New York, **1970**.
33. B.G. Cox, H. Schneider, *Pure. Appl. Chem.* **1990**, 62, 2259-2268.
34. E. Grell, T. Funck, F. Eggers, *"Membranes- A Series of Advances"*, Volume 3, G. Eisenman (Editor), Dekker, New York, **1975**.
35. E.F. Caldin, H.P. Bennetto, *J. Solution. Chem.* **1973**, 2, 217-238.
36. E.F. Caldin, *Pure. Appl. Chem.* **1979**, 51, 2067-2086.
37. M. Eigen, R.G. Wilkins, *Adv. Ser. Chem.* **1965**, 49, 55.
38. R.G. Wilkins, *Acc. Chem. Res.* **1970**, 3, 408-416.
39. E. Schmidt, A.I. Popov, *J. Am. Chem. Soc.* **1983**, 105, 1878-1882.
40. S.F. Lincoln, A.E. Merbach, *Adv. Inorg. Chem.* **1995**, 42, 1-87.
41. M. Shamsipur, A.I. Popov, *J. Phys. Chem.* **1987**, 91, 447-451.
42. K.J. Maynard, D.E. Irish, E.M. Eyring, S. Petrucci, *J. Phys. Chem.* **1984**, 88, 729-736.
43. W. Wallace, C. Chen, E.M. Eyring, S. Petrucci, *J. Phys. Chem.* **1985**, 89, 1357-1366.
44. D.P. Cobranchi, G.R. Phillips, D.E. Johnson, R.M. Barton, D.J. Rose, E.M. Eyring, L.J. Rodriguez, S. Petrucci, *J. Phys. Chem.* **1989**, 93, 1396-1398.
45. L.J. Rodriguez, E.M. Eyring, S. Petrucci, *J. Phys. Chem.* **1989**, 93, 5916-5924.
46. H. Schneider, K.H. Richmann, T. Funck, P. Firman, F. Eggers, E.M. Eyring, S. Petrucci, *J. Phys. Chem.* **1988**, 92, 2798-2804.
47. W.F. K. Wynne-Jones, H. Eyring, *J. Phys. Chem.* **1935**, 3, 492.
48. S. Glasstone, K.J. Laidler, H. Eyring, *"Theory of Rate Processes"*, McGraw-Hill, New York, **1941**.
49. S.F. Lincoln, *Prog. Reaction Kinetics* **1977**, 9, 1-91.

50. B. Dey, J.H. Coates, S.F. Lincoln, K.P. Wainwright, *J. Chem. Soc., Dalton Trans.* In press.
51. J.R. Roper, H. Elias, *Inorg. Chem.* **1992**, 31, 1202-1210.
52. N.W. Alcock, E.H. Curson, N. Herron, P. Moore, *J. Chem. Soc., Dalton Trans.* **1979**, 1987-1993.
53. N. Herron, O.W. Howarth, P. Moore, *Inorg. Chim. Acta.* **1976**, 20, L43-L44.
54. F. McLaren, P. Moore, A.M. Wynn, *J. Chem. Soc., Chem. Commun.* **1989**, 798-800.
55. T. Rodopoulos, P.-A. Pittet, S.F. Lincoln, *J. Chem. Soc., Dalton Trans.* **1993**, 1055-1060.
56. S.L. Whitbread, P. Valente, M.A. Buntine, P. Clements, S.F. Lincoln, K.P. Wainwright, *J. Am. Chem. Soc.* **1998**, 120, 2862-2869.
57. B.G. Cox, I. Schneider, H. Schneider, *Ber. Bunsenges, Phys. Chem.* **1980**, 84, 470-474.
58. S.F. Lincoln, A. Abou-Hamdan, *Inorg. Chem.* **1990**, 29, 3584-3589.
59. S.F. Lincoln, I.M. Brereton, T.M. Spotswood, *J. Chem. Soc., Faraday. Trans. I* **1985**, 1623-1630.
60. P.G. Graham, D.C. Weatherbun, *Aust. J. Chem.* **1981**, 34, 291-300.
61. T.J. Reido, T.A. Kaden, *Helv. Chim. Acta.* **1979**, 62, 1089-1096.
62. P. Chaudhuri, K. Weighardt, *Prog. Inorg. Chem.* **1987**, 35, 329-436.
63. R.K. Harris, *"NMR Spectroscopy"*, Pitman U.K. (London), **1983**.
64. (a) V. Gutmann, *"Coordination Chemistry in Non-Aqueous Solvents"*, Springer-Verlag:Wien, **1968**.
(b) W.J. Dewitte, A.I. Popov, *J. Solution. Chem.* **1976**, 5, 231-240.
(c) R.H. Erlich, E. Roach, A.I. Popov, *J. Am. Chem. Soc.* **1970**, 92, 4989-4990.

CHAPTER 5

EXCHANGE PROCESSES IN METAL ION COMPLEXES OF (*R*)-THPEC12 AND THEC12

5.1 INTRODUCTION

The addition of pendant arms to macrocyclic ligands has attracted substantial attention in the search for complexes with enhanced stability and ligands selective for specific metal ions.[1-6] The nature of the pendant arm is often influential in determining both the structure and lability of complexes involving pendant donor arm polyaza macrocyclic ligands,[7-11] as observed by the addition of hydroxy-, acetato- and amino- pendant arms to CYCLAM.[7,9,10] Incorporation of additional donor atoms onto the macrocyclic ligand backbone can allow the ligand to fulfil the coordination number requirements of the metal ion by completely enclosing it upon complexation. Moreover, the increased denticity of the ligand affords its metal complexes stereochemistries and intramolecular processes that are not available to complexes of the parent macrocyclic ligand.[12-14] Such phenomena have already been observed in the intramolecular exchange processes characterising several metal complexes of TMEC12,[15] (*S*)-THPC12,[16] TMEC14 and (*S*)-THPC14,[17,18] and heavy metal complexes of THEC12.[19]

The structure of a metal complex either determined by X-ray crystallography or modelled through molecular orbital calculations can be used to approximate those in solution and to gain further insight into selectivity trends (as discussed in Chapters 2 and 3). Dynamic NMR spectroscopy has proved to be a powerful technique for the study of intramolecular processes occurring in solution.[20-24] In particular, the use of variable temperature ^{13}C NMR spectroscopy is useful in the deduction of coordination geometries and macrocyclic ring conformations from separate isomers of a macrocyclic ligand complex in slow exchange with each other on the NMR timescale.[14,15-19,25,26] Thus, this chapter seeks to extend the understanding of the kinetic aspects of pendant arm macrocyclic ligands and their metal ion complexes through the study of alkali metal complexes of (*R*)-THPEC12 (1,4,7,10-tetrakis((*R*)-2-hydroxy-2-phenylethyl)-1,4,7,10-tetraazacyclododecane), and alkali and divalent metal complexes of THEC12 (1,4,7,10-tetrakis(2-hydroxyethyl)-1,4,7,10-tetraazacyclododecane) and THEC9 (1,4,7,-tris(2-hydroxyethyl)-1,4,7-triazacyclononane). The results obtained in this study are then compared with those obtained for metal complexes of the related pendant arm macrocyclic ligands (*S*)-THPC12 and TMEC12.

5.2 ^{13}C INTRAMOLECULAR EXCHANGE IN ALKALI METAL ION COMPLEXES

5.2.1 INTRAMOLECULAR EXCHANGE IN [M((*R*)-THPEC12)]$^+$

The natural abundance broad-band ^{1}H decoupled 75.47 MHz ^{13}C NMR spectra of (*R*)-THPEC12 and [M((*R*)-THPEC12)]$^+$, where $M^+ = Li^+$, Na^+, K^+, Rb^+ and Cs^+, in d_7-DMF consist of 7 resonances at the temperatures shown in Table 5.1. These 7 observed ^{13}C resonances arise from the 7 different chemical environments of the carbons in the ligand (*R*)-THPEC12. At 260.1 K, the resonance at 51.91 ppm for the (*R*)-THPEC12 spectra is assigned to the carbons of the 1,2-diaminoethane moiety of the macrocyclic ring (site *a* in Figure 5.1), and the resonances at 64.33 and 70.09 ppm are respectively assigned to the carbons of the >N*C*H$_2$- and the –*C*H(C$_6$H$_5$)OH moieties of the (*R*)-2-hydroxy-2-phenylethyl pendant arms of (*R*)-THPEC12 (sites *b* and *c*, respectively, in Figure 5.1). The resonances at 126.63, 127.48, 128.54 and 144.33 ppm correspond to the carbons of the –CH(*C*$_6$H$_5$)OH moiety of the pendant arms of (*R*)-THPEC12 (site *d* in Figure 5.1). (In $CDCl_3$, the analogous frequencies at 260.1 K are 51.44, 64.95, 69.82, 125.98, 127.22, 128.31 and 142.12 ppm). For the [Li((*R*)-THPEC12)]$^+$ spectra in d_7-DMF at 260.1 K, these correspond to the resonances at 49.93 and 51.74, 62.09, 69.95, 126.62, 127.71, 128.77 and 144.62 ppm, respectively. For Δ[Na((*R*)-THPEC12)]$^+$ in d_7-DMF at 260.1 K, these correspond to the resonances at 49.82 and 52.35, 63.31, 70.13, 126.62, 127.62, 128.59 and 144.83 ppm, respectively. For the spectra of Λ[K((*R*)-THPEC12)]$^+$ in d_7-DMF at 259.1 K, these correspond to the resonances at 51.30 and 52.32, 65.24, 70.51, 126.76, 127.80, 128.73 and 145.10 ppm, respectively. For the spectra of Λ[Rb((*R*)-THPEC12)]$^+$ in d_7-DMF at 260.1 K, these correspond to the resonances at 51.74, 64.33, 69.97, 126.49, 127.26, 128.43 and 144.24 ppm, respectively. For the Λ[Cs((*R*)-THPEC12)]$^+$ spectra in d_7-DMF at 254.9 K, these correspond to the resonances at 51.77, 64.31, 70.04, 126.60, 127.60, 128.59 and 144.31 ppm, respectively.

As the temperature decreases, the resonance characterising the macrocyclic ring carbons for (*R*)-THPEC12 and [M((*R*)-THPEC12)]$^+$ broadens and then splits into 2 separate resonances, whereas those characterising the carbons of the (*R*)-2-hydroxy-2-phenylethyl arms remain as singlets (Table 5.2). This is consistent with the macrocyclic ring carbons of (*R*)-THPEC12 exchanging between two magnetically inequivalent environments in [M((*R*)-THPEC12)]$^+$ and (*R*)-THPEC12. (At low temperature, the two macrocyclic ring carbon resonances of (*R*)-THPEC12 and [M((*R*)-THPEC12)]$^+$ are not of equal

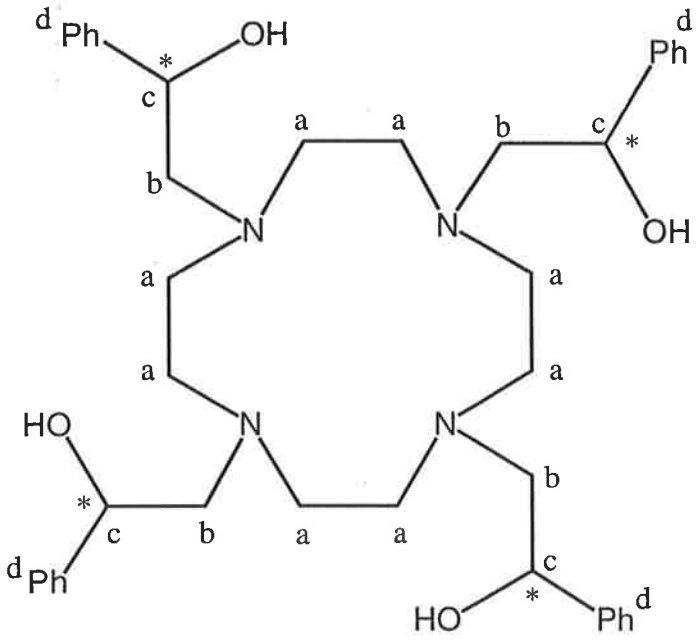

Figure 5.1: Assignment of the ^{13}C resonances of (*R*)-THPEC12 and the alkali metal ion complexes, [M((*R*)-THPEC12)]$^+$.

intensity. This may be a result of differences in the effectiveness of the Nuclear Overhauser Effect at different sites).[27]

The coordination geometries of (*R*)-THPEC12 and [M((*R*)-THPEC12)]$^+$ may be deduced from the ^{13}C NMR spectra in the slow exchange region of the NMR timescale. The pendant arms can exchange between being coordinated to M^+ and being uncoordinated, so that the resonances observed at sites *b*, *c* and *d* correspond to the weighted average of the coordinated and uncoordinated pendant arm resonance frequencies. Since the resonances assigned to these sites remain essentially unchanged over the observed temperature range, the carbons remain equivalent within their respective environments. (Certainly, the possibility that any given side arm is in rapid on-off exchange on the NMR timescale cannot be dismissed). In addition, if fewer than four pendant arms are involved in the coordination of M^+, additional resonances will be observed in the slow exchange ^{13}C NMR spectra. Therefore, the exchange mechanism generating the coalescence of the two resonances at site *a* does not change the

Table 5.1: Comparison of the ^{13}C chemical shifts of L and $[ML]^+$, where L = (*R*)-THPEC12, in d_7-DMF.

Complex	T	δ[a]						
	K	ppm						
L	260.1	51.91	64.33	70.09	126.63	127.48	128.54	144.33
[b]L	260.1	51.44	64.95	69.82	125.98	127.22	128.31	142.12
$[LiL]^+$	260.1	49.93 51.74	62.09	69.95	126.62	127.71	128.77	144.62
$\Delta[NaL]^+$	260.1	49.82 52.35	63.31	70.13	126.62	127.62	128.59	144.83
$\Lambda[KL]^+$	259.1	51.30 52.32	65.24	70.51	126.76	127.80	128.73	145.10
$\Lambda[RbL]^+$	260.1	51.74	64.33	69.97	126.49	127.26	128.43	144.24
$\Lambda[CsL]^+$	254.9	51.77	64.31	70.04	126.60	127.60	128.59	144.31

[a] ^{13}C chemical shifts are referenced to natural abundance d_7-DMF, where the amide carbon is assigned a chemical shift of 162.67 ppm. [b]In $CDCl_3$, which is assigned a chemical shift of 77.0 ppm.

Table 5.2: Slow exchange ^{13}C chemical shifts at 216.3 K of L and $[ML]^+$, where L = (*R*)-THPEC12, in d_7-DMF.

Complex	δ[a]							
	ppm							
L	49.65	52.46	63.91	69.83	126.70	127.51	128.67	144.36
[b]L	49.62	51.91	64.80	69.60	126.07	127.40	128.47	142.03
[c]$[LiL]^+$	49.57	51.31	61.91	69.42	126.44	127.63	128.63	144.68
[c]$\Delta[NaL]^+$	49.45	52.20	63.16	69.76	126.55	127.55	128.57	145.02
[c]$\Lambda[KL]^+$	50.31	52.32	65.49	70.30	126.67	127.54	128.60	145.44
$\Lambda[RbL]^+$	49.98	52.60	63.90	69.79	126.69	127.80	128.68	144.33
$\Lambda[CsL]^+$	49.68	52.54	64.02	69.81	126.62	127.80	128.66	144.33

[a] ^{13}C chemical shifts are referenced to natural abundance d_7-DMF, where the amide carbon is assigned a chemical shift of 162.67 ppm. [b]In $CDCl_3$, where $CDCl_3$ is assigned a chemical shift of 77.0 ppm. [c]Reference 74.

magnetic environment of the carbons at sites *b*, *c* and *d*. Thus, M^+ is bound by all four nitrogens of the tetraaza ring and the four pendant arms of (*R*)-THPEC12.

The configurations of the tetraaza ring with four coplanar nitrogens coordinating M^+ are TRANS I – TRANS V (Figure 5.2).[28] The spectrum of a complex adopting the TRANS II conformation should exhibit 19 resonances in the slow exchange regime of the NMR timescale. In addition, for an 8-coordinate complex adopting the TRANS II – TRANS V configurations, the metal ion is coordinated within the plane of the macrocyclic ring. However, the metal ions in this study are generally too large to be coordinated within the plane of the tetraaza ring,[28] so adoption of such conformations generates considerable steric strain in the complex. Therefore, the TRANS II – V configurations are discounted as a possibility for the $[M((R)\text{-THPEC12})]^+$ complexes.

The observed ^{13}C NMR spectra of (*R*)-THPEC12 and $[M((R)\text{-THPEC12})]^+$ are best accounted for by a structure incorporating the TRANS I conformation. In such a structure, M^+ lies above the tetraaza plane and is coordinated to the four coplanar nitrogens and the four (*R*)-2-hydroxy-2-phenylethyl pendant arms of (*R*)-THPEC12. Molecular mechanics calculations and X-ray crystallographic data lend support to this proposal. Molecular mechanics calculations have shown that TRANS I is the lowest energy configuration, and is able to accommodate metal ions of different sizes, provided they do not require octahedral coordination.[29-31] In addition, molecular orbital calculations have shown that (*R*)-THPEC12 adopts the TRANS I configuration in its alkali metal complexes,[32] and numerous complexes of related macrocyclic ligands have been shown to adopt solid state or solution structures with all the pendant arms on the same side of the macrocyclic ring plane.[33-39]

A selection of the temperature dependent ^{13}C NMR spectra of (*R*)-THPEC12 and $[M((R)\text{-THPEC12})]^+$, where $M^+ = Li^+$, K^+ and Rb^+, are shown in Figures 5.3 – 5.6. (The spectra for the analogous Na^+ and Cs^+ complexes show similar temperature dependence, but over different temperature ranges). Chiral (*R*)-THPEC12, in principle, is able to form Δ and Λ(*R*)-THPEC12 diastereomers as the free ligand or on complexation of M^+, where the phenyl groups on the pendant arms all occupy either equatorial or axial positions (Figure 5.7). In this study, the Δ and Λ assignments for the two diastereomers of (*R*)-THPEC12 refer to the clockwise and anticlockwise rotation, respectively, of the four pendant arms when viewed down the C_4 axis from the oxygen plane. This type of isomerisation occurs because

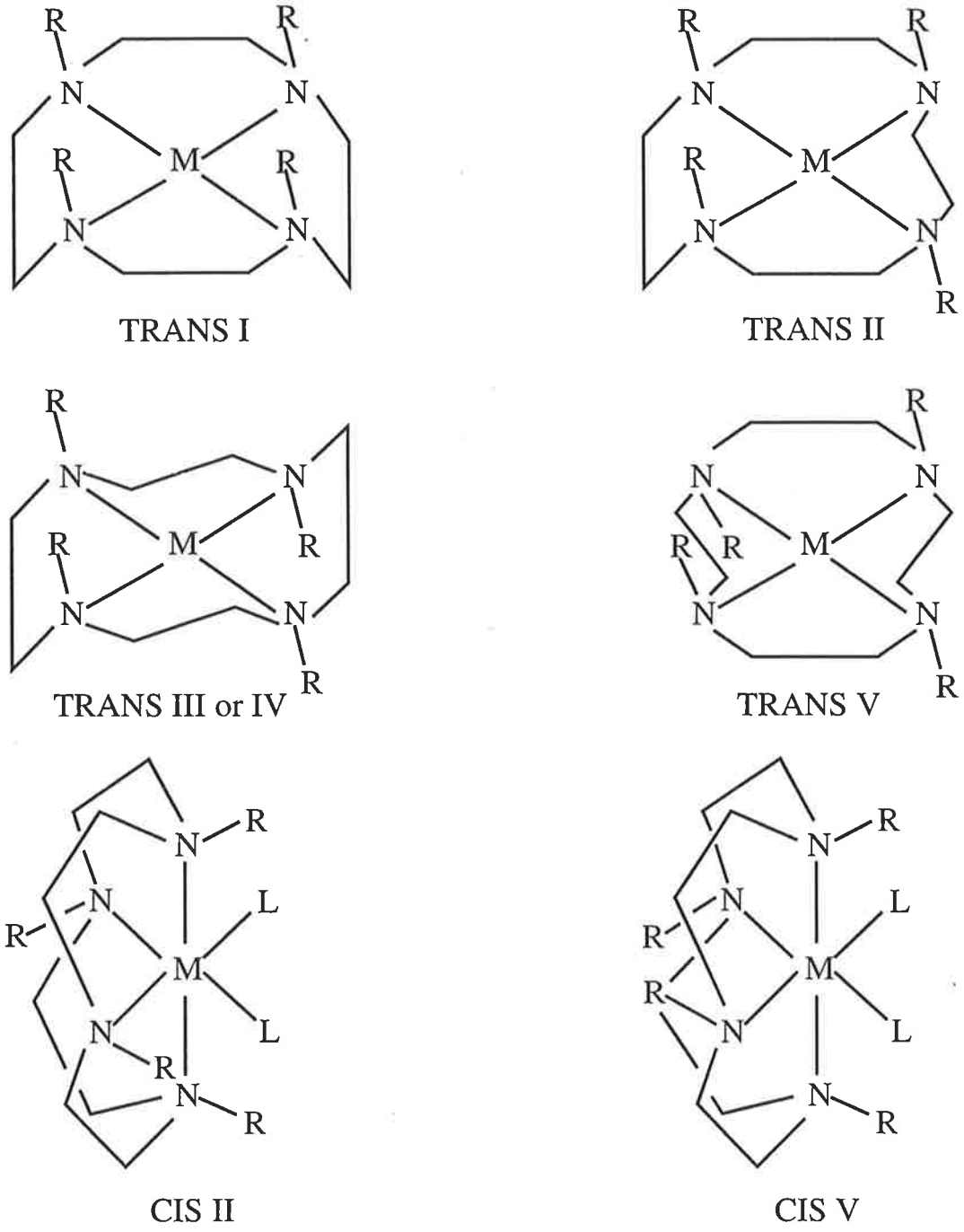

Figure 5.2: Possible configurational isomers of $[M((R)\text{-THPEC12})]^+$, where the (*R*)-2-hydroxy-2-phenylethyl arms, denoted R, are shown uncoordinated. The TRANS III and TRANS IV conformations are equivalent in the completely symmetrical (*R*)-THPEC12 system.

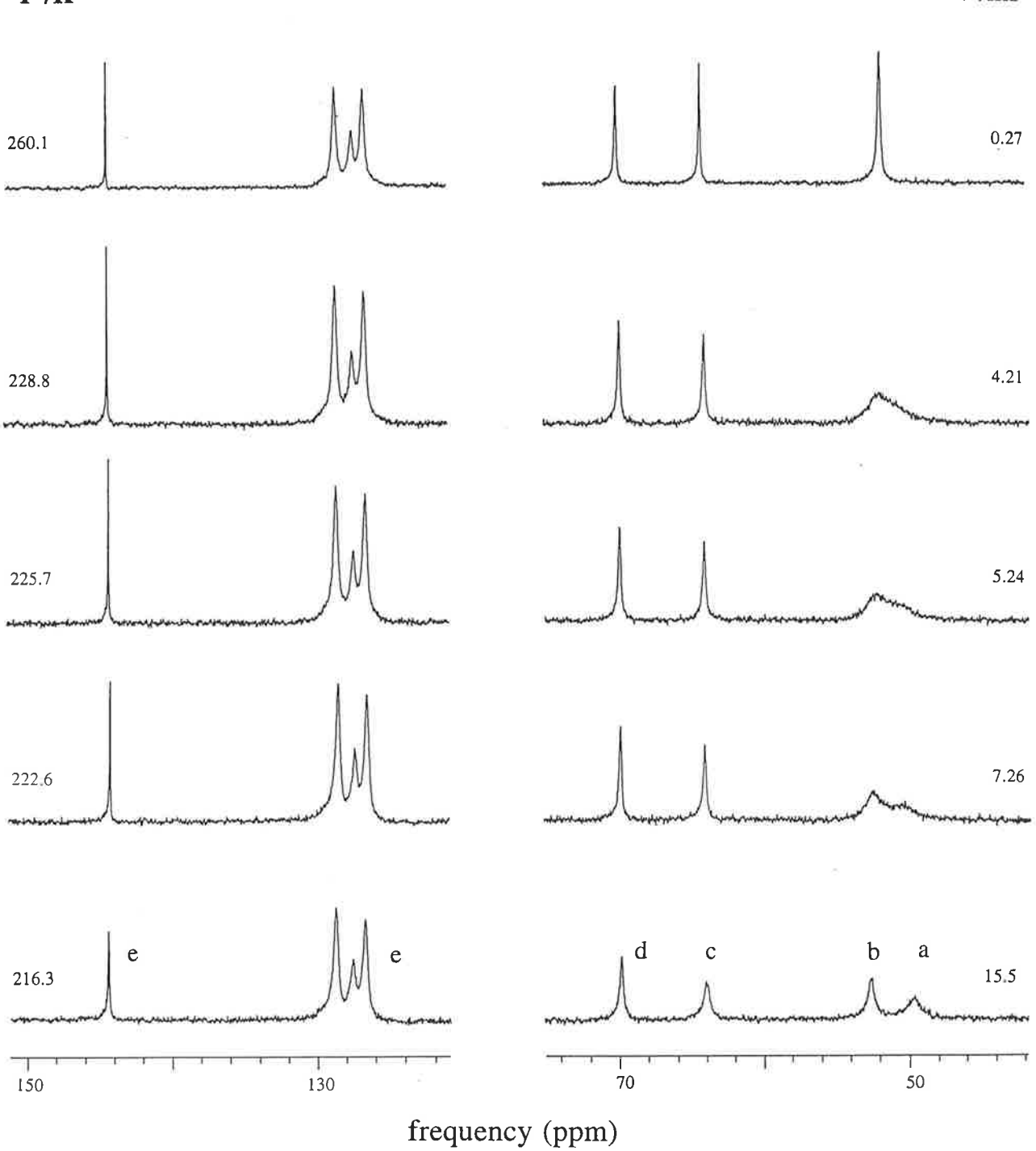

Figure 5.3: Temperature variations of the broad-band ^{1}H decoupled ^{13}C NMR spectra of (*R*)-THPEC12 (0.100 mol dm^{-3}) in d_7-DMF. Experimental temperatures and τ values derived from complete lineshape analysis of the coalescing doublet arising from the macrocyclic ring carbons, *a* and *b*, appear to the left and the right of the figure, respectively. (Slight broadening of the resonances arising from the pendant arm >N*C*H$_2$- (*c*), -*C*H(C$_6$H$_5$)OH (*d*), and the -CH(*C*$_6$H$_5$)OH (*e*) carbons are a consequence of the increase in solution viscosity with a decrease in temperature).

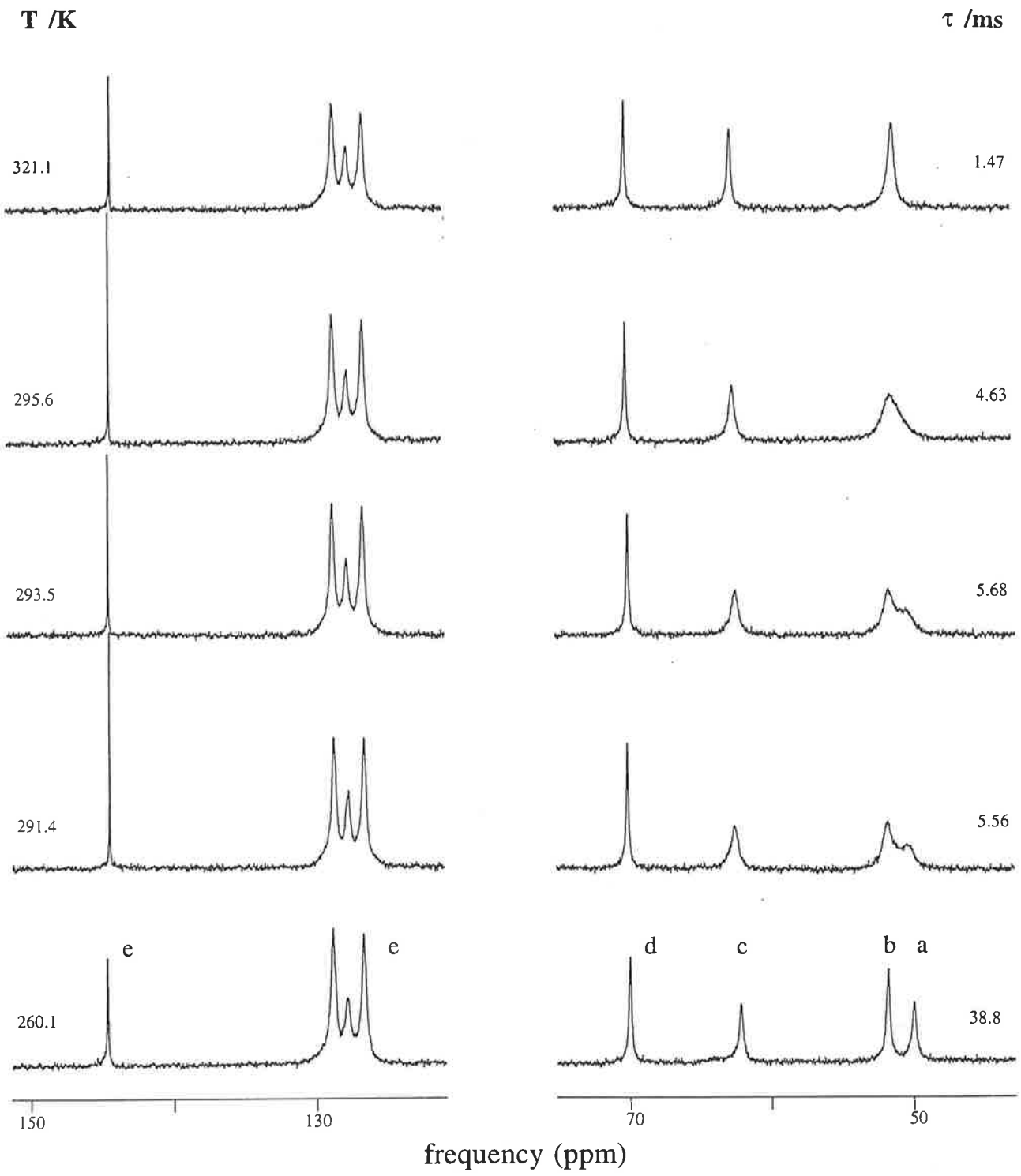

Figure 5.4: Temperature variations of the broad-band ^{1}H decoupled ^{13}C NMR spectra of $[Li((R)\text{-THPEC12})]^{+}$ (0.100 mol dm^{-3}) in d_7-DMF. Experimental temperatures and τ values derived from complete lineshape analysis of the coalescing doublet arising from the macrocyclic ring carbons, *a* and *b*, appear to the left and the right of the figure, respectively. (Slight broadening of the resonances arising from the pendant arm $>NCH_2$- (*c*), -$CH(C_6H_5)OH$ (*d*), and the -$CH(C_6H_5)OH$ (*e*) carbons are a consequence of the increase in solution viscosity with a decrease in temperature).

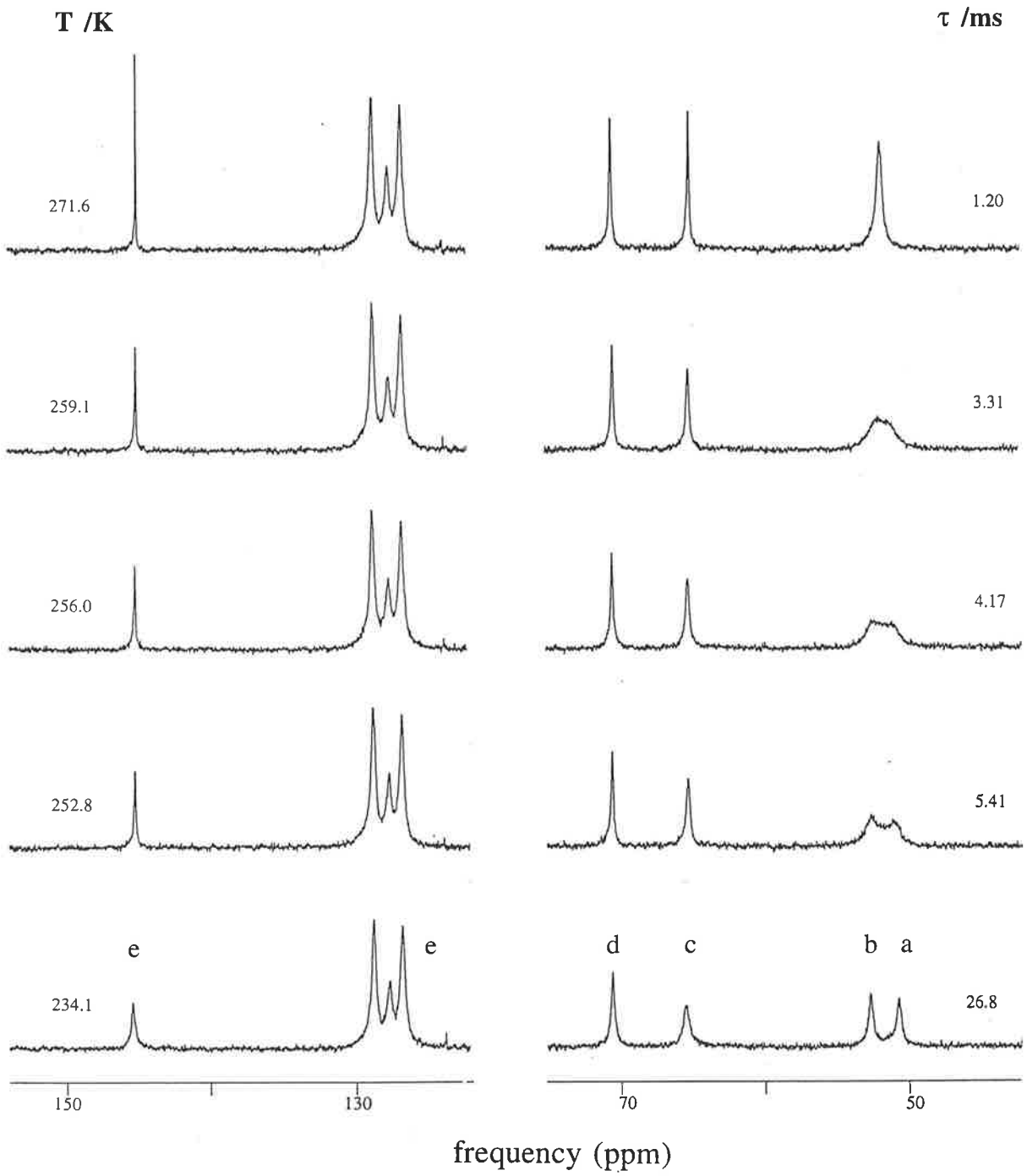

Figure 5.5: Temperature variations of the broad-band ^{1}H decoupled ^{13}C NMR spectra of Λ[K((*R*)-THPEC12)]$^{+}$ (0.099 mol dm^{-3}) in d_7-DMF. Experimental temperatures and τ values derived from complete lineshape analysis of the coalescing doublet arising from the macrocyclic ring carbons, *a* and *b*, appear to the left and the right of the figure, respectively. (Slight broadening of the resonances arising from the pendant arm >N*C*H$_2$- (*c*), -*C*H(C$_6$H$_5$)OH (*d*), and the -CH(*C*$_6$H$_5$)OH (*e*) carbons are a consequence of the increase in solution viscosity with a decrease in temperature).

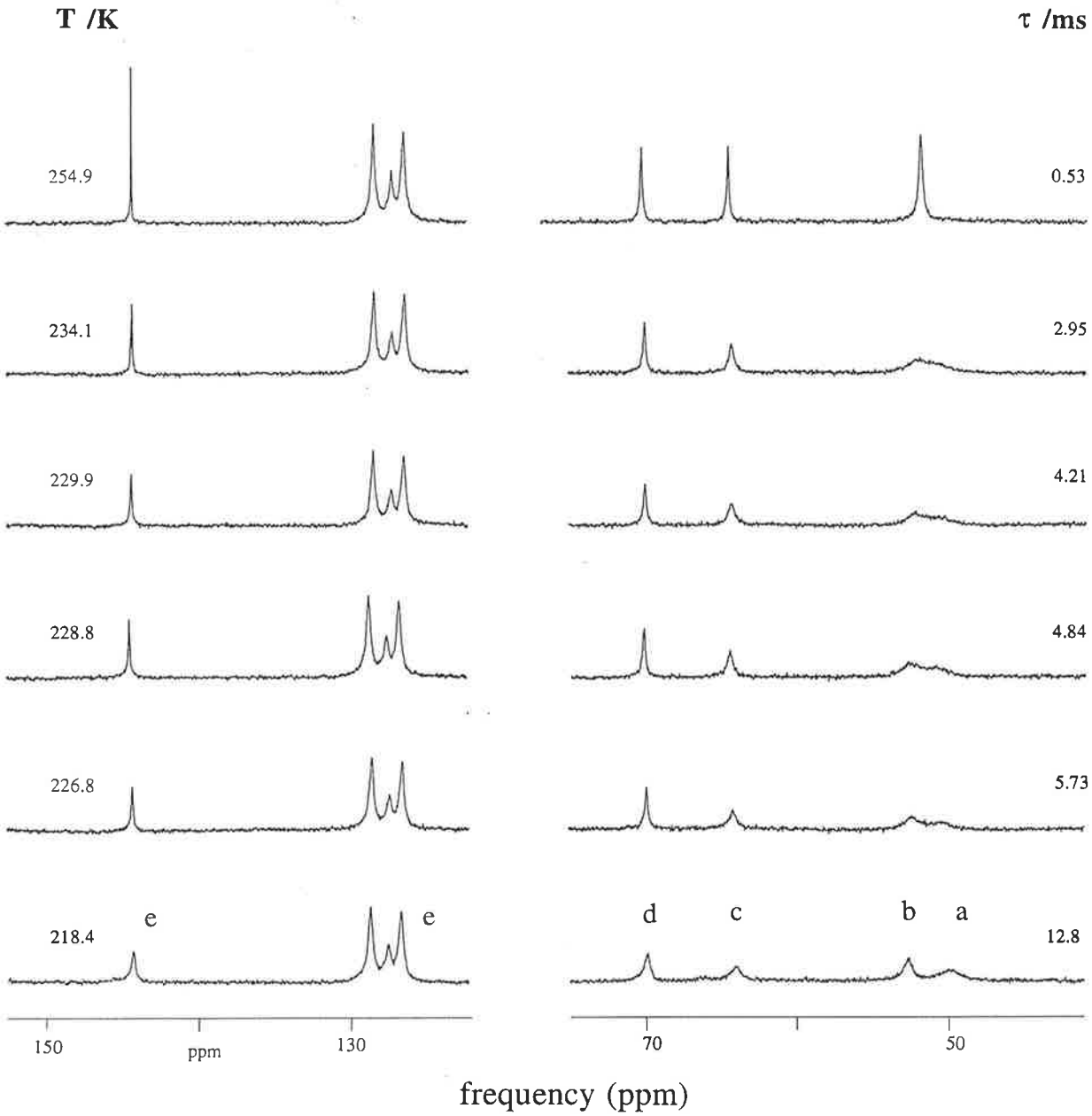

Figure 5.6: Temperature variations of the broad-band ^{1}H decoupled ^{13}C NMR spectra of Λ[Rb((*R*)-THPEC12)]$^{+}$ (0.101 mol dm^{-3}) in d_7-DMF. Experimental temperatures and τ values derived from complete lineshape analysis of the coalescing doublet arising from the macrocyclic ring carbons, *a* and *b*, appear to the left and the right of the figure, respectively. (Slight broadening of the resonances arising from the pendant arm >N*C*H$_2$- (*c*), -*C*H(C$_6$H$_5$)OH (*d*), and the -CH(*C*$_6$H$_5$)OH (*e*) carbons are a consequence of the increase in solution viscosity with a decrease in temperature).

(*R*)-THPEC12 has two independent structural features that influence its chirality. That is, the (*R*)-2-hydroxy-2-phenylethyl groups are oriented around M^+ in a propeller-like manner, and the macrocyclic ring can adopt two different conformations when coordinated to M^+. Each diastereomer should exhibit a set of 8 distinct ^{13}C resonances in the slow exchange regime of the ^{13}C NMR spectra of $[M((R)\text{-THPEC12})]^+$. However, only one such set of 8 resonances is observed (Figures 5.4 – 5.6), and it appears that only one diastereomer is present in detectable concentrations. This phenomenon is observed for (*R*)-THPEC12 in d_7-DMF and $CDCl_3$. (It must be noted that although the ^{13}C NMR solution studies refer to $\Delta(R)$-THPEC12, $\Delta[Na((R)\text{-THPEC12})]^+$ and $\Lambda[M((R)\text{-THPEC12})]^+$, for $M^+ = K^+$, Rb^+ and Cs^+, the molecular orbital calculations, discussed in Chapter 2, refer to $\Lambda(S)$-THPEC12, $\Lambda[Na((S)\text{-THPEC12})]^+$ and $\Lambda[M((R)\text{-THPEC12})]^+$, for $M^+ = K^+$, Rb^+ and Cs^+).

The variable temperature NMR spectra are consistent with intramolecular exchange of (*R*)-THPEC12 and $[M((R)\text{-THPEC12})]^+$ occurring between two equivalent square antiprismatic diastereomers of C_{4v} symmetry. This mechanism is illustrated by Figure 5.7. The macrocyclic ring carbons exchange between inequivalent sites *a* and *b*, which cannot be unequivocally identified with specific ring carbons from the available data, whereas the pendant arm carbons, denoted *c*, *d* and *e*, experience no change in magnetic environment as the diastereomers interconvert. The adoption of diastereomeric, approximately cubic structures for $[M((S)\text{-THPEC12})]^+$ from molecular orbital calculations supports this mechanism.[32] Similar structures have been predicted by molecular orbital calculations for $[M((S)\text{-THPC12})]^+$,[16] and are in accord with the approximately square antiprismatic solid state structures[33-35] of $[M(THEC12)]^+$ and the structures of related macrocyclic ligand complexes.[30,33,36-40]

By considering the square plane delineated by the four nitrogens as fixed, and the square plane delineated by the four (*R*)-2-hydroxy-2-phenylethyl pendant arms as above that of the four nitrogens (Figure 5.7A and 5.7B), the mechanism shown in Figure 5.7 for $\Delta(R)$-THPEC12 and $\Delta[M((R)\text{-THPEC12})]^+$ describes double nitrogen inversion. That is, the first nitrogen inversion of $\Delta(R)$-THPEC12 produces the less stable and more sterically crowded $\Lambda(R)$-THPEC12 diastereomer (equivalent to Figures 5.7C and 5.7F). The second nitrogen inversion restores the chirality to that of the more stable $\Delta(R)$-THPEC12 diastereomer, and the oxygen plane is now below that of the nitrogens (Figures 5.7B and 5.7E). Therefore, the double nitrogen inversion at each nitrogen of $\Delta(R)$-THPEC12 results in exchange in a single diastereomer rather than between two diastereomers. It is also possible, however, that double nitrogen inversion in $\Delta[M((R)\text{-THPEC12})]^+$ involves the passage of M^+ through the macrocyclic annulus, where the macrocyclic hole radius has been

estimated as ~ 1.27 Å.[41] This may be sufficient to allow Li^+, Na^+ and possibly K^+ (with 4- and 6-coordinate ionic radii of 0.59 and 0.76, 0.99 and 1.02, and 1.37 and 1.38 Å, respectively)[41] to pass through in a mechanism requiring dissociation of all four metal-oxygen bonds. A similar mechanism has been proposed for $[M(THEC14)]^{2+}$, where M^{2+} = Hg^{2+}, Cd^{2+} and Pb^{2+},[12,13] and related macrocycles.[25] An alternative mechanism may involve M^+ traversing the edge of the macrocycle in a process involving sequential metal-nitrogen and metal-oxygen bond breakage and formation to achieve the double nitrogen inversion at each nitrogen.

The formation of a dominant single diastereomer in solution is unusual for metal ion complexes of macrocyclic ligands, and it has been proposed that an intramolecular rearrangement via Δ to Λ conversion is generally an easier process than that via lone-pair inversion of the nitrogen atom.[20] Nonetheless, the double nitrogen inversion process has also been observed for complexes of (*S*)-THPC12,[16,42-44] and [Yb((*R*)-DOTMA]$^-$ (where DOTMA is 1,4,7,10-tetrakis((*R*)-methylacetato)-1,4,7,10-tetraazacyclododecane).[45] It was originally postulated from preliminary $[M((S)\text{-THPC12})]^+$ data that the observation of only one set of resonances in the slow exchange region of the ^{13}C NMR timescale may indicate that the difference in magnetic environments between the Λ and Δ diastereomers of $[Na((S)\text{-THPC12})]^+$ is small, so that k(298.2 K) describes an overall diastereomerisation. However, extension of this interpretation to other $[M((S)\text{-THPC12})]^+$ complexes, and to the complexes of this study, requires each of their diastereomer pairs to also possess identical ^{13}C chemical shifts which seems unlikely.

The mechanism for intramolecular exchange in $[M((R)\text{-THPEC12})]^+$ assumes that the transition state, or reactive intermediate, remains octadentate. In this circumstance, the geometry of the transition state is probably approximately cubic, where $\Delta H^{\ddagger}$ and $\Delta S^{\ddagger}$ represent the differences between the square antiprismatic and cubic geometries of $[M((R)\text{-THPEC12})]^+$. However, the possibility that one or more of the pendant arms are uncoordinated in the transition state cannot be dismissed. The differences between the ground and transition states are due to differences in: (i) metal-ligand bond lengths; (ii) coordination geometry; (iii) steric crowding; (iv) conformational strain; and (v) change in coordination number if any metal-ligand bonds are broken. These factors are mainly dependent on the ionic radius of the metal ion and the metal-ligand bond strength.

Complete lineshape analysis[46] of the coalescence of the macrocyclic resonances yielded the mean site lifetimes, τ, illustrated in Figure 5.8. The

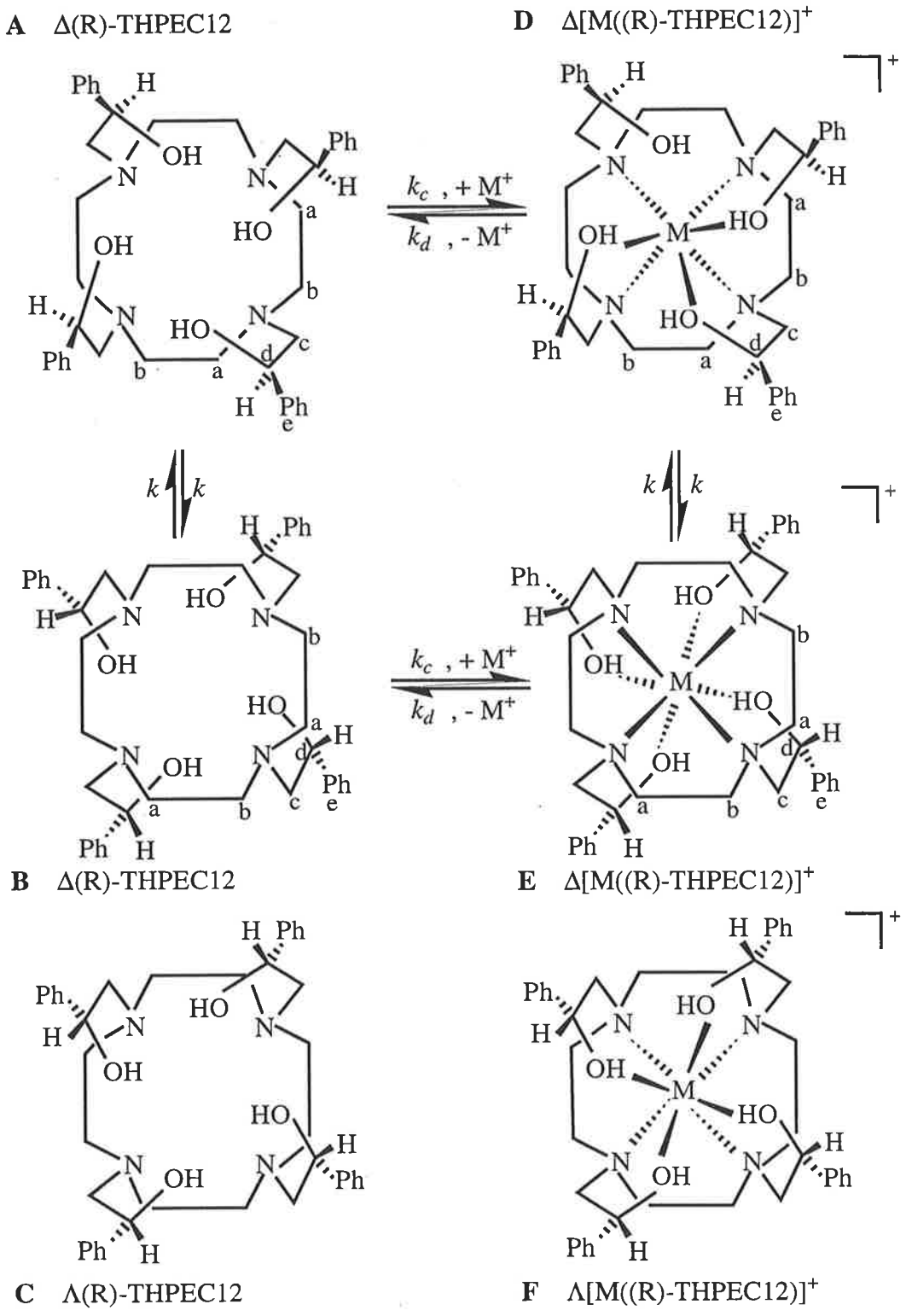

Figure 5.7: Exchange pathways. The Λ and Δ(*R*)-THPEC12 diastereomers are shown at the left of the figure, and the Λ and Δ[M((*R*)-THPEC12)]$^+$ diastereomers are shown at the right of the figure. D and E illustrate the proposed mechanism for interconversion of the square antiprismatic diastereomers of Δ[M((*R*)-THPEC12)]$^+$.

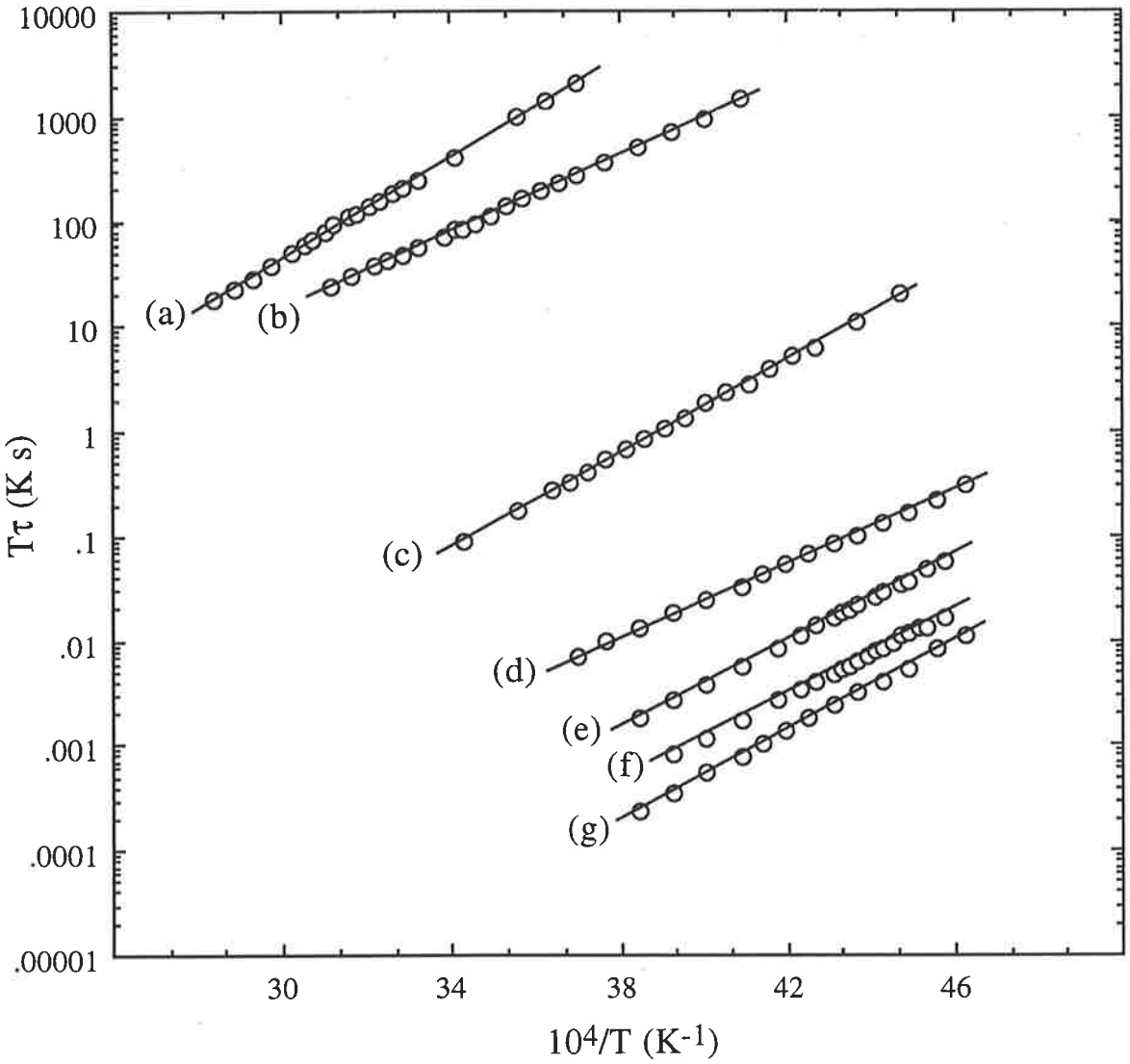

Figure 5.8: Temperature variations of τ for intramolecular exchange between the square antiprismatic diastereomers of $[M((R)\text{-THPEC12})]^+$ and (*R*)-THPEC12 and in d_7-DMF. The solid lines represent the best fit of the data to Equation 4.10 for each system.

(a) $\Delta[Na((R)\text{-THPEC12})]^+$, 100τ.
(b) $[Li((R)\text{-THPEC12})]^+$, 50τ.
(c) $\Lambda[K((R)\text{-THPEC12})]^+$, τ.
(d) (*R*)-THPEC12 in $CDCl_3$, τ/10.
(e) $\Lambda[Rb((R)\text{-THPEC12})]^+$, τ/50.
(f) $\Lambda[Cs((R)\text{-THPEC12})]^+$, τ/150.
(g) (*R*)-THPEC12, τ/300.

Table 5.3: Kinetic parameters[a] for intramolecular exchange in L and $[ML]^+$, where L = (*R*)-THPEC12, in d_7-DMF.

Complex	k (T)[b] s^{-1}	k (298.2 K) s^{-1}	$\Delta H^{\ddagger}$ kJ mol^{-1}	$\Delta S^{\ddagger}$ J K^{-1} mol^{-1}
[c]L	241 ± 3 (228.8)	46000 ± 1900	40.8 ± 0.4	-18.8 ± 1.7
[c,d]L	220 ± 3 (228.8)	16000 ± 380	33.1 ± 0.2	-53.2 ± 1.1
[c]$[LiL]^+$	184 ± 2 (293.5)	233 ± 2	34.6 ± 0.3	-83.5 ± 1.1
[e]$\Delta[NaL]^+$	276 ± 2 (314.8)	98 ± 1	46.1 ± 0.2	-52.2 ± 0.7
$\Lambda[KL]^+$	245 ± 2 (256.0)	4900 ± 100	42.7 ± 0.3	-31.1 ± 1.2
$\Lambda[RbL]^+$	238 ± 2 (229.9)	34000 ± 1000	39.1 ± 0.3	-27.2 ± 1.2
$\Lambda[CsL]^+$	239 ± 2 (228.8)	35000 ± 1100	38.5 ± 0.3	-28.9 ± 1.3

This work unless stated otherwise. [a]Errors represent 1 standard deviation for the fit of experimental τ data to Equation 4.10. [b]Exchange rate constant (k) at the coalescence temperature shown in brackets. [c]Reference 75. [d]In $CDCl_3$. [e]Reference 76.

kinetic parameters shown in Table 5.3 for this exchange process were derived from the temperature variation of τ through Equation 4.10. It is apparent from Table 5.3 that the rates of nitrogen double inversion in $[M((R)\text{-THPEC12})]^+$, where $M^+ = Li^+$, Na^+ and K^+, at 298.2 K are significantly slower than that for (*R*)-THPEC12. This is a consequence of the more negative $\Delta S^{\ddagger}$ characterising $[Li((R)\text{-THPEC12})]^+$ and the additional larger $\Delta H^{\ddagger}$ for $\Delta[Na((R)\text{-THPEC12})]^+$ and $\Lambda[K((R)\text{-THPEC12})]^+$ compared with (*R*)-THPEC12. The negative values of $\Delta S^{\ddagger}$ indicate an increase in order in going from the ground state to the transition state. Optimal bonding occurs between Na^+ and (*R*)-THPEC12 (Chapter 2), so that the larger $\Delta H^{\ddagger}$ characterising $\Delta[Na((R)\text{-THPEC12})]^+$

compared with the other complexes in Table 5.3 is consistent with the combination of a lengthening of the metal-ligand bonds and increased rigidity in the transition state for Δ[Na((*R*)-THPEC12)]$^+$.

As M^+ changes from Na^+ to Cs^+, $\Delta H^{\ddagger}$ characterising diastereomeric exchange in [M((*R*)-THPEC12)]$^+$ generally decreases while $\Delta S^{\ddagger}$ becomes less negative and k(298.2 K) substantially increases. This may indicate that the rate of intramolecular exchange at 298.2 K is largely controlled by the size of M^+. This is in agreement with the results obtained by molecular orbital calculations (Chapter 2), where from Na^+ to Cs^+, [M((*S*)-THPEC12)]$^+$ opens out so that the "basket-like" structure delineated by the four (*S*)-2-hydroxy-2-phenylethyl groups becomes shallower and wider as M^+ moves away from the tetraaza plane and closer to the tetraoxa plane. This may facilitate easier modes of intramolecular exchange. However, it is difficult to predict the relative contributions of factors (i) – (v), and although each nitrogen double inversion requires dissociation of a metal-nitrogen bond, further mechanistic detail is unclear.

For M^+ = Na^+ to Cs^+, the computed structures of [M((*S*)-THPEC12)]$^+$ (Chapter 2)[32] possess the atomic equivalence required by the corresponding ^{13}C NMR spectra, but the computed [Li((*S*)-THPEC12)]$^+$ structure does not. Thus, if the solution structure of [Li((*R*)-THPEC12)]$^+$ is similar to the computed structure, it appears that a fluxional motion in this structure renders all (*R*)-2-hydroxy-2-phenylethyl arms equivalent and all macrocyclic ring ethylenic moieties equivalent at a rate in the fast exchange limit of the ^{13}C NMR timescale which is much faster than the double nitrogen inversion process.

5.2.2 INTRAMOLECULAR EXCHANGE IN [M(THEC12)]$^+$

The natural abundance broad-band ^1H decoupled ^{13}C NMR spectra of THEC12 and [M(THEC12)]$^+$, where M^+ = Li^+, Na^+ and K^+, in methanol-^{12}C-d_4 consist of 3 resonances at the chemical shifts and temperatures shown in Table 5.4. (The solubilities of $RbCF_3SO_3$ and $CsCF_3SO_3$ were insufficient for quantitative ^{13}C NMR studies of [Rb(THEC12)]$^+$ and [Cs(THEC12)]$^+$). For free THEC12 at 291.0 K, the resonance at 50.67 ppm is assigned to the carbons of the 1,2-diaminoethane moiety of the macrocyclic ring (site *a* in Figure 5.9), and the resonances at 55.42 and 58.04 ppm are assigned to the carbons of the >N*C*H$_2$- moiety and -*C*H$_2$OH moiety of the pendant arms (sites *b* and *c*, respectively, in Figure 5.9). Apart from considerable broadening near the solution freezing point, the macrocyclic ring resonance of free THEC12

does not resolve sufficiently for the number and types of conformers to be identified, while the pendant arm resonances show little variation with decreasing temperature other than slight broadening associated with increasing viscosity. On the other hand, the resonance characterising the carbons of the macrocyclic ring in $[M(THEC12)]^+$ broadens and then splits into 2 separate resonances (Table 5.5) as the temperature decreases, while the pendant arm resonances remain as singlets. As for $[M((R)\text{-}THPEC12)]^+$, this is indicative of the macrocyclic ring carbons exchanging between two inequivalent sites in $[M(THEC12)]^+$.

A montage of the temperature dependent ^{13}C NMR spectra of $[K(THEC12)]^+$ is shown in Figure 5.10. The spectra for the analogous Li^+ and Na^+ complexes show similar temperature dependence for the macrocyclic ring resonances, but over different temperature ranges. In contrast to $[Li(THEC12)]^+$ and $[Na(THEC12)]^+$, where the pendant arm resonances exhibit small chemical shift variations with temperature, the chemical shift difference between the two pendant arm resonances of $[K(THEC12)]^+$ decreases with an increase in temperature such that they coincide at 304.4 K (Figure 5.10). Complete lineshape analysis[46] of the coalescence of the

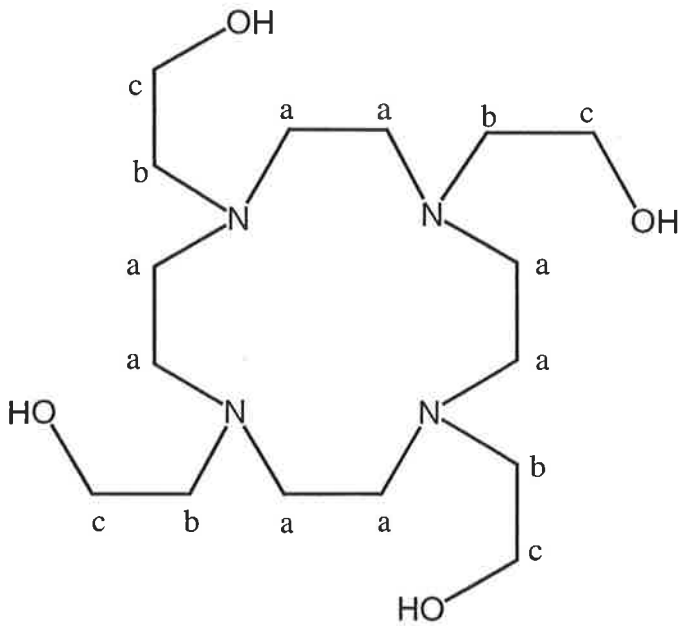

Figure 5.9: Assignment of the ^{13}C resonances of THEC12 and $[M(THEC12)]^{n+}$, where M^{n+} = alkali or alkaline earth metal ion.

Table 5.4: Fast exchange ^{13}C chemical shifts of $[M(THEC12)]^+$ at 291.0 K in methanol-^{12}C-d_4.

Complex	δ^a ppm		
THEC12	50.67	55.42	58.04
$[Li(THEC12)]^+$	49.70	54.98	57.41
$[Na(THEC12)]^+$	51.24	58.47	58.65
$[K(THEC12)]^+$	54.85	59.23	59.37

[a] ^{13}C chemical shifts are referenced to external natural abundance methanol-^{12}C-d_4, which is assigned a chemical shift of 47.05 ppm.

Table 5.5: Slow exchange ^{13}C chemical shifts of $[M(THEC12)]^+$ at 219.3 K in methanol-^{12}C-d_4.

Complex	δ^a ppm			
THEC12	49.57 (broad)		54.87	57.71
$[Li(THEC12)]^+$	49.08	49.61	53.28	57.38
$[Na(THEC12)]^+$	48.94	50.30	54.89	57.35
$[K(THEC12)]^+$	49.98	52.49	59.05	58.43

[a] ^{13}C chemical shifts are referenced to external natural abundance methanol-^{12}C-d_4, which is assigned a chemical shift of 47.05 ppm.

macrocyclic ring resonances yielded the mean site lifetimes, τ, illustrated by Figure 5.11. The kinetic parameters shown in Table 5.6 for this exchange process were derived from the temperature variations of τ through Equation 4.10.

The temperature dependence of the spectra of $[M(THEC12)]^+$ is analogous to that for (*R*)-THPEC12 and $[M((R)\text{-THPEC12})]^+$, and it is concluded from

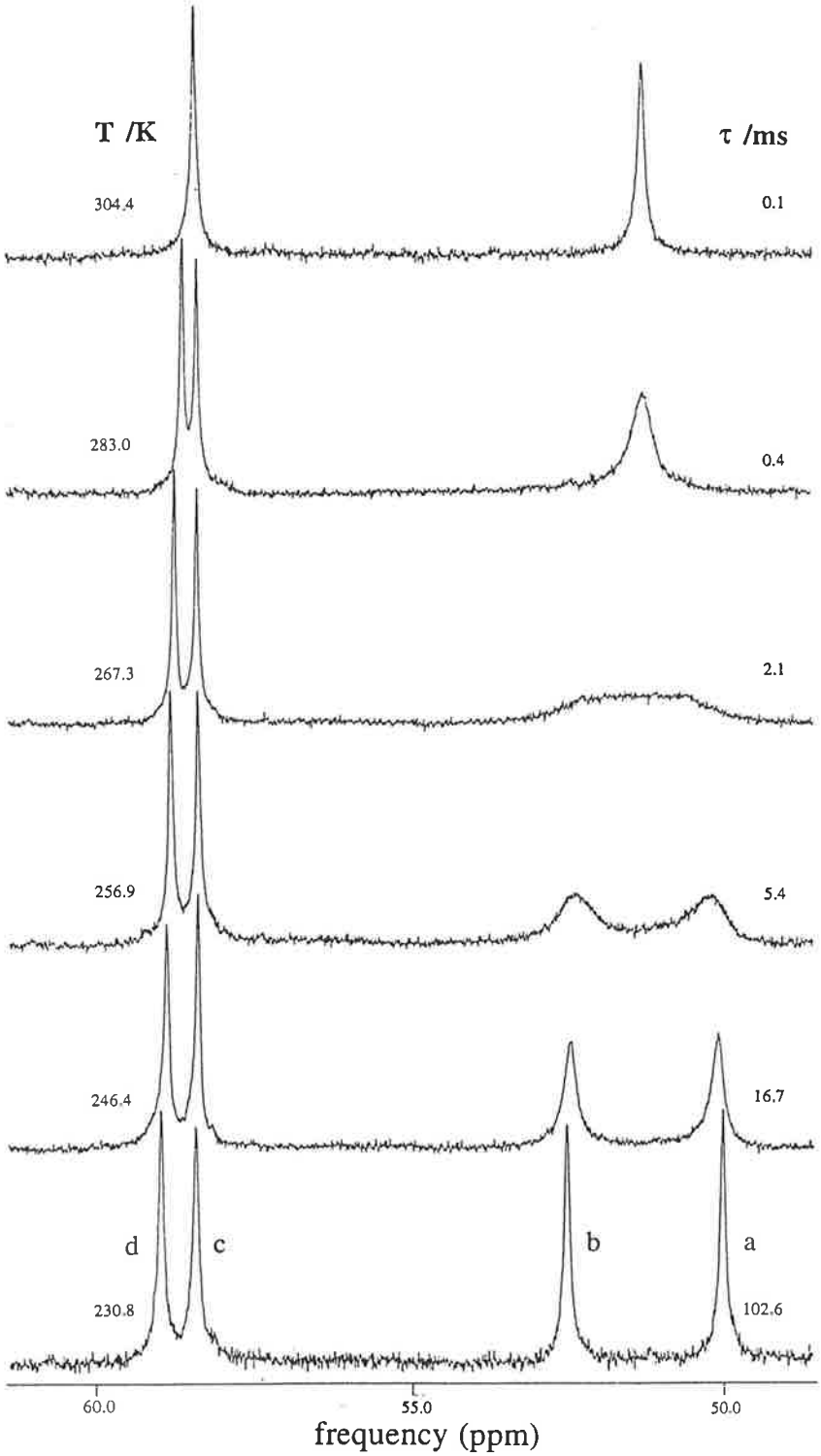

Figure 5.10: Temperature variations of the broad-band ^{1}H decoupled ^{13}C NMR spectra of $[K(THEC12)]^{+}$ (0.055 mol dm^{-3}) in methanol-^{12}C-d_4. Experimental temperatures and τ values derived from complete lineshape analysis of the coalescing doublet arising from the macrocyclic ring carbons, *a* and *b*, appear to the left and the right of the figure, respectively. (Slight broadening of the resonances arising from the pendant arm $>NCH_2$- (*c*) and the -CH_2OH (*d*) carbons are a consequence of the increase in solution viscosity with a decrease in temperature).

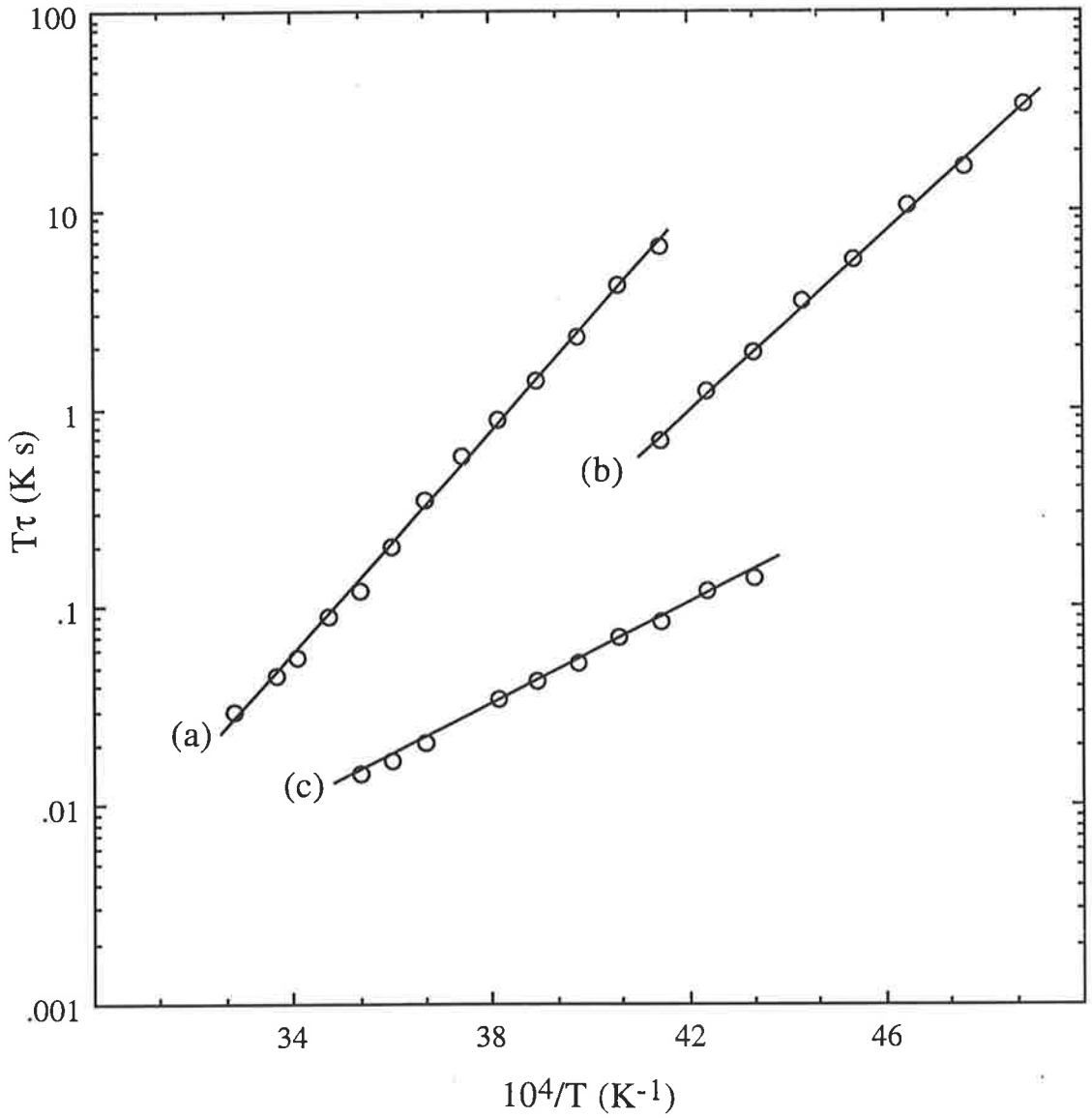

Figure 5.11: Temperature variations of τ for intramolecular exchange in methanol-^{12}C-d_4 between square antiprismatic enantiomers of $[M(THEC12)]^+$. The solid lines represent the best fit of the data to Equation 4.10 for each system.
(a) $[K(THEC12)]^+$, τ. (b) $[Li(THEC12)]^+$, τ. (c) $[Na(THEC12)]^+$, τ/5.

similar arguments to that in Section 5.2.1 that M^+ in $[M(THEC12)]^+$ is 8-coordinate in solution (Figure 5.12), where THEC12 adopts the TRANS I configuration. Stereochemistry similar to that shown in Figure 5.12 has been observed in the solid state for $[K(THEC12)]^+$, but in $[Na(THEC12)]^+$ the hydroxyethyl group of one of the pendant arms is not coordinated, so that Na^+ is 7-coordinate, and in $[Li(THEC12)]^+$ the hydroxyethyl group of three pendant arms are not coordinated so that Li^+ is only 5-coordinate.[33,34] Such structures for the Li^+ and Na^+ complexes, if retained in solution, could not produce the ^{13}C NMR spectra observed for $[Li(THEC12)]^+$ and $[Na(THEC12)]^+$ in this study. This example therefore demonstrates that solid state structures should only be used as an estimation of structures in solution.

Achiral THEC12 forms Δ and Λ enantiomeric complex ions. The convention used in this study assigns such chirality to the left and right handedness of the arrangement of pendant arms in $[M(THEC12)]^+$, respectively. Thus, the intramolecular exchange process that gives rise to the observed ^{13}C spectra of $[M(THEC12)]^+$ is described by an helicity interchange between two 8-coordinate, square antiprismatic enantiomers of C_{4v} symmetry (Figure 5.12). The macrocyclic ring carbons exchange between inequivalent sites *a* and *b*, while the pendant arm carbons (sites *c* and *d*) experience no change in magnetic environment. The mechanism shown in Figure 5.12 assumes that, as for $[M((R)\text{-THPEC12})]^+$, the transition state remains octadentate so that enantiomerisation involves a concerted twisting process. However, it is also possible that the mechanism may involve a sequence of metal-oxygen bond breakage and formation processes in which transient intermediates with monodentate pendant arms participate.

The kinetic parameters for enantiomerisation of $[M(THEC12)]^+$ do not show obviously systematic variations (Table 5.6). This is probably because the contributions to $\Delta H^{\ddagger}$ and $\Delta S^{\ddagger}$ vary in relative magnitude with M^+, and arise from changes in M^+ producing differing contributions through bonding interactions and strain in $[M(THEC12)]^+$. That is, although k(298.2 K) characterising intramolecular exchange in $[M(THEC12)]^+$ decreases with increasing metal ion size from Li^+ to K^+, the large variation in $\Delta H^{\ddagger}$ and $\Delta S^{\ddagger}$ is consistent with a large number of underlying factors contributing to the observed activation parameters for these metal complexes.

The markedly increased lability of $[M(THEC12)]^+$ towards intramolecular exchange by comparison with that of $[M((R)\text{-THPEC12})]^+$ (Table 5.6) is probably attributable to the steric hindrance of the phenyl group on each pendant arm of (*R*)-THPEC12. This is reflected in the significantly higher $\Delta H^{\ddagger}$

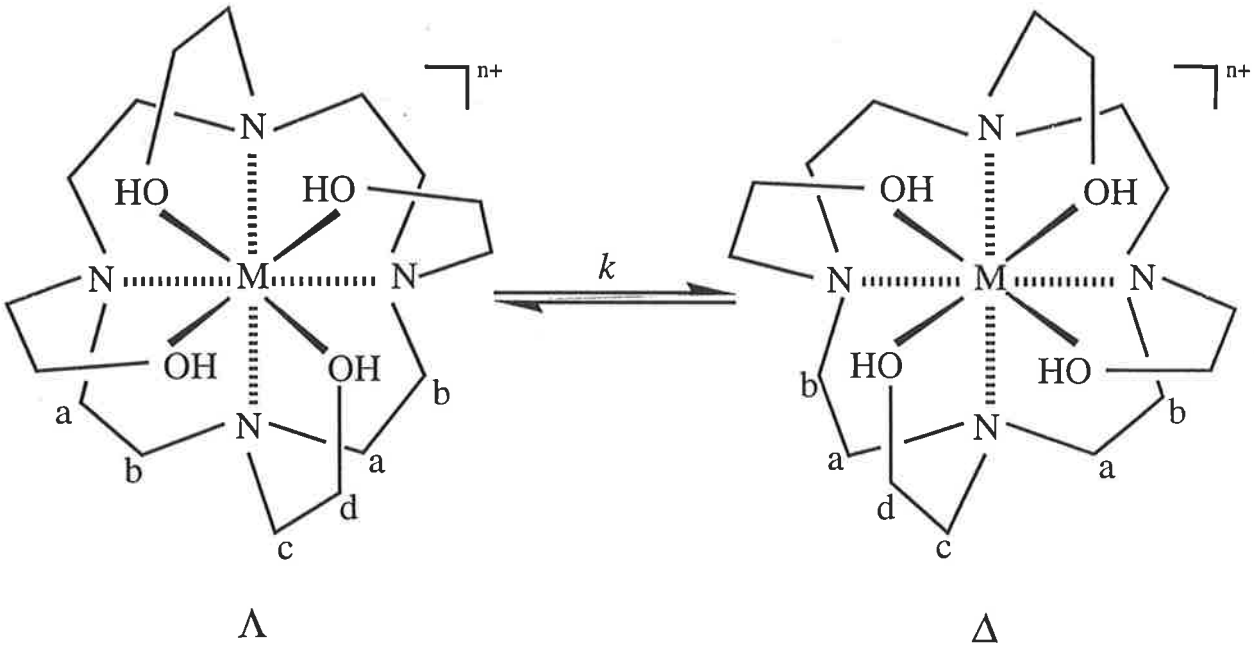

Figure 5.12: Proposed mechanism for the interconversion of the square antiprismatic enantiomers of $[M(THEC12)]^{n+}$, for n = 1 or 2, viewed from above the tetraaza macrocyclic plane.

characterising $[M((R)\text{-THPEC12})]^+$ compared with $[M(THEC12)]^+$ as a result of increasing steric hindrance in the transition state. This trend is then extended to $[M((S)\text{-THPC12})]^+$, where the temperature dependent spectra and coalescence observed for the ring carbons of $[M((S)\text{-THPC12})]^+$ indicate that M^+ in these complexes is also 8-coordinate, (*S*)-THPC12 adopts the TRANS I conformation, and intramolecular exchange in $[M((S)\text{-THPC12})]^+$ is a similar process to that of $[M((R)\text{-THPEC12})]^+$. For $[M((S)\text{-THPC12})]^+$, k(298.2 K) characterising the Li^+, Na^+ and K^+ complexes are 332, 125 and 3020 s^{-1}, respectively.[16] Thus, k(298.2 K) follows the sequence $[M(THEC12)]^+ > [M((S)\text{-THPC12})]^+ > [M((R)\text{-THPEC12})]^+$. This may be a consequence of the increasing size of the substituent at the α carbon (αC) of the ligand along this progression increasing steric hindrance in $[ML]^+$, thus slowing the rate of intramolecular exchange. Similar arguments based on steric hindrance in the ligand have been proposed in the comparison of lanthanide(III) complexes of THEC12, (*S*)-THPC12, and DOTA (1,4,7,10-tetraazacyclododecane-*N*,*N*′,*N*″,*N*‴-tetraacetic acid),[47-49] and for Cd(II) complexes of THEC12 and

Table 5.6: Kinetic parameters[a] for intramolecular exchange in $[ML]^+$, where L = (*R*)-THPEC12, $[M(THEC12)]^+$ and $[M(THEC9)]^+$.

Complex	k (T)[b] s^{-1}	k (298.2 K) s^{-1}	$\Delta H^{\ddagger}$ kJ mol^{-1}	$\Delta S^{\ddagger}$ J K^{-1} mol^{-1}
[c]$[LiL]^+$	184 ± 2 (293.5)	233 ± 2	34.6 ± 0.3	-83.5 ± 1.1
[d]$\Delta[NaL]^+$	276 ± 2 (314.8)	98 ± 1	46.1 ± 0.2	-52.2 ± 0.7
$\Lambda[KL]^+$	245 ± 2 (256.0)	4900 ± 100	42.7 ± 0.3	-31.1 ± 1.2
$\Lambda[RbL]^+$	238 ± 2 (229.9)	34000 ± 1000	39.1 ± 0.3	-27.2 ± 1.2
$\Lambda[CsL]^+$	239 ± 2 (228.8)	35000 ± 1100	38.5 ± 0.3	-28.9 ± 1.3
$[Li(THEC12)]^+$	109 ± 4 (230.8)	18000 ± 3100	41.3 ± 1.3	-24.8 ± 5.9
$[Na(THEC12)]^+$	1237 ± 17 (256.9)	7100 ± 220	24.6 ± 0.5	-88.6 ± 1.8
$[K(THEC12)]^+$	514 ± 11 (267.3)	7000 ± 200	53.7 ± 0.6	8.8 ± 2.3
$[Li(THEC9)]^+$	920 ± 20 (187.1)	1100000 ± 50000	27.7 ± 0.3	-36.3 ± 1.3
$[Na(THEC9)]^+$	791 ± 16 (187.1)	230000 ± 9000	21.7 ± 0.2	-69.6 ± 1.2
$[K(THEC9)]^+$	808 ± 8 (197.6)	24000 ± 470	14.5 ± 0.1	-112.5 ± 0.6

This work unless stated otherwise. [a]Errors represent 1 standard deviation for the fit of experimental τ data to Equation 4.10. [b]Exchange rate constant (k) at the coalescence temperature shown in brackets. [c]Reference 75. [d]Reference 76.

TCMC (1,4,7,10-tetrakis(carbamoylmethyl)-1,4,7,10-tetraazacyclododecane).[49b] A more informative comparison between these and related complexes requires further investigation, particularly involving complexes of the larger Rb^+ and Cs^+ ions.

5.2.3 INTRAMOLECULAR EXCHANGE IN $[M(THEC9)]^+$

The natural abundance broad-band ^1H decoupled ^{13}C NMR spectra of THEC9 and $[M(THEC9)]^+$, where $M^+ = Li^+$, Na^+ and K^+, in methanol-^{12}C-d_4 consist of 3 resonances at the chemical shifts and temperatures shown in Table 5.7. The solubilities of $RbCF_3SO_3$, $CsCF_3SO_3$ and their complexes with THEC9 in methanol at low temperature were insufficient for quantitative ^{13}C NMR studies of $[Rb(THEC9)]^+$ and $[Cs(THEC9)]^+$. For free THEC9 at 291.0 K, the resonance at 54.85 ppm is assigned to the carbons of the 1,2-diaminoethane moiety of the macrocyclic ring (site *a* in Figure 5.13), and the resonances at 59.23 and 59.37 ppm are assigned to the carbons of the $>NCH_2$- moiety and -CH_2OH moiety of the pendant arms (sites *b* and *c*, respectively, in Figure 5.13). The 3 resonances of free THEC9 all broaden at low temperature and are assigned the frequencies shown in Table 5.8 at 181.9 K.

For $[M(THEC9)]^+$, the resonance characterising the carbons of the macrocyclic ring broadens and then splits into 2 separate broad resonances at 181.9 K, as listed in Table 5.8. For $[Li(THEC9)]^+$ and $[Na(THEC9)]^+$, no modifications of the ^{13}C resonances assigned to the pendant arm $>NCH_2$- and -CH_2OH carbons occur apart from viscosity induced line broadening at low temperature. This is consistent with the carbons of the triaza macrocyclic ring of THEC9 exchanging between two magnetically inequivalent environments in $[M(THEC9)]^+$. The pendant arms can exchange between two environments, coordinated and uncoordinated, so that the resonances observed at sites *b* and *c* correspond to the weighted average of the coordinated and uncoordinated pendant arm resonance frequencies. However, for $[Li(THEC9)]^+$ and $[Na(THEC9)]^+$ the pendant arm resonances remain essentially unchanged over the observed temperature range, so that these carbons remain equivalent in their respective environments. In addition, all three pendant arms coordinate M^+ or additional resonances would be observed in the slow exchange ^{13}C NMR spectra of $[Li(THEC9)]^+$ and $[Na(THEC9)]^+$. Thus, Li^+ and Na^+ are 6-coordinate in $[M(THEC9)]^+$, bound by all three nitrogens of the triaza ring and the three pendant arms of THEC9.

The configurations of the triaza ring with coplanar nitrogens coordinating M^+ are shown in Figure 5.14. A complex adopting the + – + (or + – –)

conformation should exhibit 12 distinct resonances in the slow exchange regime of the ^{13}C NMR spectra of $[M(THEC9)]^+$. In addition, for a 6-coordinate complex, the + – + conformation is thermodynamically unfavourable because it places M^+ in the plane of the triaza nitrogens, a geometry which generates considerable steric strain in $[M(THEC9)]^+$. Accordingly, this configuration for the structure of $[M(THEC9)]^+$ can be eliminated. The observed ^{13}C NMR spectra of $[Li(THEC9)]^+$ and $[Na(THEC9)]^+$ are best accounted for by a structure incorporating the + + + conformation, also denoted [333],[50-52] where Li^+ and Na^+ are coordinated above the triaza ring to the three coplanar nitrogens and the three hydroxyethyl pendant arms of THEC9. Therefore, in $[M(THEC9)]^+$ all three pendant arms are coordinated on the same side of the triaza ring and the triangular plane delineated by the three oxygens of THEC9, which is parallel to the triangular plane delineated by the three nitrogens below M^+, is rotated about the C_3 axis of $[M(THEC9)]^+$ to give a distorted trigonal prismatic first coordination sphere.

Computed structures and X-ray crystallographic data add plausibility to the interpretation of the ^{13}C NMR data. That is, molecular mechanics calculations have shown that the + + + conformation is the lowest energy configuration, and the most commonly adopted conformation for cyclononane derived macrocycles.[50,51] This is in agreement with both the molecular orbital calculations of $[M(THEC9)]^+$ (discussed in Chapter 2)[56] and the solid state structures of related complexes.[52] In addition, other workers have postulated that metal complexes involving THEC9 and related ligands should experience considerable trigonal distortion because the hydroxyethyl arms are too short to permit regular octahedral coordination.[52-54]

A selection of the temperature dependent ^{13}C NMR spectra of $[Li(THEC9)]^+$ and $[K(THEC9)]^+$ are shown in Figures 5.15 and 5.16, respectively. $[Na(THEC9)]^+$ shows similar coalescence phenomena to that of $[Li(THEC9)]^+$, but over a different temperature range. Complete lineshape analysis[46] of the coalescence of the macrocyclic ring resonances *a* and *b* yielded the mean site lifetime, τ, illustrated by Figure 5.17. The kinetic parameters listed in Table 5.6 for this exchange process were derived from the temperature variation of τ through Equation 4.10. From Figures 5.15 and 5.16, it is apparent that the broadness of the resonances *a* and *b* near the solution freezing point is a result of enantiomerisation occurring just within the slow exchange regime of the NMR timescale. Thus, in deriving τ for $[Li(THEC9)]^+$ it was approximated that the unmodified macrocyclic ring carbon linewidths are the same as those of the pendant $>NCH_2-$ carbons and show the same temperature dependence, and that the chemical shift differences between resonances *a* and *b* are temperature independent.

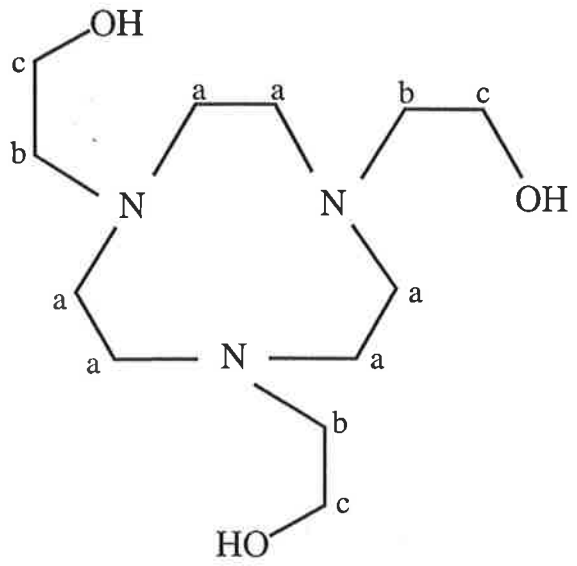

Figure 5.13: Assignment of the ^{13}C resonances of THEC9 and $[M(THEC9)]^{n+}$, where M^{n+} = alkali or alkaline earth metal ion.

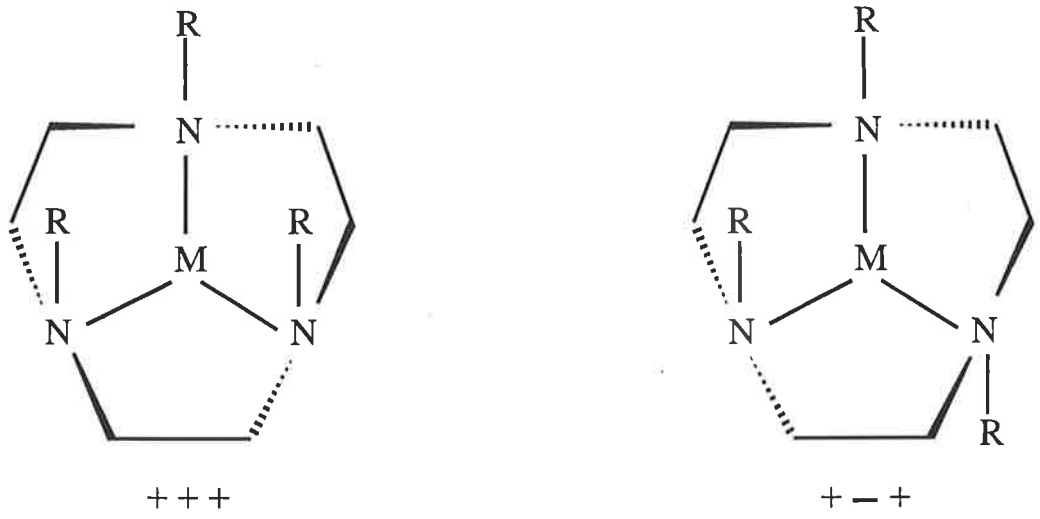

Figure 5.14: Possible configurational isomers of $[M(THEC9)]^+$, where M^+ = Li^+ and Na^+, in methanol-^{12}C-d_4. The hydroxyethyl pendant arms, denoted R, are shown uncoordinated. The R groups oriented above the nitrogen plane are indicated with a +, while those below the plane are indicated with a –.

Table 5.7: Fast exchange ^{13}C chemical shifts of $[M(THEC9)]^+$ in methanol-^{12}C-d_4.

Complex	T	δ[a]		
	K	ppm		
THEC9	291.0	54.85	59.23	59.37
$[Li(THEC9)]^+$	234.1	53.12	58.02	59.33
$[Na(THEC9)]^+$	239.3	51.95	57.81	60.05
$[K(THEC9)]^+$	249.7	53.05	58.57	60.29

[a] ^{13}C chemical shifts are referenced to external natural abundance methanol-^{12}C-d_4, which is assigned a chemical shift of 47.05 ppm.

Table 5.8: Slow exchange ^{13}C chemical shifts of $[M(THEC9)]^+$ at 181.9 K in methanol-^{12}C-d_4.

Complex	δ[a]			
	ppm			
THEC9	very broad		57.35	59.93
$[Li(THEC9)]^+$	50.01	56.66	58.13	59.33
$[Na(THEC9)]^+$	48.99	54.75	57.73	59.93
$[K(THEC9)]^+$	47.65	56.48	58.29	60.65

[a] ^{13}C chemical shifts are referenced to external natural abundance methanol-^{12}C-d_4, which is assigned a chemical shift of 47.05 ppm.

The $[K(THEC9)]^+$ macrocyclic ring resonances exhibit similar coalescence phenomena to that of $[Li(THEC9)]^+$ and $[Na(THEC9)]^+$. However, the pendant arm carbon resonances are also greatly broadened at low temperature (Figure 5.16). This may be due to K^+, with a larger 6-coordinate ionic radius (1.38 Å) than Li^+ or Na^+ (0.76 Å and 1.02 Å, respectively),[41] increasing its coordination

number by coordinating methanol in addition to THEC9. Thus, exchange between $[K(THEC9)]^+$ and a second K^+ complex ion, possibly $[K(THEC9)(methanol)_n]^+$, may be significant at low temperature. A similar phenomenon has been observed for $[K((S)\text{-}THPC9)]^+$.[55] Therefore, in deriving τ for $[K(THEC9)]^+$, it was approximated that the unmodified macrocyclic ring carbon linewidths are the same as those of the pendant arm $>NCH_2$- carbons of $[Na(THEC9)]^+$and show the same temperature dependence, and that the chemical shift differences between resonances *a* and *b* are temperature independent. (The broadness of all 3 ^{13}C resonances of free THEC9 at low temperature is probably due to the existence of several conformers which may be stabilised through hydrogen bonding with methanol. This observation contrasts with the prediction of a single enantiomeric pair through molecular orbital calculations which do not allow for such hydrogen bonding interactions).[56]

The ^{13}C NMR spectra in Figures 5.15 and 5.16 are consistent with the alkali metal complex ions of achiral THEC9 existing as 6-coordinate, rapidly interconverting Δ and Λ $[M(THEC9)]^+$ enantiomers (Figure 5.18). The convention adopted in this study refers to the pendant arms showing a clockwise and anticlockwise rotation in the Δ and Λ enantiomers, respectively, when viewed down the C_3 axis from the oxygen plane. Enantiomerisation causes the macrocyclic ring carbons to exchange between inequivalent environments, denoted *a* and *b* in Figure 5.18, while for $[Li(THEC9)]^+$ and $[Na(THEC9)]^+$ the pendant arm $>NCH_2$- and $-CH_2OH$ carbons exchange between their respective equivalent environments, *c* and *d* (Figure 5.18). The mechanism assumes that the transition state remains hexadentate, although it cannot dismissed that one or more of the pendant arms may become uncoordinated in the transition state. The activation parameters $\Delta H^{\ddagger}$ and $\Delta S^{\ddagger}$ represent the differences between the ground state and transition state geometries of $[M(THEC9)]^+$, and the same factors accounting for the differences between the ground and transition states for $[M((R)\text{-}THPEC12)]^+$ and $[M(THEC12)]^+$ (Sections 5.2.1 and 5.2.2) are also applicable for $[M(THEC9)]^+$.

As M^+ changes from Li^+ to K^+, k(298.2 K) and $\Delta H^{\ddagger}$ characterising enantiomerisation in $[M(THEC9)]^+$ decrease, and $\Delta S^{\ddagger}$ becomes progressively more negative, indicating that the rate of intramolecular exchange for $[M(THEC9)]^+$ may be controlled by the size of M^+. Nonetheless, contributions to the transition state enthalpies and entropies in $[M(THEC9)]^+$ from bonding and ligand strain vary in different ways with M^+. From a comparison of the kinetic parameters in Table 5.6, it is apparent that $[M(THEC9)]^+$ undergo

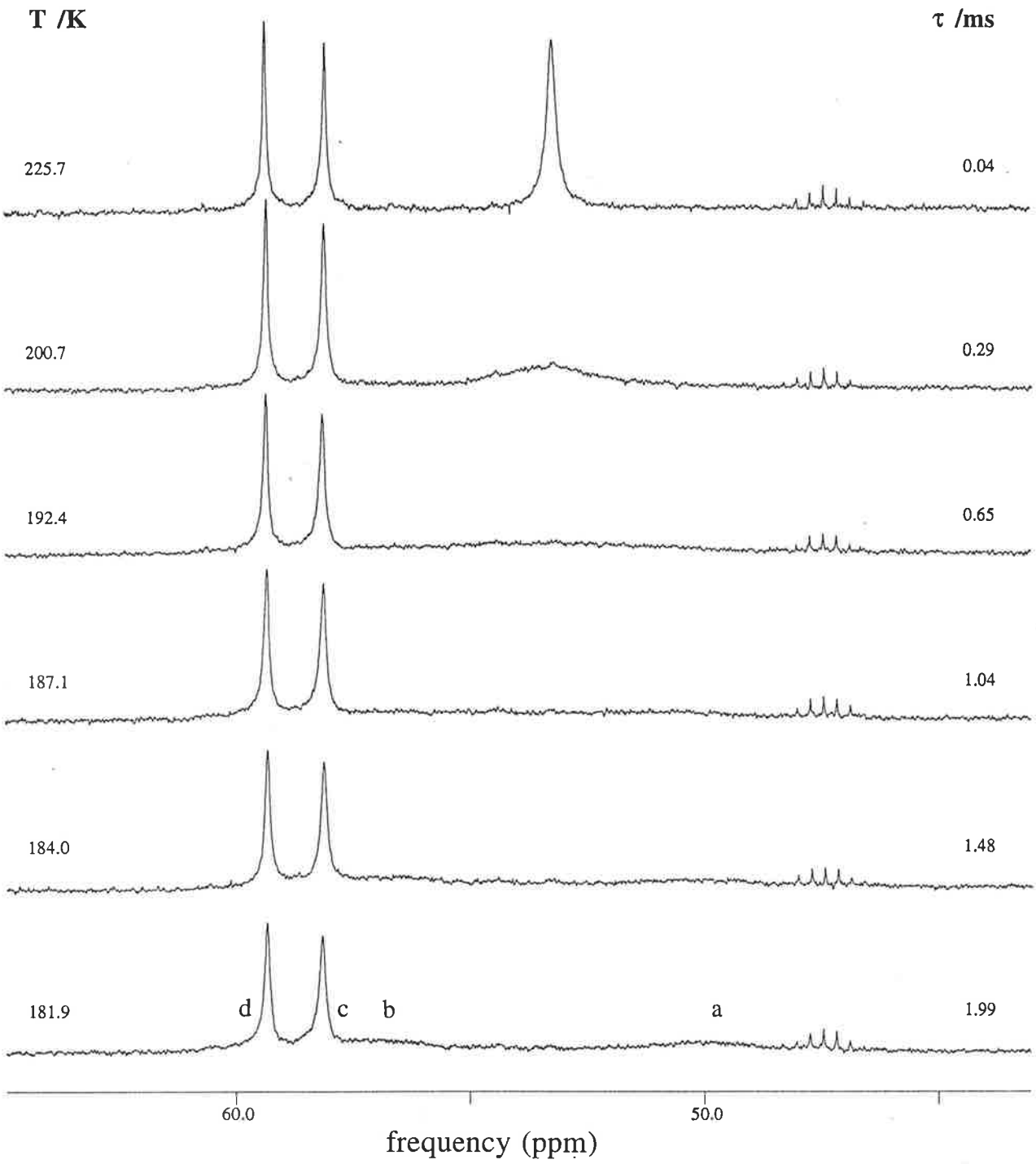

Figure 5.15: Temperature variations of the broad-band ^{1}H decoupled ^{13}C NMR spectra of $[Li(THEC9)]^{+}$ (0.101mol dm^{-3}) in methanol-^{12}C-d_4. Experimental temperatures and τ values derived from complete lineshape analysis of the coalescing doublet arising from the macrocyclic ring carbons, *a* and *b*, appear to the left and the right of the figure, respectively. (Slight broadening of the resonances arising from the pendant arm $>NCH_2$- (*c*) and the -CH_2OH (*d*) carbons are a consequence of the increase in solution viscosity with a decrease in temperature).

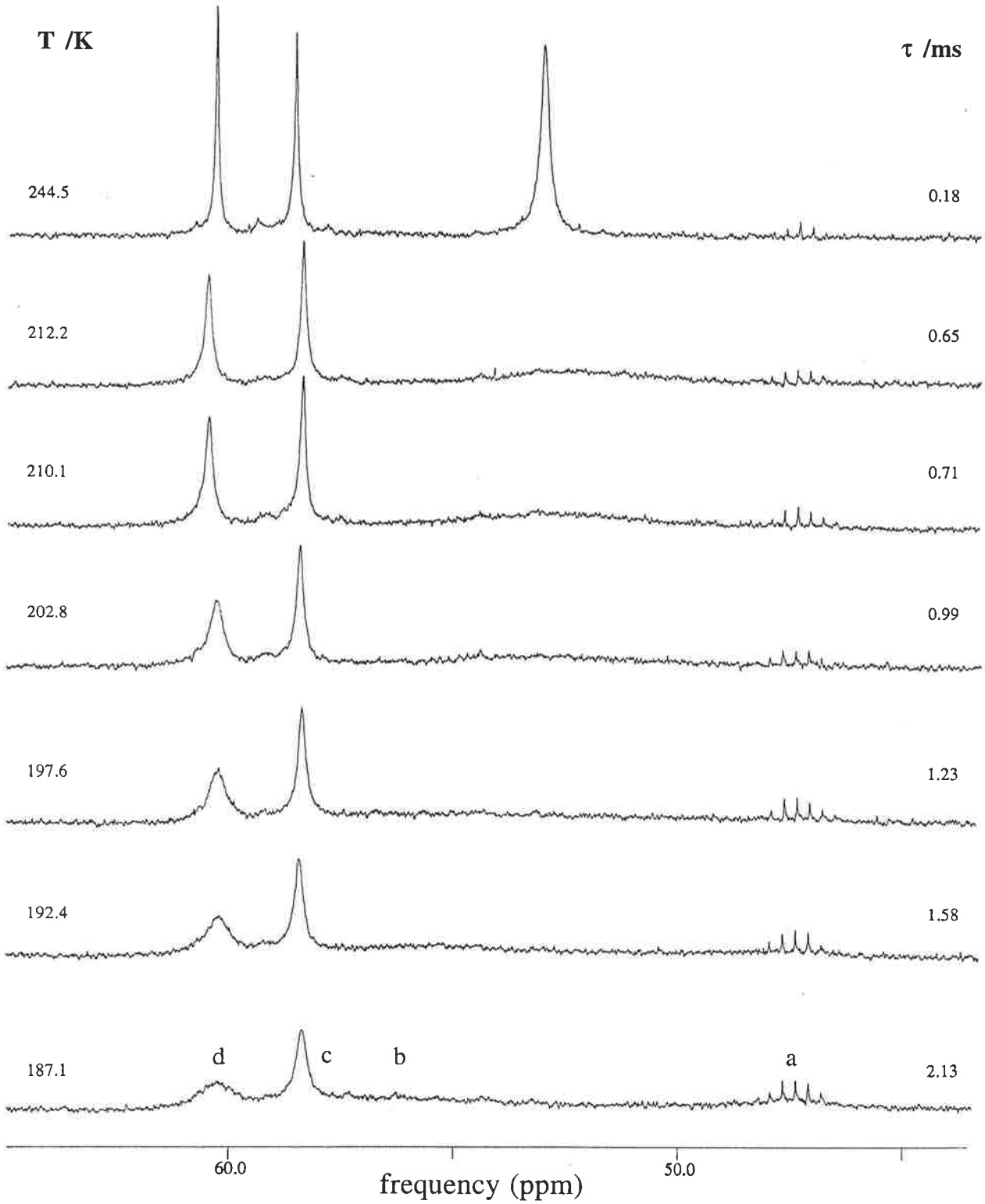

Figure 5.16: Temperature variations of the broad-band ^{1}H decoupled ^{13}C NMR spectra of $[K(THEC9)]^{+}$ (0.101 mol dm^{-3}) in methanol-^{12}C-d_4. Experimental temperatures and τ values derived from complete lineshape analysis of the coalescing doublet arising from the macrocyclic ring carbons, *a* and *b*, appear to the left and the right of the figure, respectively. (Slight broadening of the resonances arising from the pendant arm $>NCH_2$- (*c*) and the -CH_2OH (*d*) carbons are a consequence of the increase in solution viscosity with a decrease in temperature).

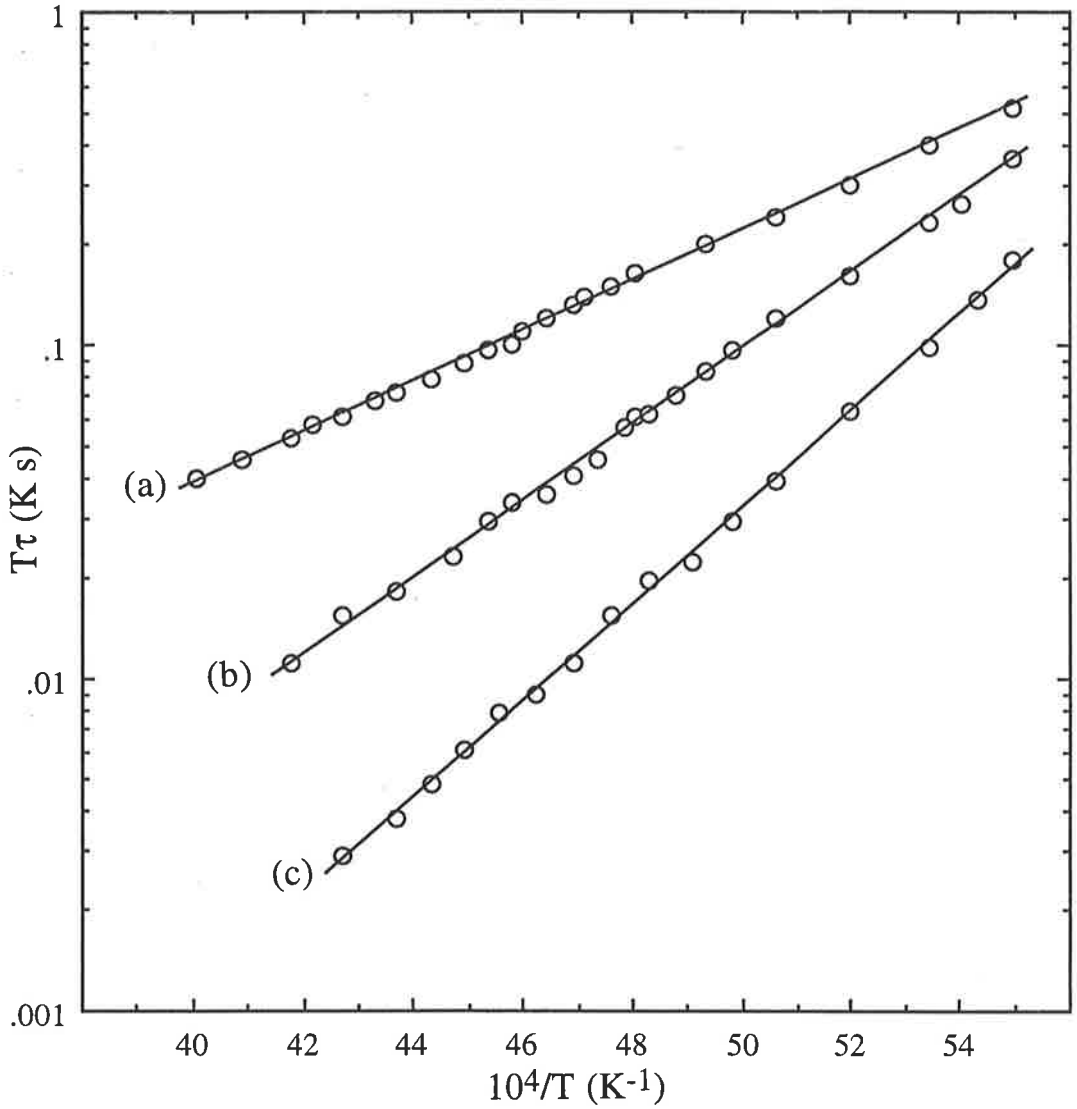

Figure 5.17: Temperature variations of τ for intramolecular exchange in methanol-^{12}C-d_4 between enantiomers of $[M(THEC9)]^+$. The solid lines represent the best fit of the data to Equation 4.10 for each system.
(a) $[K(THEC9)]^+$, τ. (b) $[Na(THEC9)]^+$, τ. (c) $[Li(THEC9)]^+$, τ/2.

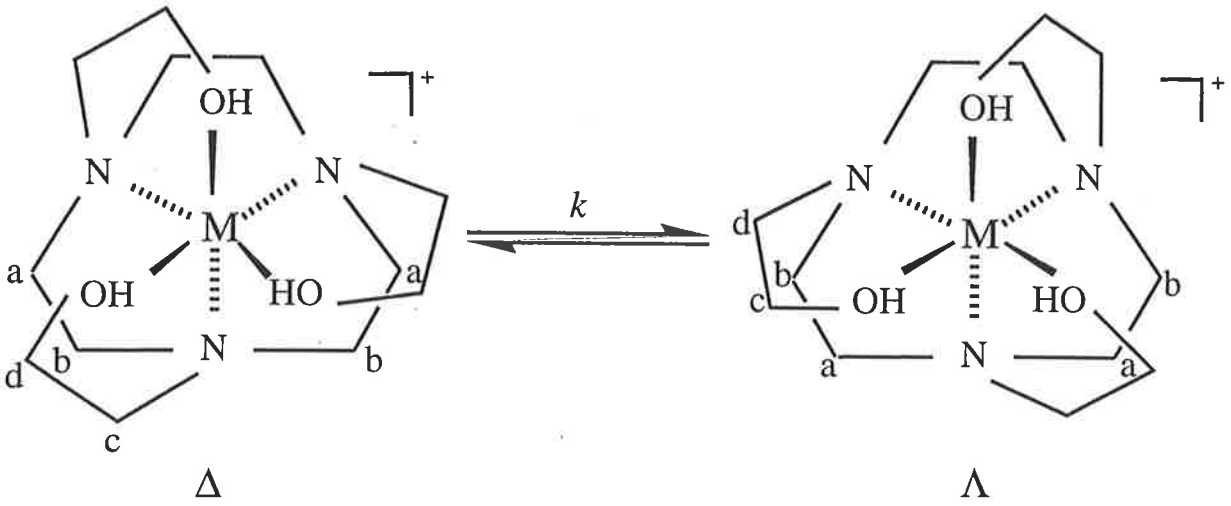

Figure 5.18: Proposed mechanism for the interconversion of the enantiomers of $[M(THEC9)]^+$ viewed from above the triaza macrocyclic plane. Assignment of the resonances *a* and *b* to specific macrocyclic ring carbons cannot be made from the present data.

faster intramolecular exchange than $[M(THEC12)]^+$ and $[M((R)\text{-}THPEC12)]^+$. This is probably a consequence of the occurrence of only 6 metal-ligand bonds in $[M(THEC9)]^+$, compared with $[M(THEC12)]^+$ and $[M((R)\text{-}THPEC12)]^+$ where 8 such bonds exist, and is reflected in the generally smaller $\Delta H^{\ddagger}$ and more negative $\Delta S^{\ddagger}$ values characterising $[M(THEC9)]^+$.

5.3 ^{13}C INTRAMOLECULAR EXCHANGE IN ALKALINE EARTH METAL ION COMPLEXES

5.3.1 INTRAMOLECULAR EXCHANGE IN $[M(THEC12)]^{2+}$

The natural abundance broad-band ^1H decoupled ^{13}C NMR spectra of $[M(THEC12)]^{2+}$, where $M^{2+} = Mg^{2+}$, Ca^{2+} and Ba^{2+}, in methanol-^{12}C-d_4 consist of 3 resonances at the temperatures shown in Table 5.9, arising from 3 different chemical carbon environments. For $[Mg(THEC12)]^{2+}$ at 296.6 K, the resonance at 49.10 ppm is assigned to the carbons of the 1,2-diaminoethane moiety of the macrocyclic ring (site *a* in Figure 5.9), and the resonances at 53.11 and 55.64 ppm are respectively assigned to the carbons of the $>NCH_2$- moiety and -CH_2OH moiety of the hydroxyethyl arms of THEC12 (sites *b* and *c*, respectively, in Figure 5.9). For $[Ca(THEC12)]^{2+}$ at 296.6 K, these correspond to the resonances at 49.02, 54.24 and 56.11 ppm, respectively. For $[Ba(THEC12)]^{2+}$ at 296.6 K, these correspond to the resonances at 49.41,

56.14 and 56.93 ppm, respectively. As the temperature decreases, the resonance characterising the carbons of the macrocyclic ring in $[M(THEC12)]^{2+}$ broadens and then splits into 2 separate resonances (Table 5.10), while the pendant arm resonances remain essentially as singlets apart from some slight broadening due to increased solution viscosity. As for the complexes discussed in Section 5.2, this is consistent with the carbons of the macrocyclic ring exchanging between two inequivalent sites in $[M(THEC12)]^{2+}$.

Table 5.9: Fast exchange ^{13}C chemical shifts of $[M(THEC12)]^{2+}$ in methanol-^{12}C-d_4.

Complex	T	δ^a		
	K	ppm		
$[Mg(THEC12)]^{2+}$	296.6	49.10	53.11	55.64
$[Ca(THEC12)]^{2+}$	296.6	49.02	54.24	56.11
$[Ba(THEC12)]^{2+}$	296.6	49.41	56.14	56.93
$[Zn(THEC12)]^{2+}$	251.6	48.44	52.17	55.92

[a] ^{13}C chemical shifts are referenced to external natural abundance methanol-^{12}C-d_4, which is assigned a chemical shift of 47.05 ppm.

Table 5.10: Slow exchange ^{13}C chemical shifts of $[M(THEC12)]^{2+}$ at 199.4 K in methanol-^{12}C-d_4.

Complex	δ^a					
	ppm					
$[Mg(THEC12)]^{2+}$	48.07	48.81	51.82	55.37		
$[Ca(THEC12)]^{2+}$	48.46	49.14	54.01	56.02		
$[Ba(THEC12)]^{2+}$	48.44	49.65	55.73	56.66		
[b]$[Zn(THEC12)]^{2+}$	46.57	48.19	49.69[c]	54.02	54.72	57.71

[a] ^{13}C chemical shifts are referenced to external natural abundance methanol-^{12}C-d_4, which is assigned a chemical shift of 47.05 ppm. [b]At 178.6 K. [c] 2 overlapping resonances.

A selection of the temperature dependent ^{13}C NMR spectra of $[Mg(THEC12)]^{2+}$ and $[Ca(THEC12)]^{2+}$ are shown in Figures 5.19 and 5.20, respectively. The spectra for the analogous Ba^{2+} complex show similar temperature dependence for the macrocyclic ring resonances but over a different temperature range. The temperature dependence of the spectra observed for $[M(THEC12)]^{2+}$ is analogous to that seen in Section 5.2 for $[M((R)\text{-}THPEC12)]^{+}$ and $[M(THEC12)]^{+}$. Thus, M^{2+} in $[M(THEC12)]^{2+}$ is 8-coordinate in solution, THEC12 adopts the TRANS I configuration, and intramolecular exchange in $[M(THEC12)]^{2+}$ is similar to that postulated for $[M(THEC12)]^{+}$, where the complex has approximately square antiprismatic (C_4) geometry and undergoes intramolecular interconversion between its two enantiomeric forms (Figure 5.12). This exchange process interchanges the magnetic environments of the macrocyclic ring carbons at sites *a* and *b* in Figure 5.12, but not those of the pendant arm carbons (sites *c* and *d*).

From the coalescence behaviour of the resonances corresponding to the carbon atoms of the macrocyclic ring, complete lineshape analysis[46] yielded the mean site lifetime, τ, for the complex in either enantiomeric form, as illustrated by Figure 5.21. The kinetic parameters shown in Table 5.11 for this exchange process were determined from the temperature variations of τ through Equation 4.10. It is apparent from the kinetic parameters characterising intramolecular exchange in $[M(THEC12)]^{2+}$ (Table 5.11) that as M^{2+} changes from Mg^{2+} to Ba^{2+}, $\Delta H^{\ddagger}$ increases, $\Delta S^{\ddagger}$ becomes progressively less negative, and k(298.2 K) dramatically decreases. Therefore, unlike the $[M(THEC12)]^{+}$ complexes which do not show a clear trend with changing M^{+} (Section 5.2), the rate of intramolecular exchange for $[M(THEC12)]^{2+}$ may be largely controlled by the size of M^{2+}. It has been shown (Chapter 3) that $[Ca(THEC12)]^{2+}$ is the most stable alkaline earth complex of THEC12, where Ca^{2+} mirrors the optimum bonding and least strain in $[M(THEC12)]^{2+}$ that was seen for $[Na(THEC12)]^{+}$. On this basis, it is anticipated that $[Ca(THEC12)]^{2+}$ should undergo the slowest rate of enantiomerisation of the $[M(THEC12)]^{2+}$ complexes in Table 5.11. The smaller Mg^{2+} ion, with an 8-coordinate radius[41] of 0.89 Å and less optimal bonding distances than Ca^{2+} in its complex with THEC12, may facilitate easier metal-ligand bond breakage and faster intramolecular exchange than $[Ca(THEC12)]^{2+}$. It is envisaged that the larger Ba^{2+} ion, with an 8-coordinate radius[41] of 1.42 Å, also induces considerable strain in $[Ba(THEC12)]^{2+}$. However, its larger size may hinder intramolecular exchange processes, so that although $[Ca(THEC12)]^{2+}$ may be anticipated to undergo the slowest enantiomerisation, it appears that as the charge density systematically decreases with increasing metal ion size from Mg^{2+} to Ba^{2+}, the rate of intramolecular exchange decreases along this progression.

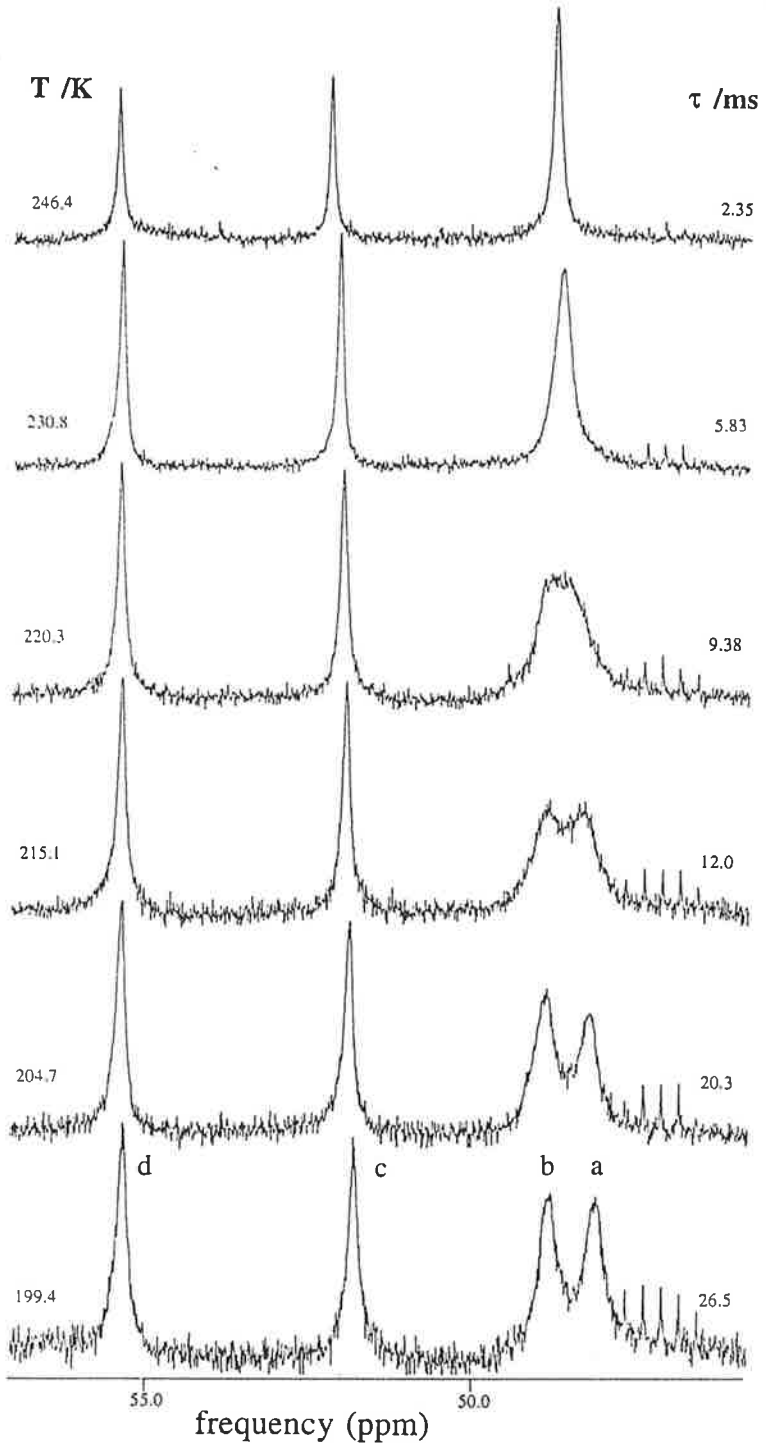

Figure 5.19: Temperature variations of the broad-band ^{1}H decoupled ^{13}C NMR spectra of $[Mg(THEC12)]^{2+}$ (0.100 mol dm^{-3}) in methanol-^{12}C-d_4. Experimental temperatures and τ values derived from complete lineshape analysis of the coalescing doublet arising from the macrocyclic ring carbons, *a* and *b*, appear to the left and the right of the figure, respectively. (Slight broadening of the resonances arising from the pendant arm $>NCH_2$- (*c*) and $-CH_2OH$ (*d*) carbons are a consequence of the increase in solution viscosity with a decrease in temperature).

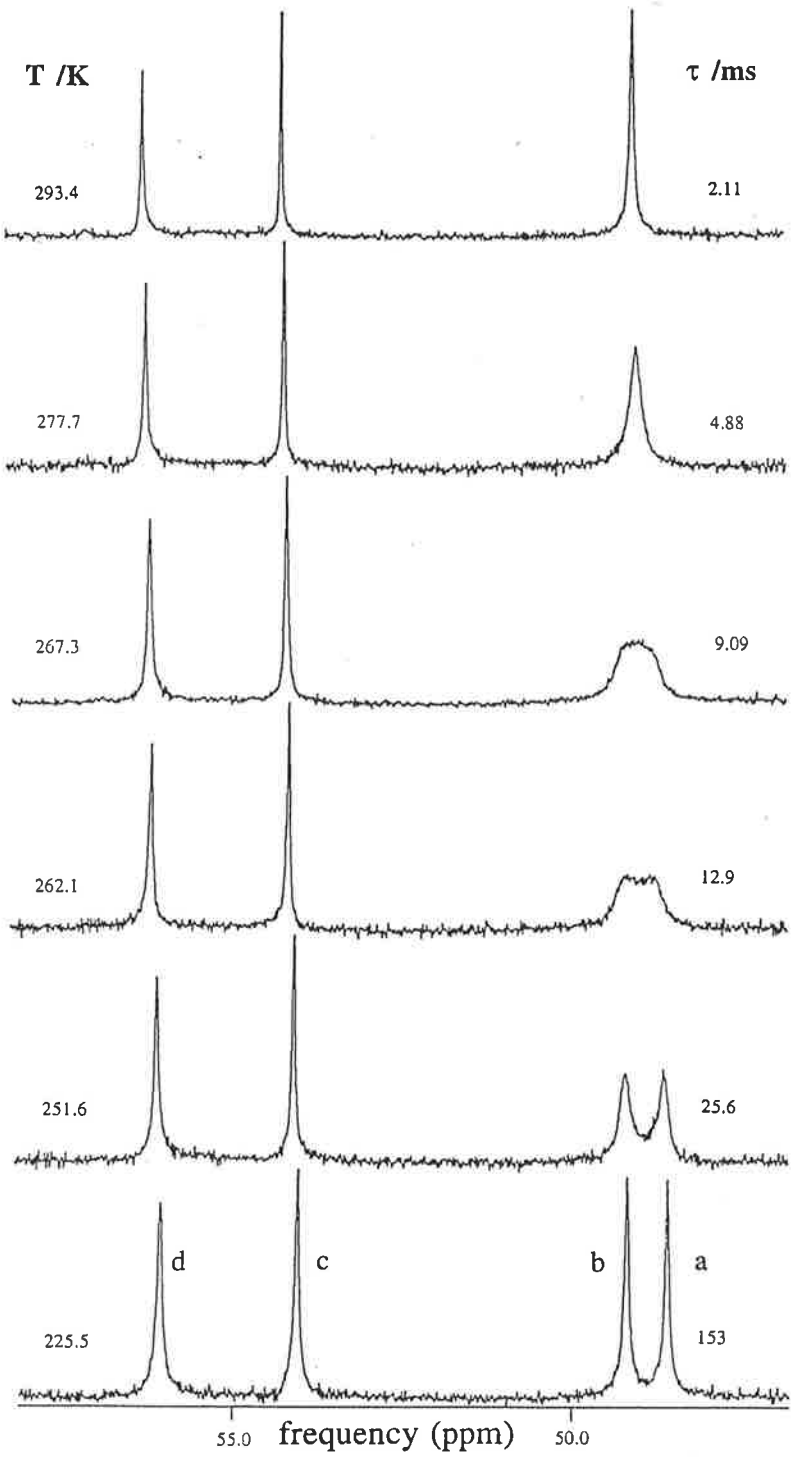

Figure 5.20: Temperature variations of the broad-band ^{1}H decoupled ^{13}C NMR spectra of $[Ca(THEC12)]^{2+}$ (0.110 mol dm^{-3}) in methanol-^{12}C-d_4. Experimental temperatures and τ values derived from complete lineshape analysis of the coalescing doublet arising from the macrocyclic ring carbons, *a* and *b*, appear to the left and the right of the figure, respectively. (Slight broadening of the resonances arising from the pendant arm $>NCH_2$- (*c*) and $-CH_2OH$ (*d*) carbons are a consequence of the increase in solution viscosity with a decrease in temperature).

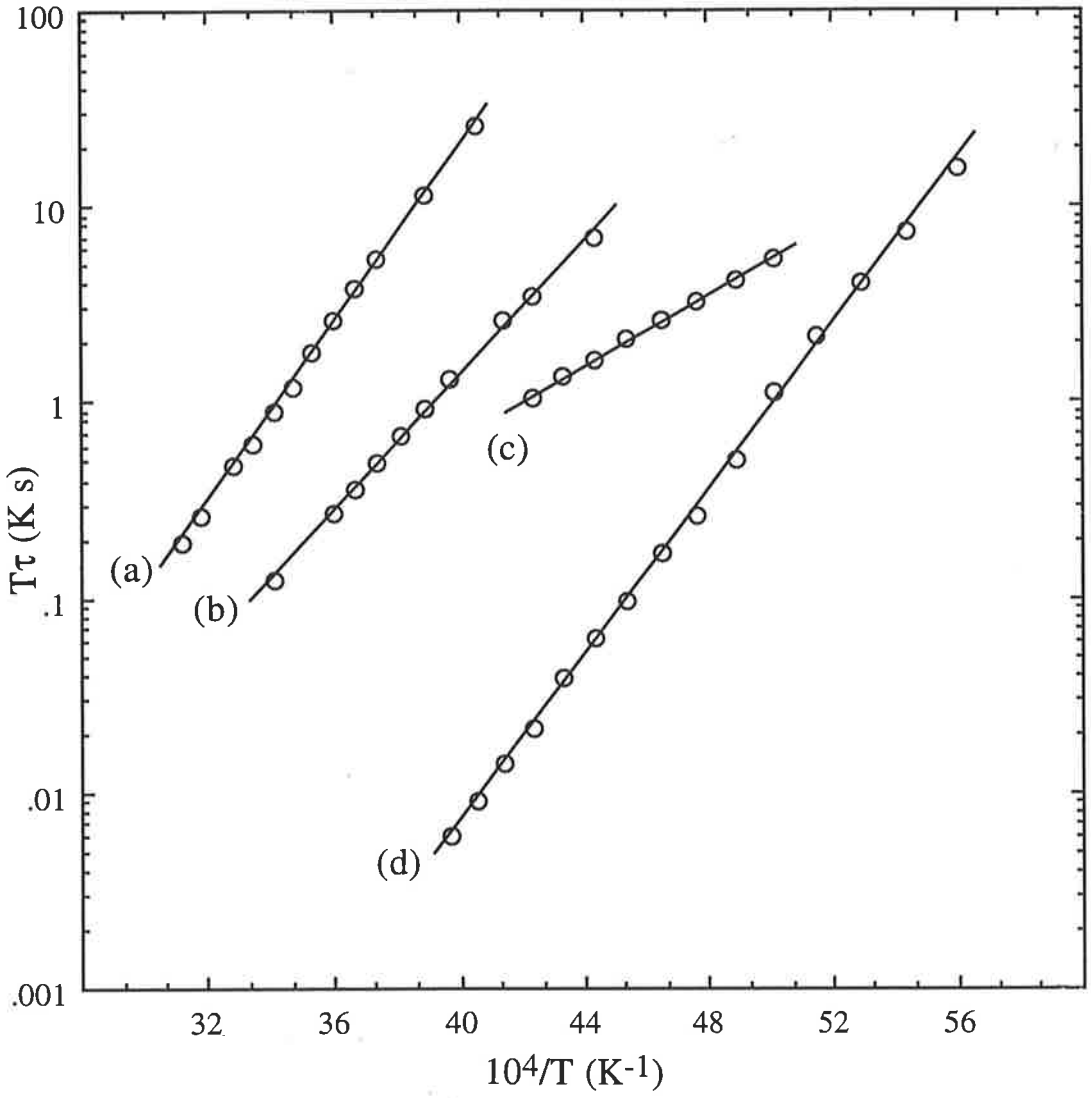

Figure 5.21: Temperature variations of τ for intramolecular exchange in methanol-^{12}C-d_4 between enantiomers of $[M(THEC12)]^{2+}$. The solid lines represent the best fit of the data to Equation 4.10 for each system.
(a) $[Ba(THEC12)]^{2+}$, τ. (b) $[Ca(THEC12)]^{2+}$, τ/5.
(c) $[Mg(THEC12)]^{2+}$, τ. (d) $[Zn(THEC12)]^{2+}$, τ.

Table 5.11: Kinetic parameters[a] for intramolecular exchange in $[M(THEC12)]^{2+}$ and $[M(THEC9)]^{2+}$ in methanol-^{12}C-d_4.

Complex	k (T)[b] s^{-1}	k (298.2 K) s^{-1}	$\Delta H^{\ddagger}$ kJ mol^{-1}	$\Delta S^{\ddagger}$ J K^{-1} mol^{-1}
$[Mg(THEC12)]^{2+}$	85 ± 3 (215.1)	2300 ± 260	19.1 ± 0.8	-116.5 ± 3.8
$[Ca(THEC12)]^{2+}$	80 ± 1 (262.1)	550 ± 20	33.3 ± 0.5	-80.3 ± 1.8
$[Ba(THEC12)]^{2+}$	112 ± 1 (277.7)	445 ± 5	43.9 ± 0.4	-47.0 ± 1.3
$[Zn(THEC12)]^{2+}$	724 ± 15[c] (209.5)	1060000 ± 50000	40.9 ± 0.3	7.6 ± 1.6
	388 ± 9[d] (204.7)			
$[Mg(THEC9)]^{2+}$	601 ± 7 (208.0)	7800 ± 150	12.6 ± 0.1	-128.1 ± 0.7
$[Ca(THEC9)]^{2+}$	450 ± 4 (208.0)	6700 ± 180	13.4 ± 0.2	-126.7 ± 0.8
$[Ba(THEC9)]^{2+}$	872 ± 8 (219.5)	69000 ± 1600	28.1 ± 0.2	-58.1 ± 0.8

This work unless stated otherwise. [a]Errors represent 1 standard deviation for the fit of experimental τ data to Equation 4.10. [b]Exchange rate constant (k) at the coalescence temperature shown in brackets, unless stated otherwise. [c]Exchange rate constant (k) at the $>NCH_2$- resonance coalescence temperature shown in brackets. [d]Exchange rate constant (k) at -CH_2OH resonance coalescence temperature shown in brackets.

The $[M(THEC12)]^{2+}$ complexes undergo slower intramolecular exchange at 298.2 K than $[M(THEC12)]^{+}$ (Table 5.6). The alkali and alkaline earth metal ions are hard acids and interact more strongly with the oxygen over nitrogen donor atoms of THEC12.[57-60] However, because of their divalent nature, slower enantiomerisation of the alkaline earth metal complexes may result from an enhanced metal-ligand bond strength for M^{2+} compared with M^{+}, obstructing the bond lengthening necessary for the complex to move through the transition state. This observation is in accord with the generally higher

stabilities observed for $[M(THEC12)]^{2+}$ compared with $[M(THEC12)]^{+}$ (Chapters 2 and 3).

The ^{13}C NMR solution studies of $[M((S)\text{-}THPC12)]^{+}$, for $M^{2+} = Mg^{2+}$, Ca^{2+} and Ba^{2+}, show that these complexes exist as two diastereomers in slow exchange with each other on the NMR timescale over the liquid temperature range of methanol.[44b] Thus, on progression from THEC12 to (*S*)-THPC12, the increasing substituent size at the αC of the ligand may induce steric hindrance in $[ML]^{2+}$, thus hindering metal-ligand bond breakage and formation. As a result, k(298.2 K) follows the order $[M(THEC12)]^{2+} >> [M((S)\text{-}THPC12)]^{2+}$, which is the same trend observed for the alkali metal analogues (Section 5.2.2). Unfortunately, the lack of available kinetic data characterising intramolecular exchange in related metal ion complexes precludes further examination of this supposition.

5.3.2 INTRAMOLECULAR EXCHANGE IN $[M(THEC9)]^{2+}$

The natural abundance broad-band ^{1}H decoupled ^{13}C NMR spectra of $[M(THEC9)]^{2+}$, for $M^{2+} = Mg^{2+}$, Ca^{2+} and Ba^{2+}, in methanol-^{12}C-d_4 consist of 3 resonances at the temperatures shown in Table 5.12, arising from 3 different chemical carbon environments. For $[Mg(THEC9)]^{2+}$ at 286.2 K, the resonance at 52.93 ppm is assigned to the carbons of the 1,2-diaminoethane moiety of the macrocyclic ring (site *a* in Figure 5.13), and the resonances at 58.46 and 58.62 ppm are respectively assigned to the carbons of the $>NCH_2$- moiety (*b*) and the $-CH_2OH$ moiety (*c*) of the hydroxyethyl arms of THEC9. For $[Ca(THEC9)]^{2+}$ at 244.5 K, these correspond to the resonances at 51.58, 57.94 and 58.39 ppm, respectively. For $[Ba(THEC9)]^{2+}$ at 265.3 K, these correspond to the resonances at 52.01, 58.94 and 59.13 ppm, respectively. As the temperature decreases, the resonance characterising the carbons of the macrocyclic ring in $[M(THEC9)]^{2+}$ broadens and then splits into 2 separate, broad resonances (Table 5.13), with signals just distinguishable above the baseline of the spectra. For $[Mg(THEC9)]^{2+}$, as the temperature is lowered from 286.2 K, the resonances assigned to the carbons of the $>NCH_2$- moiety (*c*) and $-CH_2OH$ moiety (*d*) of the pendant arms of THEC9 move towards each other so that they overlap and then interchange by 265.3 K. As the temperature is lowered below 254.9 K, these 2 resonances move towards each other again to coincide at 223.6 K, and at low temperature broadening due to chemical exchange makes identification of the pendant arm resonances difficult. For $[Ca(THEC9)]^{2+}$ and $[Ba(THEC9)]^{2+}$, there is no interchange of the resonances characterising the hydroxyethyl pendant arms. For $[Ca(THEC9)]^{2+}$, the pendant arm resonances broaden with decreasing temperature, whereas for

$[Ba(THEC9)]^{2+}$ these resonances show substantially less broadening but coincide below 223.6 K.

Montages of the temperature dependent ^{13}C NMR spectra of $[Mg(THEC9)]^{2+}$, $[Ca(THEC9)]^{2+}$ and $[Ba(THEC9)]^{2+}$ are illustrated in Figures 5.22, 5.23 and 5.24, respectively. Complete lineshape analysis[46] of the coalescence of the macrocyclic ring resonances yielded the mean site lifetimes, τ, illustrated by Figure 5.25. The kinetic parameters shown in Table 5.11 for the intramolecular exchange process were derived from the temperature variations of τ through Equation 4.10.

Table 5.12: Fast exchange ^{13}C chemical shifts of $[M(THEC9)]^{2+}$ in methanol-^{12}C-d_4.

Complex	T	δ^a		
	K	ppm		
$[Mg(THEC9)]^{2+}$	286.2	52.93	58.46	58.62
$[Ca(THEC9)]^{2+}$	244.5	51.58	57.94	58.39
$[Ba(THEC9)]^{2+}$	265.3	52.01	58.94	59.13

[a] ^{13}C chemical shifts are referenced to external natural abundance methanol-^{12}C-d_4, which is assigned a chemical shift of 47.05 ppm.

Table 5.13: Slow exchange ^{13}C chemical shifts of $[M(THEC9)]^{2+}$ at 181.9 K in methanol-^{12}C-d_4.

Complex	δ^a			
	ppm			
$[Mg(THEC9)]^{2+}$	49.53	56.85	centred ~ 58.30 ppm (broad)	
$[Ca(THEC9)]^{2+}$	48.73	56.64	~ 58.08 (broad)	~ 59.23 (broad)
$[Ba(THEC9)]^{2+}$	47.53	56.19	47.53[b]	

[a] ^{13}C chemical shifts are referenced to external natural abundance methanol-^{12}C-d_4, which is assigned a chemical shift of 47.05 ppm. [b]The ^{13}C resonances arising from the $>NCH_2$- and $-CH_2OH$ moieties coincide.

The spectra in Figures 5.22 – 5.24 at low temperature may indicate that, unlike the $[M(THEC9)]^+$ complexes (Section 5.2.3), the $[M(THEC9)]^{2+}$ complexes may not be 6-coordinate or that THEC9 may adopt the + – + configuration in $[M(THEC9)]^{2+}$. As discussed in Section 5.2.3, most triaza macrocyclic complexes adopt the + + + conformation (Figure 5.14). If THEC9 adopts the + – + conformation in $[M(THEC9)]^{2+}$, 12 distinct resonances will be observed in the slow exchange regime of the ^{13}C NMR spectra, corresponding to 6 macrocyclic ring carbon resonances (sites *a*, *b*, *c*, *d*, *e* and *f* in Figure 5.26), 3 resonances characterising the $>NCH_2$- moiety of THEC9 (*g*, *i* and *k*) and 3 resonances characterising the $-CH_2OH$ moiety of THEC9 (*h*, *j* and *l*). The ^{13}C NMR spectra observed for $[M(THEC9)]^{2+}$ may correspond to this configuration, where the spectra at the lowest attainable temperature indicate that exchange is still faster than that of the slow exchange regime. Unfortunately, the very slow exchange region for $[M(THEC9)]^{2+}$ could not be reached due to the freezing point limitations of methanol. In addition, the + – + configuration is thermodynamically unfavourable because it places M^{2+} in the plane of the triaza nitrogens, thus inducing steric strain in $[M(THEC9)]^{2+}$. This effect is more pronounced for the larger Ba^{2+} ion compared with Ca^{2+} and Mg^{2+}, with a 6-coordinate radius of 1.35 Å compared with 1.00 Å and 0.72 Å, respectively,[41] so that $[Ba(THEC9)]^{2+}$ is the most strained of the $[M(THEC9)]^{2+}$ complexes.

These factors suggest that the $[M(THEC9)]^{2+}$ complexes are more likely to adopt the + + + configuration seen for $[M(THEC9)]^+$. Thus, the M^{2+} ion in $[M(THEC9)]^{2+}$ may increase its coordination number by coordinating methanol in addition to THEC9, so that exchange between $[M(THEC9)]^{2+}$ and a second complex, possibly $[M(THEC9)(methanol)_n]^{2+}$, may be significant at low temperature. An alternative possibility is that M^{2+} in $[M(THEC9)]^{2+}$ is 6-coordinate, and that the pendant arm resonances broaden at low temperature due to increasing viscosity. However, this possibility is discounted by a comparison of the broad pendant arm resonances of $[Mg(THEC9)]^{2+}$ and $[Ca(THEC9)]^{2+}$ (Figures 5.22 and 5.23, respectively) with the narrow pendant arm resonances seen for $[Li(THEC9)]^+$ (Figure 5.15) and $[Na(THEC9)]^+$ at low temperature.

It seems more likely that the broad, unresolved pendant arm resonances exhibited by the low temperature spectra of $[Mg(THEC9)]^{2+}$ are consistent with an equilibrium between 5-coordinate and 6-coordinate Mg^{2+}. (However, the possibility that an equilibrium exists between 6-coordinate and 7-coordinate Mg^{2+} in $[Mg(THEC9)]^{2+}$ and $[M(THEC9)(methanol)]^{2+}$ cannot be dismissed. Although such an equilibrium is consistent with the spectra of

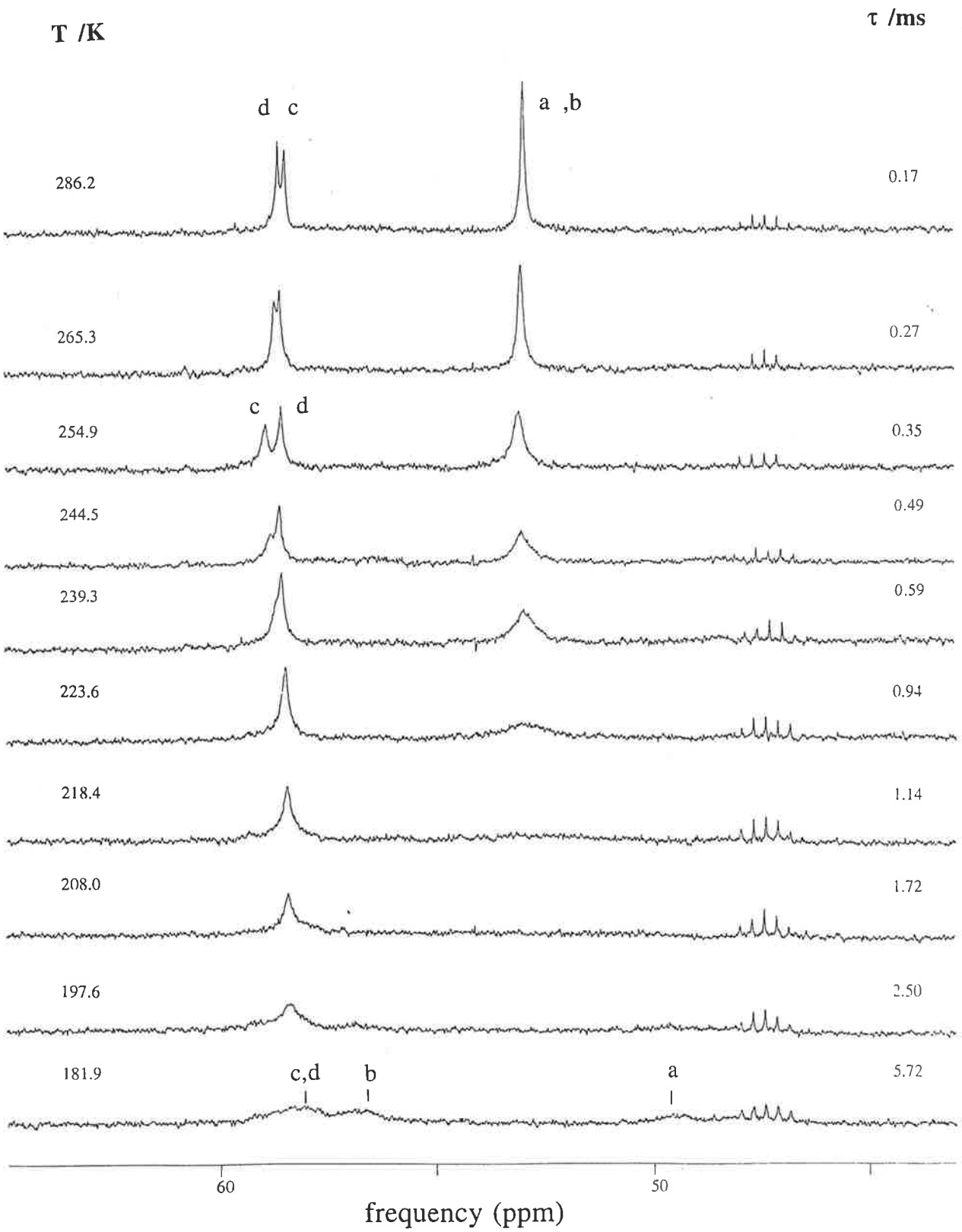

Figure 5.22: Temperature variations of the broad-band ^{1}H decoupled ^{13}C NMR spectra of $[Mg(THEC9)]^{2+}$ (0.101 mol dm^{-3}) in methanol-^{12}C-d_4. Experimental temperatures and τ values derived from complete lineshape analysis of the coalescing doublet arising from the macrocyclic ring carbons, *a* and *b*, appear to the left and the right of the figure, respectively.

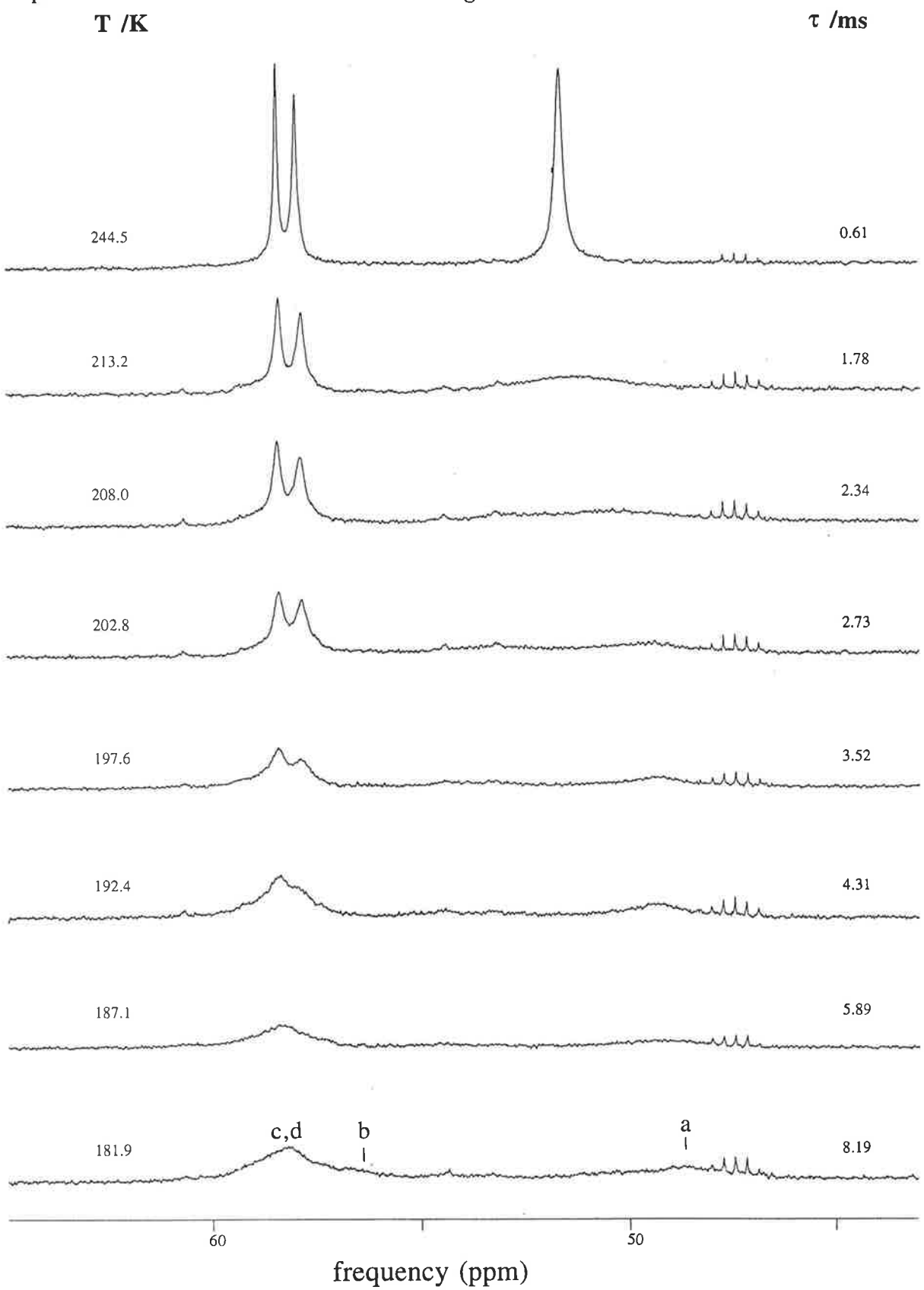

Figure 5.23: Temperature variations of the broad-band ^{1}H decoupled ^{13}C NMR spectra of $[Ca(THEC9)]^{2+}$ (0.110 mol dm^{-3}) in methanol-^{12}C-d_4. Experimental temperatures and τ values derived from complete lineshape analysis of the coalescing doublet arising from the macrocyclic ring carbons, *a* and *b*, appear to the left and the right of the figure, respectively.

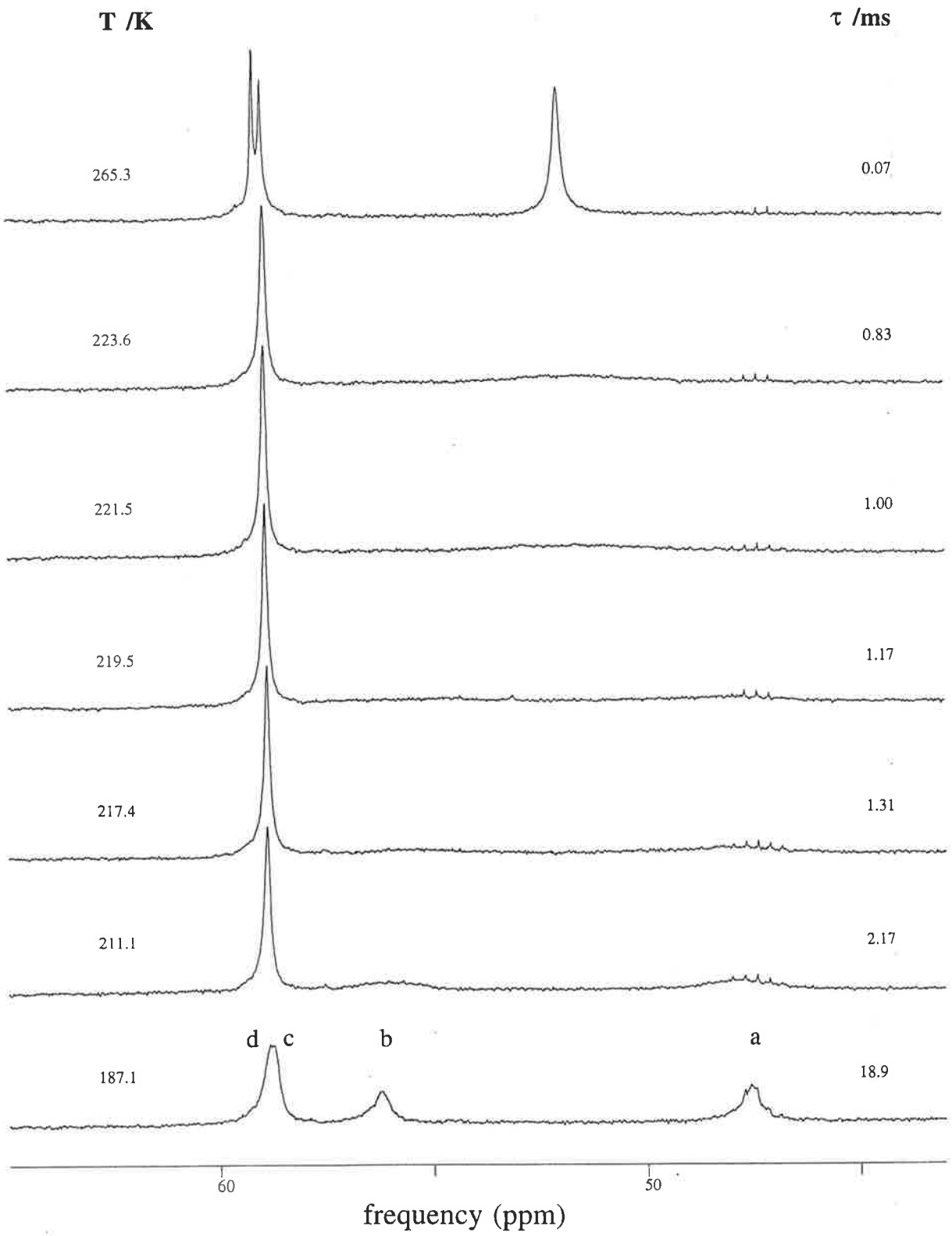

Figure 5.24: Temperature variations of the broad-band ^{1}H decoupled ^{13}C NMR spectra of $[Ba(THEC9)]^{2+}$ (0.100 mol dm^{-3}) in methanol-^{12}C-d_4. Experimental temperatures and τ values derived from complete lineshape analysis of the coalescing doublet arising from the macrocyclic ring carbons, *a* and *b*, appear to the left and the right of the figure, respectively.

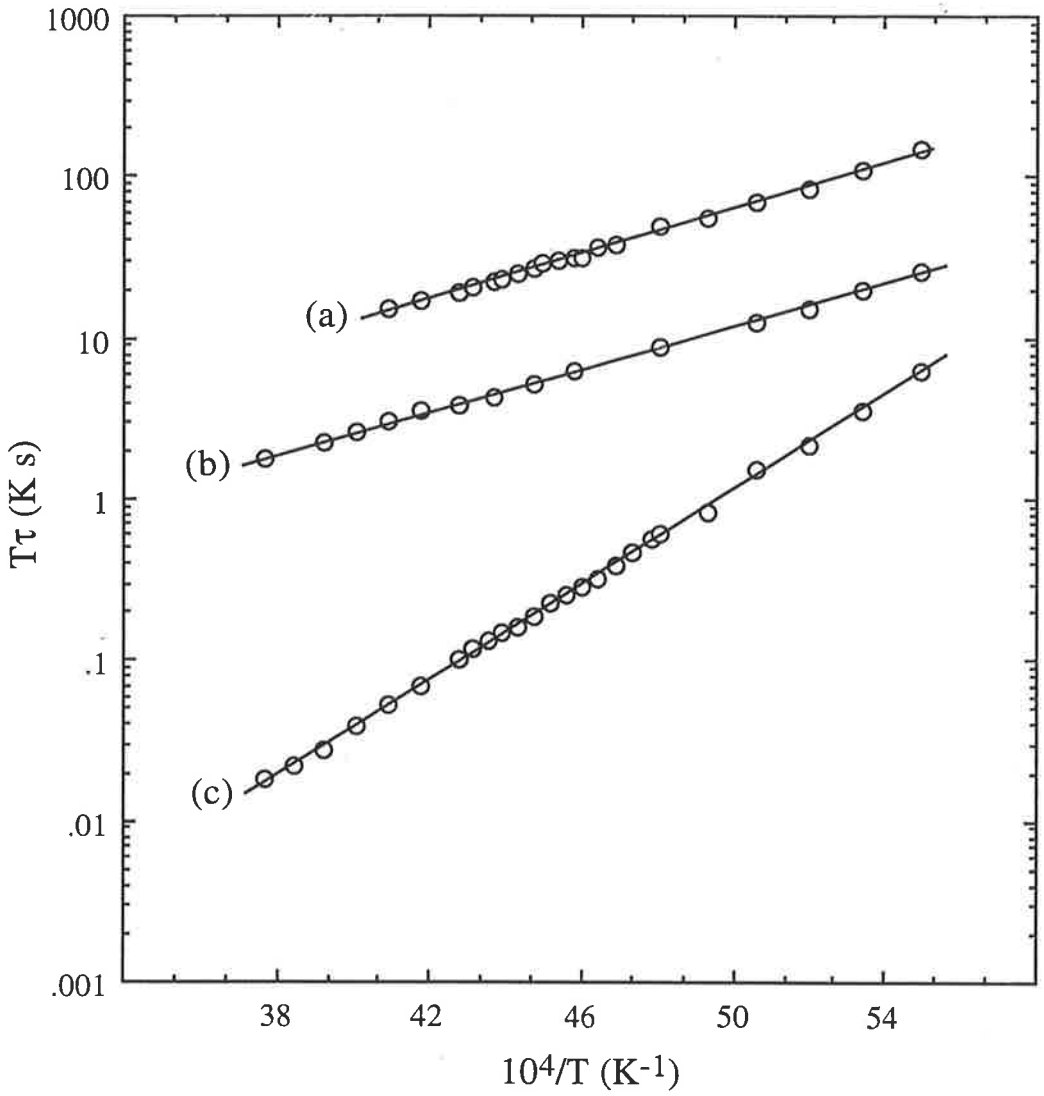

Figure 5.25: Temperature variations of τ for intramolecular exchange in methanol-^{12}C-d_4 between enantiomers of $[M(THEC9)]^{2+}$. The solid lines represent the best fit of the data to Equation 4.10 for each system.
(a) $[Ca(THEC9)]^{2+}$, 100τ. (b) $[Mg(THEC9)]^{2+}$, 25τ. (c) $[Ba(THEC9)]^{2+}$, τ.

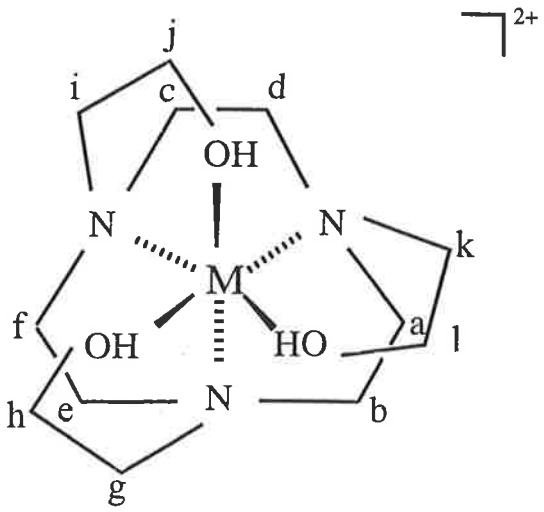

Figure 5.26: Assignment of the ^{13}C resonances of $[M(THEC9)]^{2+}$ assuming a + – + configuration of THEC9.

$[Mg(THEC9)]^{2+}$ illustrated in Figure 5.22, the combination of the smaller ring size of THEC9 compared with the larger 12-membered macrocycles THEC12 and (*R*)-THPEC12 and the small 6-coordinate radius of Mg^{2+} (0.72 Å)[41] may favour a 5-coordinate rather than a 7-coordinate geometry). In the spectra at 286.2 K characterising fast exchange in $[Mg(THEC9)]^{2+}$, the resonances assigned to the carbons of the $>NCH_2$- moiety (*c*) and the -CH_2OH moiety (*d*) of the pendant arms of THEC9 in $[Mg(THEC9)]^{2+}$ appear as sharp singlets. As the temperature is lowered, the pendant arm resonances should each broaden and then split into separate resonances as exchange enters the slow exchange regime. Unfortunately, it is not possible to observe the very slow exchange regime characterising intramolecular exchange in $[Mg(THEC9)]^{2+}$ because of the freezing point limitations of methanol, and the identification of resonances at low temperature is complicated by the signals being just distinguishable above the baseline of the spectra. Nevertheless, the variation in chemical shift of the pendant arm resonances of $[Mg(THEC9)]^{2+}$ and the very broad pendant arm resonances observed at low temperature, contrasting with the spectra of $[Li(THEC9)]^{+}$ (Figure 5.15) and $[Na(THEC9)]^{+}$ in which the pendant arm resonances show little relative variation in chemical shift with temperature and

retain their narrow linewidths at low temperature, indicate the possibility of both 5-coordinate and 6-coordinate Mg^{2+} being present in $[Mg(THEC9)]^{2+}$.

The pendant arm resonances of $[Ca(THEC9)]^{2+}$ also exhibit significant broadening at low temperature (Figure 5.23), but these resonances show much less variation in chemical shift with changing temperature than the analogous resonances of $[Mg(THEC9)]^{2+}$. This may indicate that, as for $[Mg(THEC9)]^{2+}$, an equilibrium is established between two different species. For Ca^{2+}, with a larger 6-coordinate radius of 1.00 Å compared with that of Mg^{2+},[41] it is more likely that an equilibrium exists between 6-coordinate and 7-coordinate Ca^{2+} in $[Ca(THEC9)]^{2+}$. As for 5-coordinate $[Mg(THEC9)]^{2+}$, the resonances assigned to 7-coordinate $[Ca(THEC9)]^{2+}$ are not readily observed in the spectra in Figure 5.23 due to freezing point limitations of the solvent, exchange induced broadening and low intensity signals at low temperature. The spectra for $[Ba(THEC9)]^{2+}$ at low temperature (Figure 5.24) exhibit the sharpest pendant arm resonances of the $[M(THEC9)]^{2+}$ complexes. It is envisaged that Ba^{2+}, being larger than Mg^{2+} or Ca^{2+} with a 6-coordinate radius of 1.35 Å,[41] is the most likely to adopt a higher coordination number in $[M(THEC9)]^{2+}$. However, the temperature dependence of the spectra observed for $[Ba(THEC9)]^{2+}$, specifically the narrow pendant arm resonances at low temperature, is analogous to that seen in $[Li(THEC9)]^{+}$ (Figure 5.15) and $[Na(THEC9)]^{+}$. This indicates that $[Ba(THEC9)]^{2+}$ adopts a dominant coordination geometry, which may be either 6-coordinate or 7-coordinate. If 6-coordinate $[Ba(THEC9)]^{2+}$ dominates, the process of intramolecular exchange in $[Ba(THEC9)]^{2+}$ will be similar to that postulated for $[M(THEC9)]^{+}$, where $M^{+} = Li^{+}$ and Na^{+}, (Figure 5.18).

Since the alkaline earth and alkali metal ions are both hard acids, with a preference for the oxygen over nitrogen donor atoms of THEC9, $[M(THEC9)]^{2+}$ may exhibit similar behaviour to that of $[M(THEC9)]^{+}$. However, although the 6-coordinate radii of corresponding M^{+} and M^{2+} are similar,[41] the divalent nature of the M^{2+} ions are likely to affect their complexing abilities and labilities with THEC9. The larger 12-membered macrocyclic ligands such as THEC12 may be able to stabilise the alkaline earth metal ion complexes more effectively because of their larger ring size and potential 8 donor atoms compared with only 6 such atoms in THEC9. This is reflected in the $[M(THEC9)]^{2+}$ complexes undergoing faster intramolecular exchange than $[M(THEC12)]^{2+}$ (Table 5.11), as seen for the alkali metal analogues (Section 5.2.3), and is consistent with the smaller $\Delta H^{\ddagger}$ and more negative $\Delta S^{\ddagger}$ values characterising intramolecular exchange in $[M(THEC9)]^{2+}$ compared with $[M(THEC12)]^{2+}$.

5.4 ^{13}C INTRAMOLECULAR EXCHANGE IN $[Zn(THEC12)]^{2+}$

The ^{13}C NMR spectrum of $[Zn(THEC12)]^{2+}$ in methanol-^{12}C-d_4 exhibits 3 distinct resonances in the intensity ratio 1:1:2 at 251.6 K (Table 5.9). The resonance at 48.44 ppm is assigned to the carbons of the macrocyclic ring, and the resonances at 52.17 and 55.92 ppm are respectively assigned to the carbons of the >N*C*H$_2$- moiety and -*C*H$_2$OH moiety of the hydroxyethyl arms of THEC12. All resonances broaden and then split with decreasing temperature. At very low temperature (178.6 K), the spectrum consists of 6 resonances (Table 5.10) arising from the 8 different chemical environments of the carbons in (*R*)-THPEC12, in which 2 of the resonances are partly obscured by the methanol-^{12}C-d_4 multiplet centred at 47.05 ppm and 2 resonances overlap at 49.69 ppm. Through integration it is found that the resonances at 46.57, 48.19, and 49.69 ppm pertain to the carbons of the macrocyclic ring (sites *a*, *b*, *c*, and *d* in Figure 5.27) in the intensity ratio 1:2:1, whereas the resonances at 49.69 and 54.72 ppm pertain to the carbons of the >N*C*H$_2$- moiety of the pendant arms (sites *e* and *g* in Figure 5.27), and the resonances at 54.02 and 57.71 ppm pertain to the carbons of the -*C*H$_2$OH moiety (*f* and *h*). (The carbons of the macrocyclic ring and of the >N*C*H$_2$- moiety of the pendant arms exhibit the overlapping resonance at 49.69 ppm).

A montage of the temperature dependent ^{13}C NMR spectra of $[Zn(THEC12)]^{2+}$ is shown in Figure 5.28. Complete lineshape analysis[46] of the coalescence of the pendant arm resonances yielded the mean site lifetime, τ, illustrated by Figure 5.21. The kinetic parameters listed in Table 5.11 for this exchange process were derived from the temperature variations of τ through Equation 4.10. The spectra at low temperature are not consistent with the presence of an 8-coordinate complex (observed for $[M(THEC12)]^{2+}$ and $[M(THEC12)]^{+}$), but instead the coalescence phenomena is consistent with each carbon exchanging between two inequivalent sites and the simultaneous exchange of Zn^{2+} between two sites in $[Zn(THEC12)]^{2+}$. This requires Zn^{2+} to be coordinated by the four tetraaza ring nitrogens and two pendant arms attached either to diagonally related nitrogens or nitrogens at either end of the same 1,2-diaminoethane moiety. If the two pendant arms coordinated to Zn^{2+} are attached to nitrogens diagonally opposite each other in the tetraaza ring, there are only two inequivalent sites (*a* and *b*) denoting the macrocyclic ring carbons, and thus only 6 resonances would be observed in the slow exchange ^{13}C NMR spectra of $[Zn(THEC12)]^{2+}$. For the two coordinated pendant arms attached at either end of the same 1,2-diaminoethane moiety (as shown in Figure 5.27), the macrocyclic ring carbons should ideally give rise to 4 signals in the slow exchange regime in the ratio 1:1:1:1. However, only 3 resonances

in the ratio 1:2:1 are observed for these carbons, implying that carbons *a* and *b* have similar chemical shifts and hence appear under one signal at 48.19 ppm.

The possible configurations for the THEC12 tetraaza ring with a planar array of nitrogens coordinating Zn^{2+} are shown in Figure 5.2, but no indication of the pairwise coordination of the hydroxyethyl arms is shown in this diagram. The TRANS II configuration, irrespective of the pairwise coordination of the pendant arms, produces a structure with 10 inequivalent carbon resonances in the ^{13}C spectra. Therefore, this configuration for the structure of $[Zn(THEC12)]^{2+}$ may be eliminated. In the TRANS V configuration, coordination of the two hydroxyethyl arms to Zn^{2+} attached to adjacent nitrogens requires one pendant arm to coordinate Zn^{2+} from above the plane of the ring and the other below so that Zn^{2+} is coordinated within the tetraaza ring plane. The torsional strain exhibited by such a conformation makes this coordination geometry thermodynamically unfavourable, particularly since the metal ions in this study are generally too large to sit within the plane of the tetraaza ring of THEC12.[28] (It is worth noting that molecular mechanics calculations have shown that for a metal ion to adopt an in-plane coordination geometry with THEC12, the optimum, strain free intermolecular distance between the metal ion and a ring nitrogen is ~ 1.82 Å which, in principle, corresponds to a metal ion of radius ~ 0.60 Å.[61a] The small 6-coordinate ionic radius of Zn^{2+} (0.74 Å)[41] may allow this geometry, albeit with strain in the complex). In addition, the TRANS V conformation usually folds in its metal complexes.[61b]

Octahedral geometry is allowed for the tetraaza ring folding about a diagonal axis delineated by two nitrogens so that these two nitrogen donor atoms occupy *trans* coordination sites of an octahedral metal ion and the other two nitrogen donor atoms occupy *cis* coordination sites. The CIS II and CIS V configurations (Figure 5.2) describe such conformations. The CIS II conformation has been observed in several solid state transition metal complexes of CYCLEN,[62a-65] related macrocycles have been shown to complex transition metal ions in the CIS V conformation,[62b] and the potentially octadentate ligand 1,4,7,10-tetrakis(pyrazol-1-methyl)-1,4,7,10-tetraazacyclo-dodecane folds in its 6-coordinate complexes.[66] For $[Zn(THEC12)]^{2+}$ to adopt a folded TRANS V conformation, the hydroxyethyl arms attached to the *trans* coordinated nitrogens coordinate in the remaining two *cis* coordination sites. (The hydroxyethyl arms attached to the *cis* coordinated nitrogens will not coordinate). This renders only two magnetically inequivalent 1,2-diaminoethane environments, which is incompatible with the inequivalence exhibited by these carbons in the experimental spectra of $[Zn(THEC12)]^{2+}$.

Thus, the folded TRANS V configuration is eliminated as a possibility for $[Zn(THEC12)]^{2+}$.

The TRANS I configuration readily provides pairwise coordination of the hydroxyethyl arms. However, in this configuration pairwise coordination is as conceivably allowed by the arms attached to adjacent nitrogens as from diagonally related nitrogens of THEC12. In addition, only 5,7 and 8-coordinate complexes have been observed for various metal complexes of CYCLEN and THEC12 with the ligand adopting the TRANS I conformation,[33-35,64] and the slow exchange ^{13}C NMR spectrum of $[Zn(THEC12)]^{2+}$ is only consistent with the hydroxyethyl arms attached to adjacent nitrogens. Therefore, the TRANS I configuration is also discounted as a possibility for $[Zn(THEC12)]^{2+}$ although it is the binding configuration commonly adopted by pendant arm macrocyclic ligands.

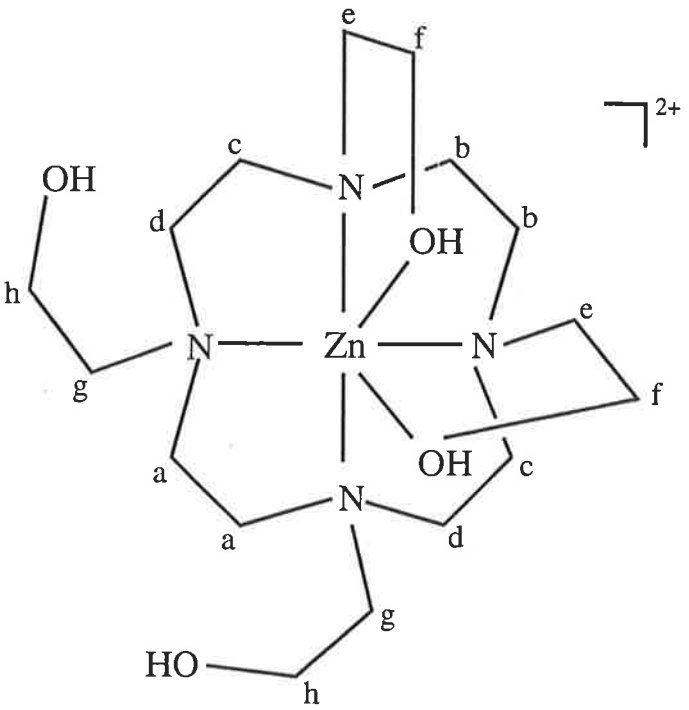

Figure 5.27: Assignment of the ^{13}C resonances of $[Zn(THEC12)]^{2+}$, assuming a 6-coordinate geometry, with the two coordinated pendant arms attached at either end of the same 1,2-diaminoethane moiety.

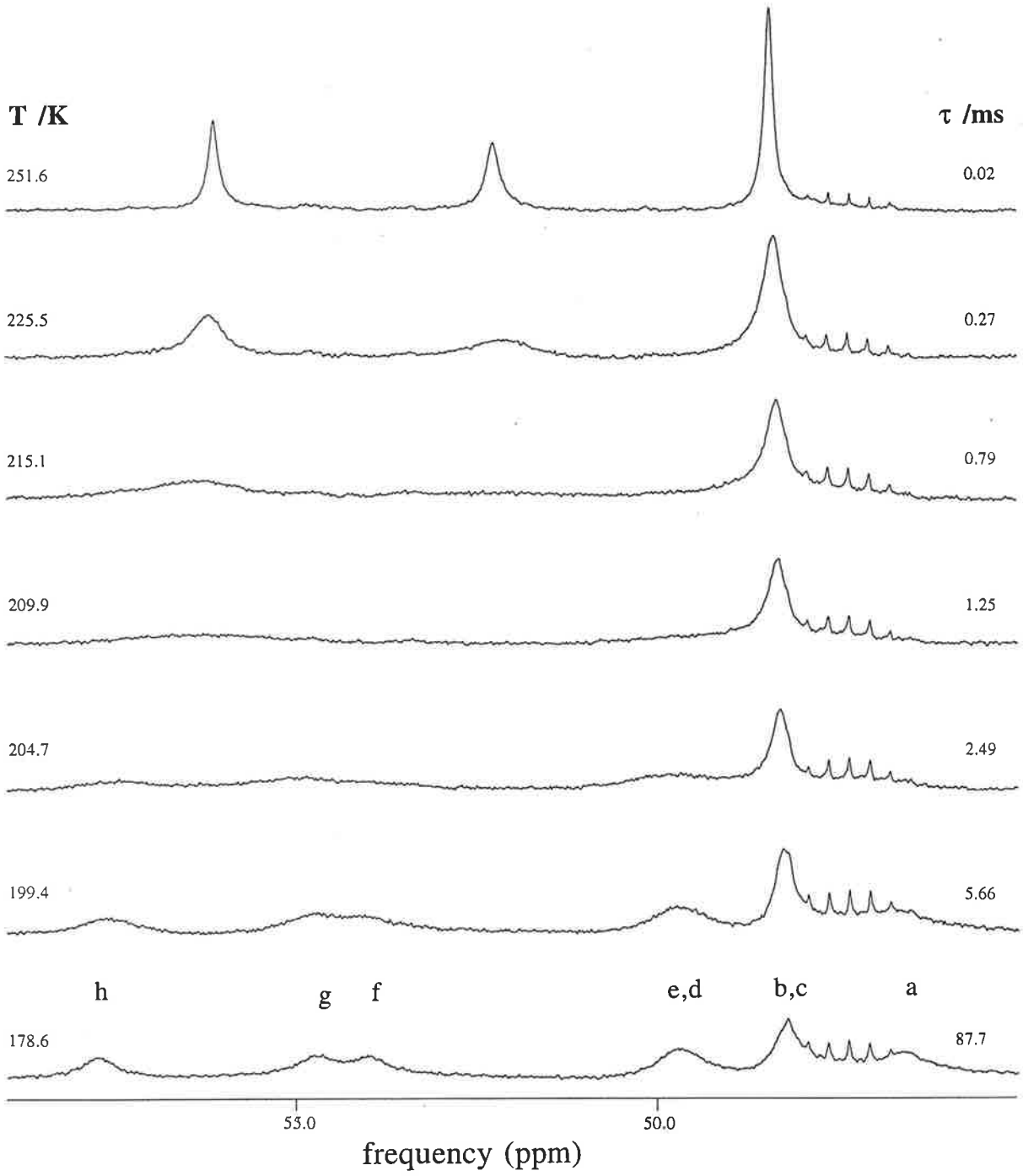

Figure 5.28: Temperature variations of the broad-band ^{1}H decoupled ^{13}C NMR spectra of $[Zn(THEC12)]^{2+}$ (0.050 mol dm^{-3}) in methanol-^{12}C-d_4. Experimental temperatures and τ values derived from complete lineshape analysis of the coalescence of the $>NCH_2$- and -CH_2OH ^{13}C resonances (denoted *e* and *g*, and *f* and *h*, respectively) appear to the left and the right of the figure, respectively.

The ^{13}C NMR spectra for 6-coordinate Zn^{2+} in $[Zn(THEC12)]^{2+}$ is best accounted for by a structure incorporating the TRANS III conformation (Figure 5.2), where Zn^{2+} is coordinated by the four ring nitrogens of THEC12 and two pendant arms attached to adjacent nitrogens (Figure 5.29). Support for this supposition comes from the X-ray diffraction studies of complexes between Zn^{2+} and 1,4,8,11-tetraazacyclotetradecane, 1,4,8,12-tetraazacyclopentane and related ligands, in which Zn^{2+} lies above the tetraaza ring plane by 0.12 Å, 0.18 Å and 0.19 Å, respectively.[38,66,67] The TRANS III conformation has also been reported in the heavy metal ion complexes of 14 and 15-membered macrocyclic ligands.[12,13,25,68] Indeed, the ability of ligands such as THEC12 to adapt to changes in the dimensions of the cage about a metal ion for a given coordination geometry, as well as their ability to yield both 6- and 8-coordinate complexes, are indicative of the considerable flexibility of pendant arm macrocyclic ligands.

Intramolecular exchange in $[Zn(THEC12)]^{2+}$ may be interpreted as being the interconversion between two octahedrally coordinated enantiomers (Figure 5.29), which may proceed by the transannular oscillation of Zn^{2+}. The transition state for the enantiomerisation process shown in Figure 5.29 can be visualised to involve Zn^{2+} in the plane of the tetraaza ring, trigonal prismatically coordinated to the four nitrogens and by two hydroxyethyl pendant arms, one from each side of the macrocyclic plane. As a consequence of the structural nature of the TRANS III configuration, it is necessary for the pendant arms to become uncoordinated during exchange. (This contrasts with the mechanism of exchange for the TRANS I isomers of the alkali and alkaline earth metal ion complexes discussed previously, which do not necessarily involve metal-ligand bond breakage in the activated complex, so their isomerisation is possible by a twisting motion of the pendant arms). This observation is in agreement with the proposition that negative $\Delta S^{\ddagger}$ values characterising intramolecular exchange are associated with twisting rather than dissociative pathways,[21] and is demonstrated by the negative $\Delta S^{\ddagger}$ values characterising intramolecular exchange in $[M((R)\text{-THPEC12})]^{+}$, $[M(THEC12)]^{n+}$ and $[M(THEC9)]^{n+}$ (Tables 5.6 and 5.11) while that of $[Zn(THEC12)]^{2+}$ has a positive value.

A knowledge of the structure of $[Zn(THEC12)]^{2+}$ is essential to the interpretation of the its ^{13}C NMR spectral coalescence to describe the mechanism characterising intramolecular exchange in solution. (Indeed, solid state structures of complexes have been very useful in postulating the transition state structure for observed solution dynamics).[14] Unfortunately, the solid state structure of $[Zn(THEC12)]^{2+}$ has not yet been determined by X-ray diffraction studies.

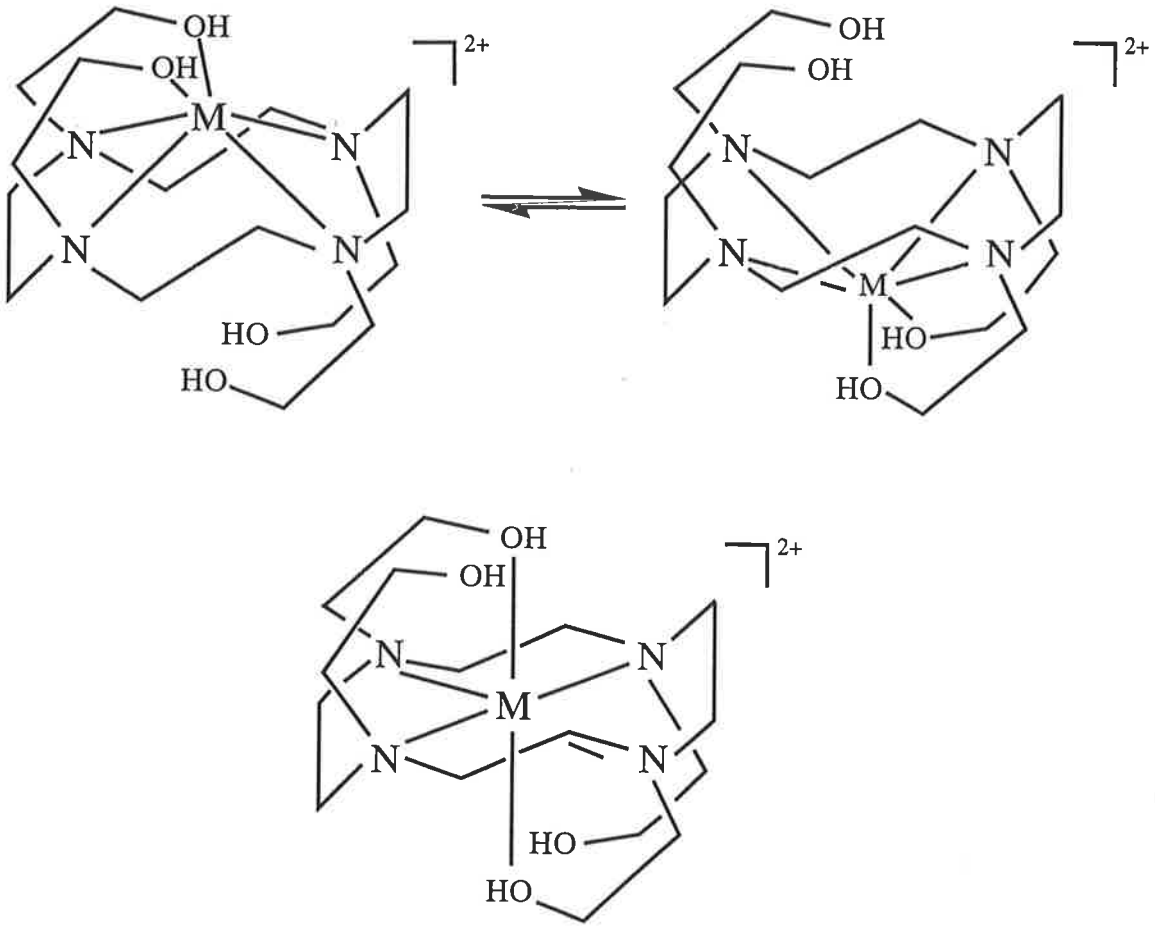

Figure 5.29: Proposed $[Zn(THEC12)]^{2+}$ structure showing the TRANS III configuration of THEC12 and the transannular exchange mechanism.

The hard acid alkaline earth metal ions interact more strongly with the oxygen rather than the nitrogen donor atoms of THEC12, whereas the predominant interaction in $[Zn(THEC12)]^{2+}$ is between the borderline soft acid Zn^{2+} and the nitrogen donor atoms of THEC12.[57-59] Therefore, two contrasting effects are important for Zn^{2+}. That is, Zn^{2+}-N interactions are favoured by the adoption of the TRANS III conformer for THEC12 since this conformer coordinates Zn^{2+} in the plane of the tetraaza nitrogens, thus enhancing metal-ligand interactions. Conversely, the TRANS III conformer has a significantly higher strain energy than the TRANS I conformer because of the in-plane

geometry. Since $[Zn(THEC12)]^{2+}$ is a stable complex, with a substantially higher stability constant (log (K_S/dm^3 mol^{-1}) = 12.83)[69] than that of the alkaline earth metal analogues (Chapter 3), the Zn^{2+}-N interaction effect appears to dominate over that of steric strain in the complex. Although Zn^{2+} has a similar size to Mg^{2+} and Li^+,[41] the latter two metal ions are 8-coordinate in $[M(THEC12)]^{n+}$ and, as discussed in Section 5.2.3, a 6-coordinate complex undergoes faster intramolecular exchange than a complex with 8 such metal-ligand bonds. On the basis of the above-mentioned factors, the rate of intramolecular exchange is expected to be greater for $[Zn(THEC12)]^{2+}$ than for the alkali or alkaline earth metal ion complexes of THEC12. This is indeed observed (Tables 5.6 and 5.11). (It is important to note that although the coordination number for pendant arm macrocyclic ligand complexes with Zn^{2+} is strongly governed by the geometric requirements of the ligand, a combination of other factors also play a part. These include the number of available donor atoms, absence of stereochemical requirements and ligand field stabilisation energy due to the d^{10} electronic configuration of Zn^{2+}, and ligand flexibility and degree of steric hindrance caused by groups on pendant arms of the ligand).[70-73]

5.5 ^{13}C INTERMOLECULAR LIGAND EXCHANGE IN ALKALI AND ALKALINE EARTH METAL ION COMPLEXES

5.5.1 INTERMOLECULAR EXCHANGE IN ALKALI METAL ION COMPLEXES

The ^{13}C NMR spectra for intermolecular (*R*)-THPEC12 exchange on Λ[K((*R*)-THPEC12)]$^+$ (Figure 5.30) consist of 11 distinct resonances at 228.8 K. The resonances at 50.72 and 52.50 ppm are assigned to both the macrocyclic ring carbons of (*R*)-THPEC12 (denoted a^* and b^* in Figure 5.30) and those of Λ[K((*R*)-THPEC12)]$^+$ (*a* and *b*). The resonances at 65.63 and 64.30 ppm are respectively assigned to the >N*C*H$_2$- moiety of (*R*)-THPEC12 (c^*) and Λ[K((*R*)-THPEC12)]$^+$ (*c*), and the resonances at 70.13 and 70.59 ppm are respectively assigned to the –*C*H(C$_6$H$_5$)OH moiety of (*R*)-THPEC12 (d^*) and Λ[K((*R*)-THPEC12)]$^+$ (*d*). The remaining resonances at 126.85, 127.64, 128.76, 144.32 and 145.49 ppm arise from the –CH(*C*$_6$H$_5$)OH moiety of both (*R*)-THPEC12 (e^*) and Λ[K((*R*)-THPEC12)]$^+$ (*e*), although the 3 resonances at ~127 ppm are not resolved. Similar assignments and coalescence phenomena are observed for the Li^+ and Na^+ analogue complexes with (*R*)-THPEC12. Intermolecular (*R*)-THPEC12 exchange on Λ[Rb((*R*)-THPEC12)]$^+$ and Λ[Cs((*R*)-THPEC12)]$^+$ is in the fast exchange regime of the ^{13}C NMR timescale at 216.3 K so that broadened environmentally averaged ^{13}C

resonances are observed.[75] Intermolecular exchange of (*R*)-THPEC12 on $[M((R)\text{-THPEC12})]^+$ is described by Equation 5.1:

$$[ML]^+ + {}^*L \underset{k_d}{\overset{k_d}{\rightleftharpoons}} [M{}^*L]^+ + L \qquad 5.1$$

Complete lineshape analysis[46] of the temperature dependent coalescence of the ^{13}C resonances arising from the $>NCH_2-$ moiety of free (*R*)-THPEC12 and complexed (*R*)-THPEC12 in $[M((R)\text{-THPEC12})]^+$, for $M^+ = Li^+$, Na^+ and K^+, yielded the mean site lifetime, τ, of (*R*)-THPEC12 in $[M((R)\text{-THPEC12})]^+$, illustrated by Figure 5.31. The kinetic parameters shown in Table 5.14 for this exchange process were determined from the temperature variations of τ through an equation analogous to Equation 4.10.

From Table 5.14 it is apparent that there is a good correlation between the kinetic parameters describing intermolecular (*R*)-THPEC12 and M^+ exchange on $[M((R)\text{-THPEC12})]^+$, for $M^+ = Li^+$ and Na^+. The larger k(298.2 K) characterising (*R*)-THPEC12 exchange on $[Li((R)\text{-THPEC12})]^+$ compared with $\Delta[Na((R)\text{-THPEC12})]^+$ is a consequence of the combination of the smaller $\Delta H^{\ddagger}$ and substantially more negative $\Delta S^{\ddagger}$ of the former complex. The significantly larger k(298.2 K) for $\Lambda[K((R)\text{-THPEC12})]^+$ is a result of the larger $\Delta H^{\ddagger}$ and $\Delta S^{\ddagger}$ compared with those of its Li^+ and Na^+ analogues. However, as for many of the intramolecular exchange processes discussed in Section 5.2, the activation parameters characterising intermolecular (*R*)-THPEC12 exchange do not show obviously systematic variations. This is probably because contributions to the activation parameters vary in relative magnitude with M^+ and the ligand, and arise from a range of sources including metal-ligand bond energies and the magnitude of strain in the ligand. (As for M^+ exchange on $[M((R)\text{-THPEC12})]^+$ (Chapter 4), although the decomplexation process (Equation 5.1) involves a series of steps it is not possible from the present data to assign a particular step as rate-determining).

It is apparent from Table 5.14 that the activation parameters describing intermolecular (*R*)-THPEC12 exchange on $[M((R)\text{-THPEC12})]^+$ and the nitrogen double inversion of $[M((R)\text{-THPEC12})]^+$ are significantly different. This is consistent with these two processes following different reaction pathways, so that intramolecular exchange in $[M((R)\text{-THPEC12})]^+$ is not the rate-determining step for decomplexation of $[M((R)\text{-THPEC12})]^+$. Nonetheless, since exchange between equivalent diastereomeric forms of

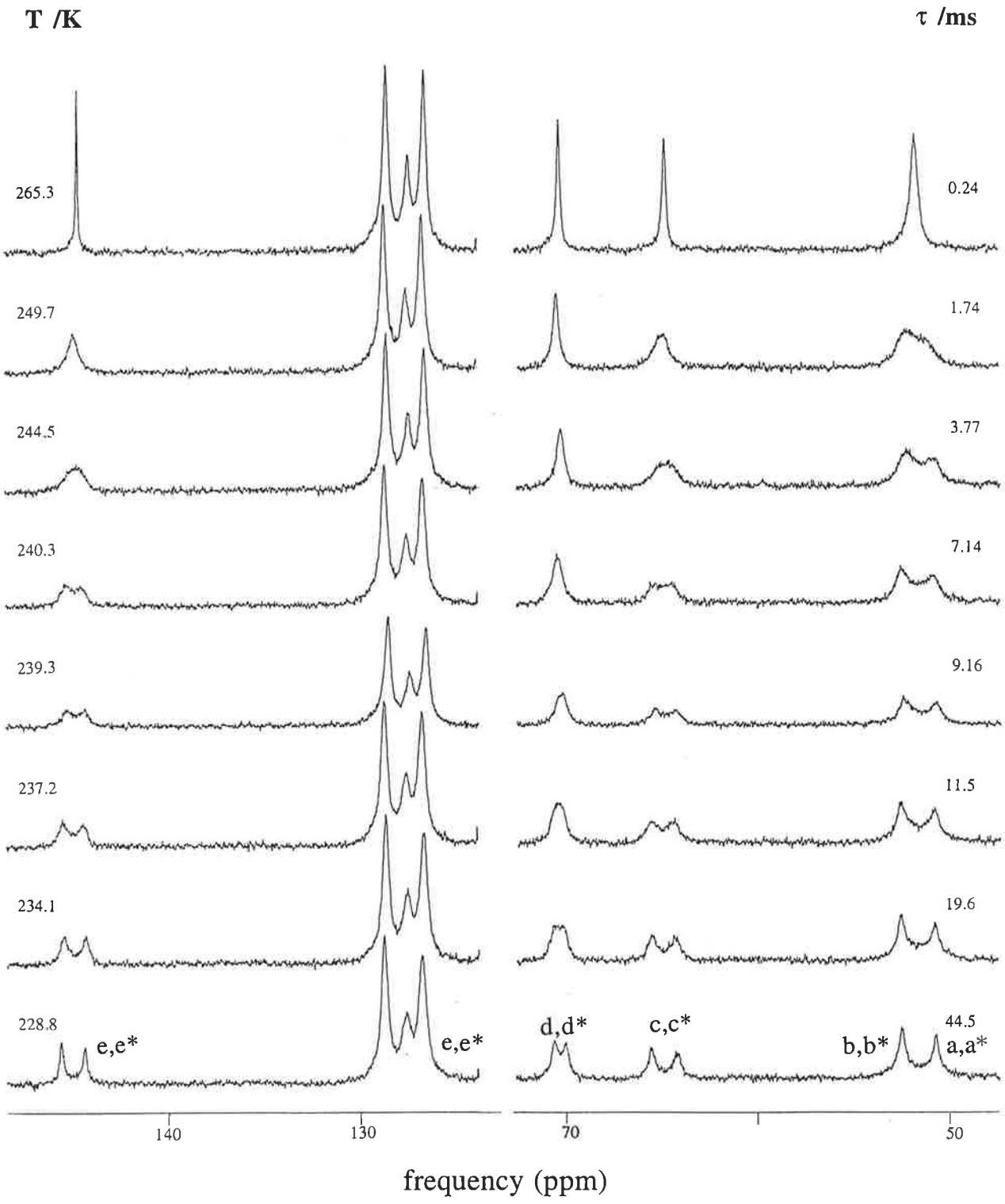

Figure 5.30: Temperature variations of the broad-band ^{1}H decoupled ^{13}C NMR spectra of Λ[K((*R*)-THPEC12)]$^{+}$ (0.099 mol dm^{-3}) and (*R*)-THPEC12 (0.089 mol dm^{-3}) in d_7-DMF. Experimental temperatures and τ values derived from complete lineshape analysis of the coalescence of the >N*C*H$_2$- ^{13}C resonances (*c* and *c**) appear to the left and the right of the figure, respectively.

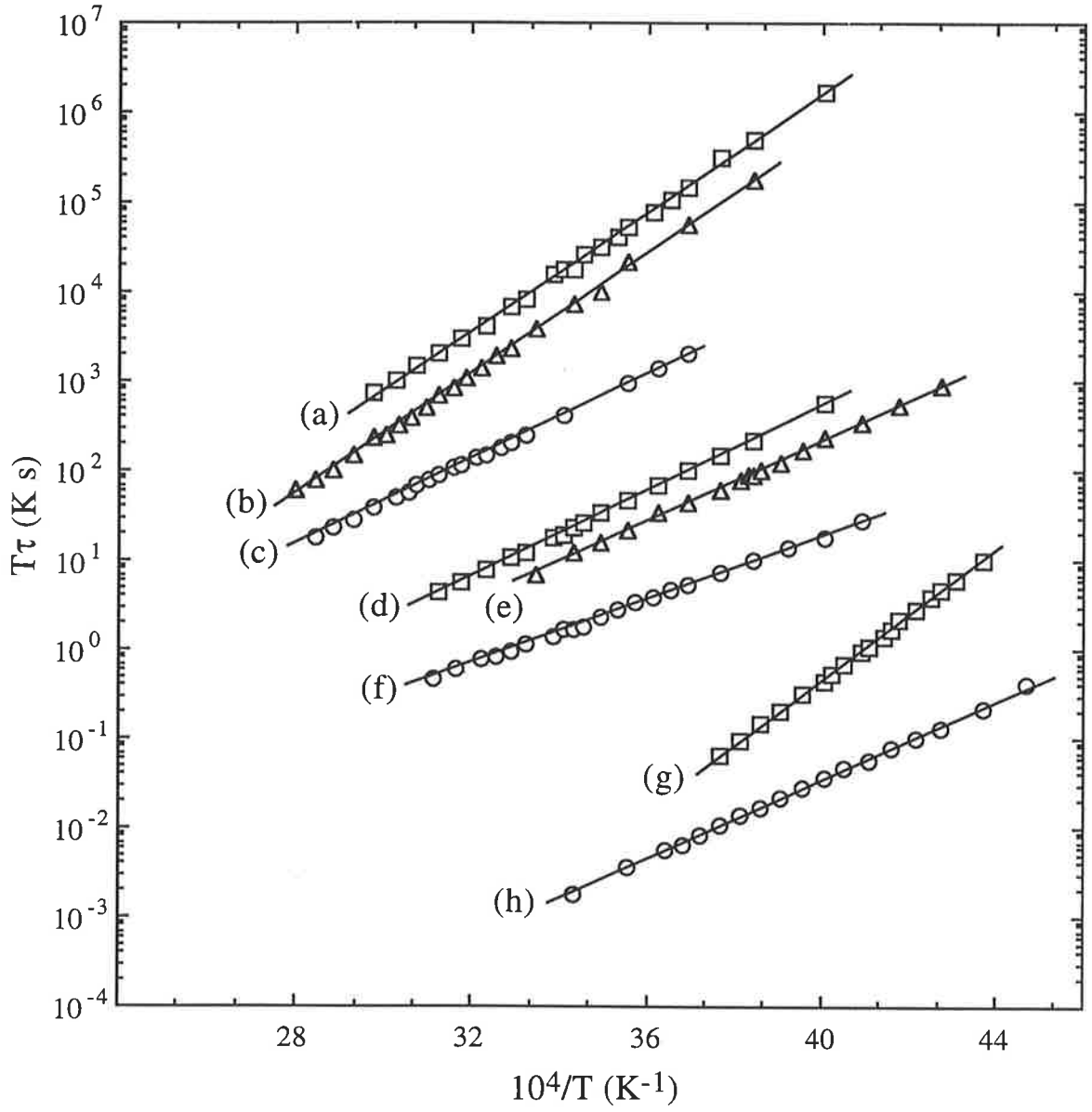

Figure 5.31: Temperature variations of τ for intramolecular and intermolecular exchange in $[M((R)\text{-THPEC12})]^+$ in d_7-DMF. The solid lines represent the best fit of the data to Equation 4.10 for each system.

Δ$[Na((R)\text{-THPEC12})]^+$: (a) L exc.,6000τ; (b) Na^+ exc.,1000τ; (c) intra.,100τ.
$[Li((R)\text{-THPEC12})]^+$: (d) L exc.,20τ; (e) Li^+ exc.,10τ; (f) intra.,τ.
Λ$[K((R)\text{-THPEC12})]^+$: (g) L exc.,τ. (h) intra.,τ/50.

Table 5.14: Kinetic parameters[a] for exchange processes in $[ML]^+$, where L = (*R*)-THPEC12, and $[M(THEC12)]^+$.

Complex	Exchange Process	*k* (298.2 K) s^{-1}	$\Delta H^{\ddagger}$ kJ mol^{-1}	$\Delta S^{\ddagger}$ J K^{-1} mol^{-1}
$[LiL]^+$	Intra.[b]	233 ± 2	34.6 ± 0.3	-83.5 ± 1.1
	Inter. L[c,d]	396 ± 3	46.0 ± 0.3	-40.9 ± 1.0
	Inter. Li^+ [e]	391 ± 12	42.6 ± 0.5	-52.3 ± 2.1
$\Delta[NaL]^+$	Intra.[c]	98 ± 1	46.1 ± 0.2	-52.2 ± 0.7
	Inter. L[c,d]	156 ± 3	62.3 ± 0.5	6.0 ± 1.9
	Inter. Na^+ [e]	73.4 ± 1.7	64.9 ± 0.5	8.4 ± 1.6
$\Lambda[KL]^+$	Intra.[e]	4900 ± 100	42.7 ± 0.3	-31.1 ± 1.2
	Inter. L[d,e]	150000 ± 6400	69.8 ± 0.5	88.4 ± 2.1
$[Li(THEC12)]^+$	Intra.[e]	18000 ± 3100	41.3 ± 1.3	-24.8 ± 5.9
	Inter. L[e,f]	424 ± 7[h]	37.7 ± 0.5	-68.2 ± 1.7
	Inter. Li^+ [g]	729 ± 7	38.0 ± 0.7	-62.8 ± 1.7
$[Na(THEC12)]^+$	Intra.[e]	7100 ± 220	24.6 ± 0.5	-88.6 ± 1.8
	Inter. L[e,f]	332 ± 8[h]	65.6 ± 0.8	23.3 ± 3.0
	Inter. Na^+ [g]	209 ± 3	68.3 ± 1.4	28.4 ± 0.8
$[K(THEC12)]^+$	Intra.[e]	7000 ± 200	53.7 ± 0.6	8.8 ± 2.3
	Inter. L[e,f]	12000 ± 700[h]	50.5 ± 0.9	2.8 ± 3.7

[a]Errors represent 1 standard deviation for the fit of experimental τ data to Equation 4.10. [b]Reference 75. [c]Reference 76. [d]$k(s^{-1})$ = 290 ± 2 (293.5 K); 102 ± 2 (293.5 K); 139 ± 1 (240.1 K) are the exchange rate constants at the $>NCH_2-$ resonance coalescence temperatures of $[M((R)\text{-THPEC12})]^+$ and (*R*)-THPEC12, where $M^+ = Li^+$, Na^+ and K^+, respectively. [e]This work. [f]$k(s^{-1})$ = 215 ± 3 (286.2 K) and 40 ± 1 (260.1 K); 62 ± 2 (281.0 K) and 105 ± 3 (286.2 K); 332 ± 12 (254.9 K) and 37 ± 2 (234.1 K) are the exchange rate constants at the $>NCH_2-$ and $-CH_2OH$ resonance coalescence temperatures for $[M(THEC12)]^+$ and THEC12, where $M^+ = Li^+$, Na^+ and K^+, respectively. [g]Reference 68. [h]Exchange rate constants (*k*) simultaneously determined from the $>NCH_2-$ and $-CH_2OH$ resonance coalescences.

$[M((R)\text{-THPEC12})]^+$ necessitates some metal-nitrogen bond breakage, it is likely that part of this exchange process is similar to that preceding decomplexation. This proposal is supported by the observation that lability towards intramolecular exchange in $[M((R)\text{-THPEC12})]^+$, which follows the sequence $K^+ > Li^+ > Na^+$, is the same trend observed for decomplexation of $[M((R)\text{-THPEC12})]^+$.

The variable temperature ^{13}C NMR spectra for intermolecular THEC12 exchange on $[Li(THEC12)]^+$ (Figure 5.32) consist of 3 distinct resonances at 325.4 K, each of which broaden and split into 2 separate resonances with decreasing temperature, so that 6 distinct resonances are observed at 239.3 K. The resonances at 49.41 and 49.77 ppm correspond to the macrocyclic ring carbons of $[Li(THEC12)]^+$ (denoted *a* in Figure 5.32) and THEC12 (a^*). The remaining resonances at 53.42, 55.05, 57.34, and 57.72 ppm are assigned to the $>NCH_2$- moiety of $[Li(THEC12)]^+$ (*b*) and THEC12 (b^*), and the $-CH_2OH$ moiety of $[Li(THEC12)]^+$ (*c*) and THEC12 (c^*), respectively. Similar assignments and coalescence phenomena are observed for the exchange of THEC12 on $[Na(THEC12)]^+$. For intermolecular THEC12 exchange on $[K(THEC12)]^+$, the ^{13}C NMR spectrum at 223.6 K differs slightly (Figure 5.33) from that of the Li^+ and Na^+ analogues. At 223.6 K, the macrocyclic ring carbons of $[K(THEC12)]^+$ resonate at 49.94 and 52.52 ppm (denoted *a* and *b* in Figure 5.33) while those of THEC12 resonate at 50.61 ppm (a^*,b^*). The resonances at 59.01 and 55.84 ppm correspond to the $>NCH_2$- moiety of $[K(THEC12)]^+$ (*c*) and THEC12 (c^*), respectively, and the remaining two resonances at 58.35 and 58.60 ppm arise from the $-CH_2OH$ moiety of $[K(THEC12)]^+$ (*d*) and THEC12 (d^*), respectively.

A montage of the calculated ^{13}C NMR spectra for alternative assignments of the resonances characterising the hydroxyethyl pendant arms of THEC12 and $[K(THEC12)]^+$ are shown in Figure 5.34. The resonances at 55.84 and 58.35 ppm are assigned to the $>NCH_2$- moiety of THEC12 (c^*) and $[K(THEC12)]^+$ (*c*), while the resonances at 58.60 and 59.01 ppm are assigned to the $-CH_2OH$ moiety of THEC12 (d^*) and $[K(THEC12)]^+$ (*d*). The temperature dependent coalescence of the resonances, using the kinetic parameters as for the system in Figure 5.33, shows that the calculated spectra display different coalescence phenomena to that of the experimental spectra in Figure 5.33. Thus, assignment of the resonances characterising the pendant arm carbons in Figure 5.33 is correct.

For $M^+ = Li^+$, Na^+ and K^+, intermolecular THEC12 exchange on $[M(THEC12)]^+$ is also described by Equation 5.1. The kinetic parameters for

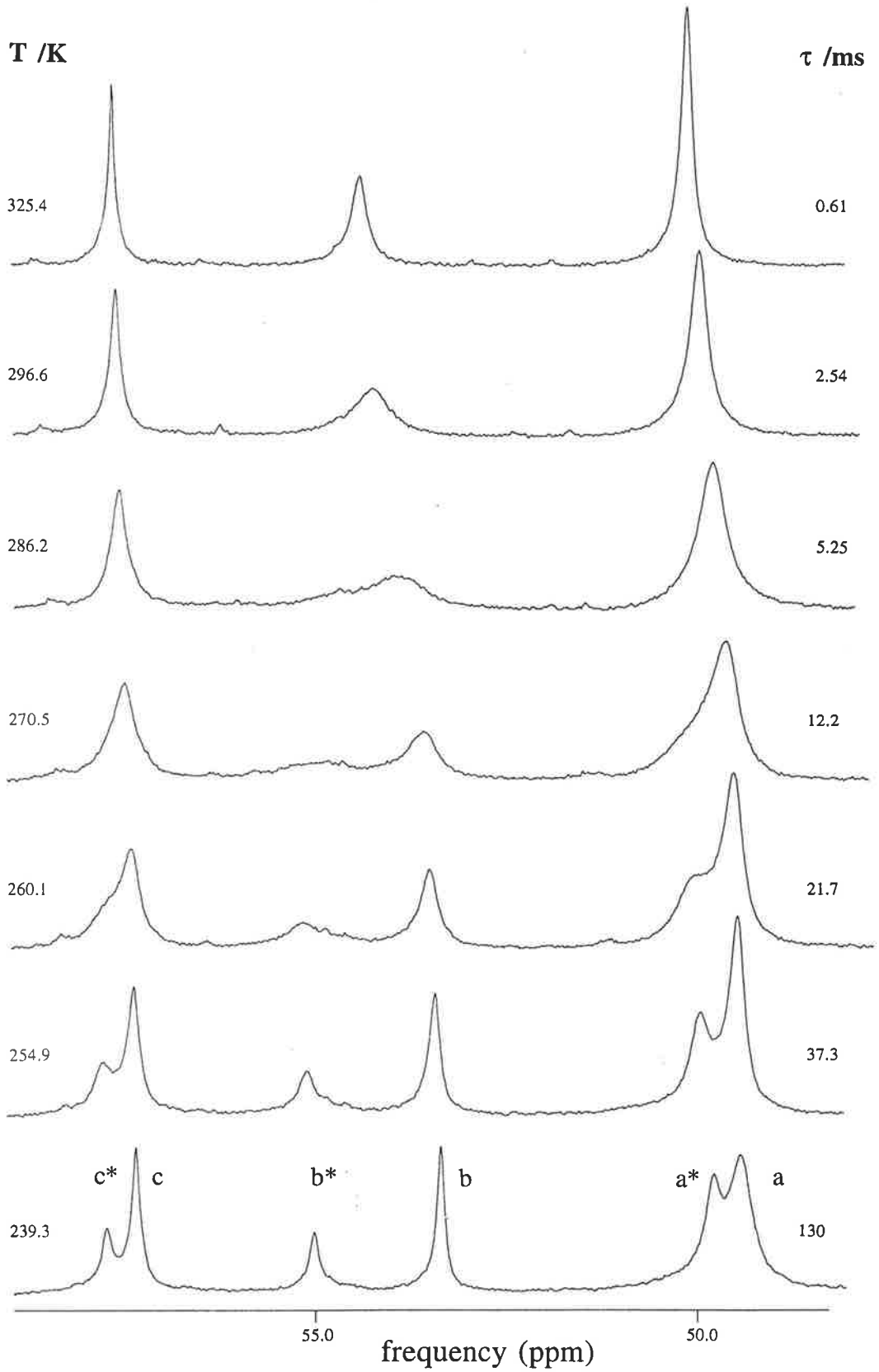

Figure 5.32: Temperature variations of the broad-band ^{13}C NMR spectra of $[Li(THEC12)]^+$ (0.111 mol dm^{-3}) and THEC12 (0.089 mol dm^{-3}) in methanol-^{12}C-d_4. Experimental temperatures and τ values derived from complete lineshape analysis of the coalescence of the >NCH_2- ^{13}C resonances (*b* and *b**) appear to the left and the right of the figure, respectively.

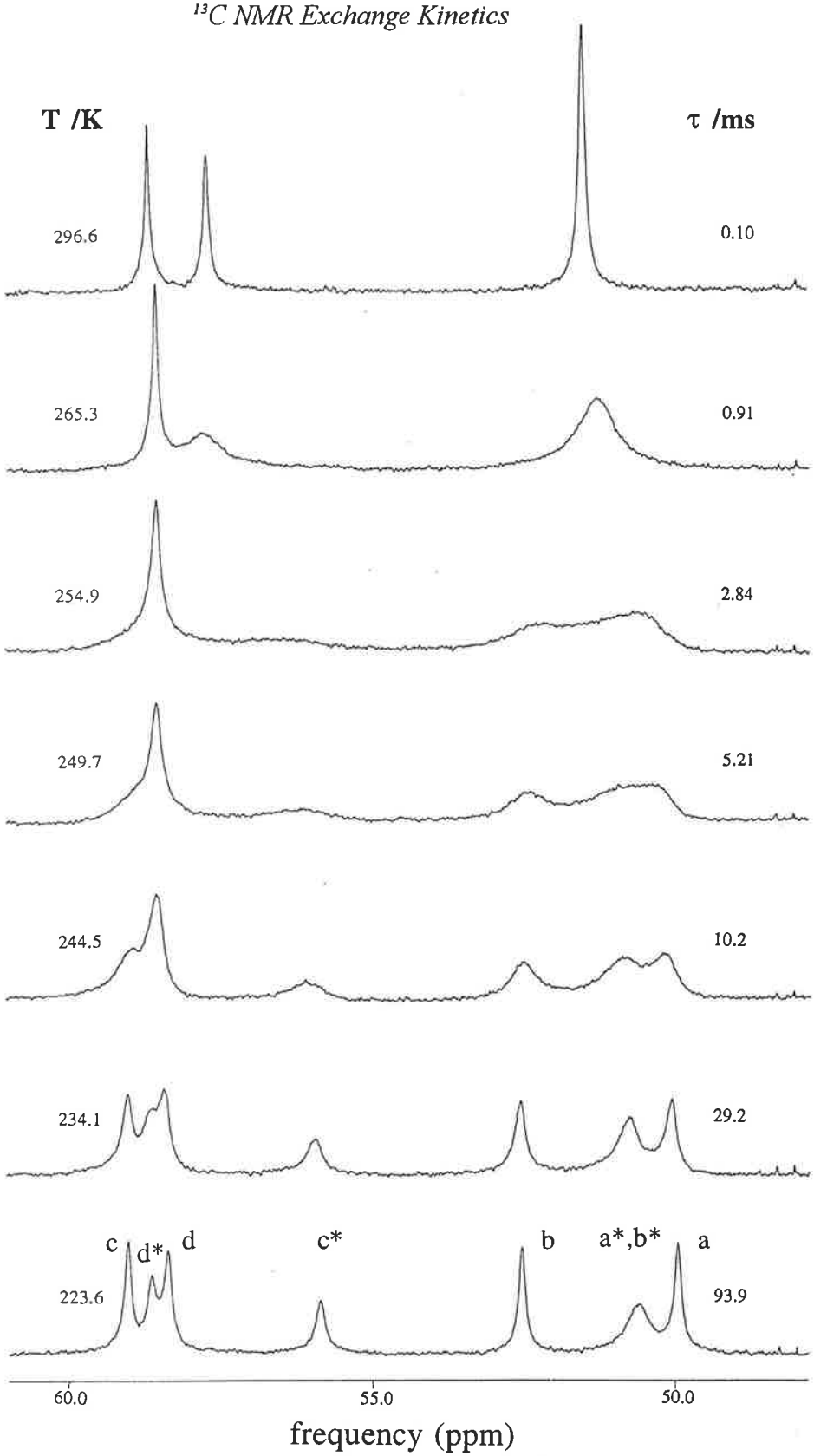

Figure 5.33: Temperature variations of the ^{13}C NMR spectra of $[K(THEC12)]^+$ (0.055 mol dm^{-3}) and THEC12 (0.042 mol dm^{-3}) in methanol-^{12}C-d_4. Experimental temperatures and τ values derived from complete lineshape analysis of the coalescence of the $>NCH_2-$ ^{13}C resonances (*c* and *c**) and the $-CH_2OH$ ^{13}C resonances (*d* and *d**) appear to the left and the right of the figure, respectively.

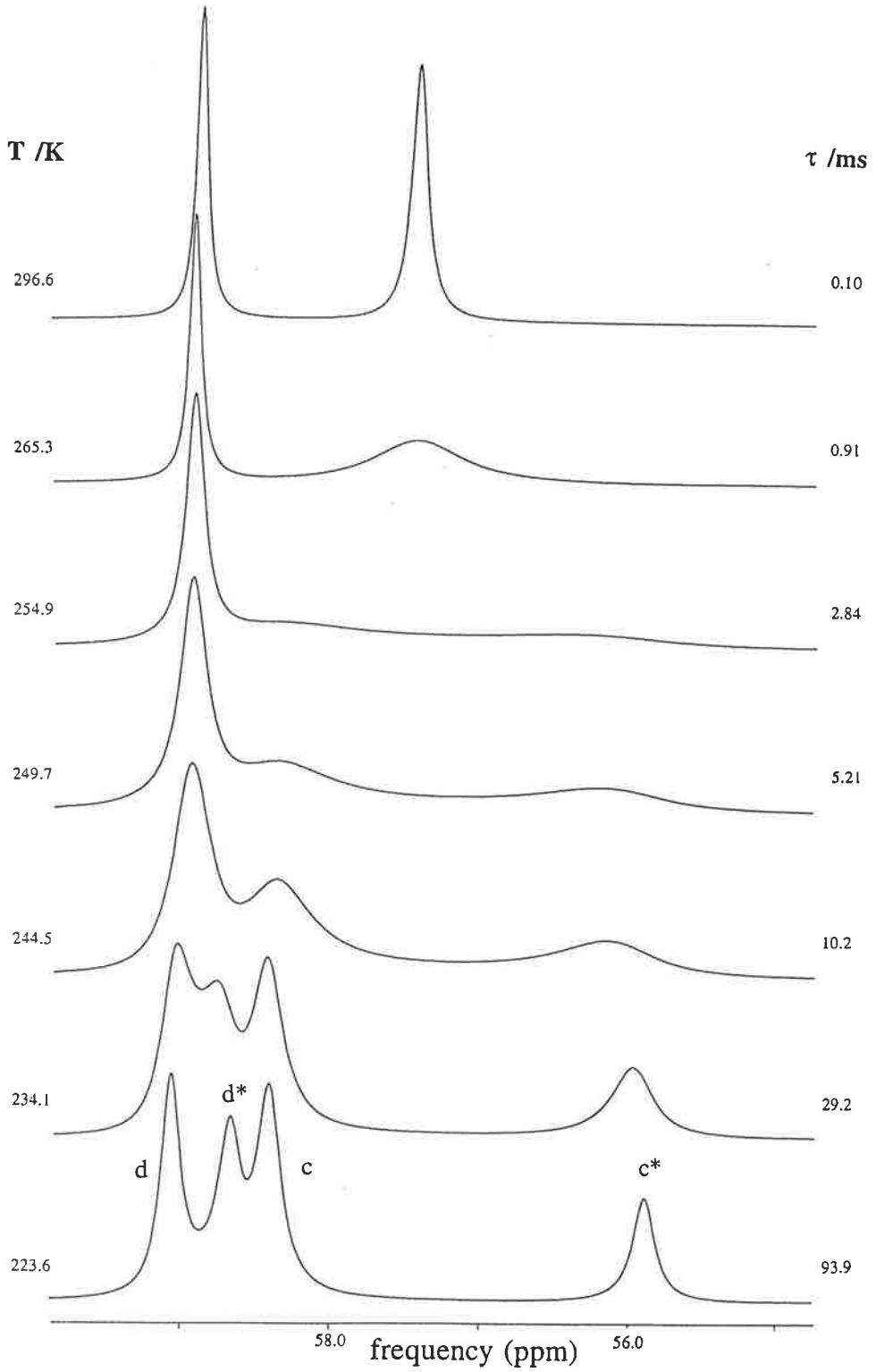

Figure 5.34: Calculated spectra for the pendant arm resonance coalescence of $[K(THEC12)]^+$ and THEC12 in methanol-^{12}C-d_4 for alternative assignment of the resonances. Temperatures and τ values derived from complete lineshape analysis of the coalescence of the $>NCH_2$- (*c* and *c**) and the -CH_2OH ^{13}C resonances (*d* and *d**) appear to the left and the right of the figure, respectively.

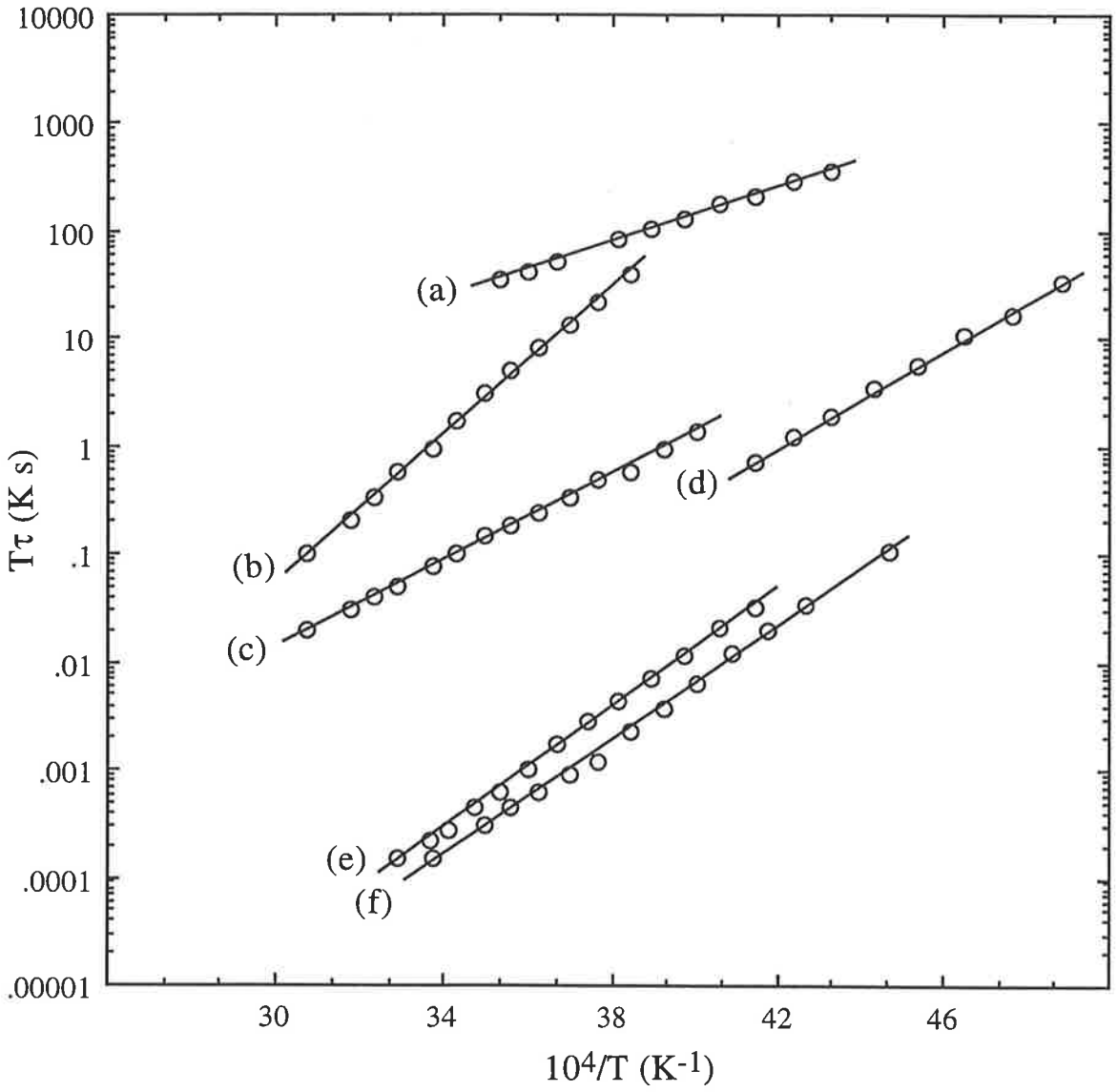

Figure 5.35: Temperature variations of τ for intramolecular and intermolecular exchange in $[M(THEC12)]^+$ in methanol-^{12}C-d_4. The solid lines represent the best fit of the data to Equation 4.10 for each system.

$[Na(THEC12)]^+$:	(a) intra., 500τ;	(b) THEC12 exc., τ.
$[Li(THEC12)]^+$:	(c) THEC12 exc., τ/10;	(d) intra., τ.
$[K(THEC12)]^+$:	(e) intra., τ/200;	(f) THEC12 exc., τ/200.

this exchange process (listed in Table 5.14 and illustrated in Figure 5.35) were determined from the coalescence of both the $>NCH_2$- and $-CH_2OH$ ^{13}C resonances of free THEC12 and $[M(THEC12)]^+$. The kinetic parameters (Table 5.14) obtained from ^{13}C NMR studies for intermolecular THEC12 exchange on $[Li(THEC12)]^+$ and $[Na(THEC12)]^+$ are similar to those obtained from ^7Li and ^{23}Na NMR studies for M^+ exchange on $[M(THEC12)]^+$.[68] This is consistent with both processes occurring through the same monomolecular mechanism. As for (*R*)-THPEC12 exchange on $[M((R)\text{-THPEC12})]^+$, where $M^+ = Li^+$ and Na^+, (Table 5.14) the larger k(298.2 K) characterising THEC12 exchange on $[Li(THEC12)]^+$ compared with $[Na(THEC12)]^+$ is due to the smaller $\Delta H^{\ddagger}$ and significantly more negative $\Delta S^{\ddagger}$ for $[Li(THEC12)]^+$. In accordance with the alkali metal complexes of (*R*)-THPEC12, the rate of THEC12 exchange on $[K(THEC12)]^+$ at 298.2 K is substantially faster than that characterising its Li^+ and Na^+ analogues. However, variations in the kinetic parameters for THEC12 exchange, as for (*R*)-THPEC12 exchange, do not show a clear trend, consistent with changes in M^+ producing differing contributions from bonding and ligand strain to the transition state in $[M(THEC12)]^+$.

For $M^+ = Li^+$ and Na^+ in $[M(THEC12)]^+$, the activation parameters characterising intermolecular exchange are dissimilar to those for intramolecular exchange, where k(298.2 K) for intermolecular exchange is much slower than that for enantiomerisation, thereby eliminating intermolecular M^+ or THEC12 exchange as a significant pathway for intramolecular exchange. However, enantiomerisation occurs through an intramolecular mechanism which may involve detachment of one or more pendant arms. Therefore, it is possible that part of the intramolecular exchange process is the same as that preceding decomplexation since lability towards intermolecular ligand exchange in $[M(THEC12)]^+$ follows the sequence $Li^+ > Na^+$, which is the same trend observed for enantiomerisation in $[M(THEC12)]^+$. A similar trend has been observed for the Li^+ and Na^+ complexes of (*S*)-THPC12 and TMEC12.[15,16]

The activation parameters at 298.2 K for THEC12 exchange on $[K(THEC12)]^+$ and enantiomerisation are very similar, and the rate of intermolecular exchange is twice that of enantiomerisation. This is consistent with intermolecular ligand exchange being the dominant enantiomerisation mechanism for $[K(THEC12)]^+$, where on average intermolecular ligand exchange produces enantiomerisation for every second exchange of THEC12. This change in the relative importance of the intermolecular and intramolecular processes for $[M(THEC12)]^+$ enantiomerisation arises from the greater lability of $[K(THEC12)]^+$ towards THEC12 exchange. Complexes between K^+ and the

related ligands (*S*)-THPC12, (*R*)-THPEC12 and TMEC12 also exhibit faster rates of ligand exchange compared with intramolecular exchange.[15,16] Intramolecular and intermolecular ligand exchange for these related K^+ complexes, however, do not proceed along similar pathways, since the activation parameters characterising these two processes are significantly different. This may be a reflection of the higher flexibility afforded to THEC12 compared with these increasingly more rigid or strained related ligands.

5.5.2 INTERMOLECULAR EXCHANGE IN ALKALINE EARTH METAL ION COMPLEXES

The ^{13}C NMR spectra for intermolecular THEC12 exchange on $[M(THEC12)]^{2+}$, for $M^{2+} = Mg^{2+}$, Ca^{2+} and Ba^{2+}, all consist of 6 distinct resonances from 293.5 K to 325.4 K, with the spectra at 325.4 K displayed in Figure 5.36. For intermolecular exchange on $[Mg(THEC12)]^{2+}$, the resonances at 49.26 and 50.48 ppm are assigned to the macrocyclic ring carbons of $[Mg(THEC12)]^{2+}$ (denoted *a* in Figure 5.36) and THEC12 (*a**), respectively, while the resonances at 53.31, 55.31, 55.70 and 57.34 ppm are assigned to the $>NCH_2$- moiety of $[Mg(THEC12)]^{2+}$ (*b*), the $>NCH_2$- moiety of THEC12 (*b**), the -CH_2OH moiety of $[Mg(THEC12)]^{2+}$ (*c*) and the -CH_2OH moiety of THEC12 (*c**), respectively. Similar spectral assignments can also be made for the Ca^{2+} (Figure 5.36) and Ba^{2+} analogue complexes. For these three complexes, the observation of separate ^{13}C resonances for THEC12 and $[M(THEC12)]^{2+}$ up to 325.4 K indicates that intermolecular exchange is in very slow exchange on the NMR timescale. Indeed, it is apparent that the higher stabilities of $[M(THEC12)]^{2+}$ compared with $[M(THEC12)]^{+}$ (Chapters 2 and 3) are reflected in their lower labilities towards intramolecular exchange (Tables 5.6 and 5.11) and very slow intermolecular ligand exchange.

The ^{13}C NMR spectra for intermolecular TMEC12 exchange on $[M(TMEC12)]^{2+}$, for $M^{2+} = Ca^{2+}$ and Ba^{2+}, consist of 8 distinct resonances from 293.5 K to 325.4 K, with the spectra at 325.4 K displayed in Figure 5.36. For intermolecular ligand exchange on $[Ca(TMEC12)]^{2+}$ at 325.4 K, the resonances at 47.41 and 51.08 ppm are assigned to the macrocyclic ring carbons of $[Ca(TMEC12)]^{2+}$ (*a*) and TMEC12 (*a**), while the resonances at 49.11 and 53.82 ppm, 56.67 and 58.64 ppm, and 67.47 and 69.60 ppm are assigned to the $>NCH_2$- moiety of $[Ca(TMEC12)]^{2+}$ (*b*) and TMEC12 (*b**), the -OCH_3 moiety of TMEC12 (*c**) and $[Ca(TMEC12)]^{2+}$ (*c*), and the -CH_2OCH_3 moiety of $[Ca(TMEC12)]^{2+}$ (*d*) and TMEC12 (*d**), respectively. Similar spectral assignments can also be made for $[Ba(TMEC12)]^{2+}$. (The broad

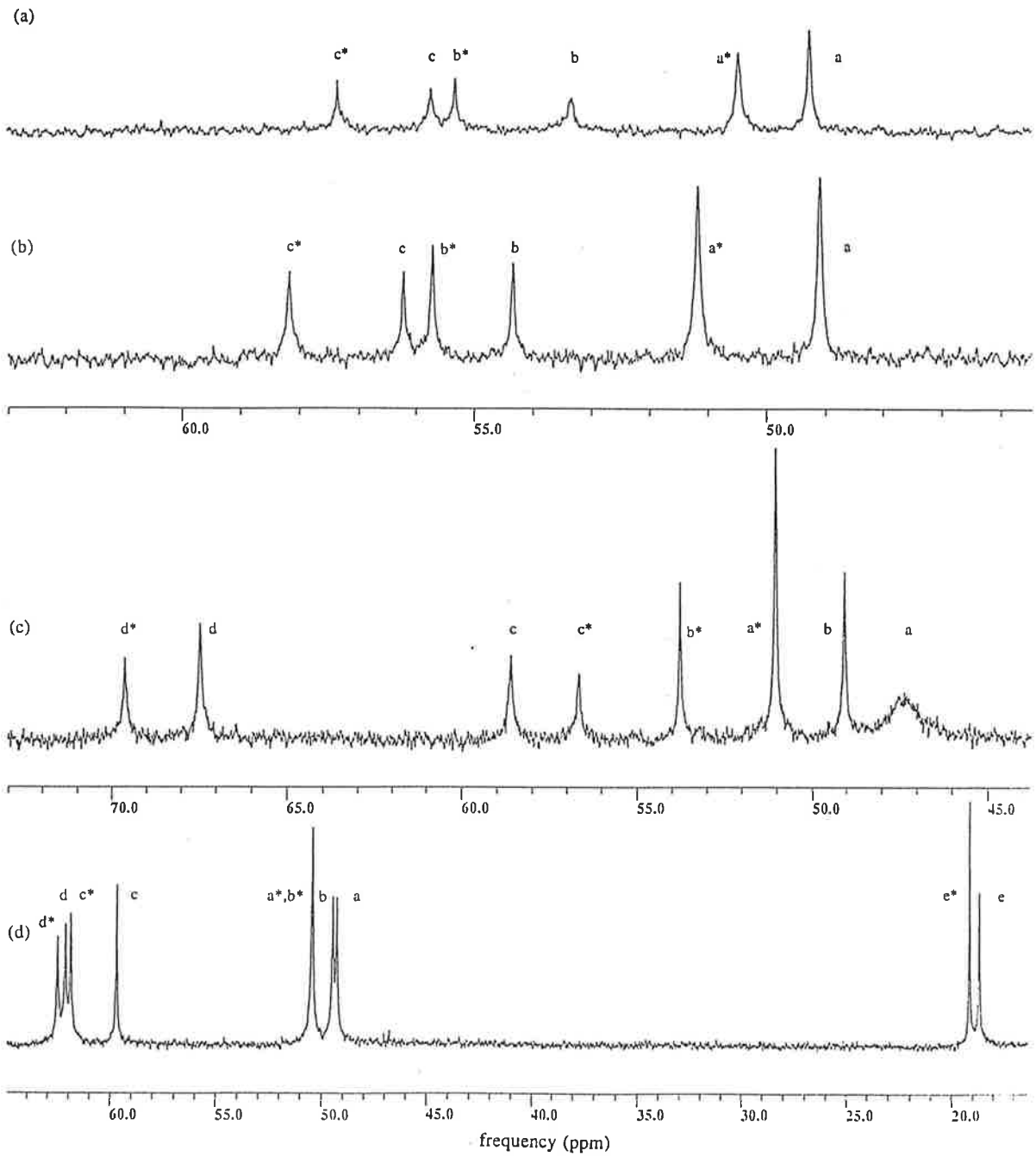

Figure 5.36: A selection of the broad-band ^{1}H decoupled ^{13}C NMR spectra in methanol-^{12}C-d_4 at 325.4 K of:
(a) $[Mg(THEC12)]^{2+}$ (0.100 mol dm^{-3}) and THEC12 (0.100 mol dm^{-3});
(b) $[Ca(THEC12)]^{2+}$ (0.110 mol dm^{-3}) and THEC12 (0.100 mol dm^{-3});
(c) $[Ca(TMEC12)]^{2+}$ (0.102 mol dm^{-3}) and TMEC12 (0.099 mol dm^{-3}); and
(d) $[Mg((S)\text{-THPC12})]^{2+}$ (0.101 mol dm^{-3}) and (*S*)-THPC12 (0.100 mol dm^{-3}).

medial carbon resonance in Figure 5.36(c), denoted *a*, at 325.4 K is due to the intramolecular exchange process in $[Ca(TMEC12)]^{2+}$). As for intermolecular ligand exchange on $[M(THEC12)]^{2+}$, no broadening or coalescence phenomena is observed for these two systems up to 325.4 K, consistent with exchange between TMEC12 and $[M(TMEC12)]^{2+}$ being in the very slow exchange limit of the NMR timescale. The intermolecular TMEC12 exchange on $[Mg(TMEC12)]^{2+}$ exhibits contrasting behaviour to that of its Ca^{2+} and Ba^{2+} analogues, and is discussed in more detail below.

For intermolecular (*S*)-THPC12 exchange on $[Mg((S)\text{-THPC12})]^{2+}$, the ^{13}C NMR spectra consist of 9 distinct resonances from 293.5 K to 325.4 K. At 325.4 K, the macrocyclic ring resonances of $[Mg((S)\text{-THPC12})]^{2+}$ (denoted *a* and *b* in Figure 5.36) are observed at 49.25 and 49.41 ppm, whereas that of (*S*)-THPC12 (a^*,b^*) is observed at 50.27 ppm. The pendant arm $-CH(CH_3)OH$ moiety of $[Mg((S)\text{-THPC12})]^{2+}$ (*c*) resonates at 59.70 ppm, whereas that of (*S*)-THPC12 (c^*) resonates at 61.95 ppm. The resonance arising from the pendant arm $>NCH_2-$ moiety of $[Mg((S)\text{-THPC12})]^{2+}$ (*d*) and (*S*)-THPC12 (d^*) are observed at 62.14 and 62.60 ppm, respectively. The $-CH(CH_3)OH$ moiety of $[Mg((S)\text{-THPC12})]^{2+}$ (*e*) and (*S*)-THPC12 (e^*) resonate at 18.70 and 19.15 ppm, respectively. Since intramolecular exchange of $[M((S)\text{-THPC12})]^{2+}$, for $M^{2+} = Mg^{2+}$, Ca^{2+} and Ba^{2+}, has been observed to be in the slow exchange limit of the NMR timescale over the liquid solvent temperature range,[44b] and intermolecular (*S*)-THPC12 exchange on $[Mg((S)\text{-THPC12})]^{2+}$ is in slow exchange up to 325.4 K, a similar situation is likely to occur for the Ca^{2+} and Ba^{2+} analogue complexes.

It has been shown from variable temperature ^{13}C NMR studies that the solution spectra of $[Mg(TMEC12)]^{2+}$ are consistent with a 7-coordinate complex where TMEC12 adopts the TRANS I configuration.[44b] (Although it is also possible that $[Mg(TMEC12)]^{2+}$ is 5-coordinate, the observation of a 7-coordinate, TRANS I complex in the solid state for $[Mg((S)\text{-THPC12})]^{2+}$ supports the preference of the 7-coordinate geometry for $[Mg(TMEC12)]^{2+}$).[43b] Intermolecular exchange between free TMEC12 and $[Mg(TMEC12)]^{2+}$ (Equation 5.1) is indicated by the coalescence of the $-CH_2OCH_3$, $>NCH_2-$ and macrocyclic ring ^{13}C resonances of free and complexed TMEC12 (Figure 5.37). The ^{13}C NMR spectrum exhibits broad, partially unresolved resonances at 187.1 K. At 223.6 K, the resonances at ~ 49.18 and ~ 50.16 ppm are assigned to the macrocyclic ring carbons of $[Mg(TMEC12)]^{2+}$ (denoted *a* in Figure 5.37) and TMEC12 (a^*), respectively. The resonances at 52.89 and 54.02 ppm are respectively assigned to the $>NCH_2-$ moiety of $[Mg(TMEC12)]^{2+}$ (*b*) and TMEC12 (b^*), while those of the $-OCH_3$ moiety for $[Mg(TMEC12)]^{2+}$ (*c*) and TMEC12 (c^*) are observed at the same chemical

shift of 56.87 ppm. The resonances at 67.94 and 69.52 ppm are assigned to the -CH_2OCH_3 moiety of $[Mg(TMEC12)]^{2+}$ (*d*) and TMEC12 (*d'*), respectively. The rate parameters listed in Table 5.15 for the intermolecular exchange process were determined from the coalescence of the -CH_2OCH_3 ^{13}C resonances of free TMEC12 and $[Mg(TMEC12)]^{2+}$, as these resonances exhibit the largest chemical shift difference.

The Mg^{2+} complex stabilities decrease in the order $[Mg((S)\text{-THPC12})]^{2+}$ > $[Mg(THEC12)]^{2+}$ > $[Mg(TMEC12)]^{2+}$. The ^{13}C NMR studies show that $[Mg((S)\text{-THPC12})]^{2+}$ and $[Mg(THEC12)]^{2+}$ both maintain an 8-coordinate geometry, where k(298.2 K) decreases in the order $[Mg(THEC12)]^{2+}$ > $[Mg((S)\text{-THPC12})]^{2+}$. The lower stability and observation of a 7-coordinate complex for $[Mg(TMEC12)]^{2+}$ are probably due to the bulky methyl group on the coordinating oxygen of the pendant arms of TMEC12 inducing strain in the complex and facilitating easier modes of intramolecular exchange. This effect is more pronounced for the smaller Mg^{2+} ion than for the other alkaline earth metals.

The observations in this chapter for intramolecular and intermolecular exchange processes follow similar trends to the stabilities of the complexes discussed in this study. That is, it is apparent that the stability of the alkali metal ion complexes follow the sequence $[M(TMEC12)]^{+}$ > $[M(THEC12)]^{+}$ (Chapter 2), but the alkaline earth metal ion complexes follow the reverse sequence (Chapter 3). This is reflected in slower rates of intramolecular exchange characterising $[M(TMEC12)]^{+}$ compared with $[M(THEC12)]^{+}$,[15,44b] whereas intramolecular exchange for $[Ba(TMEC12)]^{2+}$ proceeds at a faster rate than that of $[Ba(THEC12)]^{2+}$. Furthermore, the lower stability of $[M(THEC12)]^{2+}$ compared with $[M((S)\text{-THPC12})]^{2+}$ is envisaged to be reflected in slower intramolecular exchange for $[M((S)\text{-THPC12})]^{2+}$. This has been observed, where the parameters characterising intramolecular exchange in $[M(THEC12)]^{2+}$ are shown in Table 5.11, while intramolecular exchange in $[M((S)\text{-THPC12})]^{2+}$ is in the very slow exchange limit of the NMR timescale over the liquid solvent temperature range.[44b] However, as a consequence of the limited range of kinetic data afforded by these complexes, it would be inappropriate to speculate without further investigation.

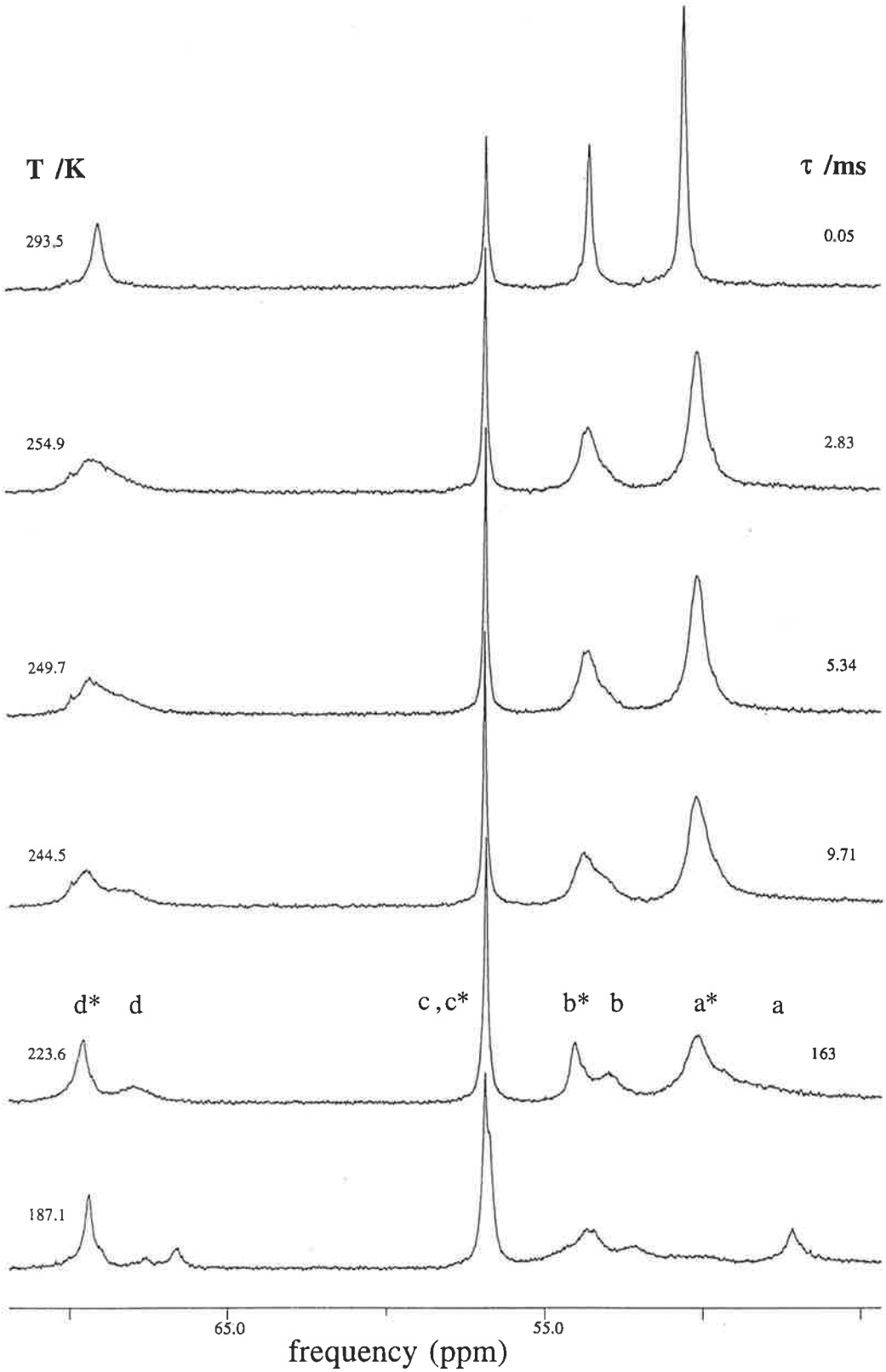

Figure 5.37: Temperature variations of the broad-band ^{1}H decoupled ^{13}C NMR spectra of $[Mg(TMEC12)]^{2+}$ (0.054 mol dm^{-3}) and TMEC12 (0.134 mol dm^{-3}) in methanol-^{12}C-d_4. Experimental temperatures and τ values derived from complete lineshape analysis of the coalescence of the $>NCH_2$- ^{13}C resonances (*b* and *b**) appear to the left and the right of the figure, respectively.

Table 5.15: Kinetic parameters[a] for intermolecular TMEC12 exchange on $[Mg(TMEC12)]^{2+}$ in methanol-^{12}C-d_4.

k (298.2 K)[b] s^{-1}	$\Delta H^{\ddagger}$ kJ mol^{-1}	$\Delta S^{\ddagger}$ J K^{-1} mol^{-1}
30000 ± 750	61.7 ± 0.4	47.7 ± 1.5

[a]Errors represent 1 standard deviation for the fit of experimental τ data to Equation 4.10. [b]$k(s^{-1})$ = 199 ± 3 (249.7 K) is the exchange rate constant at the $-CH_2OCH_3$ coalescence temperature.

BIBLIOGRAPHY

1. (a) M. Shamsipur, A.I. Popov, *J. Phys. Chem.* **1986**, 90, 5997-5999.
   (b) J.-M. Lehn, *Struct. Bond. (Berlin)* **1973**, 16, 1-69.
2. (a) R.M. Izatt, K. Pawlak, J.S. Bradshaw, R.L. Bruening, *Chem. Rev.* **1991**, 91, 1721-2085.
   (b) B.G. Cox, J. Garcia-Rosas, H. Schneider, *J. Am. Chem. Soc.* **1981**, 103, 1054-1059.
3. (a) S.F. Lincoln, A.K.W. Stephens, *Inorg. Chem.* **1991**, 30, 3529-3534.
   (b) J.M. Ceraso, J.L. Dye, *J. Am. Chem. Soc.* **1973**, 95, 4432-4434.
4. (a) A. Abou-Hamdan, S.F. Lincoln, *Inorg. Chem.* **1991**, 30, 462-466.
   (b) A. Anichini, L. Fabbrizzi, P. Paoletti, R.M. Clay, *J. Chem. Soc., Dalton Trans.* **1986**, 577-583.
5. (a) R. Gresser, D.W. Boyd, A.M. Albrecht-Gary, J.P. Schwing, *J. Am. Chem. Soc.* **1980**, 102, 651-653.
   (b) B.G. Cox, D. Knop, H. Schneider, *J. Am. Chem. Soc.* **1978**, 100, 6002-6007.
6. (a) J.M. Ceraso, P.B. Smith, J.S. Landers, J.L. Dye, *J. Phys. Chem.* **1977**, 81, 760-766.
   (b) E. Schchori, J. Jagur-Gordzinski, Z. Luz, H. Shporer, *J. Am. Chem. Soc.* **1971**, 93, 7133-7138.
7. (a) C.M. Madeyski, J.P. Michael, R.D. Hancock, *Inorg. Chem.* **1984**, 23, 1487-1489.
   (b) R.W. Hay, M.P. Pujari, W.T. Moodie, S. Craig, D.T. Richens, A. Perotti, L. Ungaretti, *J. Chem. Soc., Dalton Trans.* **1987**, 2605-2613.
8. (a) R.D. Hancock, R. Bhavan, P.W. Wade, J.C.A. Boeyens, S.M. Dobson, *Inorg. Chem.* **1989**, 28, 187-194.
   (b) T.A. Kaden, *Topp. Curr. Chem.* **1984**, 121, 157-179.
9. (a) K.P. Wainwright, *J. Chem. Soc., Dalton Trans.* **1980**, 2117-2120.
   (b) I. Murase, M. Mikuriya, H. Sonoda, S. Kida, *J. Chem. Soc., Chem. Commun.* **1984**, 692-694.
10. (a) M.K. Moi, M. Yanuck, S.V. Deshpande, H. Hope, S.J. DeNardo, C.F. Meares, *Inorg. Chem.* **1987**, 26, 3458-3463.
    (b) N.W. Alcock, K.P. Balakrishnan, P. Moore, *J. Chem. Soc., Dalton Trans.* **1986**, 1743-1745.
11. A. Reisen, M. Zehnder, T.A. Kaden, *Acta. Crystallogr., Sect. C: Cryst. Struct. Commun.* **1988**, C44, 1740-1742.
12. P. Clarke, A.M. Hounslow, R.A. Keough, S.F. Lincoln, K.P. Wainwright, *Inorg. Chem.* **1990**, 29, 1793-1797.
13. (a) P. Clarke, S.F. Lincoln, K.P. Wainwright, *Inorg. Chem.* **1991**, 30, 134-139.
    (b) J.-M. Lehn, J.-P. Sauvage, *J. Am. Chem. Soc.* **1975**, 97, 6700-6707.

14. N.W. Alcock, N. Herron, P. Moore, *J. Chem. Soc., Dalton Trans.* **1978**, 1282-1288.
15. A.K.W. Stephens, R.S. Dhillon, S.E. Madback, S.L. Whitbread, S.F. Lincoln, *Inorg. Chem.* **1996**, 35, 2019-2024.
16. R.S. Dhillon, S.E. Madback, F.G. Ciccone, M.A. Buntine, S.F. Lincoln, K.P. Wainwright, *J. Am. Chem. Soc.* **1997**, 119, 6126-6134.
17. A.K.W. Stephens, PhD Thesis, University of Adelaide, **1994**.
18. J.B. Lucas, PhD Thesis, University of Adelaide, **1994**.
19. S.F. Lincoln, G.S. Laurence, P.-A. Pittet, M.L. Turonek, K.P. Wainwright, *J. Chem. Soc., Chem. Commun.* **1991**, 1205.
20. Y. Ba, R.-F. Song, Z.-W. Qiu, *Mag. Res. in Chem.* **1989**, 27, 916-921.
21. M.C. Gennaro, P. Mirti, C. Casolino, *Polyhedron* **1983**, 2, 13-18.
22. P. Mirti, M.C. Gennaro, M. Vallinotto, *Transition Met. Chem.* **1982**, 2, 2-5.
23. L.M. Jackman, F.A. Cotton, *"DNMR Spectroscopy"*, Academic Press, London and New York, **1975**.
24. R.J. Day, C.N. Reilley, *Anal. Chem.* **1965**, 37, 1326-1333.
25. N.W. Alcock, N. Herron, P. Moore, *J. Chem. Soc., Dalton Trans.* **1979**, 1486-1491.
26. T. Alfheim, S. Buøen, J. Dale, K.D. Krautwurst, *Acta. Chem. Scand.*, **1986**, B40, 40-49.
27. F.A. Bovey, *"NMR Spectroscopy"*, Academic Press, London, **1988**.
28. V.J. Thöm, G.D. Hosken, R.D. Hancock, *Inorg. Chem.* **1985**, 24, 3378-3381.
29. V.J. Thöm, C.C. Fox, J.C.A. Boeyens, R.D. Hancock, *J. Am. Chem. Soc.* **1984**, 106, 5947-5955.
30. J.F. Desreux, *Inorg. Chem.* **1980**, 19, 1319-1324.
31. J. Dale, *Acta. Chem. Scand.* **1973**, 27, 1115-1129 and 1130-1148.
32. M.A. Buntine, University of Adelaide.
33. S. Buøen, J. Dale, P. Groth, J. Krane, *J. Chem. Soc., Chem. Commun.* **1982**, 1172-1174.
34. P. Groth, *Acta. Chem. Scand.* **1983**, 71-77.
35. P. Groth, *Acta. Chem. Scand.* **1983**, 283-291.
36. T. Sakurai, K. Kobayashi, K. Tsuboyama, S. Tsuboyama, *Acta. Crystallogr. Sect. B* **1978**, 34, 1144-1148.
37. (a) J.H. Coates, D.A. Hadi, S.F. Lincoln, *Aust. J. Chem.* **1982**, 35, 903-909.
    (b) F.K. Barefield, F. Wagner, *Inorg. Chem.* **1973**, 12, 2435-2439.
38. (a) K.R. Adam, B.J. McCool, A.J. Leong, L.F. Lindoy, C.W.G. Ansell, P.J. Baillie, K.P. Dancey, L.A. Drummond, K. Henrick, M. McPartlin, D.K Uppal, P.A. Tasker, *J. Chem. Soc., Dalton Trans.* **1990**, 3435-3444.

(b) C.W.G. Ansell, K.P. Dancey, M. McPartlin, P.A. Tasker, L.F. Lindoy, *J. Chem. Soc., Dalton Trans.* **1983**, 1789-1791.
(c) M. Kato, T. Ito, *Inorg. Chem.* **1985**, 24, 509-514.

39. (a) M. Shionoya, E. Kimura, M. Shiro, *J. Am. Chem. Soc.* **1993**, 115, 6730-6737.
(b) N.W. Alcock, K.P. Balakrishnan, P. Moore, *J. Chem. Soc., Chem. Commun.* **1985**, 1731-1733.
(b) G. de Martino Norante, M. Di Vaira, F. Mani, S. Mazzi, P. Stoppioni, *J. Chem. Soc., Chem. Commun.* **1990**, 438-439.
40. A. Bencini, A. Bianchi, M. Castello, M. DiVaira, J. Faus, E. Garcia Espana, M. Micheloni, P. Paoletti, *Inorg. Chem.* **1989**, 28, 347-351.
41. R.D. Shannon, *Acta. Crystallogr. Sect. A: Cryst. Phys. Diffr. Theor. Gen. Crystallogr.* **1976**, 32, 751-767.
42. (a) R.D. Hancock, M.S. Shaikjee, S.M. Dobson, J.C.A. Boeyens, *Inorg. Chim. Acta.* **1988**, 154, 229-238.
(b) R. Luckay, J.H. Reibenspies, R.D. Hancock, *J. Chem. Soc., Chem. Commun.* **1995**, 2365-2366.
43. (a) A.K.W. Stephens, R.S. Dhillon, S.F. Lincoln, K.P. Wainwright, *Inorg. Chim. Acta.* **1995**, 236, 185-188.
(b) J.R. Morrow, K.O.A. Chin, *Inorg. Chem.* **1993**, 32, 3357-3361.
44. (a) R.S. Dhillon, A.K.W. Stephens, S.L. Whitbread, S.F. Lincoln, K.P. Wainwright, *J. Chem. Soc., Chem. Commun.* **1995**, 1, 97-98.
(b) S.E. Madback, Honours Thesis, University of Adelaide, **1994**.
45. H.G. Brittain, J.F. Desreux, *Inorg. Chem.* **1984**, 23, 4459-4466.
46. S.F. Lincoln, *Prog. Reaction Kinetics* **1977**, 9, 1-91.
47. K.O.A. Chin, J.R. Morrow, C.H. Lake, M.R. Churchill, *Inorg. Chem.* **1994**, 33, 656-664.
48. S.I. Kang, R.S. Ranganathan, J.E. Emswiler, K. Kumar, J.Z. Gougoutas, M.F. Malley, M.F. Tweedle, *Inorg. Chem.* **1993**, 32, 2912-2918.
49. L. Carlton, R.D. Hancock, H. Maumela, K.P. Wainwright, *J. Chem. Soc., Chem. Commun.* **1994**, 1007-1008.
50. R.D. Hancock, S.M. Dobson, J.C.A. Boeyens, *Inorg. Chim. Acta.* **1987**, 133, 221-231.
51. (a) *"Stereochemical and Stereophysical Behaviour of Macrocycles"*, Volume 2, Ivan Bernal (Editor), **1987**.
(b) R.D. Hancock, A.E. Martell, *Chem. Rev.* **1989**, 89, 1875-1914.
52. (a) M.J. Van der Merwe, J.C.A. Boeyens, R.D. Hancock, *Inorg. Chem.* **1985**, 24, 1208-1213.
(b) R.S. Glass, G.S. Wilson, W.N. Setzer, *J. Am. Chem. Soc.* **1980**, 102, 5068-5069.
53. B.A. Sayer, J.P. Michael, R.D. Hancock, *Inorg. Chim. Acta.* **1983**, 77, L63-L64.

54. K. Wieghardt, U. Bossek, P. Chaudhuri, W. Hermann, B.C. Menke, J. Weiss, *Inorg. Chem.* **1982**, 21, 4308-4314.
55. F.G. Ciccone, Honours Thesis, University of Adelaide, **1996**.
56. S.L. Whitbread, J.M. Weeks, P. Valente, M.A. Buntine, S.F. Lincoln, K.P. Wainwright, *Aust. J. Chem.* **1997**, 50, 853-856.
57. (a) R.G. Pearson, *J. Am. Chem. Soc.* **1963**, 85, 3533-3539.
(b) R.G. Pearson, *Coord. Chem. Rev.* **1990**, 100, 403-425.
58. E. Luboch, A. Cygan, J.F. Biernat, *Inorg. Chim. Acta.* **1983**, 68, 201-204.
59. I. Lazar, R. Ramasamy, E. Brücher, C.F.G.C. Geraldes, A.D. Sherry, *Inorg. Chim. Acta.* **1992**, 195, 89-93.
60. R.D. Hancock, M.S. Shaikjee, S.M. Dobson, J.C.A. Boeyens, *Inorg. Chim. Acta.* **1988**, 154, 229-238.
61. (a) R.D. Hancock, *Pure. Appl. Chem.* **1986**, 58, 1445-1452.
(b) E.K. Barefield, A. Bianchi, E.J. Billo, P.J. Connolly, P. Paoeletti, J.S. Summers, D.G. Van Derveer, *Inorg. Chem.* **1986**, 25, 4197-4202.
62. (a) M. Kojima, K. Nakabayashi, S. Ohba, S. Okumoto, Y. Saito, J. Fujita, *Bull. Chem. Soc. Jpn.* **1986**, 59, 277-283.
(b) J. Giusti, S. Chimichi, M. Ciampolini, *Inorg. Chim. Acta.* **1984**, 88, 51-54.
63. (a) T. Ito, M. Kato, H. Ito, *Bull. Chem. Soc. Jpn.* **1984**, 57, 2634-2640.
(b) M. Di Vaira, F. Mani, P. Stoppioni, *J. Chem. Soc., Dalton Trans.* **1992**, 1127-1130.
(c) G. de Martino Norante, M. Di Vaira, F. Mani, S. Mazzi, P. Stoppioni, *Inorg. Chem.* **1990**, 29, 2822-2829.
64. R. Clay, P. Murray-Rust, J. Murray-Rust, *J. Acta. Cryst.* **1979**, B35, 1894-1895.
65. Y. Iitaka, M. Shina, E. Kimura, *Inorg. Chem.* **1974**, 13, 2886-2891.
66. J.H. Lochlin, E.B. Fleischer, *J. Acta. Cryst.* **1976**, B32, 3063-3066.
67. (a) N. Matsumoto, A. Hirano, T. Hara, A. Ohyoshi, *J. Chem. Soc., Dalton Trans.* **1983**, 2405-2410.
(b) B. Scott, K.J. Brewer, L.O. Spreer, C.A. Craig, J.W. Otves, M. Calvin, S. Taylor, *J. Coord. Chem.* **1990**, 21, 307-313.
68. M.L. Turonek, P. Clarke, G.S. Laurence, S.F. Lincoln, P.-A. Pittet, S.Politis, K.P. Wainwright, *Inorg. Chem.* **1993**, 32, 2195-2198.
69. M.L. Turonek, PhD Thesis, University of Adelaide, **1993**.
70. (a) A.F. Cameron, D.W. Taylor, R.H. Nuttall, *J. Chem. Soc., Dalton Trans.* **1972**, 1603-1608.
(b) D. Wester, G.J. Palenik, *Inorg. Chem.* **1976**, 15, 755-761.
71. (a) Z.P. Haque, D.C. Liles, M. McPartlin, P.A. Tasker, *Inorg. Chim. Acta.* **1973**, 23, L21-L22.

(b) A.H. White, A.C. Willis, *J. Chem. Soc., Dalton Trans.* **1977**, 1377-1381.
72. G.J. Palenik, D.W. Wester, *Inorg. Chem.* **1978**, 17, 864-870.
73. D.C. Liles, M. McPartlin, P.A. Tasker, *J. Chem. Soc., Dalton Trans.* **1987**, 1631-1636.
74. Spectral assignment at 216.3 K made by P. Clements (NMR Officer), University of Adelaide.
75. P. Valente, Flinders University of South Australia.
76. NMR data collected by P. Valente, lineshaping analysis done by this author.

CHAPTER 6

EXPERIMENTAL

6.1 SYNTHESIS OF LIGANDS

CYCLEN was prepared by the method described in the literature,[1] and used the starting materials *N,O,O'*-tris(toluene-*p*-sulphonyl)bis(2-hydroxy-ethyl)amine and the disodium salt of 1,4,7-tris(toluene-*p*-sulphonyl)-1,4,7-triazaheptane. These starting materials were prepared by a method derived from the literature.[2] Various pendant arms can then be attached to the unsubstituted macrocycle CYCLEN. The synthesis of *N* functionalised aza macrocycles, reviewed in the literature, is often straightforward,[3] whereby the unsubstituted macrocycle is reacted with an excess of alkylating agent in the presence of a base. (The base is necessary to neutralise acid liberated in the reaction). Therefore, many pendant arm macrocycles are synthesised by this general method,[4-9] and this method was used to synthesise THEC12, TMEC12 and THEC9. The ligands (*S*)-THPC12 and (*R*)-THPEC12 were used as supplied.[10,11]

6.1.1 PREPARATION OF CYCLEN

PREPARATION OF 1,4,7-TRIS(TOLUENE-*P*-SULPHONYL)-1,4,7-TRIAZAHEPTANE AND ITS DISODIUM SALT

A solution of *p*-toluenesulphonyl chloride (114.4 g, 0.6 mol) (BDH) in diethylether (600 cm^3) was added dropwise to a stirred solution of diethylene-triamine (20.6 g, 22 cm^3, 0.2 mol) (BDH) and NaOH (24 g, 0.6 mol) (Aldrich) in water (200 cm^3) at room temperature. Excess NaOH was added to ensure complete deprotonation of the amine. After addition was complete, the solution was stirred for a further hour, and the white precipitate of 1,4,7-tris(toluene-*p*-sulphonyl)-1,4,7-triazaheptane was filtered from solution and recrystallised from ethanol. Yield 87.6 g, 78%.

The disodium salt was prepared by addition of small amounts of 1,4,7-tris(toluene-*p*-sulphonyl)-1,4,7-triazaheptane to a mechanically stirred solution of sodium (12.3 g) (Aldrich) in ethanol (1400 cm^3) (Aldrich) under a nitrogen atmosphere. The solution was stirred for one hour, and the pasty white precipitate of the disodium salt of 1,4,7-tris(toluene-*p*-sulphonyl)-1,4,7-

triazaheptane was filtered from solution under nitrogen, washed with large portions of diethyl ether and dried under vacuum. Yield 72.0 g, 76%.

PREPARATION OF *N,O,O'*-TRIS(TOLUENE-*P*-SULPHONYL)BIS(2-HYDROXYETHYL)AMINE

A solution of *p*-toluenesulphonyl chloride (114.4 g, 0.6 mol) (BDH) in diethyl ether (600 cm^3) (BDH) was added dropwise to a mechanically stirred solution of bis(2-hydroxyethyl)amine (20.4 g, 0.2 mol) (BDH) in triethylamine (200 cm^3) at room temperature. The solution was stirred for a further hour and water (900 cm^3) was added. The solution was stirred for a further 8 hours and the white precipitate of *N,O,O'*-tris(toluene-*p*-sulphonyl)bis(2-hydroxyethyl)-amine was filtered from solution, washed with diethyl ether (200 cm^3), dried on a water pump and then air dried overnight. Yield 68.0 g, 62%.

PREPARATION OF TETRATOSYL CYCLEN

A solution of *N,O,O'*-tris(toluene-*p*-sulphonyl)bis(2-hydroxyethyl)amine (68 g, 0.120 mol) in anhydrous DMF (450 cm^3) was added dropwise to a mechanically stirred solution containing the disodium salt of 1,4,7-tris(toluene-*p*-sulphonyl)-1,4,7-triazaheptane (72 g, 0.120 mol) in anhydrous DMF (900 cm^3) at 383 K under a nitrogen atmosphere. After complete addition (2 hours), the solution was cooled, and water was added dropwise to dilute the solution to 3 dm^3. The solution was then stirred for a further 8 hours, and the white precipitate of tetratosyl cyclen was filtered from solution, washed with ethanol (2×200 cm^3) and diethyl ether (200 cm^3) and dried under vacuum. Yield 45.0 g, 40%.

PREPARATION OF CYCLEN

To remove the tosyl functional groups, tetratosyl cyclen (45 g, 0.076 mol) was added to a stirred solution containing deoxygenated concentrated H_2SO_4 (220 cm^3) and H_2O (5 cm^3) at 373 K. The solution was stirred for 50 hours, then cooled in ice. Diethyl ether (550 cm^3) was added to the ice-cooled, stirred black solution, and the resulting sticky precipitate was filtered from solution and washed with diethylether (200 cm^3). The crude CYCLEN was then dissolved in H_2O (200 cm^3), and NaOH (50 g) (Aldrich) was slowly added to the aqueous layer until the solution turned highly basic. The CYCLEN was extracted with $CHCl_3$ (5×250 cm^3), dried with anhydrous $MgSO_4$ and the solvent was removed by a rotary evaporator. Yield 5.8 g, 67%. The product was shown to be pure by NMR: ^{13}C NMR ($CDCl_3$) δ(ppm): 45.95, and ^1H

NMR ($CDCl_3$) δ(ppm): 2.60. A reaction scheme for this synthesis appears in Figure 6.1.

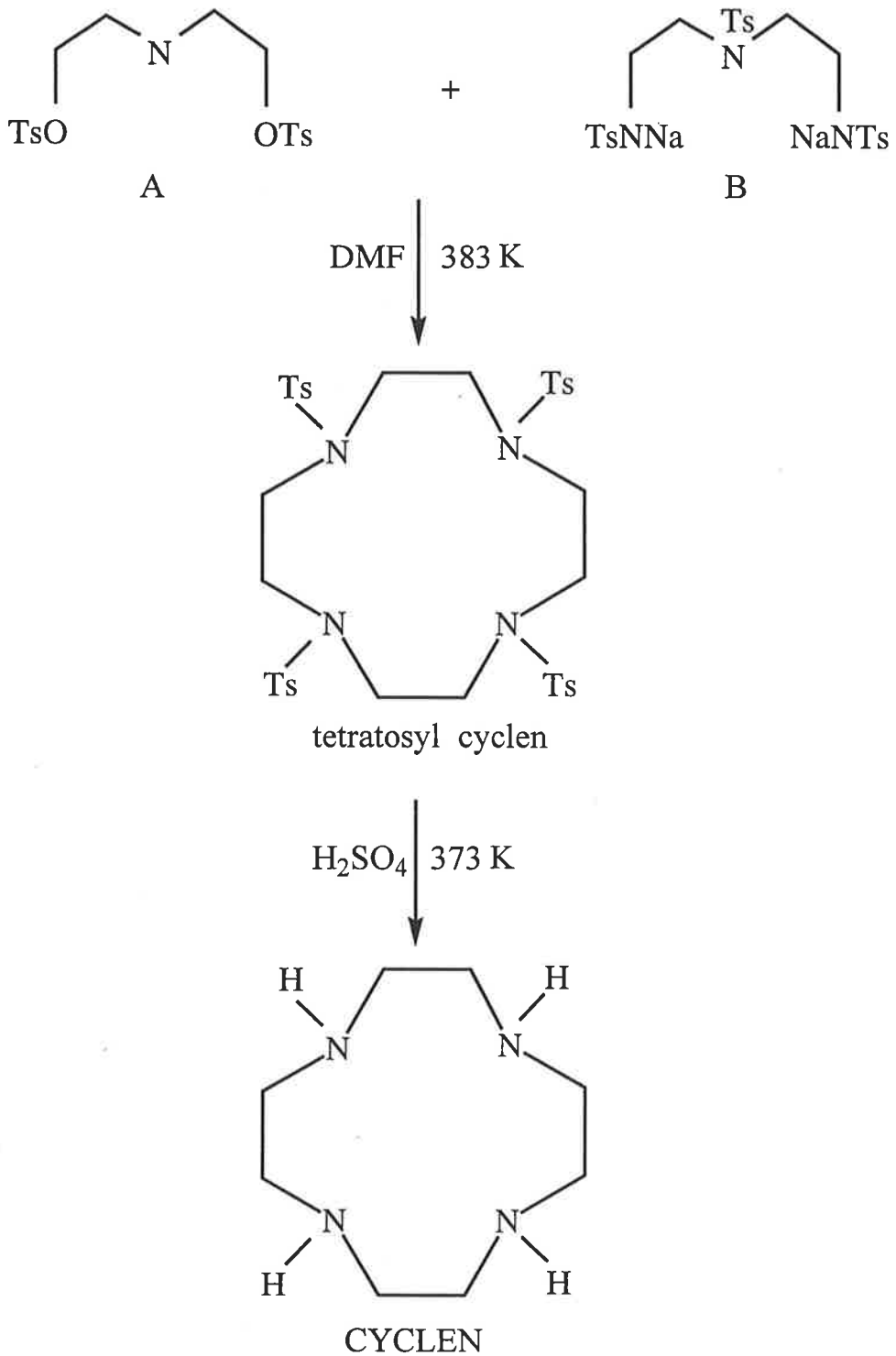

Figure 6.1: Structural representation for the synthesis of CYCLEN, where A is *N,O,O'*-tris(toluene-*p*-sulphonyl)bis(2-hydroxyethyl)amine, B is the disodium salt of 1,4,7-tris(toluene-*p*-sulphonyl)-1,4,7-triazaheptane, and Ts is *p*-$CH_3C_6H_4SO_2$.

6.1.2 PREPARATION OF THEC12

Attachment of hydroxyethyl pendant arms to a parent macrocycle such as CYCLEN may be done by reacting the parent macrocycle with 2-bromoethanol or ethylene oxide under a variety of conditions.[6,12-16a] Reactions with ethylene oxide afford a more direct route and shorter reaction times than for other methods of synthesising THEC12, but ethylene oxide can be very hazardous and inconvenient to use. That is, due to its high volatility, ethylene oxide must always be used at low temperatures, and only a 100 - 200% stoichiometric excess of ethylene oxide should be used in the reaction, since high concentrations of ethylene oxide in H_2O produces a crystalline clathrate at temperatures below 284 K which makes stirring difficult.[16b-16d] In addition, extended reaction times result in elongated side-chains of the product and formation of polyethylene glycols.[16a]

THEC12 was prepared by a slight modification of the method described in the literature.[16a] Cooled ethylene oxide (2.27 cm^3, 2 g, 0.045 mol) (Fluka) was added to a stirred solution of CYCLEN (0.97 g, 0.006 mol) in H_2O (10 cm^3), which was kept at 273 K for 2 hours 20 minutes. The reaction was then stopped by removing excess ethylene oxide on a rotary evaporator. The mixture was concentrated to half its original volume on the rotary evaporator, and concentrated further by evaporation at room temperature. The THEC12 crystals were filtered from the sticky mother liquor, washed with ice cold H_2O (2 × 1 cm^3) and dried under vacuum. Yield 0.90 g, 46%. Analysis of the solid by NMR spectroscopy revealed a product requiring no further purification: ^{13}C NMR ($CDCl_3$) δ(ppm): 49.57 (ring); 54.87 (>NCH_2-); 57.71 (-CH_2OH), and ^1H NMR ($CDCl_3$) δ(ppm): 2.47 (*t*, 8H, >NCH_2-); 2.51 (*s*, 16H, ring); 3.59 (*t*, 8H, -CH_2OH). A reaction scheme for this synthesis appears in Figure 6.2.

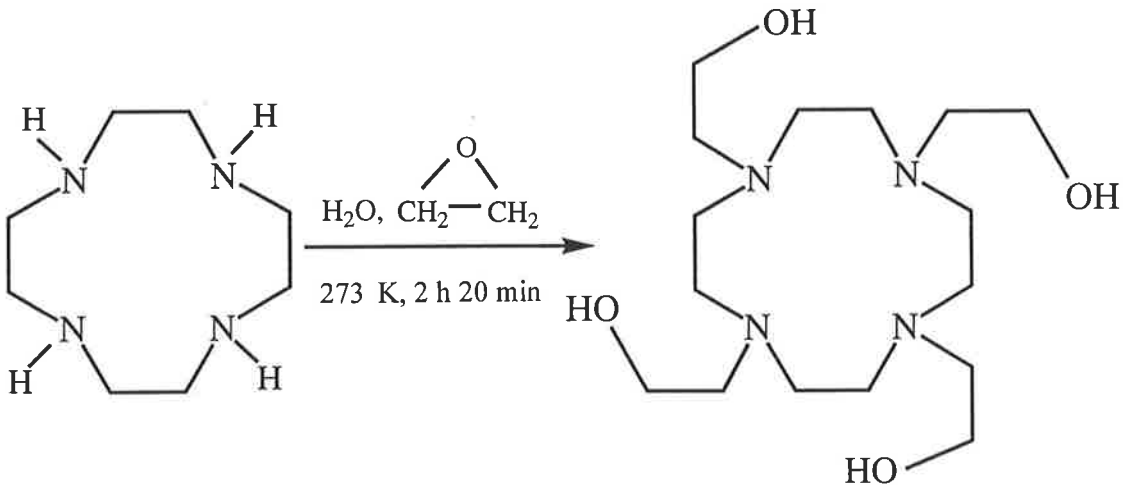

CYCLEN THEC12

Figure 6.2: Structural representation for the synthesis of THEC12.

6.1.3 PREPARATION OF TMEC12

CYCLEN (0.6 g, 0.035 mol), NaOH (0.53 g, 0.013 mol) (Aldrich) and 2-chloroethylmethyl ether (12.4 g, 0.131 mol) (Aldrich) were dissolved in 50% ethanol/H_2O mixture (25 cm^3). The solution was refluxed under nitrogen for several days. NaOH was added regularly to the reaction mixture as it is necessary to maintain the pH above 11 to prevent a side reaction between the chloride and NaOH. The solvent was then removed by rotary evaporation, and the solid residue was dissolved in H_2O (25 cm^3). NaOH was then added, and the solution was extracted with $CHCl_3$ (5 × 50 cm^3). The $CHCl_3$ was removed by rotary evaporation to give yellow [Na(TMEC12)]Cl, which was then heated under vacuum at 373 K, 0.05 mm Hg to dissociate the complex. Distillation of the solid on a sublimator at 413 K, 0.015 mm Hg produced pure TMEC12 as a colourless oil. Yield 0.94 g, 67%. The product was shown to be pure by NMR: ^{13}C NMR ($CDCl_3$) δ(ppm): 52.59 (ring); 55.02 (>NCH_2-); 58.71ppm (-OCH_3); 71.01 (-CH_2OCH_3), and ^1H NMR ($CDCl_3$) δ(ppm): 2.56 (*t*, 8H, >NCH_2-); 2.63 (*s*, 16H, ring); 3.28 (*s*, 12H, -OCH_3); 3.42 (*t*, 8H, -CH_2OCH_3). Figure 6.3 shows the reaction scheme for this synthesis.

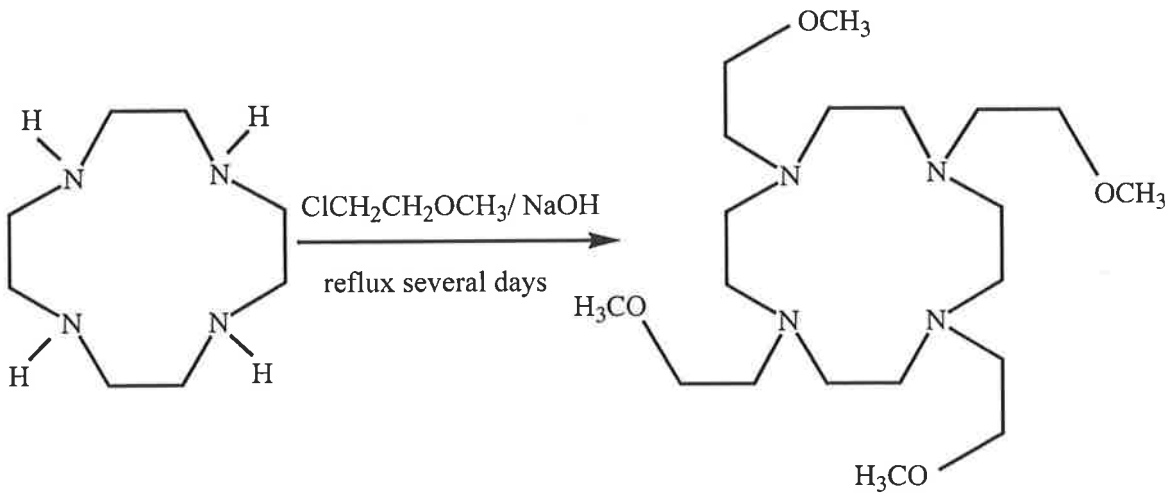

CYCLEN TMEC12

Figure 6.3: Structural representation for the synthesis of TMEC12.

6.1.4 PREPARATION OF THEC9

THEC9 was prepared according to the method described in the literature.[17] Cooled liquid ethylene oxide (0.52 cm^3, 0.44 g, 0.01 mol) was added to a solution of TACN (0.3 g, 0.002 mol)[1,18] in dry distilled ethanol (5 cm^3). The

solution was stirred overnight, and the reaction was stopped by removing unreacted ethylene oxide on a rotary evaporator. Solvent was removed under vacuum to give THEC9 as a yellow oil. Yield 0.43 g, 71%. The product was shown to be pure by NMR: ^{13}C NMR ($CDCl_3$) δ(ppm): 54.85 (ring); 59.23 (>N*C*H_2-); 59.37 (-*C*H_2OH), and ^{1}H NMR ($CDCl_3$) δ(ppm): 2.83 (*t*, 6H, >NC*H*$_2$-); 2.84 (*s*, 12H, ring); 3.67 (*t*, 6H, -C*H*$_2$OH). The reaction route is shown in Figure 6.4.

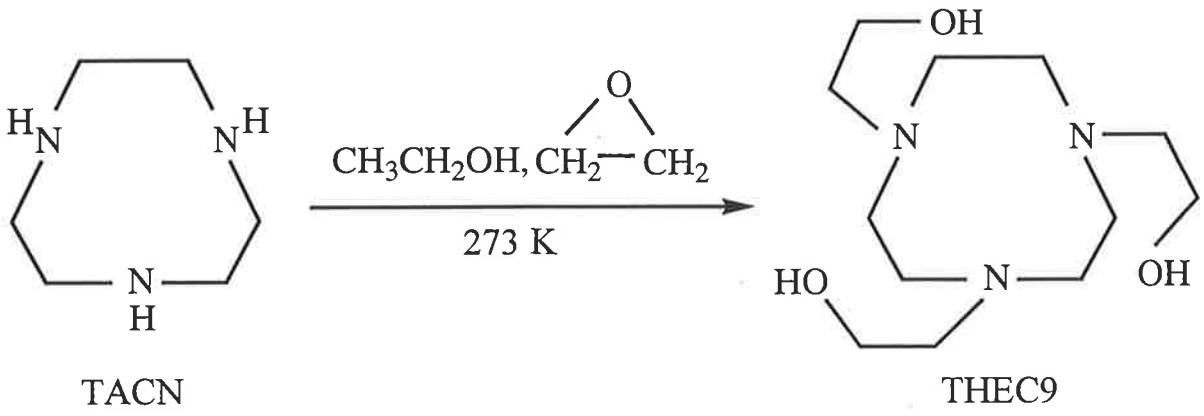

Figure 6.4: Structural representation for the synthesis of THEC9.

6.2 NON-AQUEOUS TITRATIONS

6.2.1 MATERIALS

Synthesis of the ligands TMEC12, CYCLEN and THEC9 used in this study is outlined in Section 6.1. (*R*)-THPEC12 was used as previously prepared.[11] Acetonitrile (AR, Ajax), propylene carbonate (AR, Aldrich), methanol (AR, CSR) and *N,N*-dimethylformamide (AR, BDH) were purified and dried by literature methods.[19] Acetonitrile and methanol were then stored over Linde 3 Å molecular sieves, whereas propylene carbonate and *N,N*-dimethylformamide were stored over Linde 4 Å molecular sieves under dry nitrogen. (Linde 3 Å and 4 Å molecular sieves (BDH) were activated by heating in a furnace at 450 K for 8 hours). The water level of these solvents was below the Karl-Fischer detection level of *ca.* 50 ppm. Anhydrous $LiClO_4$ (Fluka), $NaClO_4$ (Fluka), $KClO_4$ (BDH), $AgClO_4$ (BDH) and $AgNO_3$ (Mattthey-Garrett) were purchased. Anhydrous $RbClO_4$ and $CsClO_4$ were used as previously prepared after drying.[20] All $MClO_4$ salts and $AgNO_3$ were dried

under vacuum for 48 hours and then stored over P_2O_5 under a nitrogen atmosphere. NEt_4ClO_4 was prepared by addition of $HClO_4$ (1.0 mol dm^{-3}, 1.7 dm^3) to NEt_4Br (300 g) (Aldrich) in H_2O (500 cm^3). The resulting NEt_4ClO_4 precipitate was recrystallised from H_2O until free of bromide (using an aqueous $AgNO_3$ solution) and acid (using indicator strips). The crystalline white NEt_4ClO_4 was dried under high vacuum for 48 hours until it maintained constant weight, and then stored over P_2O_5 under vacuum. All solutions were prepared in 0.05 mol dm^{-3} NEt_4ClO_4 (to maintain a constant Ag^+ activity coefficient), the appropriate solvent, and deionised H_2O that was ultra purified with a MilliQ™-Reagent system to produce H_2O with a specific resistance > 15 MΩcm.

6.2.2 MEASUREMENTS

Potentiometric titrations were performed manually using 2 vessels, each with a capacity in excess of 40 cm^3, connected by a salt bridge containing 0.05 mol dm^{-3} NEt_4ClO_4 electrolyte solution. The potential readings during the titration were monitored by an Orion Research 720 Digital voltmeter. The reference electrode, in the reference cell, was a Ag^+ wire in a reference solution of 20 cm^3 of 0.005 mol dm^{-3} $AgClO_4$ or $AgNO_3$ in the same solvent in which the titrations were carried out. The Ag^+ concentration in the sample cell was also monitored by a Ag^+ wire electrode. The vessels were thermostatted at 298.2 ± 0.1 K by an outer water-jacket, through which H_2O from a constant H_2O bath was circulated. High purity nitrogen, which was constantly bubbled through a solution of NEt_4ClO_4 in the appropriate solvent before entering the vessels, was used to saturate the nitrogen and exclude atmospheric CO_2, prevent solution evaporation and stir the solutions during titrations. In addition, a drying tube with Carbosorb soda lime (10-16 mesh) (BDH) was attached to the burette, and all joints were sealed with teflon tape to prevent evaporation from the vessels. In view of the hygroscopicity of the solvents, ligands and $M(ClO_4)_n$ salts, all solutions were prepared under a dry nitrogen atmosphere in a glove box.[21] Solutions of the $M(ClO_4)_n$ salts were prepared by volume. Equilibrium times for a stable potential reading varied with solvent, but generally a maximum delay time of 2 minutes between titrant additions was sufficient.

The electrode response to Ag^+ concentration was calibrated several times a day by the titration of 5 cm^3 of 0.005 mol dm^{-3} $AgClO_4$ or $AgNO_3$ in 0.01 cm^3 increments with 20 cm^3 of 0.05 mol dm^{-3} NEt_4ClO_4 solution in the appropriate solvent. This calibration was necessary to avoid the possibility of systematic errors resulting from incorrect potential measurements. The electrode response

to the change in Ag^+ concentration in solution is pseudo-Nernstian and is given by Equation 6.1:

$$E = E_0 + C \ln [Ag^+] \qquad 6.1$$

The calibration constants E_0 and C were determined from a linear plot of potential, E (mV), against the logarithm of the Ag^+ concentration, $\ln[Ag^+]$. The values for E_0 and C are solvent dependent, but generally C was found to lie in the range 19 - 28 mV, consistent with the values quoted in the literature.[22]

The stability constants for $[AgL]^+$, where L = (*R*)-THPEC12, TMEC12, CYCLEN and THEC9, were determined in triplicate by the direct titration of 5 cm^3 of 0.005 mol dm^{-3} ligand solution with 20 cm^3 of 0.0005 mol dm^{-3} $AgClO_4$ or $AgNO_3$ in the appropriate solvent. Stability constants for $[ML]^+$, where $M^+ = Li^+$, Na^+ and K^+, were determined in triplicate by the indirect (competitive) potentiometric titration of a 5 cm^3 solution containing 0.01 mol dm^{-3} $MClO_4$ and 0.005 mol dm^{-3} ligand with 20 cm^3 of 0.0005 mol dm^{-3} $AgClO_4$ or $AgNO_3$. Due to the low solubility of $RbClO_4$ and $CsClO_4$, concentrations at 1/10th of those stated above were used for competitive titrations involving these metal ions. The stability constants for $[ML]^+$ were then determined from the data using the programs VISP and STAB, as described in Chapter 7.[23]

The limit of detectability of the Ag^+ concentration by the Ag^+ ion selective electrode is solvent dependent, but is always able to be determined from the calibration. For all solvents studied here, the response of the Ag^+ electrode obeyed Equation 6.1 for all concentrations used in the titrations. Generally, for direct titrations reliable and reproducible results are obtained when the stability constants for $[AgL]^+$ are in the range 10^2 - 10^{12} mol^{-1} dm^3. The stability of $[ML]^+$ needs to be at least 10 times less than that of $[AgL]^+$ in order to be determined by the competitive potentiometric titration method.

6.3 AQUEOUS TITRATIONS

6.3.1 MATERIALS

The ligands THEC12 and THEC9 of this study were used as prepared in Section 6.1. Deionised H_2O was purified with a MilliQ™-Reagant system to give H_2O with a specific resistance > 15 MΩcm, and then boiled to remove any CO_2. This ultra-pure H_2O was then used in all solution preparations. Anhydrous $LiClO_4$ (Fluka), $NaClO_4$ (Fluka) and $KClO_4$ (BDH) were purchased. Anhydrous $RbClO_4$ and $CsClO_4$ were used as previously prepared

by the method reported in the literature.[20] Anhydrous $Mg(ClO_4)_2$ and $Ca(ClO_4)_2$ were prepared by addition of the corresponding metal carbonate (AR, BDH) to concentrated $HClO_4$. The solutions were left stirring for 2 days. Excess carbonate was filtered off, and the solutions were concentrated to give crystalline solids, which were recrystallised twice from H_2O. Anhydrous $Sr(ClO_4)_2$ and $Ba(ClO_4)_2$ were purchased (Aldrich). All $M(ClO_4)_n$ salts were dried under high vacuum for 48 hours until at constant weight, and then stored over P_2O_5 under vacuum. (CAUTION: Anhydrous perchlorate salts are potentially powerful oxidants and should be handled with care). Stock solutions of $M(ClO_4)_n$ (*ca.* 0.1 mol dm^{-3}), prepared from the AR grade salts, and 0.1053 mol dm^{-3} of NEt_4OH (40% w/w, Fluka) were standardised by conventional complexiometric titration techniques.[24,25] NEt_4ClO_4 was prepared and stored as described in Section 6.2.1. Solutions were prepared in both 0.1 mol dm^{-3} NEt_4ClO_4 (to maintain constant ionic strength) and $HClO_4$ (to ensure complete protonation of the tertiary amines in the aza ring of the ligand). For titrations involving THEC12, 0.005 mol dm^{-3} $HClO_4$ was used, and for titrations involving THEC9, 0.004 mol dm^{-3} $HClO_4$ was used.

6.3.2 MEASUREMENTS

Potentiometric titrations were carried out using a Metrohm E665 Dosimat Autoburette which was equipped with a 5 cm^3 burette (with a capillary tip placed below the surface of the solution in the vessel) to deliver the titrant, NEt_4OH, into the titration vessel. An Orion Ross Sureflow 81-72BN combination electrode (with 0.1 mol dm^{-3} NEt_4ClO_4 in H_2O as the filling solution) connected to an Orion SA 720 potentiometer was used to measure the potential. The autoburette and potentiometer were interfaced to a Laser 286/3 personal computer, and the autoburette was computer controlled to either deliver constant volume aliquots of the titrant to the titration vessel or add successive additions of titrant to give a decrease in potential of approximately 4 mV.[26] For all titrations, a maximum delay time of 300 seconds between each titrant addition was sufficient for equilibrium to be established. Therefore, no problems with long equilibration times during the potentiometric titrations, as is often found with nitrogen donor macrocycles, were experienced. The titration vessel was thermostatted at 298.2 ± 0.1 K by an outer water-jacket, through which H_2O from a constant H_2O bath was circulated. All solution preparations and titrations were done under a high purity nitrogen atmosphere,[21] and nitrogen was also bubbled through a solution of NEt_4ClO_4 (0.1 mol dm^{-3}) prior to entry into the titration vessel to saturate the nitrogen, exclude atmospheric CO_2 and prevent evaporation from the vessel. In addition, a drying tube with Carbosorb soda lime (10-16 mesh) (BDH) was attached to

the bottle containing NEt_4OH to further prevent contamination of the titration by CO_2. (The presence of CO_2 may lead to the formation of a carbonic acid-carbonate buffer, which will effect the pH of the solution).[27] All solutions were equilibrated in the vessel for 20 minutes prior to titration, and the solutions were constantly stirred with a magnetic stirrer.

The electrode, initially calibrated with pH 4 and pH 7 buffers, was calibrated several times a day by titrating 0.1053 mol dm^{-3} NEt_4OH with NEt_4ClO_4 and $HClO_4$ (either 0.005 or 0.004 mol dm^{-3}). The resulting data was fitted to the Nernst Equation (Equation 6.2) to determine E_0 and pK_w:

$$E = E_0 + \frac{RT}{F} \ln [H^+] \qquad 6.2$$

where E = observed potential (V)
E_0 = standard electrode potential (V)
R = Gas constant (8.314 J mol^{-1} K^{-1})
T = temperature (K)
F = Faraday's constant (9.6487×10^4 Coulombs mol^{-1})
$\ln[H^+]$ = hydrogen ion concentration.

At 298.2 K, with E in millivolts and converting to logarithm to base 10, Equation 6.2 becomes:

$$pH = \frac{E_0 - E}{59.15} \qquad 6.3$$

where E = observed potential (mV)
$pH = -\log[H^+]$

and

$$pK_w = \frac{E_0 - E}{59.15} + pOH \qquad 6.4$$

The program MacCalib[28] was used to calculate the endpoint (and hence the exact concentration of H^+ used) and the calibration parameters E_0 and pK_w, with the appropriate diffusion correction terms for 0.1 mol dm^{-3} NEt_4ClO_4 in H_2O.[29]

Protonation constants of THEC12 and THEC9 were determined by titrating 1 cm^3 of 0.1053 mol dm^{-3} NEt_4OH with 10 cm^3 of 0.001 mol dm^{-3} ligand solution in NEt_4ClO_4 and $HClO_4$. The titration of 1 cm^3 of 0.1053 mol dm^{-3} NEt_4OH with a 10 cm^3 solution containing 0.001 mol dm^{-3} ligand, $HClO_4$ (0.005 mol dm^{-3} for THEC12 or 0.004 mol dm^{-3} for THEC9), and 0.001-0.002 mol dm^{-3} of $M(ClO_4)_n$, where n = 1 or 2, was carried out to determine the stability constant of $[ML]^{n+}$. The $M(ClO_4)_n$ solution was added to the titration vessel by a Gibson Microman positive displacement pipette. All titrations were performed in triplicate, and for each metal ion studied, titrations with differing metal:ligand ratios (1:1 and 2:1) were carried out. Analysis of the data was carried out with the use of the FORTRAN-77 program SUPERQUAD,[30] which showed that apart from the $[ML]^{n+}$ complexes of 1:1 stoichiometry, no other species, including polymeric forms of the complexes, were present.

6.4 NMR SPECTROSCOPY

6.4.1 MATERIALS FOR ^{7}Li AND ^{23}Na NMR STUDIES

The preparation of materials used in this section has been described in the previous sections. The solvents acetonitrile (AR, Ajax), propylene carbonate (AR, Aldrich), methanol (AR, CSR) and *N,N*-dimethylformamide (AR, BDH) were purified and stored as described in Section 6.2.1. The solvents acetone-d_6 (AR, 99% ^{2}H, Aldrich) and dimethylsulphoxide-d_6 (AR, Aldrich) acted as the lock solvents and were used as supplied.

6.4.2 MEASUREMENTS FOR ^{7}Li AND ^{23}Na NMR STUDIES

All solutions were prepared under dry nitrogen in a glove box to exclude moisture.[23] For L = (*R*)-THPEC12, THEC12 and CYCLEN, a 1 cm^3 solution of the $[LiL]^+$ or $[NaL]^+$ complex was prepared by addition of equimolar amounts of ligand and either $LiClO_4$ (0.02 mol dm^{-3}) or $NaClO_4$ (0.1 mol dm^{-3}) in the various solvents. Three different $[M]^+$: $[ML]^+$ ratios were used for each system (typically 2:1, 1:1 and 1:2) with constant total metal ion concentration. The solutions were then placed in 5 mm outer diameter NMR tubes (507-PP, Wilmad Glass Co., modified by placing a glass joint at the open end to allow sealing under vacuum) which were degassed and sealed under vacuum. These tubes were then coaxially mounted in 10 mm outer diameter NMR tubes (513-PP, Wilmad Glass Co.) containing either acetone-d_6 (for variable temperature studies within the temperature range 200-300 K) or dimethylsulphoxide-d_6 (for studies 300-370 K) to provide the deuterium lock signal. All spectra were

collected on a Bruker CXP-300 NMR spectrometer, using a Bruker B-VT 1000 variable temperature unit that controlled the sample temperature to within ± 0.3 K. The variable temperature unit was calibrated using the temperature dependence of the ^{1}H chemical shifts of neat ethylene glycol (for the temperature range 300-360 K) and neat methanol (for the temperature range 190-300 K).[31-33] The samples were equilibrated for 20 minutes at each temperature before acquisition.

For the variable temperature ^{23}Na NMR spectroscopic studies, an average of 1000-10000 transients were collected at each temperature in an 8192 point data base over an average spectral width of 10000 Hz, prior to Fourier transformation. Spectra were recorded on a Bruker CXP-300 NMR spectrometer operating at a frequency of 79.39 MHz. For the variable temperature ^{7}Li NMR spectroscopic studies, an average of 500-1000 transients were collected at each temperature in an 8192 point data base over a spectral width of 10000 Hz, prior to Fourier transformation. Spectra were recorded on a Bruker CXP-300 NMR spectrometer operating at a frequency of 116.64 MHz.

The Fourier transformed data were then transferred to an ACER 486 computer, on which complete lineshape analysis[34] was carried out using the FORTRAN-77 program LINSHP.[35] For $M^+ = {}^{7}Li$ or ^{23}Na, the M^+ linewidths and chemical shifts (and their temperature dependences) employed in the lineshape analysis were obtained through a combination of extrapolation from low temperature, where no exchange induced modification occurred, and from the linewidths and shift variations of solutions containing either solvated M^+ or $[ML]^+$ alone in the coalescence temperature range observed for the solutions containing both species. A more detailed description of data treatment is given in Chapter 7.

6.4.3 MATERIALS FOR ^{13}C NMR STUDIES

Preparation of the ligands THEC12, TMEC12 and THEC9 in this study have already been described in Section 6.1. The ligands (*R*)-THPEC12 and (*S*)-THPC12 were used as previously prepared.[10,11] Anhydrous $LiClO_4$ (Fluka), $NaClO_4$ (Fluka) and $KClO_4$ (BDH) were purchased and dried as described in Section 6.2.1. Anhydrous KCF_3SO_3, $RbCF_3SO_3$, $CsCF_3SO_3$ and $Ba(CF_3SO_3)_2$ were used as previously prepared after drying.[36-38] Anhydrous $Mg(CF_3SO_3)_2$ and $Ca(CF_3SO_3)_2$ were prepared by addition of an excess of the metal carbonate (AR, BDH) to CF_3SO_3H (98%, Aldrich), and the solution was stirred for 2 days. Excess carbonate was filtered off, and the solutions were concentrated to give white crystalline solids, which were recrystallised from

H_2O, dried under vacuum and stored over P_2O_5 under nitrogen. Anhydrous $Zn(ClO_4)_2$ (Fluka) was purchased and dried. Methanol-^{12}C-d_4 (99.95 atom % ^{12}C and 99.5% ^2H, Aldrich), $CDCl_3$ (99.8% ^2H, Aldrich) and DMF-d_7 (99.5% ^2H, Aldrich) were stored under nitrogen over Linde molecular sieves (3 Å for methanol-^{12}C-d_4 and $CDCl_3$, and 4 Å for DMF-d_7). Methanol-^{12}C-d_4 was used in preference to natural abundance methanol-d_4 to avoid problems of overlap between the ^{13}C NMR resonances of the complex and those arising from methanol-d_4.

6.4.4 MEASUREMENTS FOR ^{13}C NMR STUDIES

All solutions were prepared under dry nitrogen in a glove box to exclude moisture.[21] The $[ML]^{n+}$ complexes were prepared in 1 cm^3 volumetric flasks by addition of equimolar amounts of the metal salt with the macrocyclic ligand in the appropriate solvent. All solutions had a concentration *ca.* 0.1 mol dm^{-3}, and were placed in 5 mm outer diameter NMR tubes (507-PP, Wilmad Glass Co.) which were tightly stoppered. For $M^{n+} = K^+$, Rb^+, Cs^+, Mg^{2+}, Ca^{2+} or Ba^{2+} and n = 1 or 2, $M(CF_3SO_3)_n$ salts were used in preference to the corresponding perchlorates because of the insufficient solubility of the latter salts to give reasonable resonance intensities. The stabilities of $[ML]^{n+}$, for L = THEC12, TMEC12, (*S*)-THPC12, (*R*)-THPEC12 and THEC9 and n = 1 or 2, were sufficiently high for the concentrations of $[ML]^{n+}$, free M^{n+} and free L in the solutions prepared for the NMR studies to be those arising from the simple stoichiometric complexation of M^{n+} by L. (By using stoichiometric amounts of the metal salt, for most ligands studied here the fraction found in the complexed form is essentially 100% under these conditions. Even ligands with the smallest binding constants have complexed fractions well over 90%).

Broad-band ^1H decoupled ^{13}C variable temperature NMR spectroscopic studies were carried out on a Bruker CXP-300 NMR spectrometer operating at a frequency of 75.47 MHz. A Bruker B-VT 1000 variable temperature unit, calibrated by the procedure discussed in Section 6.4.2, controlled the sample temperature to within ± 0.3 K, and the samples were equilibrated for 20 minutes at each temperature before acquisition. The deuterated solvent in the sample solution provided the deuterium lock signal. The ^{13}C chemical shifts were referenced to the appropriate external solvent, where natural abundance methanol-d_4, dimethylformamide-d_7 and $CDCl_3$ are assigned chemical shifts of 47.05, 162.7, and 77.0 ppm, respectively.[39]

For each solution, an average of 3000-9000 transients were accumulated at each temperature in an 8192 point data base over an average spectral width of

3000 Hz. The data was Fourier transformed, transferred to an ACER 486 computer, and subject to complete lineshape analysis[34] using the FORTRAN-77 program LINSHP[35] to determine the kinetic parameters characterising the exchange processes. The temperature dependences of the chemical shifts and linewidths in the absence of chemical exchange were needed for lineshape analysis. These were determined by extrapolation from the spectra at low temperatures where no chemical induced broadening of the spectra occurred. All spectra were recorded to within 5 K of the freezing point of the solvent in order to obtain accurate extrapolation and to minimise the introduction of systematic errors. However, due to the freezing point constraints of the solvents, it was not always possible to attain low enough temperatures for observation of very slow exchange. In this circumstance, the linewidths and chemical shifts used for lineshaping were derived from the resonances corresponding to the $>NCH_2$- moiety of the pendant arm of the ligand in $[ML]^{n+}$. This was necessary for intramolecular exchange processes (of $[M(THEC9)]^+$ and $[Zn(THEC12)]^{2+}$) and for intermolecular ligand exchange processes (in $[M((R)\text{-}THPEC12)]^+$, $[M(THEC12)]^+$ and $[Mg(TMEC12)]^{2+}$). For all complexes studied, there was little or no variation in the relative populations with variation in temperature for the lineshaped systems.

BIBLIOGRAPHY

1. J.E. Richman, T.J. Atkins, *J. Am. Chem. Soc.* **1974**, 96, 2268-2270.
2. L. Fabbrizzi, *J. Chem. Soc., Dalton Trans.* **1979**, 1857-1861.
3. T.A. Kaden, *Topp. Curr. Chem.* **1984**, 121, 157-179.
4. H. Hafliger, T.A. Kaden, *Helv. Chim. Acta.* **1979**, 62, 683-688.
5. N.W. Alcock, K.P. Balakrishnan, P. Moore, *J. Chem. Soc., Dalton Trans.* **1986**, 1743-1745.
6. P.S.K. Chia, A. Elkstrom, I. Liepa, L.F. Lindoy, M. McPartlin, S.V. Smith, P.A. Tasker, *Aust. J. Chem.* **1991**, 44, 737-746.
7. H. Stetter, W. Frank, R. Mertens, *Tetrahedron* **1981**, 37, 767-772.
8. M. Takahashi, S. Takamoto, *Bull. Chem. Soc. Jpn.* **1977**, 50, 3413-3414.
9. F.L. Weitl, K.N. Raymond, *J. Am. Chem. Soc.* **1979**, 101, 2728-2731.
10. R.S. Dhillon, S.E. Madback, F.G. Ciccone, M.A. Buntine, S.F. Lincoln, K.P. Wainwright, *J. Am. Chem. Soc.* **1997**, 119, 6126-6134.
11. S.L. Whitbread, P. Valente, M.A. Buntine, P. Clements, S.F. Lincoln, K.P. Wainwright, *J. Am. Chem. Soc.* **1998**, 120, 2862-2869.
12. C.G. Krespan, *J. Org. Chem.* **1975**, 40, 1205-1209.
13. L.C. Hodgkinsoon, S.L. Leigh, I.O. Sutherland, *J. Chem. Soc., Chem. Commun.* **1976**, 640-642.
14. S. Kulstad, L.A. Malmsten, *Acta. Chem. Scand.* **1979**, B33, 469-474.
15. E. Amble, J. Dale, *Acta. Chem. Scand.* **1979**, B33, 698-700.
16. (a) S. Buøen, J. Dale, *Acta. Chem. Scand.* **1984**, B38, 773-778.
    (b) R.K. McMullan, G.A. Jeffrey, *J. Chem. Phys.* **1965**, 42, 2725-2732.
    (c) D.N. Glew, N.S. Rath, *J. Chem. Phys.* **1966**, 44, 1710-1711.
    (d) L. Carbonnel, J.C. Rosso, *J. Solid State Chem.* **1973**, 8, 304-311.
17. R. Luckay, R.D. Hancock, I. Cukrowski, J.H. Reibenspies, *Inorg. Chim. Acta.* **1996**, 246, 159-169.
18. P. Chaudhuri, K. Wieghardt, *Prog. Inorg. Chem.* **1987**, 35, 329-436.
19. D.D. Perrin, W.L.F. Aramaego, D.R. Perrin, *"Purification of Laboratory Chemicals"*, Second Edition, Pergamon, Oxford England, **1980**.
20. A.K.W. Stephens, S.F. Lincoln, *J. Chem. Soc., Dalton Trans.* **1993**, 2123-2126.
21. D.F. Shriver, *"The Manipulation of Air-Sensitive Compounds"*, McGraw-Hill, New York, **1969**.
22. J.-M. Lehn, J.-P. Sauvage, *J. Am. Chem. Soc.* **1975**, 97, 6700-6707.
23. P. Clarke, PhD Thesis, University of Adelaide, **1992**.
24. A.I. Vogel, *"Quantitative Inorganic Analysis"*, Longmans, Greens and Co., London, **1955**.
25. G. Schwarzenbach, H. Flaschka, H.M.N.H. Irving, *"Complexiometric Titrations"*, Methuen, London, Second edition, **1969**.
26. P.A. Duckworth, University of Adelaide, private communication.

27. A.E. Martel, P.J. Motekaitus, *"The Determination and Use of Stability Constants"*, VCH Publishers, **1988**.
28. A. Sabatini, A. Vacca, P. Gans, *Talanta.* **1974**, 21, 53-77.
29. S. Kulstad, L.A. Malmstem, *J. Inorg. Nucl. Lett.* **1980**, 42, 573-578.
30. P. Gans, A. Sabatini, A. Vacca, *J. Chem. Soc., Dalton Trans.* **1985**, 1195-1200.
31. A.L. Van Geet, *Anal. Chem.* **1970**, 42, 679-680.
32. A.L. Van Geet, *Anal. Chem.* **1968**, 40, 2227-2229.
33. D.S. Raiford, C.L. Fisk, E.D. Becker, *Anal. Chem.* **1979**, 51, 2050-2051.
34. S.F. Lincoln, *Prog. Reaction Kinetics* **1977**, 9, 1-91.
35. LINSHP program by T.M. Spotswood, **1973**. Converted to Nicolet BNC-12 machine code by E. Williams, **1980**. Modified and converted to FORTRAN-5 by A. White, **1983**. Modified and converted to FORTRAN-77 by P. Clarke, **1987**.
36. S.E. Madback, Honours Thesis, University of Adelaide, **1994**.
37. A.K.W. Stephens, R.S. Dhillon, S.E. Madback, S.L. Whitbread, S.F. Lincoln, *Inorg. Chem.* **1996**, 35, 2019-2024.
38. F.G. Ciccone, Honours Thesis, University of Adelaide, **1996**.
39. E. Breitmaier, G. Haas, W. Voelter, *"Atlas of Carbon-13 NMR Data"*, Volume 2, Heyden, London, **1979**.

CHAPTER 7

POTENTIOMETRIC TITRATION AND NMR SPECTROSCOPIC DATA ANALYSIS

7.1 ANALYSIS OF POTENTIOMETRIC TITRATION DATA

7.1.1 STABILITY CONSTANT DETERMINATION OF $[ML]^+$ IN NON-AQUEOUS SOLUTION

Stability constants of metal complexes in non-aqueous solution have been determined by several experimental techniques. These include NMR spectroscopy, calorimetry, polarography, spectrophotometry, cyclic voltammetry and conductivity.[1-4] However, the predominant literature method is that of potentiometric titration, which is applicable over a wide stability constant range and requires only small amounts of ligand. The potentiometric titration technique involves the direct titration of a ligand solution into a solution of a metal ion being studied and measuring the free metal ion concentration, $[M^+]$, with an ion selective electrode (ISE). The electrode response to change in free metal ion concentration in solution is pseudo-Nernstian and is given by Equation 7.1:

$$E = E_0 + C \ln [M^+] \qquad 7.1$$

to describe complexation between a metal ion, M^+, and ligand, L:

$$M^+ + L \underset{}{\overset{K_s}{\rightleftharpoons}} [ML]^+ \qquad 7.2$$

where

$$K_s = \frac{[ML^+]}{[M^+][L]} \qquad 7.3$$

The constants E_0 and C are determined from calibration of the electrode (discussed in Chapter 6), so that the concentration of the free metal ion after equilibrium has been established can then be determined from Equation 7.1. Knowing the initial, or total, metal ion and ligand concentrations allows the calculation of the concentration stability constant, K_s, of the complex. This technique was adopted to determine the stability constants of the Ag^+

complexes in this study, and can also be used to determine stability constants for Na^+ complexes using a Na^+ ISE.[5-7]

Although the direct potentiometric titration is very versatile, allowing stability constant determination of many metal ions, this method is best suited[1] to stabilities in the range $10 < K_s > 10^6$ dm^3 mol^{-1}. For metal complex stability constants higher than 10^6 dm^3 mol^{-1}, the concentration of the free metal ion being studied in solution becomes too low to be reliably determined by the ISE, such that the electrode behaviour may no longer be described as pseudo-Nernstian. In this circumstance, an indirect, competitive titration technique was employed,[1,8,9] which involves measuring the stability constant of the Ag^+ complex in the presence of a competing metal ion, M^+. A solution of $[ML]^+$ (with M^+ in excess) is titrated with a solution of Ag^+, and the competition between Ag^+ and M^+ for the ligand, L, is monitored with an Ag^+ ISE:

$$Ag^+ + [ML]^+ \overset{K_e}{\rightleftharpoons} [AgL]^+ + M^+ \qquad 7.4$$

where the equilibrium constant, K_e, for the competitive reaction is defined by:

$$K_e = \frac{[AgL^+][M^+]}{[Ag^+][ML^+]} \qquad 7.5$$

To be able to calculate the equilibrium constant, K_e, the stability constant of the Ag^+ complex, denoted $K_s(Ag^+)$, described by Equation 7.6, must first be determined by a direct potentiometric titration.

$$Ag^+ + L \overset{K_s(Ag^+)}{\rightleftharpoons} [AgL]^+ \qquad 7.6$$

where

$$K_s(Ag^+) = \frac{[AgL^+]}{[Ag^+][L]} \qquad 7.7$$

Then, for a known value of $K_s(Ag^+)$, the equilibrium concentrations of the species required to calculate K_e (Equation 7.5) can be determined from the titration of a solution of $[ML]^+$ with a solution of standard Ag^+, as described by Equation 7.4, where the initial concentrations of $[ML]^+$, Ag^+ and M^+ are known, and the equilibrium concentration of Ag^+ is determined from the electrode potential of the Ag^+ ISE. Thus, combining Equations 7.5 and 7.7

allows the stability constant of the competing metal ion, $K_s(M^+)$, to be calculated:

$$K_s(M^+) = \frac{K_s(Ag^+)}{K_e} \qquad 7.8$$

or

$$\log K_s(M^+) = \log K_s(Ag^+) - \log K_e \qquad 7.9$$

The stability constants of Li^+, Na^+, K^+, Rb^+ and Cs^+ complexes in this study were determined by this method.

This titration technique can be extended to metal ions other than Ag^+ as the auxiliary ion for which an ISE is available, where the Ag^+ solutions and electrodes are replaced by the appropriate metal ion solutions and metal ISE. However, its complex must be less stable than that of the competing metal ion, $[ML]^+$, or the concentration of free metal ion will be negligible and the electrode potential will not change significantly during the titration to allow monitoring of the competitive equilibrium.

It should be noted that the thermodynamic stability constant, K_{th}, for the formation of a 1:1 metal complex is defined as:

$$K_{th} = \frac{f_{ML^+}[ML^+]}{f_{M^+}[M^+] f_L [L]} \qquad 7.10$$

where f_L, f_{M^+} and f_{ML^+} are the activity coefficients of the uncomplexed ligand, uncomplexed metal ion, and the metal complex, respectively. Activity corrections must be considered if the ionic strength varies during the titration, so the potentiometric titrations were carried out at a high ionic strength using the inert supporting electrolyte NEt_4ClO_4 to maintain ionic strength nearly constant throughout the titration. Since the pendant arm macrocyclic ligands in this study are neutral molecules, the complexation process described by Equation 7.2 does not involve the separation of charges. In addition, it may be assumed that in dilute solution the activity coefficients of the complex and the metal ion are equal and that of the neutral ligand is zero. Therefore, the activity coefficients are generally not taken into account. Thus, Equation 7.10 can be restated as Equation 7.3.

Extraction of the stability constants from the experimental potentiometric titration data is discussed in more detail below, and uses the method described by Rossotti and Rossotti[10] which is straightforward for the formation of 1:1 metal complexes. The stability constants were determined by the linear solution method, as discussed below, and used the FORTRAN-77 program STAB.[11] The results obtained by this method were then confirmed by a second method of analysis, using the FORTRAN-77 program VISP,[11] which determines the stability constant, K_s, for a calculated titration curve that best fits the experimental data.

7.1.1.1 LINEAR SOLUTION METHOD

For the direct potentiometric titration, the total concentrations of metal and ligand are defined as:

$$[M^+]_{tot} = [M^+] + [ML^+] \qquad 7.11$$

and

$$[L]_{tot} = [L] + [ML^+] \qquad 7.12$$

where M^+ refers to the alkali metal ion of interest or Ag^+.

The total concentrations of the metal ion and ligand are known, so the concentration of the metal complex and the free ligand can be calculated. That is, for the addition of V_{titre} cm^3 of a solution of ligand, L, to 20 cm^3 of a solution of M^+, the following relationship holds:

$$[M^+]_{tot} = \frac{20\,[M^+]_{in}}{20 + V_{titre}} \qquad 7.13$$

and

$$[L]_{tot} = \frac{V_{titre}\,[L]_{in}}{20 + V_{titre}} \qquad 7.14$$

where $[M^+]_{in}$ and $[L]_{in}$ are the initial concentrations of M^+ and L, respectively. At each point of the titration, the potential, E, is related to the concentration of solvated M^+, $[M^+]$, by Equation 7.1. Thus:

$$[M^+] = \exp\left(\frac{E - E_0}{C}\right) \qquad 7.15$$

Rearrangement of Equations 7.11 and 7.12 gives:

$$[ML^+] = [M^+]_{tot} - [M^+] \qquad 7.16$$

and

$$[L] = [L]_{tot} - [ML^+]$$

$$= [L]_{tot} - [M^+]_{tot} + [M^+] \qquad 7.17$$

So, substituting Equation 7.16 into Equation 7.3 gives:

$$K_s = \frac{[M^+]_{tot} - [M^+]}{[M^+]\,[L]} \qquad 7.18$$

which can be expressed as:

$$K_s\,[L] = \frac{1 - \alpha_1}{\alpha_1} \qquad 7.19$$

where $\alpha_1 = \dfrac{[M^+]}{[M^+]_{tot}}$ is the mole fraction of solvated metal ion.

Therefore, by calculating the values of $\dfrac{1-\alpha_1}{\alpha_1}$ and concentration of free ligand, [L], for each data point in the direct titration, a plot of $\dfrac{1-\alpha_1}{\alpha_1}$ versus [L] (described by Equation 7.19) gives a straight line which passes through the origin and has a slope of K_s.

For the competitive potentiometric titration, Equation 7.5 can be rewritten as:

$$K_e\,[ML^+] = \frac{[AgL^+][M^+]}{[Ag^+]} \qquad 7.20$$

which may be expressed as:

$$K_e[ML^+] = \frac{1 - \alpha_1}{\alpha_1}[M^+] \quad 7.21$$

where $\alpha_1 = \frac{[Ag^+]}{[Ag^+]_{tot}}$ is the mole fraction of solvated Ag^+.

The total concentrations of M^+, Ag^+, and ligand are now defined as:

$$[M^+]_{tot} = [M^+] + [ML^+] \quad 7.22$$

$$[Ag^+]_{tot} = [Ag^+] + [AgL^+] \quad 7.23$$

$$[L]_{tot} = [L] + [AgL^+] + [ML^+] \quad 7.24$$

Rearrangement of Equation 7.24 gives:

$$[ML^+] = [L]_{tot} - [AgL^+] - [L]$$

$$= [L]_{tot} - [Ag^+]_{tot} + [Ag^+] - [L] \quad 7.25$$

However, the total metal ion (Ag^+ and M^+) concentration is always greater than that of the total ligand concentration (by about a 5-fold excess) so that the concentration of the uncomplexed ligand at equilibrium is assumed to be negligible,[8] and $\log(K_s/dm^3\ mol^{-1}) > 2$. Therefore:

$$[ML^+] = [L]_{tot} - [Ag^+]_{tot} + [Ag^+] \quad 7.26$$

For the addition of V_{titre} cm^3 of a solution of L and M^+ to a 20 cm^3 solution of Ag^+, the following relationships hold:

$$[Ag^+]_{tot} = \frac{20\,[Ag^+]_{in}}{20 + V_{titre}} \quad 7.27$$

$$[M^+]_{tot} = \frac{V_{titre}\,[M^+]_{in}}{20 + V_{titre}} \quad 7.28$$

$$[L]_{tot} = \frac{V_{titre}\,[L]_{in}}{20 + V_{titre}} \quad 7.29$$

where $[Ag^+]_{in}$, $[M^+]_{in}$, and $[L]_{in}$ are the initial concentrations of Ag^+, M^+ and L, respectively.

For the direct and competitive potentiometric titration, the FORTRAN-77 program STAB[11] was used to calculate the values of $\frac{1-\alpha_1}{\alpha_1}$ versus [L] (using Equations 7.11 and 7.12) and the values of $\frac{1-\alpha_1}{\alpha_1}$ [M^+] versus [ML^+] (using Equations 7.22 - 7.24), respectively, and the known electrode calibration parameters C and E_0 (Equation 7.1). Simple linear regression of Equation 7.19 and 7.21, respectively, were used to determine K_s and K_e, respectively. Once K_e and $K_s(Ag^+)$ are known, the stability constant of the competing metal ion, $K_s(M^+)$, can be determined from Equation 7.9. Examples of a direct and competitive titration are discussed below, where the K_s values quoted in Chapter 2 are the mean values determined from three titration experiments. The quoted errors are one standard deviation of the slope based on experimental scatter of the points.

To determine the stability constant of $[Ag((R)\text{-THPEC12})]^+$ in DMF, a solution of 5 cm^3 of 0.0035 mol dm^{-3} (*R*)-THPEC12 was titrated with 20 cm^3 of 0.0003 mol dm^{-3} $AgClO_4$ ($[Ag^+]_{in}$) solution. The Ag^+ electrode used to measure [Ag^+] was calibrated over the concentration range 1.0×10^{-8}-2.0×10^{-3} mol dm^{-3}. The values for solvated [Ag^+] were derived from a calibration which yielded the calibration constants C = 36.49 mV and E_0 = 228.54 mV. Linear regression of Equation 7.19 was used to obtain the value of $\log(K_s/dm^3\ mol^{-1})$ = 8.03 ± 0.05. The titration data and parameters calculated by the program STAB for the determination of the stability constant of $[Ag((R)\text{-THPEC12})]^+$ in DMF are given in Table 7.1. The plot of $\frac{1-\alpha_1}{\alpha_1}$ versus [(*R*)-THPEC12] for this system is illustrated in Figure 7.1.

To determine the stability constant of $[Li((R)\text{-THPEC12})]^+$ in DMF, a solution of 5 cm^3 containing 0.0040 mol dm^{-3} (*R*)-THPEC12 and 0.0055 mol dm^{-3} $LiClO_4$ was titrated with 20 cm^3 of 0.0003 mol dm^{-3} $AgClO_4$ ($[Ag^+]_{in}$) solution. The values for solvated [Ag^+] were derived from a calibration which yielded the calibration constants C = 36.74 mV and E_0 = 210.44 mV. Linear regression of Equation 7.21 was used to obtain the value of $\log(K_e/dm^3\ mol^{-1})$ = 5.08 ± 0.05. Therefore, $\log K_s(M^+)$ ($dm^3\ mol^{-1}$) = $\log K_s(Ag^+)$ - $\log K_e$ = 3.06 ± 0.05. The titration data and parameters calculated by the program STAB for the determination of the stability constant of $[Li((R)\text{-THPEC12})]^+$ in DMF are given in Table 7.2. For this system, the plot of $\frac{1-\alpha_1}{\alpha_1}$[$Li^+$] versus [$Li((R)\text{-THPEC12})^+$] is illustrated in Figure 7.3.

7.1.1.2 CURVE FITTING METHOD

For the titration of a ligand solution into a solution containing $AgClO_4$, the concentration of free L, [L], is very small before the equivalence point, so that the experimental parameters used to derive [L] (Equation 7.17) have large errors. Therefore, only data points after the equivalence point are used to determine the stability constants using the program STAB. A more appropriate method would use all data points to determine K_S, so the method of curve fitting described by Rossotti and Rossotti[10] was used to confirm the values of K_S determined by use of Equations 7.19 and 7.21. The FORTRAN-77 program VISP[11] calculates a theoretical titration curve from known initial concentrations of the various species, volumes of the solutions, the calibrated electrode response and the stability constant, K_S (for direct titrations) and K_e (for competitive titrations). The following paragraphs provide a mathematical description for the derivation of this theoretical curve.

For the direct potentiometric titration, substituting Equations 7.11 and 7.12 into Equation 7.3 gives:

$$K_s = \frac{[M^+]_{tot} - [M^+]}{([L]_{tot} - [M^+]_{tot} + [M^+])\,[M^+]} \qquad 7.30$$

so that rearranging Equation 7.30 gives the following quadratic in $[M^+]$:

$$K_s[M^+]^2 + (K_s[L]_{tot} - K_s[M^+]_{tot} + 1)\,[M^+] - [M^+]_{tot} = 0 \qquad 7.31$$

which can be solved for $[M^+]$:

$$[M^+] = \frac{K_s([M^+]_{tot} - [L]_{tot}) - 1 + \sqrt{A}}{2K_s} \qquad 7.32$$

where $A = K_s^2([L]_{tot} - [M^+]_{tot})^2 + 2K_s([L]_{tot} + [M^+]_{tot}) + 1$

All terms in Equation 7.32 must be positive to be physically meaningful.

For the competitive potentiometric titration, substituting Equations 7.22 - 7.24 into Equation 7.5 gives:

$$K_e = \frac{([Ag^+]_{tot} - [Ag^+])([M^+]_{tot} - [L]_{tot} + [Ag^+]_{tot} - [Ag^+])}{[Ag^+]([L]_{tot} - [Ag^+]_{tot} + [Ag^+])} \quad 7.33$$

Rearranging Equation 7.33 gives the following quadratic in $[Ag^+]$:

$$[Ag^+]^2(K_e - 1) + [Ag^+]A + [Ag^+]_{tot}B = 0 \quad 7.34$$

where $A = K_e[L]_{tot} - K_e[Ag^+]_{tot} + 2[Ag^+]_{tot} - [L]_{tot} + [M^+]_{tot}$

and $B = [L]_{tot} - [M^+]_{tot} - [Ag^+]_{tot}$

Since $[Ag^+]$ is the experimentally determined variable, the quadratic in Equation 7.34 is solved for $[Ag^+]$:

$$[Ag^+] = \frac{(K_e - 2)[Ag^+]_{tot} + (1 - K_e)[L]_{tot} - [M^+]_{tot} + \sqrt{K_e^2X + Y}}{2(K_e - 1)} \quad 7.35$$

where

$$X = ([L]_{tot} - [Ag^+]_{tot})^2 + K_e([M^+]_{tot}(2[Ag^+]_{tot} + [L]_{tot}) + 2[L]_{tot}([Ag^+]_{tot} - [L]_{tot}))$$

and $Y = ([L]_{tot} - [M^+]_{tot})^2$

All terms in Equation 7.35 must be positive to be physically meaningful.

The program VISP generates a theoretical curve of EMF versus titre by determining free metal ion concentration, $[M^+]$, from Equation 7.32 or free Ag^+ ion concentration, $[Ag^+]$, from Equation 7.35 for initial estimates of K_s or K_e. The theoretical EMF is then generated by the substitution of these concentrations into Equation 7.1. The values of K_s or K_e are systematically varied to obtain the best fit of the experimental EMF data to the theoretical curve. The results may be presented graphically for visual comparison as in Figures 7.2 and 7.4. The results obtained from VISP (using Equations 7.32 and 7.35) are identical to those obtained from STAB (using Equations 7.19 and 7.21) within experimental error.

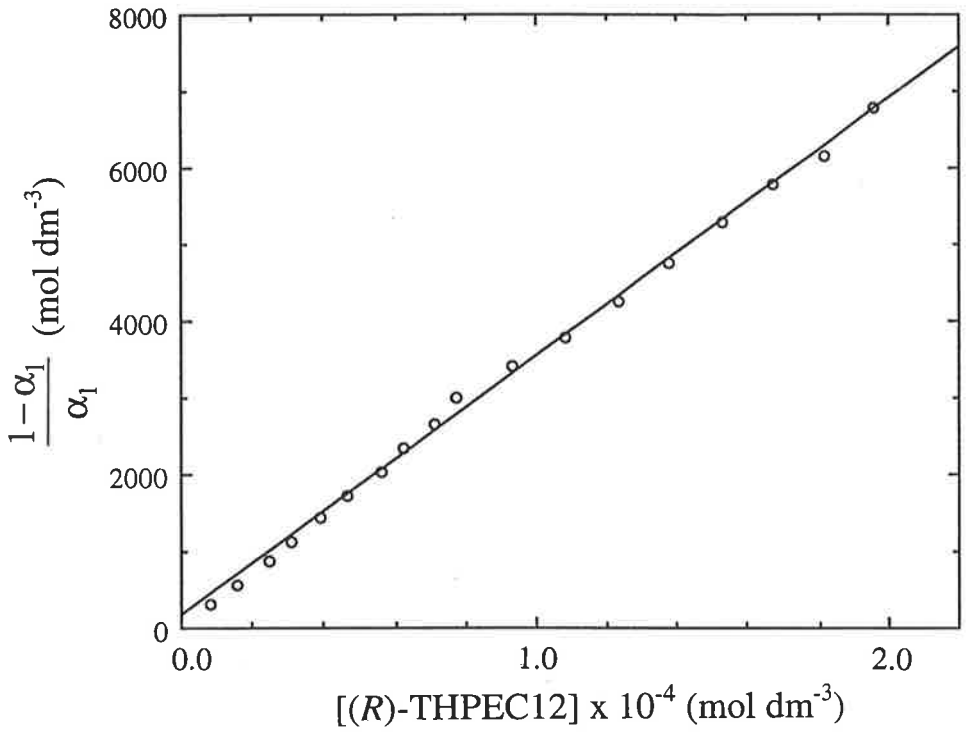

Figure 7.1: The plot of $\frac{1-\alpha_1}{\alpha_1}$ versus [(*R*)-THPEC12] for the titration of (*R*)-THPEC12 with Ag^+ in DMF at 298.2 K and I = 0.05 mol dm^{-3} NEt_4ClO_4. The straight line is the best fit of the data to Equation 7.19.

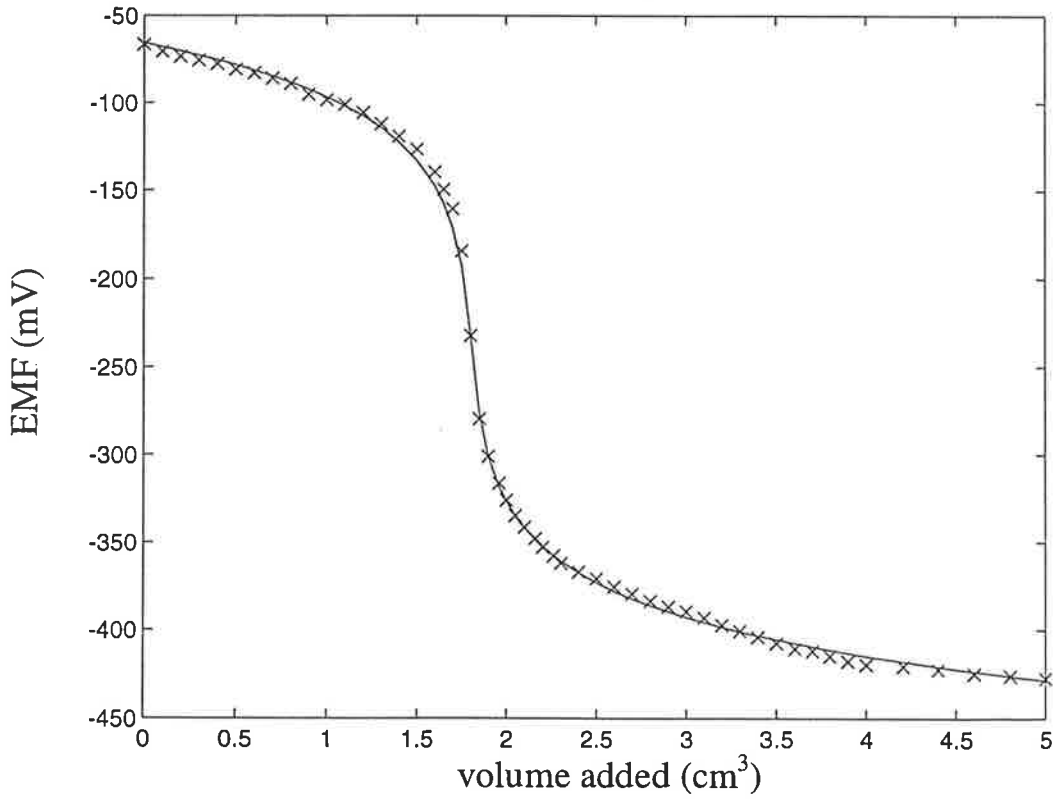

Figure 7.2: Plot of experimental (x) and calculated (solid curve) EMF (mV) versus titre (cm^3) for the titration of (*R*)-THPEC12 with Ag^+ in DMF at 298.2 K and I = 0.05 mol dm^{-3} NEt_4ClO_4.

Table 7.1: Experimental and calculated parameters using STAB for the stability constant determination of $[Ag((R)\text{-THPEC12})]^+$ in DMF at 298.2 K and $I = 0.10$ mol dm^{-3} NEt_4ClO_4.

Titre	EMF (exp)	EMF (theor)	[L]	$\frac{1-\alpha_1}{\alpha_1}$
cm^3	mV	mV	$\times 10^5$ mol dm^{-3}	mol dm^{-3}
1.85	-279.700	-276.962	0.799	322.747
1.90	-300.900	-301.019	1.557	576.471
1.96	-316.200	-318.237	2.492	874.868
2.00	-325.900	-326.474	3.116	1139.499
2.05	-334.600	-334.719	3.897	1443.289
2.10	-341.200	-341.452	4.677	1725.720
2.16	-347.500	-348.180	5.610	2045.565
2.20	-352.600	-352.065	6.228	2348.314
2.26	-357.400	-357.214	7.153	2671.374
2.30	-361.600	-360.284	7.767	2991.987
2.40	-366.600	-366.991	9.294	3416.200
2.50	-370.400	-372.656	10.807	3774.396
2.60	-375.000	-377.560	12.307	4262.680
2.70	-379.100	-381.882	13.794	4748.680
2.80	-383.200	-385.746	15.268	5290.179
2.90	-386.500	-389.241	16.730	5765.703
3.00	-389.000	-392.430	18.178	6147.508
3.10	-392.700	-395.362	19.614	6774.508

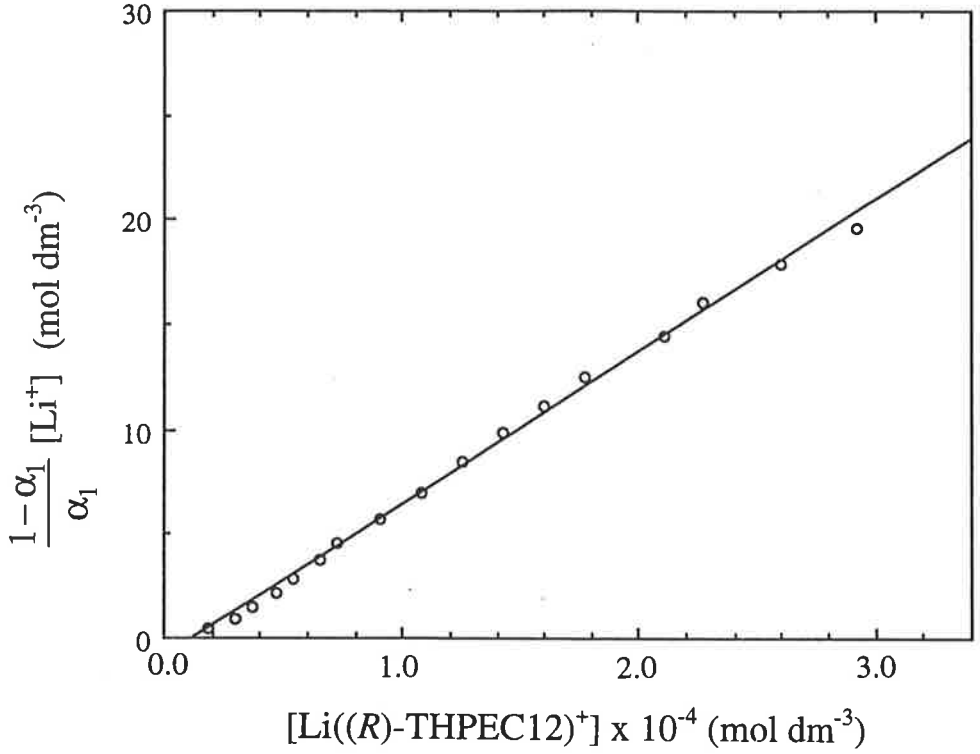

Figure 7.3: Plot of $\frac{1-\alpha_1}{\alpha_1}$ [Li$^+$] versus [(Li((*R*)-THPEC12))$^+$] for stability constant determination of [Li((*R*)-THPEC12)]$^+$ in DMF at 298.2 K and I = 0.05 mol dm^{-3} NEt_4ClO_4. The straight line is the best fit of data to Equation 7.21.

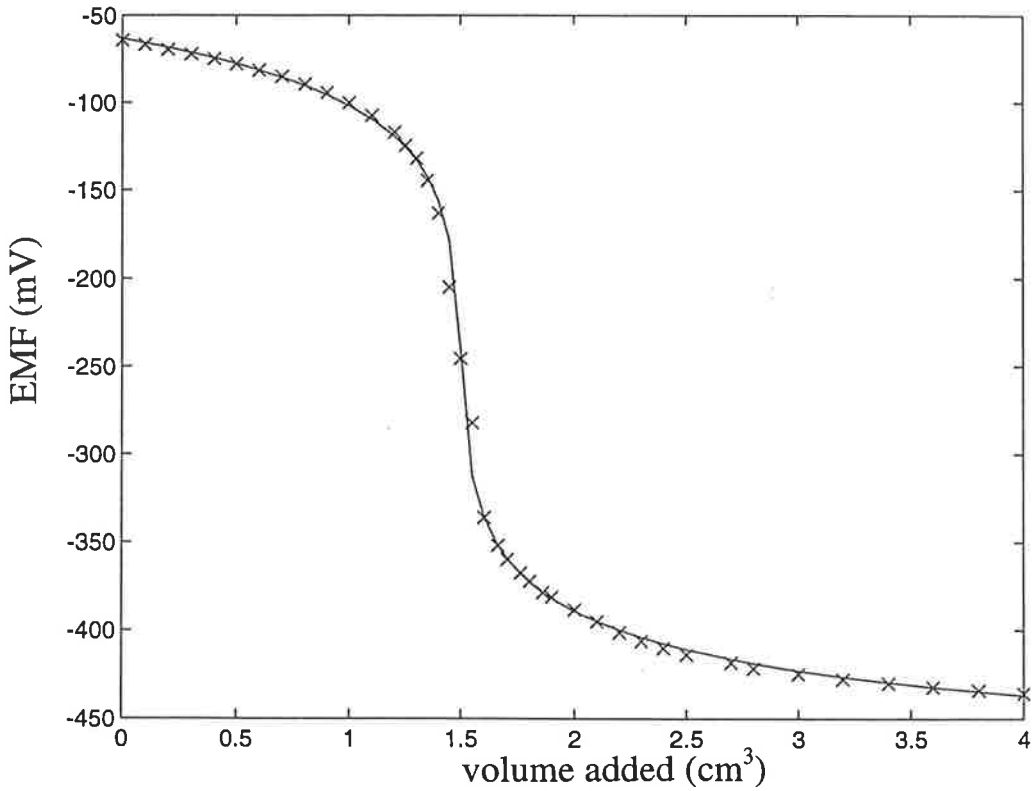

Figure 7.4: Plot of experimental (x) and calculated (solid curve) EMF (mV) versus titre (cm^3) for the titration of [Li((*R*)-THPEC12)]$^+$ with Ag^+ in DMF at 298.2 K and I = 0.05 mol dm^{-3} NEt_4ClO_4.

Table 7.2: Experimental and calculated parameters using STAB for the stability constant determination of $[Li((R)\text{-THPEC12})]^+$ in DMF at 298.2 K and $I = 0.10$ mol dm^{-3} NEt_4ClO_4.

Titre	EMF (exp)	EMF (theor)	[L]	$\frac{1-\alpha_1}{\alpha_1}[Li^+]$
cm^3	mV	mV	$\times 10^4$ mol dm^{-3}	mol dm^{-3}
1.60	-335.700	-335.925	0.182	0.489
1.66	-351.000	-351.793	0.291	0.924
1.70	-359.700	-359.249	0.363	1.434
1.76	-367.300	-367.941	0.472	2.157
1.80	-372.100	-372.643	0.544	2.894
1.86	-378.600	-378.590	0.652	3.741
1.90	-381.100	-382.003	0.724	4.550
2.00	-388.400	-389.166	0.902	5.693
2.10	-395.000	-394.944	1.079	6.975
2.20	-401.200	-399.772	1.254	8.443
2.30	-406.100	-403.907	1.427	9.831
2.40	-410.100	-407.515	1.598	11.144
2.50	-413.700	-410.708	1.769	12.481
2.70	-418.200	-416.153	2.105	14.442
2.80	-421.500	-418.509	2.271	16.022
3.00	-424.700	-422.665	2.598	17.819
3.20	-427.600	-426.238	2.920	19.630

7.1.2 STABILITY CONSTANT DETERMINATION OF $[ML]^{n+}$ IN AQUEOUS SOLUTION

The stability constants of $[M(THEC12)]^{n+}$, where n = 1 or 2, and $[M(THEC9)]^{2+}$ were determined by the pH-metric titration technique. This technique uses a pH electrode to determine the concentration of H^+ in solution rather than an ISE to determine the concentration of free metal ion in solution, and is best suited for stability constants $\log(K_s/dm^3\ mol^{-1}) \geq 2$.[1] The determination of stability constants in aqueous solution is similar to that in non-aqueous solution but also involves protonation equilibria of the tetrabasic tetraaza macrocycle THEC12 and tribasic triaza macrocycle THEC9 (as described in Chapter 3). Since the basicity, or pH, of a solution of these ligands can be altered by the complexation of a metal ion (Figure 7.6), comparison and analysis of the pH-metric titration curves of a ligand in the presence and absence of a metal ion yields the apparent stability constant, K_s, for the complex. That is, for known total concentrations of the ligand, metal ion and acid, measurement of the solution pH establishes the extent of the metal ion-ligand equilibria so that the stability constant of the metal complex can be determined. The ligand pK_a values, described overall by Equation 7.36, and in expanded form in Chapter 3, must first be known before the stability constant, described by Equation 7.37, can be determined.

$$K_n = \frac{[LH_n^{n+}]}{[LH_{n-1}^{(n-1)+}]\,[H^+]} \qquad 7.36$$

where $pK_{an} = -\log(K_{an})$ and n = 1 - 4 for THEC12, or 1 - 3 for THEC9.

$$K_s = \frac{[ML^{n+}]}{[M^{n+}]\,[L]} \qquad 7.37$$

The protonation constants of the ligand are determined by the titration of a base with an acidified solution of the ligand, and analysis using the FORTRAN-77 program SUPERQUAD.[12] The stability constant, K_s, can then be determined by titration of a base with an acidified solution of the ligand in the presence of the metal ion to be studied. The resulting titration curve is modified by the formation of the metal complex, and analysis of the titration data is carried out by the FORTRAN-77 program SUPERQUAD[12] to determine K_s. A more detailed description of the experimental procedures and conditions is given in Chapter 6.

The protonation constants and stability constants quoted in Chapter 3 are the mean values determined from three titration experiments, where errors represent one standard deviation of experimental to calculated data as generated by the program SUPERQUAD. For each metal ion studied, the ratio of M^{n+}:L was varied between titrations (typically 2:1 and 1:1). Some data points from the titration were not used to calculate the derived protonation or stability constant values. These points were either at high or low pH, where hydroxide precipitates occurred or where no appreciable amounts of the relevant species had formed, respectively. For SUPERQUAD, a good fit of the experimental titration data to the theoretical curve is defined by a lower parameter, c^2, where a value of $c^2 \leq 12.60$ implies that the titration data fits the protonation or complexation model satisfactorily. For each metal ion studied, the possibility of the presence of species other than that of $[ML]^{n+}$ must be considered. These species include $[ML_2]^{n+}$, $[M_2L]^{(n+2)+}$, $[MHL]^{(n+1)+}$, and $[M(OH)L]^{(n-1)+}$ and, if present, may greatly improve the fit of the data, where such species can exist in concentrations $\geq$ 10% of the total metal ion concentration. However, methodical analysis of the titration curves revealed no evidence of the formation of species other than the 1:1 $[ML]^{n+}$ complexes. An example of a typical titration for the determination of protonation and stability constant values is discussed below.

To determine the protonation constants, pK_n, for n = 1 - 4, of THEC12, a solution of 1 cm^3 of 0.1053 mol dm^{-3} of NEt_4OH solution was titrated with 10 cm^3 of a solution of 0.0010 mol dm^{-3} THEC12 in 0.0048 mol dm^{-3} $HClO_4$, with 0.1 mol dm^{-3} NEt_4ClO_4 as the background electrolyte. The electrode calibration parameters for this titration were pK_w = 13.68 and E_0 = 410.033. The protonation constants calculated for this titration by SUPERQUAD were $\log(K_1/dm^3\ mol^{-1})$ = 10.72 ± 0.03, $\log(K_2/dm^3\ mol^{-1})$ = 8.18 ± 0.05 and $\log(K_3/dm^3\ mol^{-1})$ = 1.99 ± 0.07 (c^2 = 2.22). The value of the fourth protonation constant, $\log(K_4/dm^3\ mol^{-1})$, was too low to be determined. The best fit curve obtained by SUPERQUAD is represented by the solid curve in Figure 7.5 and the experimental data is represented by a x.

To determine the apparent stability constant, K_s, of $[Ca(THEC12)]^{2+}$, a solution of 1 cm^3 of 0.1053 mol dm^{-3} of NEt_4OH solution was titrated with 10.2 cm^3 of a solution containing 0.0010 mol dm^{-3} THEC12 and 0.0021 mol dm^{-3} of $Ca(ClO_4)_2$ in 0.0049 mol dm^{-3} $HClO_4$, with 0.1 mol dm^{-3} NEt_4ClO_4 as the background electrolyte. The electrode calibration parameters for this titration were pK_w = 13.69 and E_0 = 419.412 mV, and the protonation constants log K_1, log K_2 and log K_3 used in the refinement were 10.74, 8.16 and 1.94, respectively. The result calculated using SUPERQUAD for this titration was $\log(K_s/dm^3\ mol^{-1})$ = 7.40 ± 0.01, and Figure 7.6 shows the

titration curve, where the best fit curve obtained by SUPERQUAD is represented by the solid curve and the experimental data is represented by a o. Similar titrations involving $Sr(ClO_4)_2$ and $Ba(ClO_4)_2$ yielded $\log(K_s/dm^3\ mol^{-1})$ = 6.50 ± 0.01 and 4.73 ± 0.02 for $[Sr(THEC12)]^{2+}$ and $[Ba(THEC12)]^{2+}$, respectively, which are shown graphically for comparison in Figure 7.6.

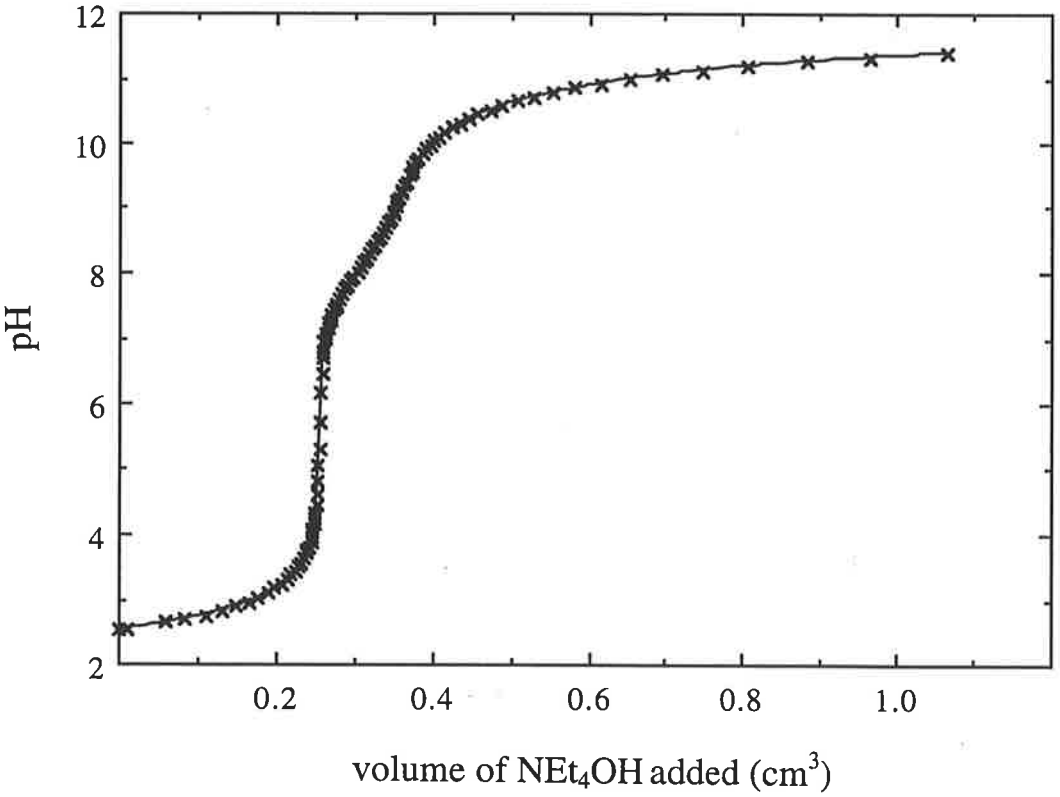

Figure 7.5: Typical titration curve for the determination of the protonation constants of THEC12 at 298.2 K and I = 0.10 mol dm^{-3} NEt_4ClO_4. The experimental data is represented by a x and the solid curve is the best fit of the data by SUPERQUAD.

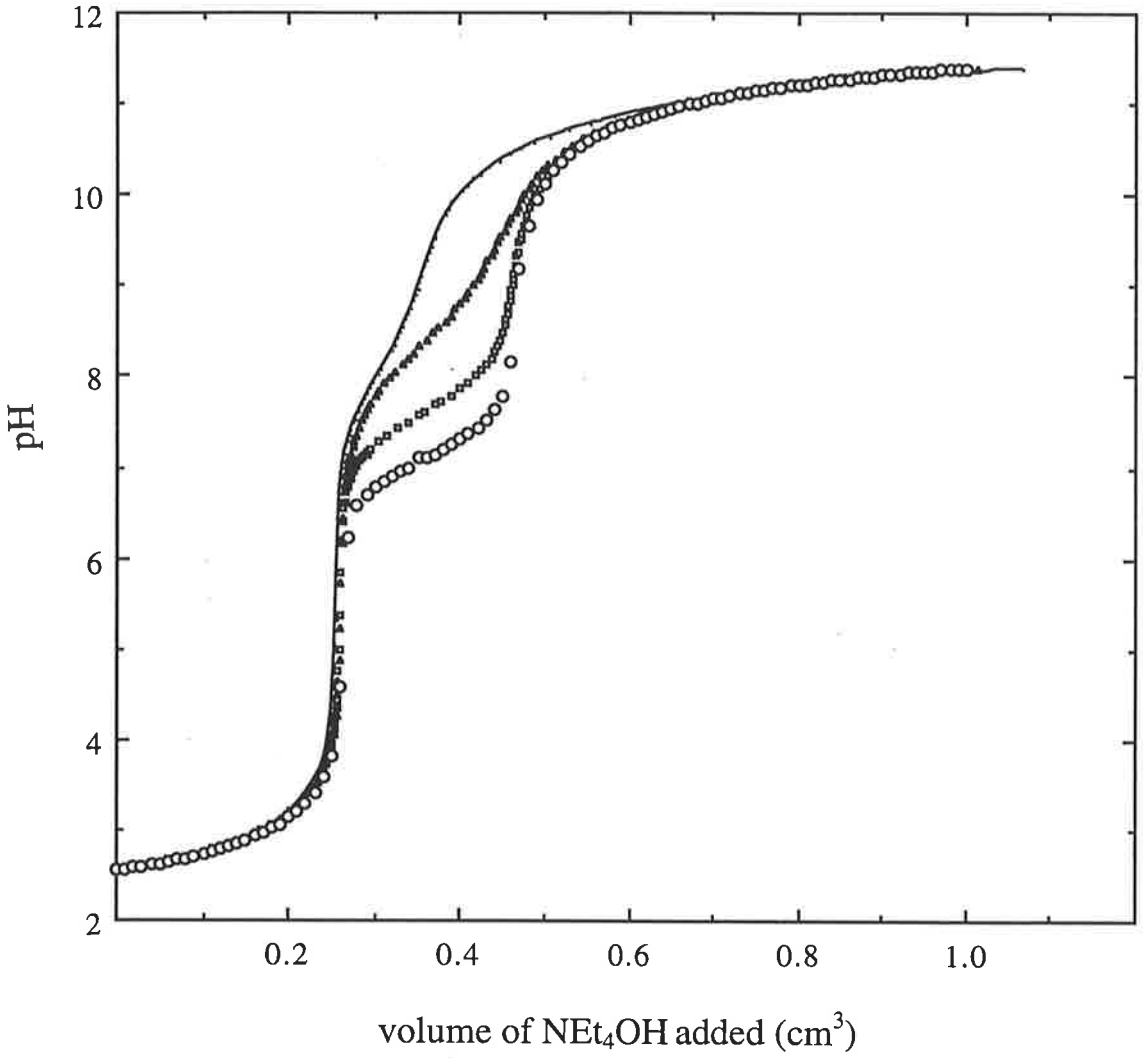

Figure 7.6: Typical titration curve used for the calculation of the apparent stability constant, K_s, of $[Ca(THEC12)]^{2+}$ at 298.2 K and I = 0.10 mol dm^{-3} NEt_4ClO_4. The titration of THEC12 in aqueous solution in the absence of a metal ion is represented by the solid curve and is the best fit of the data by SUPERQUAD, while those in the presence of Ca^{2+}, Sr^{2+} and Ba^{2+} are represented by a O, □ and ▲, respectively. The stability constant titration curve deviates more from the protonation constant titration curve as the complex stability increases.
log $K_s(M(THEC12)]^{2+}$) = 7.40 ± 0.01 (c^2 = 2.07), 6.50 ± 0.01 (c^2 = 3.43), and 4.73 ± 0.02 (c^2 = 1.54), for M^{2+} = Ca^{2+}, Sr^{2+} and Ba^{2+}, respectively.

7.2 ANALYSIS OF NMR SPECTROSCOPIC DATA

7.2.1 NMR ANALYSIS OF TWO-SITE CHEMICAL EXCHANGE

NMR spectroscopy is a very versatile technique for the determination of intramolecular and intermolecular chemical exchange dynamics in labile systems at thermodynamic equilibrium. Intramolecular and intermolecular chemical site exchange processes of numerous inorganic, organic and biochemical systems in solution can be studied if the process involves the exchange of nuclear spins between different magnetic environments.[13-15] The spectral coalescence describing intermolecular exchange of Na^+ and Li^+ between complexed and solvated states, as studied by ^{23}Na and ^{7}Li NMR spectroscopy, respectively, was discussed in Chapter 4. The spectral coalescence describing intramolecular exchange between two conformers of alkali and alkaline earth metal complexes of several pendant arm macrocyclic ligands and intermolecular ligand exchange, as studied by broad-band ^{1}H decoupled ^{13}C NMR spectroscopy, was discussed in Chapter 5.

The chemical shifts of alkali metal nuclei are very sensitive to the immediate environment of an alkali metal ion in solution. Therefore, NMR spectroscopy is a powerful and sensitive method for the resolution and assignment of separate signals due to alkali nuclei in different chemical environments. In addition, the biological importance of metal ions such as Li^+, Na^+ and K^+ has led to the use of alkali metal NMR spectroscopy in kinetic studies. The ^{23}Na nucleus has a natural isotopic abundance of 100% and an intrinsic NMR sensitivity which is 9.3% of that of the ^{1}H nucleus.[16,17] The ^{7}Li nucleus has a natural isotopic abundance of 92.6% and an intrinsic NMR sensitivity which is 29.4% of that of the ^{1}H nucleus.[16,17] Although ^{23}Na and ^{7}Li both have a nuclear spin of 3/2, giving rise to quadrupolar charge distribution, the natural linewidths of these nuclei in solution are usually quite narrow,[18] so that the chemical shifts of the Lorentzian resonance lines corresponding to the complexed and solvated alkali metal environments can be measured easily. These alkali metal ion nuclei show a large range of chemical shifts in different solvents, where the ^{23}Na chemical shifts vary linearly with solvent D_N, whereas the ^{7}Li chemical shifts do not.[16] The above-mentioned properties of the ^{23}Na and ^{7}Li nuclei facilitate the application of variable temperature ^{23}Na and ^{7}Li NMR spectroscopy in numerous solvents for intermolecular exchange processes of Na^+ and Li^+ complexes of many pendant arm macrocyclic ligands, where (*R*)-THPEC12, THEC12 and CYCLEN have been the subject of this study by this NMR technique.

The rates of exchange, activation parameters, and mechanism by which exchange occurs may be derived from the temperature variation of the NMR spectral lineshapes. This study is particularly concerned with the influences of the intramolecular and intermolecular chemical site exchange processes in solution on the spectral lineshapes. (These two processes are similar in that they involve time averaging of the nuclear environment). Dynamic NMR spectroscopy (DNMR) describes the study of the resultant spectral changes, and has been extensively studied.[19-24] This technique may be used to derive exchange rate constants in the range 10^{-1} - 10^{6} s^{-1}, at temperatures from 100-500 K, and determine activation parameters from the temperature dependence of the exchange modified NMR spectrum.[25] The theoretical treatment of DNMR spectroscopy discussed below uses a classical mechanical model and only applies for simple two-site exchange between uncoupled nuclei. More complex systems, such as multi-site exchange or exchange between coupled systems, require a more sophisticated quantum mathematical method and, although described in the literature,[25-27] are not the subject of this study.

The application of a magnetic field, B_0, to a nucleus along the z axis causes the individual magnetic moments, μ, of the sample nuclei to precess about the z axis at the Larmor frequency, ω_0. The nuclear spins and their populations are assigned according to the Boltzmann distribution law. The lowest nuclear spin state occurs when the nuclear spins of the samples are aligned with B_0, and gives rise to a net magnetic moment, $\boldsymbol{M}$. The z component of this magnetic moment is denoted M_z, and the x and y components, M_x and M_y, are zero. When a smaller second oscillating magnetic field, B_1, rotating clockwise in the xy (transverse) plane at a frequency ω is applied, it induces magnetic field components along the x and y axes such that the total magnetic field, $\boldsymbol{B}$, can be described by:

$$B = (B_1\cos\omega t, -B_1\sin\omega t, B_0) \qquad 7.38$$

The effect of $\boldsymbol{B}$ causes $\boldsymbol{M}$ to tilt away from the z axis into the xy plane, so that M_z decreases and magnetisations in the x and y directions are generated. (M_x and M_y have maximum values when $\omega = \omega_0$). The time required for M_z to reach its thermal equilibrium value, M_{zeq}, is characterised by a first order rate law and is called the spin-lattice or longitudinal relaxation time, T_1. The decay of the transverse components M_x and M_y to their equilibrium values of zero as a result of dephasing also follows a first order process which is characterised by the spin-spin or transverse relaxation time, T_2.

For stationary Cartesian coordinates (x,y,z), the time dependence of $\boldsymbol{M}$ in the stationary frame is described by the Bloch equations.[28] These equations

incorporate the effect of B_1 on M and the effects of longitudinal and transverse relaxation.

$$\frac{dM_x}{dt} = \gamma(M_y B_0 + M_z B_1 \sin\omega t) - \frac{M_x}{T_2} \qquad 7.39$$

$$\frac{dM_y}{dt} = \gamma(-M_x B_0 + M_z B_1 \cos\omega t) - \frac{M_y}{T_2} \qquad 7.40$$

$$\frac{dM_z}{dt} = \gamma(-M_x B_1 \sin\omega t - M_y B_1 \sin\omega t) - \frac{(M_z - M_{zeq})}{T_2} \qquad 7.41$$

where γ is nuclear gyromagnetic ratio.

If the stationary set of Cartesian axes (x,y,z) is replaced by a set of axes (x',y',z') rotating at an angular frequency, ω, about the z axis, so that B_1 is stationary, the Bloch equations may be expressed as:[25]

$$\frac{dM_{xy}}{dt} = -\alpha M_{xy} - i\gamma B_1 M_{zeq} \qquad 7.42$$

$$\frac{dM_z}{dt} = \gamma \upsilon B_1 + \frac{(M_{zeq} - M_z)}{T_1} \qquad 7.43$$

where M_{xy} is the transverse magnetisation.

υ is the component of M along the y' axis, which is 90° out of phase with B_1

$$\alpha = \frac{1}{T_2} - i(\omega_0 - \omega)$$

From Equation 7.43 it is evident that the variation of M_z, and hence the energy of the system, is dependent on υ, the observed absorption mode of the NMR signal.

Although the pulsed Fourier transform technique was used to carry out the NMR measurements in this study, the discussions below are based on the continuous wave slow passage NMR technique because it is an easier model to envisage. However, it is demonstrated in Section 7.2.2 that the NMR

absorption mode lineshape (derived from the total lineshape for all frequencies, ω) obtained from the pulsed Fourier transform experiment is, in general, equivalent to that obtained from the continuous wave slow passage experiment.[29,30]

For the continuous wave slow passage NMR, ω is varied through ω_0 so that dM_{xy}/dt and $dM_z/dt = 0$, and if B_1 is smaller than B_0, such that $M_z \sim M_{zeq}$ and M_{xy} is small, then the absorption mode lineshape, υ, may be described as:

$$\upsilon = -M_{zeq} \frac{\gamma B_1 T_2}{1 + T_2^2(\omega_0 - \omega)^2 + \gamma^2 B_1^2 T_1 T_2} \qquad 7.44$$

Since B_1 is small, $\gamma^2 B_1^2 T_1 T_2$ is negligible. Therefore, υ approximates a Lorentzian function:

$$\upsilon = -M_{zeq} \frac{\gamma B_1 T_2}{1 + T_2^2(\omega_0 - \omega)^2} \qquad 7.45$$

The Bloch equations are modified when the effects of chemical exchange are taken into account.[31,32] These modifications only apply for the exchange of nuclear spins inducing only transverse relaxation (adiabatic exchange) and for no spin-spin coupling between exchanging nuclear spins. Therefore, for uncoupled two-site exchange, the nucleus exchanges between two different magnetic sites, sites **a** and **b**, at a rate defined by:

$$k_a \chi_a = k_b \chi_b \qquad 7.46$$

with $k_a = \frac{1}{\tau_a}$ and $k_b = \frac{1}{\tau_b}$

where χ_n and τ_n are the relative populations and mean site lifetimes, respectively, of the nucleus at site **n**.

The time required for a nuclear spin to transfer from site **a** to **b** is assumed to be sufficiently small such that no nuclear spin precession occurs during the transfer, and that a nucleus arriving at site **b** has an intact phase memory of site **a**, and vice versa. This results in dephasing of the nuclear spins at site **b** and an increase in the transverse magnetisation of site **b**, at the rate M_{xya}/τ_a, and a consequent decrease in M_{xya} at the same rate. (Similarly, transfer of a nuclear

spin from site **b** to **a** causes dephasing at site **a**, increases M_{xya} at the rate M_{xyb}/τ_b, and decreases M_{xyb} at the same rate). This can be illustrated by the following equations:

$$\frac{dM_{xya}}{dt} = \frac{M_{xyb}}{\tau_b} - \frac{M_{xya}}{\tau_a} \qquad 7.47$$

and

$$\frac{dM_{xyb}}{dt} = \frac{M_{xya}}{\tau_a} - \frac{M_{xyb}}{\tau_b} \qquad 7.48$$

Incorporation of these chemical exchange induced dephasing effects into Equation 7.42 gives:[32,33]

$$\frac{dM_{xya}}{dt} = -\alpha_a M_{xya} - i\gamma B_1 M_{zeqa} + \frac{M_{xyb}}{\tau_b} - \frac{M_{xya}}{\tau_a} \qquad 7.49$$

and

$$\frac{dM_{xyb}}{dt} = -\alpha_b M_{xyb} - i\gamma B_1 M_{zeqb} + \frac{M_{xya}}{\tau_a} - \frac{M_{xyb}}{\tau_b} \qquad 7.50$$

where $\alpha_a = \frac{1}{T_{2a}} - i(\omega_{0a} - \omega)$

$$\alpha_b = \frac{1}{T_{2b}} - i(\omega_{0b} - \omega)$$

ω_{0n} is the Larmor frequency of site **n** in the absence of chemical exchange.

For the condition of continuous wave slow passage NMR, $M_z \sim M_{zeq}$, so that:

$$M_{za} = M_{zeqa} = \chi_a M_{zeq} \qquad 7.51$$

$$M_{zb} = M_{zeqb} = \chi_b M_{zeq} \qquad 7.52$$

and

$$\frac{dM_{xya}}{dt} = \frac{dM_{xyb}}{dt} = 0 \qquad 7.53$$

Therefore, the total transverse magnetisation, $M_{xy} = M_{xya} + M_{xyb}$, may be expressed in terms of τ_a and τ_b:[18,25,28,34]

$$M_{xy} = \frac{-i\gamma B_1 M_{zeq}[\tau_a + \tau_b + \tau_a\tau_b(\alpha_a\chi_a + \alpha_b\chi_b)]}{(1 + \alpha_a\tau_a)(1 + \alpha_b\tau_b) - 1} \qquad 7.54$$

The NMR absorption lineshape υ at frequency ω (rad s^{-1}) is proportional to the imaginary part of M_{xy} and can be expressed as:[21(b),25,35]

$$\upsilon = \frac{-\gamma B_1 M_{zeq}\left\{Y\left[1 + \tau\left(\frac{\chi_b}{T_{2a}} + \frac{\chi_a}{T_{2b}}\right)\right] + QR\right\}}{Y^2 + R^2} \qquad 7.55$$

where $\tau = \chi_b\tau_a = \chi_a\tau_b$

$\Delta\omega = \omega_{0a} - \omega_{0b}$

$$\delta\omega = \frac{1}{2}\left|\omega_{0a} - \omega_{0b}\right| - \omega$$

$$Y = \tau\left(\frac{1}{T_{2a}T_{2b}} - \delta\omega^2 + \frac{\Delta\omega^2}{4}\right) + \frac{\chi_a}{T_{2a}} + \frac{\chi_b}{T_{2b}}$$

$$Q = \tau\left(\delta\omega - \frac{\Delta\omega}{2}(\chi_a - \chi_b)\right)$$

$$R = \delta\omega\left[1 + \tau\left(\frac{1}{T_{2a}} + \frac{1}{T_{2b}}\right)\right] + \frac{\Delta\omega}{2}\tau\left(\frac{1}{T_{2b}} - \frac{1}{T_{2a}}\right) + \frac{\Delta\omega}{2}(\chi_a - \chi_b)$$

Therefore, the NMR lineshape for exchanging chemical systems may be calculated from Equation 7.55. When the rate of exchange is slow, τ_a and τ_b are very large and the NMR spectrum consists of two Lorentzian lineshapes

centred at ω_{0a} and ω_{0b}. As the rate of exchange increases, τ_a and τ_b decrease and the two resonances broaden and coalesce to form a single resonance. The very slow exchange limit occurs when the rate of exchange between sites **a** and **b** is too slow to cause any significant broadening of the two resonances. Conversely, the very fast exchange limit occurs when the rate of exchange between these sites is so fast that the coalesced singlet is characterised by a chemical shift and linewidth which is the weighted average of the two singlets characterising sites **a** and **b** in the absence of exchange. The best kinetic results are obtained within the temperature range defined by these two limiting conditions, where the singlets coalesce and the total lineshape is very sensitive to variations in τ_a and τ_b. These exchange rate limiting conditions are discussed in more detail below.

7.2.1.1 KINETIC ANALYSIS FOR SYSTEMS IN SLOW EXCHANGE

VERY SLOW EXCHANGE

Under these conditions:

$$\tau_a^{-1},\ \tau_b^{-1} << |\omega_{0a} - \omega_{0b}|,\ T_{2a}^{-1},\ T_{2b}^{-1}$$

That is, the rate of exchange between sites **a** and **b** is sufficiently small compared to the chemical shift difference (or frequency separation) between the two states. Equation 7.55 approximates to:

$$\upsilon = \frac{-\gamma B_1 \chi_a M_{zeq} T_{2a}^{-1}}{T_{2a}^{-2} + (\omega_{0a} - \omega)^2} + \frac{-\gamma B_1 \chi_b M_{zeq} T_{2b}^{-1}}{T_{2b}^{-2} + (\omega_{0b} - \omega)^2} \qquad 7.56$$

which contains no chemical exchange parameters, and describes two distinct Lorentzian lineshapes centred at ω_{0a} and ω_{0b}.

SLOW EXCHANGE

Under these conditions:

$$\tau_a^{-1},\ \tau_b^{-1} << |\omega_{0a} - \omega_{0b}| \text{ and } \tau_a^{-1} \sim T_{2a}^{-1},\ \tau_b^{-1} \sim T_{2b}^{-1}$$

The rate of exchange is now greater than that of the very slow exchange limit, although it is still small compared to the chemical shift difference between sites

a and **b**. For the slow exchange limit, the absorption mode lineshape approximates to:

$$\upsilon = \frac{-\gamma B_1 \chi_a M_{zeq} T'_{2a}{}^{-1}}{T'_{2a}{}^{-2} + (\omega_{0a} - \omega)^2} + \frac{-\gamma B_1 \chi_b M_{zeq} T'_{2b}{}^{-1}}{T'_{2b}{}^{-2} + (\omega_{0b} - \omega)^2} \qquad 7.57$$

where T'_{2n} is the observed transverse relaxation time of site **n**.

$$T'_{2a}{}^{-1} = T_{2a}{}^{-1} + \tau_a{}^{-1}$$
$$T'_{2b}{}^{-1} = T_{2b}{}^{-1} + \tau_b{}^{-1}$$

Equation 7.57, as for Equation 7.56, describes two Lorentzian lineshapes centred at ω_{0a} and ω_{0b}. However, the additional dephasing effect of the exchange process on the transverse magnetisation leads to observed relaxation times, T'_{2a} and T'_{2b}, which are shorter than those characterising these sites in the absence of exchange, T_{2a} and T_{2b}. Therefore, the resonance characterising sites **a** and **b** are broader than those in the absence of exchange. The difference between the full width at half maximum amplitude of the resonance at site **a** in the absence of exchange, $W_{\frac{1}{2}a}$, and the corresponding width of the exchange broadened resonance, $W'_{\frac{1}{2}a}$, may be used to estimate τ_a:

$$\pi W_{\frac{1}{2}a} = \frac{1}{T_{2a}} \qquad 7.58$$

$$\pi W'_{\frac{1}{2}a} - \pi W_{\frac{1}{2}a} = \frac{1}{T'_{2a}} - \frac{1}{T_{2a}} = \frac{1}{\tau_a} \qquad 7.59$$

Therefore, for resonances at the slow exchange limit, one method to obtain a minimum lifetime, τ_a, and thus a maximum rate of exchange, is to calculate the lifetime of the exchanging species that would cause a broadening of each resonance by 50%. This means that $W_{\frac{1}{2}a}$ becomes:

$$W'_{\frac{1}{2}a} = 1.5 W_{\frac{1}{2}a} \qquad 7.60$$

so that

$$\tau_a = \frac{2}{\pi W_{\frac{1}{2}a}} \qquad 7.61$$

A similar expression for τ_b can be derived, where $\tau_b = \frac{\tau_a \chi_b}{\chi_a}$.

7.2.1.2 KINETIC ANALYSIS FOR SYSTEMS AT INTERMEDIATE RATES OF EXCHANGE

The region of intermediate rates of exchange is defined as that region where the rate of exchange is faster than that in the slow exchange limit, and slower than the fast exchange limit. That is, in the slow exchange region, the two separate resonances of sites **a** and **b** have achieved a sufficient rate of chemical exchange such that they become broadened from their natural linewidths, and their inherent chemical shifts begin to approach each other as the rate of exchange increases. As the rate of exchange increases further, the two separate resonances coalesce to a single broadened resonance when the lifetimes τ_a and τ_b are of the order $(\omega_{0a} - \omega_{0b})^{-1}$. This single resonance continues to narrow as the rate of exchange increases, and τ_a and τ_b decrease, until exchange reaches the very fast exchange limit.

For the simplifying conditions $\chi_a = \chi_b = ½$ and $\tau_a = \tau_b$ applied to the coalescing resonances, and the widths of the resonances in the absence of exchange are small compared with their separation, then $\frac{1}{T_{2a}} = \frac{1}{T_{2b}} = 0$, and:

$$M_{za} = M_{zb} = \frac{1}{2} M_{zeq} \qquad 7.62$$

Therefore, the NMR absorption mode lineshape becomes:

$$\upsilon = \frac{\frac{1}{2}\gamma B_1 M_{zeq} \tau_a (\omega_{0a} - \omega_{0b})^2}{(\omega_{0a} + \omega_{0b} - 2\omega)^2 + \tau_a^2 (\omega_{0a} - \omega)^2 (\omega_{0b} - \omega)^2} \qquad 7.63$$

Converting to frequency units, υ (Hz) = $\omega/2\pi$, gives:

$$g(\upsilon) = \frac{2\tau_a (\upsilon_a - \upsilon_b)^2}{[\upsilon - \frac{1}{2}(\upsilon_a + \upsilon_b)]^2 + \pi^2 \tau_a^2 (\upsilon - \upsilon_a)^2 (\upsilon - \upsilon_b)^2} \qquad 7.64$$

By expressing the absorption lineshape as a function of the dimensionless quantity, x, Equation 7.64 can be simplified:[34]

$$g(x) = \frac{2\tau_a}{[x^2 + q^2(x^2 - 1)^2]} \qquad 7.65$$

where $x = \frac{\Delta\upsilon}{\Delta}$

$$\Delta\upsilon = \upsilon - \frac{1}{2}(\upsilon_a + \upsilon_b)$$

$$\Delta = \frac{1}{2}(\upsilon_a - \upsilon_b)$$

$$q = \pi\tau_a\Delta$$

The lineshapes predicted by Equation 7.65 are the same as those derived from Equation 7.55, for $\chi_a = \chi_b$.

The shape of the NMR spectra described by g(x) depends on the product q. For $q >> 1$, characterising slow exchange conditions, Equation 7.65 predicts two Lorentzian signals centred at υ_a and υ_b. As q decreases, τ_a decreases, and the two individual signals broaden so that their maxima draw closer together until $q = 1/\sqrt{2}$. At this point, the two resonances coalesce into a single broad signal with a maximum amplitude at the mean of the frequency of the individual resonances, $\frac{1}{2}(\upsilon_a + \upsilon_b)$. For $q << 1$, characterising fast exchange, Equation 7.65 predicts that the single broad resonance narrows further to give rise to a single Lorentzian line centred at $\frac{1}{2}(\upsilon_a + \upsilon_b)$. Therefore, for systems undergoing two-site chemical exchange, the site lifetime of the exchanging species, τ, can be estimated at the coalescence temperature, where the two resonances of the spectrum coalesce into a single broad resonance. That is, at coalescence, $q = 1/\sqrt{2}$ and:

$$\tau = \tau_a = \tau_b = \frac{\sqrt{2}}{\pi(\upsilon_a - \upsilon_b)} \qquad 7.66$$

Therefore, if the chemical shifts characterising sites **a** and **b** in the absence of exchange, υ_a and υ_b, can be determined or estimated, an approximate value of τ may be calculated through complete lineshape analysis using Equation 7.66.

7.2.1.3 KINETIC ANALYSIS FOR SYSTEMS IN FAST EXCHANGE

VERY FAST EXCHANGE

Under these conditions:

$$\tau_a^{-1},\ \tau_b^{-1} >> |\omega_{0a} - \omega_{0b}|,\ T_{2a}^{-1},\ T_{2b}^{-1}$$

That is, the two broadened resonances, centred at ω_{0a} and ω_{0b}, have coalesced to form a single Lorentzian resonance, centred at $\omega = \chi_a\omega_{0a} + \chi_b\omega_{0b}$, as complete environmental averaging is experienced by the exchanging nuclear spins. The linewidth, $W_{\frac{1}{2}}$, at half-height of the single resonance is also the weighted average of the individual resonances in the absence of exchange, and is described by:

$$W_{\frac{1}{2}} = \frac{1}{\pi T'_2} = \frac{\chi_a}{\pi T_{2a}} + \frac{\chi_b}{\pi T_{2b}} \qquad 7.67$$

Substitution of Equation 7.67 into Equation 7.55 gives the following expression for the absorption mode lineshape:

$$\upsilon = \frac{-\gamma B_1 M_{zeq} T'_2}{1 + (T'_2)^2(\chi_a\omega_{0a} + \chi_b\omega_{0b} - \omega)^2} \qquad 7.68$$

where $\frac{1}{T'_2} = \frac{\chi_a}{T_{2a}} + \frac{\chi_b}{T_{2b}}$

Equation 7.68, as for Equation 7.56 describing the very slow exchange limit, contains no chemical exchange parameters, because the rate of exchange is so fast that the exchanging nuclear spins experience the weighted average of the two different environments **a** and **b**.

For the fast exchange limit, the rate of exchange is slightly slower, so that $\tau_a^{-1},\ \tau_b^{-1} > |\omega_{0a} - \omega_{0b}|$, with the observation of a single Lorentzian lineshape, centred at $\omega = \chi_a\omega_{0a} + \chi_b\omega_{0b}$. The linewidth describing this resonance, $W'_{\frac{1}{2}a}$, at half-height of the single resonance is greater than that given in Equation 7.67 and is described by:

$$\pi W'_{\frac{1}{2}} = \pi\chi_a W_{\frac{1}{2}a} + \pi\chi_b W_{\frac{1}{2}b} + \chi_a^2\chi_b^2\Delta\omega_0^2(\tau_a + \tau_b) \qquad 7.69$$

where $\Delta\omega_0 = |\omega_{0a} - \omega_{0b}|$

$$\frac{1}{T'_2} = \frac{\chi_a}{T_{2a}} + \frac{\chi_b}{T_{2b}} + \chi_a^2\chi_b^2(\omega_{0a} - \omega_{0b})^2(\tau_a + \tau_b)$$

Converting to frequency units, υ (Hz) = $\omega/2\pi$, gives:

$$\pi W'_{\frac{1}{2}} = \pi\chi_a W_{\frac{1}{2}a} + \pi\chi_b W_{\frac{1}{2}b} + 4\pi^2\chi_a^2\chi_b^2\Delta\upsilon_0^2(\tau_a + \tau_b) \qquad 7.70$$

where $\Delta\upsilon_0 = |\upsilon_{0a} - \upsilon_{0b}|$

So, if the linewidths, $W_{\frac{1}{2}a}$ and $W_{\frac{1}{2}b}$, and chemical shift difference, $\Delta\upsilon_0$, of the two resonances in the absence of exchange can be determined or estimated, then τ_a (or τ_b) can be calculated from Equation 7.70 and the relationship $\frac{\tau_a}{\chi_a} = \frac{\tau_b}{\chi_b}$.

7.2.2 PULSED FOURIER TRANSFORM NMR

Pulsed NMR allows site lifetimes down to 10^{-6} s to be measured in chemically exchanging systems, whereas continuous wave slow passage NMR is limited to values $\geq 10^{-3}$ s.[25] For the condition of the pulsed NMR experiment, in the rotating frame (x',y',z'), B_0 is applied continuously along the z' axis (as for the continuous wave slow passage experiment) but B_1 is now applied along the x' axis. The magnetic field B_1 is applied as a short (10^{-6}-10^{-4} s), high intensity pulse, whose frequency, centred about ω_0, applies a torque to $\boldsymbol{M}$. This in turn causes $\boldsymbol{M}$ to tilt away from its alignment with the z' axis and rotate about the x' axis towards the y' axis, thus generating a transverse component, M_{xy}. Once the pulse of B_1 ceases ($B_1 = 0$), $\boldsymbol{M}$ relaxes back to its equilibrium position aligned with the z' axis by spin-lattice relaxation. The transverse component, M_{xy}, decays exponentially to zero by transverse relaxation and thus generates a free induction decay (FID) signal. The FID (or time domain spectrum) is acquired and accumulated in the computer of the NMR spectrometer. For $B_1 = 0$, the modified Bloch equations (Equations 7.42 and 7.43) may be solved to give an equation describing the FID:[30(c)]

$$M_{xy} = C_1 e^{-\Phi+t} + C_2 e^{-\Phi-t} \qquad 7.71$$

where C_1 and C_2 are the constants of integration

$$2\Phi_{\pm} = \left(\alpha_a + \frac{1}{\tau_a} + \alpha_b + \frac{1}{\tau_b}\right) \pm \left[\left(\alpha_a + \frac{1}{\tau_a} - \alpha_b - \frac{1}{\tau_b}\right)^2 + \frac{4}{\tau_a \tau_b}\right]^{\frac{1}{2}} \quad 7.72$$

The Fourier transform (or frequency domain spectrum) of the FID, S, is given by:

$$S = \int_0^{\infty} M_{zeq} e^{-i(\omega - \omega_1)t} dt \quad 7.73$$

$$= \frac{iM_{zeq}\left[\tau_a + \tau_b + \tau_a \tau_b (\alpha_a \chi_a + \alpha_b \chi_b)\right]}{(1 + \alpha_a \tau_a)(1 + \alpha_b \tau_b) - 1} \quad 7.74$$

where $\alpha_a = \frac{1}{T_{2a}} + i(\omega_{0a} - \omega)$

$$\alpha_b = \frac{1}{T_{2b}} + i(\omega_{0b} - \omega)$$

ω is the variable frequency
ω_1 is the fixed pulse carrier frequency.

The absorption mode lineshape, derived from the imaginary part of Equation 7.73, is the same as that derived from the continuous wave slow passage experiment (Equation 7.55), which is generally the case for an uncoupled spin system undergoing chemical exchange.[29,30]

7.2.3 TWO-SITE LINESHAPE ANALYSIS

A series of ^{23}Na, ^{7}Li and ^{13}C variable temperature NMR spectra were accumulated and Fourier transformed on a Bruker CXP-300 NMR spectrometer for Na^+, Li^+, and M^{n+} complex systems, respectively, whose rate of exchange falls within the NMR timescale. In general, the temperature range spans the slow and fast exchange limits of the particular system being studied. The Fourier transformed spectra were then transferred to an ACER 486

computer and subject to complete lineshape analysis[25] using the FORTRAN-77 program LINSHP.[36]

For two-site uncoupled intramolecular or intermolecular exchange, a theoretical NMR spectrum is generated at each temperature by the non-interactive FORTRAN-77 program LINSHP[36], using the input parameters υ_a and υ_b (the frequency, in Hz, of the two coalescing resonances characterising sites **a** and **b** in the absence of exchange); $W_{\frac{1}{2}\,a}$ and $W_{\frac{1}{2}\,b}$ (the full width, in Hz, at half maximum amplitude of each resonance in the absence of exchange); χ_a and χ_b (the relative populations, or mole fractions, of each site); and R (the estimated rate of exchange, where $R = (\tau_a\chi_b)^{-1} = (\tau_b\chi_a)^{-1}$). Once the range of R, the number of iterations to be made and the input parameters are defined, the LINSHP program iteratively determines the best R value in which the difference between the experimental and theoretical spectra is minimal at each temperature. The exchange rate constant, $k = 1/\tau$, characterising intramolecular or intermolecular exchange can then be determined at each temperature. For all the NMR systems studied, the experimental spectrum over a full range of temperatures were displayed simultaneously against the theoretical spectrum, generated from the input parameters, on a VDU for comparison. Examples of the best fit theoretical and corresponding experimental spectra over a full range of temperatures are shown in Chapters 4 and 5.

The chemical shifts and linewidths of the site resonances in the absence of exchange must be known accurately over the temperature range for which NMR measurements of the exchange process are carried out in order to reduce the introduction of systematic errors. For ^{23}Na and ^{7}Li NMR spectroscopic studies, the linewidths and chemical shifts (and their temperature dependences) employed in the lineshape analysis were obtained through a combination of extrapolation from low temperature, where no chemical induced modification occurred, and from the linewidths and chemical shift variations of solutions containing either solvated M^+ or $[ML]^+$ alone, where $M^+ = {}^{23}$Na or ^{7}Li, in the coalescence temperature range observed for solutions containing both species. For ^{13}C NMR spectroscopic studies, the temperature dependence of the chemical shifts and linewidths in the absence of exchange were determined by extrapolation from the spectra at low temperature where no chemical induced broadening of the spectra occurred. For certain systems studied by ^{13}C NMR spectroscopy, it was necessary to use the chemical shifts and linewidths of the resonances corresponding to the $>NCH_2$- moiety of the pendant arm of the ligand in $[ML]^{n+}$ rather than that of the ring resonance for the lineshape analysis (as detailed in Chapter 6).

7.2.4 CALCULATION OF ACTIVATION PARAMETERS

For variable temperature NMR analysis, the intramolecular or intermolecular exchange rate constant, k, determined at each temperature by complete lineshape analysis is related to the activation parameters and temperature according to the Eyring equation:[37,38]

$$k = \frac{1}{\tau} = \frac{k_B T}{h} \exp\left(\frac{-\Delta H^{\ddagger}}{RT} + \frac{\Delta S^{\ddagger}}{R}\right) \qquad 7.75$$

where τ = mean lifetime (ms)
k_B = Boltzmann's constant (1.3806×10^{-23} J K^{-1})
h = Planck's constant (6.6262×10^{-34} J s)
R = gas constant (8.3143 J mol^{-1} K^{-1})
T = temperature (K)
$\Delta H^{\ddagger}$ and $\Delta S^{\ddagger}$ are the enthalpy (J mol^{-1}) and entropy (J mol^{-1} K^{-1}) of activation, respectively.

The linear form of Equation 7.75 is given by:

$$\ln(T\tau) = \frac{\Delta H^{\ddagger}}{RT} + \ln\left(\frac{h}{k_B}\right) - \frac{\Delta S^{\ddagger}}{R} \qquad 7.76$$

so that a plot of $\ln(T\tau)$ versus $1/T$ yields a straight line with slope $\frac{\Delta H^{\ddagger}}{R}$ and an intercept of $\ln\left(\frac{h}{k_B}\right) - \frac{\Delta S^{\ddagger}}{R}$, from which $\Delta H^{\ddagger}$ and $\Delta S^{\ddagger}$ can be obtained. Examples of such plots are shown in Chapters 4 and 5.

A non-linear, weighted least squares method of fitting was used to determine k(298.2 K), k at the coalescence temperature for each system, $\Delta H^{\ddagger}$ and $\Delta S^{\ddagger}$, using the program DATAFIT[39,40] on an ACER 486 computer. This program was used to fit the experimentally determined variation of k with T using Equation 7.75, where the program DATAFIT minimises the residual differences in an n-dimensional sum of squares space set, between a calculated and experimental surface (ie: k and T, respectively), using the method described by Pitha and Jones.[41] The errors quoted in Chapters 4 and 5 for the activation parameters derived by this method are the standard deviations for each parameter in the sum of squares space. These errors only take the errors

between the input parameters into account, and not any systematic errors associated with the individual input parameters k and T.

BIBLIOGRAPHY

1. (a) J.-M. Lehn, J.-P. Sauvage, *J. Am. Chem. Soc.* **1975**, 97, 6700-6707.
   (b) H.J. Buschmann, *J. Solution. Chem.* **1986**, 15, 453.
2. (a) G. Ritzler, F. Peter, M. Grass, *J. Electroanal. Chem.* **1983**, 146, 285-301.
   (b) B. Tümmler, G. Maas, E. Weber, W.Wehner, F. Vögtle, *J. Am. Chem. Soc.* **1977**, 99, 4683-4690.
3. (a) T. Alfheim, J. Dale, P. Groth, K.D. Krautwurst, *J. Chem. Soc., Chem. Commun.* **1984**, 1502-1504.
   (b) G. Boras, C. Bosso, M.R. Vignon, *J. Inclusion Phenom.* **1989**, 7, 637-647.
4. Y.M. Cahen, J.L. Dye, A.I. Popov, *J. Phys. Chem.* **1975**, 79, 1289-1295.
5. A.K.W. Stephens, PhD Thesis, University of Adelaide, **1994**.
6. J.B. Lucas, PhD Thesis, University of Adelaide, **1994**.
7. T. Rodopoulos, PhD Thesis, University of Adelaide, **1993**.
8. B.G. Cox, H. Schneider, J. Stroka, *J. Am. Chem. Soc.* **1978**, 100, 4746-4749.
9. J. Gutknecht, H. Schneider, J. Stroka, *Inorg. Chem.* **1978**, 17, 3326-3329.
10. F.J.C. Rossotti, H. Rossotti, *"The Determination of Stability Constants"*, McGraw-Hill, New York, **1961**.
11. P. Clarke, PhD Thesis, University of Adelaide, **1992**.
12. P. Gans, A. Sabatini, A. Vacca, *J. Chem. Soc., Dalton Trans.* **1985**, 1195-1200.
13. (a) S. Forsen, B. Lindman, *"Ion Binding in Biological Systems as Studied by NMR Spectroscopy"* in *"Methods of Biochemical Analysis"*, Academic Press, New York, **1981**.
    (b) H.S. Gutowsky, C.H. Holm, *J. Chem. Phys.* **1956**, 25, 1228.
14. (a) T.S. Piper, G. Wilkinson, *J. Inorg. Nucl. Chem.* **1956**, 3, 104-124.
    (b) D. Gamliel, Z. Luz, S. Vega, *J. Chem. Phys.* **1988**, 88, 25-42.
15. (a) H.S. Gutowsky, L.M. Jackman, F.A. Cotton, *"Time Dependent Magnetic Perturbations"* in *"Dynamic NMR Spectroscopy"*, Academic Press, New York, **1975**.
    (b) T.E. Bull, *J. Mag. Reson.* **1972**, 8, 344-353.
16. A.I. Popov, *Pure. Appl. Chem.* **1979**, 51, 101-110.
17. A.I. Popov, J.-M. Lehn, *"Coordination Chemistry of Macrocyclic Compounds"*, G.A. Melson (Editor), Plenum Press, New York, **1979**.
18. Y.M. Cahen, P.R. Handy, E.T. Roach, A.I. Popov, *J. Phys. Chem.* **1975**, 79, 80-85.
19. (a) S.F. Lincoln, I.M. Brereton, T.M. Spotswood, *J. Chem. Soc., Faraday Trans.* **1985**, 81, 1623-1630.

(b) S.F. Lincoln, A. White, A.M. Hounslow, *J. Chem. Soc., Faraday Trans.* **1987**, 83, 2459-2466.

20. (a) P. Clarke, S.F. Lincoln, K.P. Wainwright, *Inorg. Chem.* **1991**, 30, 134-139.
(b) Y.M. Cahen, J.L. Dye, A.I. Popov, *J. Phys. Chem.* **1975**, 79, 1292-1295.
21. (a) J.M. Ceraso, P.B. Smith, J.S. Launders, J.L. Dye, *J. Phys. Chem.* **1977**, 81, 760-766.
(b) I.O. Sutherland, *Ann. Reports. NMR. Spectros.* **1971**, 4, 71-235.
22. (a) K. Orrell, V. Šik, D. Stephenson, *Prog. NMR. Spec.* **1990**, 22, 141-208.
(b) L.M. Jackman, S. Sternhell, *"Applications of NMR Spectroscopy in Organic Chemistry"*, Pergamon Press, Second Edition, **1969**.
23. (a) C.L. Perrin, T.J. Dwyer, *Chem. Rev.* **1990**, 90, 935-967.
(b) J. Sandström, *"Dynamic NMR Spectroscopy"*, Academic Press, London, **1982**.
24. M. Oki, *"Applications of Dynamic NMR Spectroscopy to Organic Chemistry"*, VCH, **1985**.
25. S.F. Lincoln, *Prog. Reaction Kinetics* **1977**, 9, 1-91.
26. (a) R.M. Lynden-Bell, *Prog. NMR. Spec.* **1967**, 2, 163-204.
(b) J.I. Kaplan, G. Fraenkel, *"NMR of Chemically Exchanging Systems"*, Academic Press, New York, **1980**.
27. (a) A. Steigel in *"NMR Basic Principles and Progress"*, P. Diehl, E. Fluck, R. Rosfeld (Editors), **1978**.
(b) S. Alexander, *Prog. NMR. Spec.* **1962**, 37, 967-974.
(c) S. Alexander, *Prog. NMR. Spec.* **1962**, 37, 974-980.
28. F. Bloch, *Phys. Rev.* **1946**, 70, 460-474.
29. (a) J.I. Kaplan, *J. Chem. Phys.* **1972**, 57, 5615-5616.
(b) R.R. Ernst, *J. Chem. Phys.* **1973**, 59, 989.
30. (a) J.I. Kaplan, *J. Chem. Phys.* **1973**, 59, 990.
(b) T.C. Farrar, E.D. Becker, *"Pulse and Fourier Transform NMR"*, Academic Press, New York, **1971**.
(c) R.K. Gupta, T.P. Pitner, R. Wasyrishen, *J. Mag. Reson.* **1974**, 13, 383-385.
31. E.L. Hahn, D.E. Maxwell, *Phys. Rev.* **1952**, 88, 1070-1084.
32. H.M. McConnell, *J. Chem. Phys.* **1958**, 28, 430-431.
33. H.S. Gutowsky, D.M. McCall, C.P. Slitcher, *J. Chem. Phys.* **1953**, 21, 279.
34. R.K. Harris, *"NMR Spectroscopy"*, Pitman, London UK, **1983**.
35. M.T. Rogers, J.C. Woodbrey, *J. Chem. Phys.* **1962**, 66, 540-544.
36. LINSHP program by T.M. Spotswood, **1973**. Converted to Nicolet BNC-12 machine code by E. Williams, **1980**. Modified and converted to

FORTRAN-5 by A. White, **1983**. Modified and converted to FORTRAN-77 by P. Clarke, **1987**.
37. W.K.F. Wynne-Jones, H. Eyring, *J. Chem. Phys.* **1935**, 3, 492.
38. S. Gladstone, K.J. Laidler, H. Eyring, *"Theory of Rate Processes"*, McGraw-Hill, New York, **1941**.
39. T. Kuruscev, *J. Chem. Educ.* **1978**, 55, 128-129.
40. T. Kuruscev, University of Adelaide. Unpublished material.
41. J. Pitha, R.N. Jones, *Can. J. Chem.* **1966**, 44. 3031-3050.

APPENDIX i

GUTMANN DONOR NUMBER, D_N

In solution, the complexation of a metal ion by a ligand involves competition between the ligand and solvent for coordination of the metal ion. This arises because most solvents are electron pair donors, with the ability to donate electron density to an electron pair acceptor such as a metal ion. Therefore, a measure of the ability of the solvent to compete for a metal ion is important. The Gutmann donor number, D_N, is an empirical measurement of the strength of the electron pair donating ability (or donor strength) of the solvent, and may be used as a measure of cation solvation energy. The D_N is defined as the enthalpy of formation, $-\Delta H^{\ddagger}$ (kJ mol^{-1}), of the 1:1 complex between a donor solvent and the reference electron pair acceptor antimony (V) chloride, $SbCl_5$, in the non-coordinating solvent 1,2-dichloroethane, and is described by Equation A.1:

$$SbCl_5 + \text{Solvent} \xrightarrow{ClCH_2CH_2Cl} [SbCl_5.(\text{Solvent})] \qquad \text{A.1}$$

Numerous equilibrium and kinetic studies of metal complexes in non-aqueous solution have been investigated with respect to the D_N.[1-7] In general, as the electron donating power of the solvent increases, D_N increases and metal complex stability decreases.[4,8] The D_N values for the solvents used in this study are shown in Table A.1.

The D_N has been successfully used in this study, and elsewhere, as a measure of the strength of metal ion-solvent interactions in solution, with a good correlation between D_N and the stabilities and labilities of metal complexes. However, the D_N does not take into account particular steric interactions that may exist between certain donor-acceptor species. That is, there is a good correlation between D_N and the stability of Ag^+ complexes in oxygen donor solvents, but not so in nitrogen donor solvents because of the high affinity of Ag^+ for nitrogen donor atoms. Therefore, it may not always be applicable to determine the magnitude of metal ion-solvent interactions by the relationship between D_N and solvent donor strength. In addition, the D_N does not take steric effects, such as the coordination of a metal ion by bulky solvent molecules, into account. That is, D_N is proportional to the electron donating strength of a single solvent molecule, whereas the number of solvent molecules coordinating a metal ion in solution depends on the size of the metal ion and the size and structure of the solvent.

For the solvents H_2O and MeOH, D_N = 33.0 and 23.5, respectively, are probably more appropriate values than D_N = 18.0 and 19.0, respectively, (Table A.1) because the former values refer to the bulk solvent, whereas the latter values are those obtained for H_2O and MeOH in 1,2-dichloroethane where the intermolecular hydrogen bonding of these protic solvents is disrupted.[9,10] However, it is also likely that neither of these values are an accurate measurement of the metal ion hydration energies in H_2O and MeOH.

Table A.1: The Gutmann Donor Number, D_N, for selected solvents.

Solvent	D_N[a]	D_N[b]
1,2-dichlorethane	0.0	
Acetonitrile	14.1	
Propylene Carbonate	15.1	
MeOH	19.0	23.5
DMF	26.6	
H_2O	18.0	33.0

[a]Reference 11,12. [b]Reference 9,10.

BIBLIOGRAPHY

1. B.G. Cox, J. Garcia-Ross, H. Schneider, *J. Am. Chem. Soc.* **1981**, 103, 1054-1059.
2. P. Clarke, A. Abou-Hamdan, A.M. Hounslow, S.F. Lincoln, *Inorg. Chim. Acta.* **1988**, 154, 83-87.
3. S.F. Lincoln, I.M. Brereton, T.M. Spotswood, *J. Am. Chem. Soc.* **1986**, 108, 8134-8138.
4. S.F. Lincoln, A. Abou-Hamdan, *Inorg. Chim. Acta.* **1990**, 30, 462-466.
5. M. Shamsipur, A.I. Popov, *Inorg. Chim. Acta.* **1980**, 43, 243-247.
6. R. Dhillon, S.F. Lincoln, *Aust. J. Chem.* **1972**, 27, 113-140.
7. (a) S.F. Lincoln, B.J. Steel, I.M. Brereton, T.M. Spotswood, *Polyhedron* **1986**, 5, 1597-1600.
   (b) S. Kulstad, L.A. Malmsten, *J. Inorg. Nucl. Chem.* **1980**, 42, 573-578.
8. S.F. Lincoln, A.K.W. Stephens, *Inorg. Chem.* **1991**, 30, 3529-3534.
9. R.H. Erlich, E. Roach, A.I. Popov, *J. Am. Chem. Soc.* **1970**, 92, 4989-4990.
10. W.J. Dewitte, A.I. Popov, *J. Solution Chem.* **1976**, 5, 231-240.
11. U. Mayer, V. Gutmann, *Topp. Curr. Chem.* **1972**, 27, 113-140.
12. V. Gutmann, *"Coordination Chemistry in Non-Aqueous Solvents"*, Springer-Verlag, Wien, **1968**.

PUBLICATIONS

"Diastereomeric Δ-1,4,7,10-Tetrakis((*R*)-2-hydroxy-2-phenylethyl)-1,4,7,10-tetraazacyclododecane and Its Alkali-Metal Complex Ions. A Potentiometric Titration, Nuclear Magnetic Resonance, and Molecular Orbital Study".
S.L. Whitbread, P. Valente, M.A. Buntine, P. Clements, S.F. Lincoln, K.P. Wainwright.
J. Am. Chem. Soc. **1998**, 120, 2862-2869.

"Enantiomerisation of Pendant-Arm Triaza Macrocyclic Lithium(I) and Sodium (I) Complex Ions".
S.L. Whitbread, J.M. Weeks, P. Valente, M.A. Buntine, S.F. Lincoln, K.P. Wainwright.
Aust. J. Chem. **1997**, 50, 853-856.

"Alkali Metal Complexes of a Pendant Arm Tetraaza Macrocycle. Equilibrium, Inter- and Intramolecular Exchange Processes".
S.L. Whitbread, S. Politis, A.K.W. Stephens, J. Lucas, R.S. Dhillon, S.F. Lincoln, K.P. Wainwright.
J. Chem. Soc., Dalton Trans. **1996**, 79, 1379-1384.

"Alkali Metal Complexes of the Pendant Arm Macrocyclic Ligand 1,4,7,10-tetrakis(2-methoxyethyl)-1,4,7,10-tetraazacyclododecane. An Equilibrium and Inter- and Intramolecular Exchange Study".
A.K.W. Stephens, R.S. Dhillon, S.E. Madback, S.L. Whitbread, S.F. Lincoln.
Inorg. Chem. **1996**, 35, 2019-2024.

"Helicity Interchange in Pendant Arm Tetraaza Macrocyclic Sodium(I) Complexes".
R.S. Dhillon, A.K.W. Stephens, S.L. Whitbread, S.F. Lincoln, K.P. Wainwright.
J. Chem. Soc., Chem. Commun. **1995**, 1, 97-98.